2008-01-01

Novel Photoelectrochemical Cell for the Remediation of Organic Compounds in Water

Patrick Enright
Technological University Dublin

Novel Photoelectrochemical Cell For The Remediation Of Organic Compounds in Water

By

Patrick Enright BSc. (Hons)

A thesis presented to
Dublin Institute of Technology for the award of Ph.D

Prepared under the supervision of Prof. J.F. Cassidy,
School of Chemical and Pharmaceutical Sciences, Dublin Institute of Technology,
Kevin St, Dublin 8 and Dr A.J. Betts,
Directorate of Research and Enterprise, Dublin Institute of Technology,
143 – 149 Rathmines Road, Dublin 6

School of Chemical and Pharmaceutical Sciences
November 2008

Abstract

Titanium dioxide (TiO_2) suspensions have widely been used as photocatalysts, either alone or in a doped form to degrade organic compounds and kill bacteria. Because of its relatively large band gap, UV light has been the most efficient radiation used to allow this catalysis to occur. TiO_2 has also been immobilised on electrodes in order to separate the 'reduction' and 'oxidation' reactions. Typical systems involve the oxidation of a 'fuel' at a TiO_2 coated anode and the reduction of oxygen at a separate cathode, where the passage of current can be monitored, and this work utilises such a system.

In this work, there are two systems described. TiO_2 coatings have been prepared on carbon ink based electrodes as anodes, while the cathodes were ink electrodes loaded with cobalt (II) phthalocyanine (CoPc). These electrodes are characterised and used in a fuel cell configuration with formic acid as a substrate in a one compartment cell. In this case the light source was modelled on visible radiation using either a 60 W tungsten lamp or a Q Sun system.

The second system involves the use of TiO_2 coated electrodes with air electrodes as cathodes in either one or two compartment set ups, using many water soluble organic compounds as fuels.

Such a system can be used to degrade many organics such as benzaldehyde, 1,2-dihydroxybenzene (CAT) potassium hydrogen phthalate, 2-propanol, phthalic acid (HHP), 4-chlorophenol, and ascorbic acid to mention but a few. The rate of degradation depends on the light source used, amount of lumens from the light source reaching the catalytically coated surface, passivation, chemical nature and stability of the organic compound, pH and cell configuration.

With daylight as the source, at room temperature the photoelectrocatalyic (pec) cell connected for 11 days brought about an 88 % degradation of CAT, 4 times more than a similar surface confined photocatalytic (pc) cell could offer. Another pec cell also produced over 4 times more degradation than its equivalent pc cell; this time eliminating 90 % of the initial amount of the common vitamin ascorbic acid, using visible light and within 3 hours. There was over 3 times as much HHP degraded in a one compartment pec cell using UV light and an air cathode rather than for a similar surface confined pc cell, with half of the concentration of the aromatic chemical eliminated within 3 hours.

A qualitative model was developed for the cyclic voltammetric behaviour of formic acid, where a reversible system was transformed into a steady state system, depending on Langmuir Hinshelwood parameters; k' and K.

In separate work square wave voltammetry was applied to microelectrodes to obtain a peaked current response. Parameters such as pulse height, frequency and step height were varied and a simple model was applied.

DECLARATION

I certify that this thesis which I now submit for examination for the award of Doctor of Philosophy is entirely my own work and has not been taken from the work of others, save and to the extent that such work has been cited and acknowledged within the text of my work.

This thesis was prepared according to the regulations for postgraduate study by research of the Dublin Institute of Technology and has not been submitted in whole or in part for another award in any Institute.

The work reported on in this thesis conforms to the principles and requirements of the Institute's guidelines for ethics in research.

The Institute has permission to keep, lend or copy this thesis in whole or in part, on condition that any such use of the material of the thesis be duly acknowledged.

Signature _____ Date _____

Candidate

ID No.: _____

Acknowledgements

Firstly I would like to thank both of my supervisors, Prof. J.F. Cassidy and Dr. A.J. Betts for their help, guidance, enthusiasm and encouragement over the past three or four years. Their enthusiasm about the project was infectious, even at times when my motivation had dropped due to experiments not working out or whatever. Both supervisors' guidance for this project was excellent, with both having a great ability to make even the most complex mathematical processes comprehendible. Their generosity meant that they always made time for me regardless of whatever else was on, meeting up at least once a week and often many times more per week.

I would like to thank the DIT for affording me the use of their equipment and facilities. I owe a lot of thanks to many of the lecturers, particularly my internal reader and fellow photochemist Dr M. Seery for the time he spent reading my work and offering many suggestions along the way.

Without Dr M. McNamara and Prof. H. Byrne acquiring the funding to build the FOCAS research building and working endless and often thankless hours so that postgraduate students could have an easier life, none of this would be possible.

I owe many thanks to the undergrad students I supervised, particularly Lisa Ceysennes, Paul O Brien and John Beggan. The laboratory technicians in DIT, Kevin Street - Brian, Peter, Caoimhe, Howard and Martin were always there to provide any chemicals that I may not have had. I would like to thank Brian Devine from the school of physics for his help in acquiring emission spectra of light sources; while I'd also like to thank fellow photocatalysis researchers Nicholas Nolan, Vinod Kumar, Dr R. George and Dr. H. Hayden for their information and tips. Dr J. Walsh from the school of physics was also very helpful in our research lab, as was Dr B. Duffy.

I owe many thanks to Dr K.G. McGuigan and Eunice Ubomba-Jaswa from RCSI for their loan of an Oriel 150 W Xe light source. I would also like to thank Dr. S.C. Pillai and Dr. J.A. Byrne for reading through my thesis.

Most of all I would like to thank my parents for this wonderful education I have received. It has been described by many governments as free but this is far form the case, and now there is talk of bringing in third level fees. I am very grateful for my parents' assistance with some of my rent over the last couple of years. I am grateful to my fellow members of the electrochemistry and fuel cells group here in Kevin Street and anyone else that I forgot to mention.

To Dad and Mam

Abbreviations used

4CP	-	4-Chlorophenol
4-HBz	-	4-Hydroxybenzoic acid
AA	-	Ascorbic Acid
ACE	-	Acetone
BA	-	Benzamide
Bz	-	Benzaldehyde
CAT	-	1,2–Hydroxybenzene
CB	-	Conduction Band
CE	-	Counter Electrode
CE mechanism	-	Homogenous chemical process preceding heterogeneous electron transfer
CI	-	Carbon Ink
COD	-	Chemical Oxygen Demand
CoPc	-	Cobalt Phthalocyanine
CV	-	Cyclic Voltammetry
DIT	-	Dublin Institute of Technology
E. coli	-	Escherichia coli
E_g	-	Band Gap Energy
eV	-	Electron volts
FA	-	Formic Acid
FeoCN	-	Potassium (II) Hexacyanoferrate
GC	-	Gas Chromatography
GCE	-	Glassy Carbon Electrode

GCMS	-	Gas Chromatography Mass Spectroscopy
HOMO	-	Highest Occupied Molecular Orbital
IBA	-	2-Butanol
IPA	-	2-Propanol
KHP	-	Potassium Hydrogen Phthalate
LSV	-	Linear Sweep Voltammetry
LUMO	-	Lowest Unoccupied Molecular Orbital
MeOH	-	Methanol
NHE	-	Normal Hydrogen Electrode
nm	-	Nanometres
PA	-	Polyaniline
PCB	-	Polychlorinated BiPhenyls
PEG	-	Polyethyleneglycol
PEM	-	Polymer Electrolyte Membrane
PS	-	Polystyrene
PtME	-	Platinum Micro Electrode
PVC	-	Poly(vinyl chloride)
PVP	-	Poly(4-vinylpyridine)
RCSI	-	Royal College of Surgeons in Ireland
RDE	-	Rotating Disc Electrode
RE	-	Reference Electrode
SCE	-	Mercury (I) Chloride Reference Electrode
SWV	-	Square Wave Voltammetry
THF	-	Tetrahydrofuran
UV	-	Ultraviolet

UVA	-	Ultraviolet radiation, 400 – 320 nm
UVB	-	Ultraviolet radiation, 320 – 280 nm
UVC	-	Ultraviolet radiation, 280 – 200 nm
VB	-	Valence Band
WE	-	Working Electrode

TABLE OF CONTENTS

LIST OF FIGURES AND ILLUSTRATIONS

PAGE

LIST OF TABLES

LIST OF SCHEMES

PAGE

Chapter 1

General Introduction

Chapter 1 – General introduction

1.1 Background

There are many sources of organic waste in the world. Some of these are natural while others are man made wastes, often as a result of agricultural and industrial activities. From time to time there is microbiological contamination of waters. A recent example of this in Ireland was the *cryptosporidium* outbreaks in Galway and Ennis [1].

Waste treatment therefore becomes a priority, as water is vital to sustain life. In developed countries, there are traditional methods of treating water in order to make it potable. Filtration can take place using sand, diatomaceous earth filter, membranes and cartridge filters. During sedimentation, aluminium sulphates are used to coagulate solids to form a floc. In reverse osmosis and deionisation, ions are removed from water which is pumped through a stationary phase of the opposite charge and so these ions can form salts within the column. Boiling proved to be an effective method to rid drinking water of the *cryptosporidium* outbreak cited above.

The most common treatments for water contaminated with organic pollutants are adsorption and air stripping. However, as non-destructive technologies, they merely transfer contaminants from water to adsorbents or to the air. The spent adsorbents (activated granular carbon or synthetic resin) or stripping tower off-gas often requires further treatment. Moreover, some toxic organic compounds are not removed by adsorption or air stripping because of their low adsorbabilities or low volatilities.

Disinfection kills pathogenic microorganisms. Chlorination oxidises the pathogens, as chlorine is easily reduced to chloride. Ozone works in the same way although it is more costly. Chlorination can be harmful, as humic acid (naturally present

in water and soil) gets electrophillically attacked to form halogenated organics. However, trihalomethanes formed during chlorination are suspected to be carcinogenic.

A solar photocatalytic process can destroy many toxic organic compounds. Such processes can also destroy nuisance, colour, taste and odour compounds. These systems have been known to remove naturally occurring organic matter that contain the precursors to trihalomethanes. Additionally, the solar process can be used on-site, and avoid the risk of transporting and handling hazardous wastes (e.g., spent carbon). An ideal photocatalyst should be stable, cheap, non-toxic and, of course, highly photoactive.

Novel methods of treating waste water involve UV light, fuel cells or both combined in the case of the fuel cell presented in this work. In microbial fuel cells microbes such as *Escherichia coli* [2], *Shewanella putrefaciens* and *Geobacter metallireducens* [3], *Clostridium butyricum* and *Desulfovibrio desulfuricans* [4] and *Aeromonas hydrophila* are used as catalysts at a platinum loaded carbon anode often to oxidise dairy manure [5], swine wastewater [6] sugary food processing wastewater [7], corn waste [8] and cysteine [9]. Oxygen is normally the electron acceptor, often through the use of air electrodes [10]. Not only does this process clean up the water in what has been termed as an 'underwater incineration', but there is also generation of electricity. This makes such fuel cells very useful devices.

1.2 Fuel cells

A fuel cell operates similarly to a battery, and for both devices electrons flow to the positive terminal. Batteries deliver electricity given off by reactions between the stored chemicals inside the container. For fuel cells, as long as there is a steady, constant

supply of material, electrons can be taken from it and transferred to a different electrode, so the fuel cell may run indefinitely. A diagram of a fuel cell is shown in figure 1.1.

Waste organics in water may actually come in useful as a substrate for fuel cells, and this is the case in the fuel cell presented in this work. This is because organics yield many electrons due to their high energy density, many more per mole than hydrogen, which is the typical compound of choice for most commercial fuel cells.

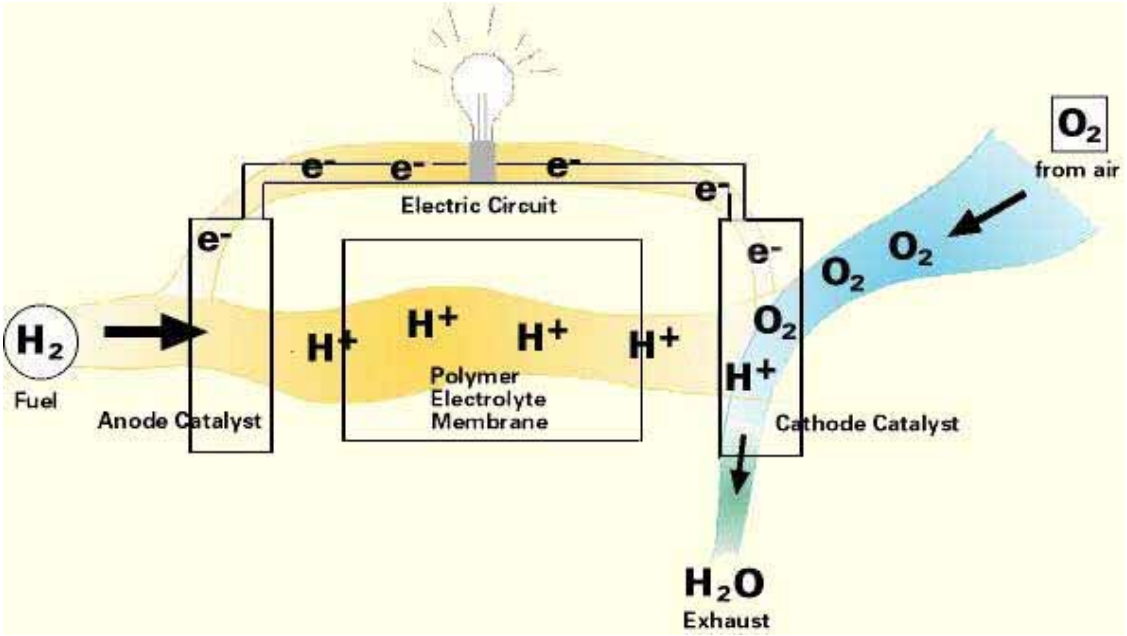

Figure 1.1: A hydrogen fuel cell that creates a current that may power a light bulb in this example [11]

For the hydrogen fuel cell, hydrogen is oxidised, oxygen is reduced and overall gaseous water is created. Such fuel cells normally run at high temperatures and have found commercial viability for buses and a car produced by Ballard. Chrysler lead the way for hydrogen powered cars though Honda, Volkswagen, Mercedes and many others have followed suit. The world's first hydrogen filling station opened in Reykjavik in 2003. There are many problems as well, such as storage of such high pressurised gasses

on board vehicles. There are expenses involved in trying to obtain pure sources of hydrogen, mostly from the reforming of methanol. Vehicles which run on hydrogen are of low power and speed (often a maximum of 80 kph) as it is not a dense fuel supply energetically (it only provides 2 electrons per mole of hydrogen oxidised). There is also only a certain distance that these vehicles can travel (~ 100 kilometres) before the fuel supply runs out.

In this work, organics found commonly in waste water are used to power a low temperature photoelectrochemical cell, and so the problems associated with hydrogen fuel cells are avoided. Most fuel cells rely on O_2 reduction as their cathodic reaction, so two chapters in this work are devoted to this process. After over 150 years of research, fuel cells can be divided into categories named after the electrolyte used in each and are shown in table 1.1 [12].

Table 1.1: Some common commercially viable fuel cell types

Type	Electrolyte	Temperature / °C	Power	Comments
Direct formic acid	Organic nafion	< 40	< 50 W	
Alkaline	Aqueous KOH	< 80	< 100 kW	Medium temp, high pH, KOH a good conductor
Direct methanol	Nafion in methanol	< 120	< 1 MW	
Solid polymer PEM	Nafion in methanol	< 200	< 500 kW	Acidic, 2 Pt electrodes, cathode sensitive to CO poisoning[1]
Phosphoric acid	Aqueous H_3PO_4	< 200	10 MW	Medium temp, Teflon - coated anode, 40 % efficiency
Molten carbonate	Molten alkaline 68 % $LiHCO_3$ 32 % K_2CO_3 in alumina	< 650	100 MW	Electrodes made of Ni salts[2]
Solid oxide	ZrO_2	< 1100	100 MW	Poorly conducting[3]

[1] Carbon monoxide contamination arises from incomplete combustion of the solid polymer. If the concentration of carbon monoxide becomes greater than 0.17 % adsorbed onto the platinum surface, the fuel cell fails to operate.

[2] At the cathode CO_2 can be reduced, and the high temperature can reform methanol into the hydrogen needed at the anode

[3] Cheap and need no catalysts or fuel treatment equipment

1.3 Photoelectrochemical cells

In addition to the main commercially viable fuel cells listed in table 1.1, some cells can harvest sunlight as a mode of operation. A photoelectrochemical cell consists of a semiconductor either dispersed in solution or immobilised on an electrode. The cell also contains an auxiliary and /or reference electrode; neither of which are light sensitive. There are many types of photoelectrochemical cell, some may require a potentiostat to deliver potential and others may not [13].

1.3.1 Photoelectrolytic cells

This is a cell in which a net chemical conversion is caused by absorption of radiant energy e.g. so as to produce hydrogen as a useful fuel, scheme 1.1.

$$2\ H_2O\ (l) \rightarrow 2\ H_2\ (g) + O_2\ (g)$$

Scheme 1.1: Photosynthetic splitting of water

Such cells are also described as being photocatalytic or photosynthetic. A photogenerated hole is used to oxidise one species and the electron is used to reduce another species. Chemical compounds, often toxic and noxious like hydrogen sulphide (scheme 1.2), can be converted irreversibly in the presence of a catalyst.

$$8\ H_2S\ (g) \rightarrow 8\ H\text{-}H\ (g) + S_8\ (s)$$

Scheme 1.2: Conversion of hydrogen sulphide

Radiant energy drives a reaction such as the splitting of water (scheme 1.2), and electrical or thermal energy may be later recovered by allowing the reverse reaction to proceed.

In a photocatalytic cell the photon absorption promotes a reaction with $\Delta G < 0$ so there is no net storage of chemical energy, but the radiant energy speeds up a reaction. When the semiconductor (bound to an electrode) is illuminated, the electrons and holes move to the surface. The electrons will reduce species at the surface and the holes will oxidise species at the surface. If not, however, permanent chemical changes will occur in the medium in which the semiconductor is immersed; such photoinduced chemical changes are termed photocatalytic effects. Typical examples occur within this work, where 2-propanol is decomposed into carbon dioxide and water (scheme 1.3).

$$TiO_2 \mid H_3C\text{-}CHOH\text{-}CH_3,\ O_2 \mid Pt/Ti$$

Scheme 1.3: 2-propanol oxidation accompanied by oxygen reduction

1.3.2 Photogalvanic cell

In this type of cell, the incident light is absorbed by molecular species in solution, and electrical power is generated by charge transfer from excited molecular species to the electrodes in contact with the light absorbing system. Just like photoelectrolytic cells it is concerned with non spontaneous processes. So not only does it require solar energy to work but it also needs an electrical input. When the external circuit of the cell is

connected, the cell supplies a current that regenerates the initial chemical compounds used such as thionine (figure 1.2).

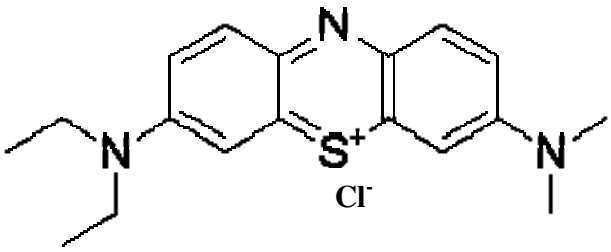

Figure 1.2: Chemical structure of thionine

1.3.3 Photovoltaic cells

In this case, the reaction that occurs at counter electrode is simply the reverse of the photo-assisted process at the semiconductor electrode. Light energy (in the form of photons) is converted into electrical energy (in the form of electric current). It relates to the application of solar cells for energy by converting sunlight directly into electricity. A good example of their use is in solar panels.

1.4 Semiconductors and band gap theory

Photoelectrochemical cells (such as the one presented in this work) consist of light activated semiconductors. Semiconductors share some of the conducting properties of metals, while they also possess some of the insulating character that is typical of organic compounds. There is a separation between the electronic levels – namely the occupied valence band and the unoccupied conduction band. In an attempt to explain some of these activities, valence band theory has been established. This is displayed in figure 1.3.

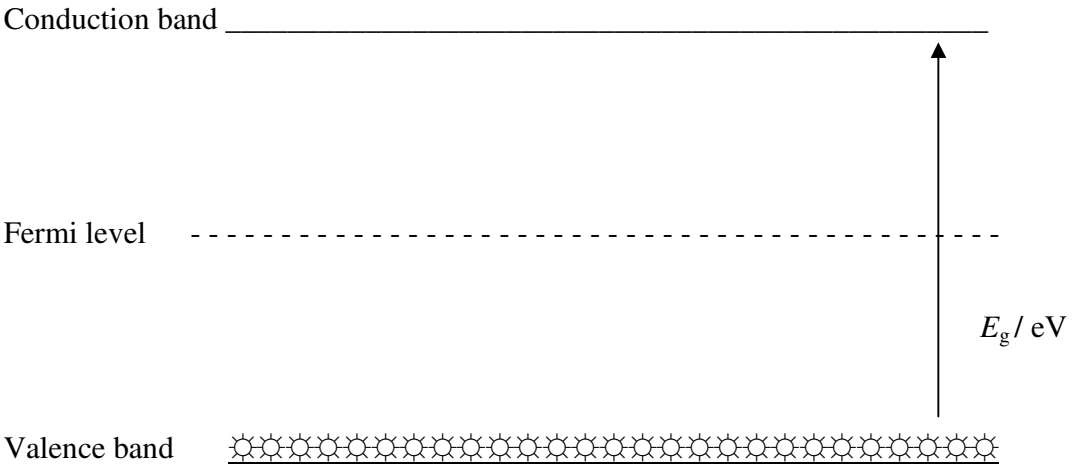

Figure 1.3: Valence band model for an undoped, intrinsic semiconductor (where the number of charge carriers is determined by the properties of the material itself and not the amount of impurities). The valence band is filled with electrons [14].

The Fermi level lies halfway between valence and conduction bands for an intrinsic semiconductor. Like all models, certain things are assumed beforehand. One of the assumptions of the model is that the conductivity of these semiconductors can be due to crystal defects or to thermal or photon excitation. Conduction happens through the promotion of electrons from the valence to conduction bands. Electrons in the valence band must absorb significant energy to achieve that promotion. This promotion leaves a hole in the valence band (caused by the lack of an electron), resulting in a positive charge. Conduction is achieved by movement of the hole in the valence band and also by movement of this new electron in the conduction band.

Table 1.2: Bandgap energy, E_g, and corresponding wavelength λ_{bg} for a selected few semiconductors that are in widespread use [15].

Semiconductor	λ_{bg} / nm	E_g / eV
SnO_2	350	3.5
ZnO	390	3.2
$SrTiO_3$	390	3.2
TiO_2 (anatase crystal form)	390	3.2
TiO_2 (rutile crystal form)	410	3.0
CdS	520	2.4
GaP	540	2.3
Fe_2O_3	590	2.1
CdSe	730	1.7
CdTe	890	1.4
GaAs	890	1.4
InP	950	1.3
Si	1130	1.1

1.5 Photochemistry

The most important concept in photocatalysis is that the flow of electrons and holes must be equal. If they are not either (a) the surface becomes electro statically charged and the process stops, or (b) another electrode must be present to complete the electrical circuit and the process is termed as photoelectrocatalysis [16].

When the incidence of photons of light excites a species in solution or else when they excite an electron on an electrode surface, a photoelectrochemical reaction has taken place. Such reactions are of interest as they harvest solar energy to power various appliances. Upon absorption of energy (thermal or in this case light), conduction can be achieved through movement of holes or electrons.

One such semiconductor that has received a lot of interest in recent times is TiO_2. It is used in printing inks but has also found use as a potent photocatalyst, for the photodegradation of *o*-chloroaniline; particularly when iodate [17] and hydrogen

peroxide [18] and other oxyhalogens like bromate and chlorate [19] are added in as oxidising agents.

The energy bandgap for many semiconductors (table 1.1) falls in the region of 1 – 3 eV and is in the visible daylight region of the electromagnetic spectrum. For a typical semiconductor like TiO_2, its rather large bandgap is listed in this table as 3 eV. It has 3 crystal forms with different spatial configurations of its atoms, and the band gap for the rutile crystal form is 3 eV. It can be calculated what wavelength this corresponds to from equation 1.1.

$$E = h\frac{c}{\lambda} \qquad 1.1$$

Where:

E	=	Energy / J normally but eV in this case
h	=	Planck's constant = 4.14×10^{-15} eV s
c	=	Speed of light = 2.99×10^{8} m s^{-1}
λ	=	Wavelength of light / nm
f	=	Frequency of light / Hz ($\equiv s^{-1}$)

$$3 \text{ eV} = \frac{(4.14 \times 10^{-15} \text{ eV s})\,(2.99 \times 10^{8} \text{ m s}^{-1})}{\lambda}$$

$$\lambda = \frac{(4.14 \times 10^{-15} \text{ eV s})\,(2.99 \times 10^{8} \text{ m s}^{-1})}{3 \text{ eV}}$$

$$\lambda = 412 \text{ nm}$$

$$f = \frac{c}{\lambda} \qquad 1.2$$

$$f = \frac{(2.99 \times 10^{8} \text{ m s}^{-1})}{412 \times 10^{-9} \text{ m}}$$

$$f = 7.26 \times 10^{14} \text{ s}^{-1}$$

This means that visible light with wavelength $\leq$ 412 nm at a frequency of 726 teraphotons per second will be absorbed by TiO_2 and promote an electron from its

valence to its conduction bands. An electron volt is the amount of energy gained by a single unbound electron when it accelerates through an electrostatic potential difference of one volt.

Incidentally, the band gap of the anatase crystal form is 3.2 eV, meaning that it will absorb near ultraviolet light of wavelength 387.5 nm at a frequency of 772 teraphotons per second.

Semiconductors absorb light below a threshold wavelength λ_g, the fundamental absorption edge, which is related to the band gap energy via: [20]

$$\lambda_g \text{ (nm)} = \frac{1240}{E_g \text{ (eV)}} \qquad 1.3$$

Equation 1.3 is a facile way of expressing the relationship between band gap wavelength and energy. At the ground level, solar irradiation starts at about 300 nm, and around 4 % of the total solar spectrum can activate TiO_2. As rutile TiO_2 absorbs only light of < 412 nm, it does not use sunlight very effectively. This is because 95 % of the total energy of the solar spectrum lies at energies below this value [14].

1.6 TiO_2 photocatalysis

Both hydroxyl radicals and valence band holes are powerful and indiscriminate oxidizing species and will attack organic pollutants to yield more oxidised forms of the organic compound [21]. The photocatalyst may be used either in a slurry or immobilized form. Using an immobilised system one can obtain a configuration in which all the catalyst is illuminated and further eliminates the need for post treatment catalyst recovery. A disadvantage with an immobilised system is that mass transfer limitations can reduce reactor efficiency and/or interfere with the measurement of true degradation

kinetics. Post-treatment catalyst recovery would be undesirable at industrial scale as it would add to the capital and operating costs of the treatment process.

1.7 Mechanism of photocatalysis

Titanium dioxide photocatalysis is a useful technique for the breakdown of organic pollutants in water and air. Photocatalysis, as the name suggests, involves light and a catalyst to bring about a chemical reaction. In titanium dioxide photocatalysis for water purification, the pollutants are usually organic compounds.

During a photocatalytic process, light activates the photocatalyst and establishes a redox environment in the water. When a photon of light, of sufficient energy ($E > E_{bg}$), strikes a TiO_2 particle, the energy of the photon is absorbed and used to promote an electron (e^-) from the valence band to the conduction band. This movement of an electron leaves a hole (h^+) in the valence band. These species (h^+ and e^-), produced by the absorption of light, can either recombine or they migrate to the surface of the TiO_2 particle, where they can react with other species at the interface.

Holes react with adsorbed water molecules or hydroxide anions (OH^-) and produce hydroxyl radicals ($OH^\bullet$), which are very strong oxidants capable of oxidising virtually any organic compound [22, 23]. Indeed, the only organic that can't be completely mineralised is cyanuric acid [24, 25]; which is non-toxic.

(a) (b)

Figure 1.4: Hydroxyl radical (a) and superoxide anion (b)

Within a few nanoseconds the electron/hole pair can recombine, emitting the stored energy as fluorescence. When this happens, the electrons return to the ground state of the semiconductor, and the semiconductor has not been put to good use. However if some species is capable of seizing the photogenerated electron (e.g. Ag^+, CeO_2), then recombination is prevented; and this can allow the holes to do their job more effectively.

$$TiO_2 + h\nu \rightarrow TiO_2(h^+ \ldots e^-) \quad 1$$

$$TiO_2(h^+) + OH^- \rightarrow OH^\bullet \quad 2$$

Scheme 1.4: Absorption of light energy by TiO_2 and subsequent combination with anions to form radicals

These charge carriers, amongst other possible routes, can recombine as mentioned previously, or react with electron donors and acceptors adsorbed on the surface or bound within the electrical double layer. In order to maintain charge neutrality there must be species present capable of interacting with both hole and electron.

Therefore it is vital that the organic compound adsorbs onto the TiO_2 surface in the first place if any direct degradation is to happen. This process finally results in the formation of carbon dioxide and water, if the reaction proceeds to completion.

Figure 1.5 shows a schematic representation of TiO_2 photocatalysis. If air is present, oxygen can be reduced, while if it is in aqueous solution the hydroxyl radical can be formed when the holes react with water.

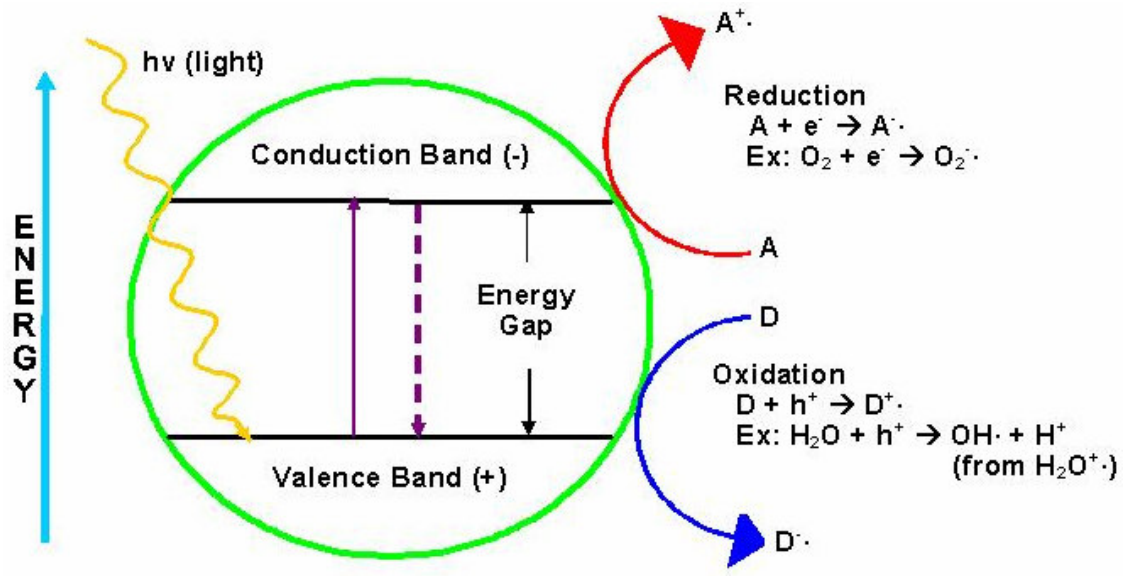

Figure 1.5: Photocatalysis of TiO_2 in aqueous solution and subsequent degradation of organics present [26]

ESR studies have shown the presence of hydroxyl and hydroperoxyl radicals in aqueous solutions of illuminated TiO_2 [27]. In the same work it has been conversely shown that substances which have no hydrogen atoms available for abstraction by hydroxyl radicals are primarily oxidised by valence band holes.

Immobilized TiO_2 particles collectively yield anodic photocurrent similar to that of an n-type semiconductor material [28, 29]. The destruction rate in a photocatalytic process is as a function of light intensity: starting with a linear dependency at low light intensity, having a transition at moderate light, and becoming light independent after light exceeding a certain value [30]. This type of light dependency originates from the compromise of a number of reactions involved in the photocatalytic process, such as the generation and annihilation of the oxidation sites, and the production of $OH^{\bullet}$ radicals and their self recombination.

1.8 Different crystal forms of TiO_2

Studies on its crystal structure have revealed that TiO_2 is a multi faceted ionic compound, and that there are three different arrangements of its titanium and oxygen atoms – brookite (orthorhombic), anatase and rutile (both tetragonal), each with many different properties. The photocatalytic activity of rutile TiO_2 was found to be negligible even when it was loaded with platinum black [31]. Nishimoto *et al* also found that its anatase form produced almost 3 times more acetone from the photoelectrodehydrogenation of 2-propanol than the rutile equivalent; but vast amounts of acetone was produced from the oxidation when anatase was mixed with Pt black and RuO_2. They also found that photoirradiation at wavelengths longer than 400 nm produced negligible amounts of acetone. This suggests that anatase is the best crystal form for photochemical experiments, in agreement with Linsbigler *et al* [32] and Tanaka *et al* [33]. However, many authors believe that for the best photocatalysis to occur a mixture of anatase (70 – 80 %) and rutile (20 – 30 %) is necessary as recombination effects are minimized [34 – 36] and due to better electron - hole separation because of the fact that the particles are in two separate phases [37].

Rutile is the stable phase at high temperatures. In a study of phase transformation behaviour of nanocrystalline aggregates during their growth, Zhang and Banfield [38] found that anatase was thermodynamically stable for sizes smaller than 11 nm, rutile was more stable for particles larger than 35 nm and brookite was the intermediate phase.

The performance of TiO_2 based devices depends largely on the sizes of the building units, with smaller units facilitating charge transfer and leading to huge surface areas. In this work a commercial photocatalyst Degussa P-25 is used, with the average

particle size smaller than 30 nm and the surface area being 50 m^2 g^{-1}. It is 80 % anatase and 20 % rutile [39].

1.9 Doping of TiO_2 and other semiconductors

To use more available solar irradiation and increase visible light efficiency, a great deal of research has been done on modifying TiO_2 and testing other semiconductors [40]. The activity of a photocatalyst can be enhanced by surface modification or substitutional doping. Surface deposition with metals, for example platinum, prolongs the life time of the oxidation site at the exterior catalyst surface and enhances the hydroxyl radical production [41]. Absorption of visible light by TiO_2 has been attempted by doping TiO_2 with transition metals [42]. A semiconductor photocatalyst can also be sensitised by attaching dyes to its surface. Sensitisation allows the available visible portion of the solar spectrum to be used.

1.10 History of TiO_2 use

TiO_2 is highly available in minerals and has even been found in rocks brought back from the moon. It has been produced since the early 1900s and has normally been used in paints and toothpaste as a white pigment. In the middle half of the century it was used in sun barrier cream, by absorbing the UV component from the sun and thus leaving the skin free from harmful damage.

In the early 1970s, Fujishima and Honda discovered that cleavage of water could be achieved (scheme 1.2) [43 - 45]. In this work a two compartment (twin cell) separated by a porous glass frit consisted of a TiO_2 coated anode in one compartment (for water oxidation to oxygen) and a platinum electrode (for O_2 reduction to hydrogen) in the other. They had discovered that when a titanium dioxide electrode in an aqueous solution was

exposed to sunlight, gas bubbles were evolved. It was found that these were in fact oxygen bubbles. Incorporated into an electrochemical cell, it was found that hydrogen gas was evolved at a platinum counter electrode. Water molecules are reduced by electrons to form hydrogen and oxidised by the holes to form oxygen. A similar system is used in chapters 4 and 5 of this work. This was the number one piece of work that turned the sod for photocatalytic fuel cells from which millions of workers worldwide followed (obviously with different variations on it); and it is one of the most widely researched topics to this day.

In the late 70's, it was discovered that TiO_2 photocatalysis was useful in the remediation of harmful organics in wastewater [46 - 48]. Finding a rate for the photodestruction *via* current doubling of cyanide ions dissolved in water at a rate of 6 μM per cm^2 per day in a simple 3 electrode cell, this paper opened the way for thousands of scientists to use TiO_2 photocatalysis for the annihilation of many organics.

Broadly speaking, use of semiconductors can be divided up into energy (photovoltaics and water spitting) and environmental (photocatalysis and sensing) applications.

1.11 TiO_2 immobilised on an electrode

TiO_2 may be immobilized onto a suitable solid support matrix which would eliminate the need for post-treatment removal, but this decreases the surface area available for reaction [26]. The application of a small positive potential to a conducting anode coated with TiO_2 was useful in the degradation of formic acid, with oxygen and also cupric nitrate used as the electron acceptors [49].

Much work has also been done on the use of titanium dioxide based systems for waste water remediation as demonstrated by Palmer *et al* [50] for the removal of humic acid. In a particularly clever system ensuing electrons from oxalate photooxidation at an anode were used to recover copper from cupric solutions in a photoelectrochemical cell. In this way the COD of a sample of waste water was reduced while the heavy metal content of a different waste water sample was reduced simultaneously without the supply of external energy (Byrne *et al*) [51].

1.12 Degradation of dyes using TiO_2 photocatalysis

Dyes are stable, highly coloured organic compounds that present danger from an environmental standpoint when they enter aquatic systems. Industrial processes in the textile and clothing manufacturing industries has seen an increasing concentration of many synthetic dyes in streams. Yizhong *et al* showed that the degradation of many commercial dyes were possible using the photocatalysis of aqueous suspensions of TiO_2 [52].

In recent work many other azo, formazan, anthraquinone and phthalocyanine based dyes were photodegraded with the aid of TiO_2 homogenously and 90 % of their colour was removed within two hours [53]. In similar work with TiO_2 immobilised on a glass slide the same group found a COD removal rate of similar days of 0.5 g h^{-1} m^{-2} [54]. The same group added hydrogen peroxide to their TiO_2 suspension of dyes and found an enhancement of the rate of photodecolourisation [55].

For aqueous suspensions of TiO_2 coupled with a 250 W Hg lamp, the concentration of the non-biodegradable dye intermediate H-acid (figure 1.6) decreased due to the photocatalysis [56].

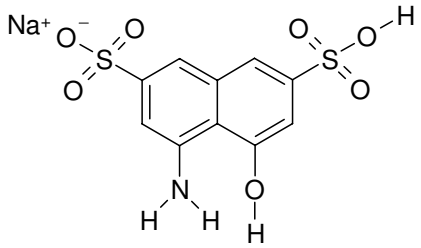

Figure 1.6: Chemical structure of H-acid, a dye intermediate

When immobilised on stainless steel, a mesoporous TiO_2 layer incorporating polyethyleneglycol showed a good performance for the degradation of rhodamine B when irradiated with 20 W light at 365 nm [57]. This group followed up this work with spectral and micro graphical studies of the TiO_2 film [58].

1.13 The use of solar light for the degradation of organics

In areas rich in sunlight, visible light irradiance can reach 3 W m^{-2}, so it makes sense to make use of it for photocatalysis. Such TiO_2 photolysis was used in the degradation of cyanides and formates [39]. Suspensions of titania doped with iron were also irradiated with daylight in order to photodegrade ethidium bromide [59].

An aqueous suspension of benzamide (BA) and 4-hydroxybenzoic acid (4-HBz) were photodegraded by TiO_2 absorbing solar light in the Mediterranean [60]. In the binary mixture they found that it was possible to degrade 4-HBz while the concentration of BA remained constant (as it doesn't adsorb as well onto TiO_2). At a low concentration of TiO_2 (200 ppm), the rates of photodegradation of both compounds were similar and not selective. At a high TiO_2 concentration (2000 ppm), whichever organic is the better competitor for hydroxyl radicals or better to bind to TiO_2 will degrade faster while the concentration of the other organic remains relatively stable.

1.14 Photodegradation of polymers and bacteria

Cho *et al* found that the presence of oxygen was essential for efficient photolytic degradation of PVC, and monitored its breakdown by FT-IR [61]. This was in the solid state using a 200 W Hg lamp with a flux of 1.5 mW cm^{-2}.

While chlorination of swimming pools and normal water is a common method used to kill bacteria, it doesn't remove cysts, spores and some viruses [62]. TiO_2 suspensions have reduced bacterial levels [63] because photocatalysis is non - discriminate between bacterial colonies. The elimination of *E. coli* spores is enhanced by the application of a positive potential bias to an irradiated TiO_2 electrode [64].

Dunlop *et al* found that applying a potential to 150 W Xe illuminated TiO_2 immobilised on electrodes increased the rate of disinfection of *E. coli* relative to when the same electrode was used in open circuit conditions [65].

1.15 Photodegradation of aromatics

Suspensions of TiO_2 have also been used to degrade aromatics such as aniline [66] (incorporating silver) and benzoic acid [67]. The electrochemical benefit of the oxidation of organic compounds which is an indirect combustion has also been realised with oxidation of *p*-nitrophenol [68].

1.16 pH effects

TiO_2 is an amphoteric compound, and pH plays a role in the photodegradation of organic compounds. It is specific for each organic though, and firstly depends on how well the organic adsorbs to the semiconductor surface before pH effects are significant. Piscopo *et al* studied the pH effects of TiO_2 suspensions of benzamide (BA) and 4-

hydroxybenzoic acid (4-HBz) [69]. They found that the pseudo-first-order rate constant for the degradation of 4-HBz decreased with increasing pH (4-HBz is strongly adsorbing). For BA this photodegradation rate constant increased with increasing pH but only very slightly. BA has no change in its molecular form right through from pH 3 – 11. The reason why pH had no great effect on BA degradation is that BA does not adsorb well to TiO_2.

The zero point charge pH of TiO_2 P25 is 6.3. At a pH less than this, TiO_2 will exist as TiOH and $TiOH_2^+$, and so will attract anions to adsorb to it. However many organics will be present in their protonated form at low pH. In alkaline solution, most protic organics will be in their anionic form, and so can often repel the electron rich and negatively charged TiO_2. In this work it was found that acidification of potassium hydrogen phthalate (and formation of phthalic acid, pKa_1 2.98 and pKa_2 5.28 [70]) has a positive impact on its photodegradation.

If a chemical species adsorbs to TiO_2, TiO_2's ability to partake in photoinitiated electron transfer depends on the band energy potential of TiO_2 and the redox potential of the adsorbate [71]. The LUMO of the conduction band equals the redox potential of the photogenerated electrons, while the HOMO of the valence band determines just how oxidising the photogenerated holes will be. In order to find the energy of the photogenerated electrons and holes at a semiconductor - electrolyte interface, the flatband potential (where no space charge layer exists, V_{fb}) is used [72]. Chemical species adsorbed to TiO_2 (be it a suspension or at an electrode) can be reduced by the electrons ensuing from photocatalysis if they have a redox potential more positive than V_{fb} (- 0.4 V V's NHE) of the TiO_2 valence band [73]. Similarly the adsorbed chemical may be

oxidised by the photogenerated holes left behind in the valence band provided that the chemicals have a more negative redox potential than the valence band V_{fb}. However it must be remembered that the band edge potential of a semiconductor can shift up or down with increasing or decreasing pH [74]. This is because V_{fb} follows a Nerstian pH dependence, decreasing by 59 mV per pH unit [75].

Some groups recently added millimolar levels of nitric acid (lessening pH) to their TiO_2 suspension during the photocatalytic degradation of benzene (slowly to carbon monoxide and dioxide) in order to prevent aggregation during mixing the TiO_2 suspension [76].

1.17 New work in this field

With the ever increasing problem of global warming, photocatalytic reduction of CO_2 to methane was studied in CO_2-saturated aqueous solution containing a suspension of TiO_2 photo-catalyst using 350 nm light [77]. Hydrogen production *via* water splitting took place at a TiO_2 coated anode in a twin cell (Pt cathode) [78], following up on Fujishima and Honda's work [43].

1.18 Novelty of this work

Currently there is a group in Japan actively pursuing research into photoelectrochemical cells, similar to this work [79]. TiO_2 was annealed onto a fluoride doped tin oxide glass electrode which was irradiated with a 500 W Xe lamp (0.5 W cm^{-2}) in the aqueous organic. The wide variety of substrates tested ranged from biomass like polysaccharides, proteins, lignin and cellulose to simple alcohols and sugars, ammonia, urea and even synthetic polymers like PEG and poly(acrylamide). The electrons produced

travelled through a resistance towards the positive oxygen sparged air cathode made of Pt/Pt black, where O_2 was reduced. Evolved gases (N_2, H_2, O_2 and CO_2) were analysed by gas chromatography, and compounds underwent mineralisation.

This work is different due to having cheaper, flexible conducting carbon – based anodes; and the reason for their flexibility is that they were applied onto acetate transparencies that are normally used for presentation of data *via* overhead projectors. This work is also different as alternative preparation methods of TiO_2 coated anodes were employed to that of other researchers. While sol gel preparation methods, addition of detergents to trap electrons and calcination [79] are common, the method in this work involved creating an organic suspension of titania and creating a thick film by dip coating. Different organic substrates were used such as formic acid, ascorbic acid, catechol, potassium hydrogen phthalate, 4-chlorophenol, benzaldehyde, phthalic acid and 2-propanol.

A similar cell was reported for the degradation of human urine with promising results [80]. Other work by this group relating to surface confined TiO_2 photocatalysis has included sensitisation of the semi conductor with Pt and $Ru(bpy)^{2+}$ for degradation of EDTA [81] and polysaccharides like agarose [82, 83]. In a suspension, platinised TiO_2 was used as a photocatalyst in combination with a Pt counter electrode for ammonia degradation to nitrogen and hydrogen [84].

1.19 Aim of this work

Characterisation of a photoelectrochemical cell is described in this work. The cell involves a carbon ink anode with light active TiO_2 coated on it. Mineralisation of

organics takes place here, and the electrons produced flow through to the cathode where they reduce O_2.

O_2 reduction is the primary reaction at the cathode. This may also involve carbon ink incorporating cobalt phthalocyanine or in some cases it is an air cathode. During the transformation and depletion of organics that are abundant in nature, some of which are harmful to the environment; a small and useful current is produced. The system provides an environmentally friendly mechanism of degrading organic matter in wastewater, and at the same time it provides energy. The overall reaction scheme when formic acid was the substrate is shown in figure 1.7.

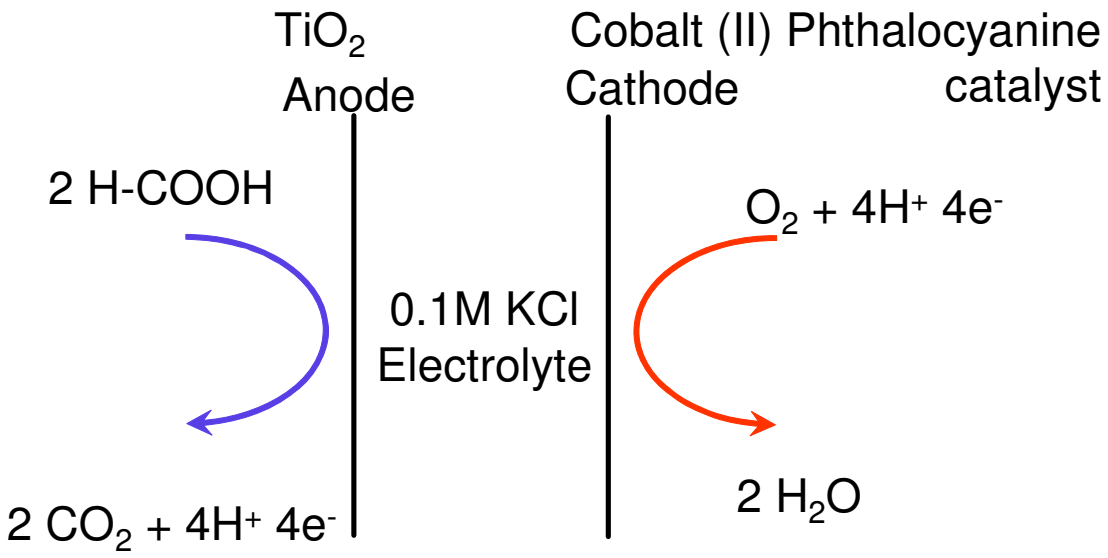

Figure 1.7: Photoelectrochemical cell reaction scheme

The objectives are:

1. To characterise planar ink based electrodes
2. To characterise ink electrodes modified by either a photocatalyst or a mediator

3. To employ these electrodes in photoelectrocatalysis and determine if there is any benefit over photocatalysis
4. To examine these systems using visible and UV light for the degradation of model organic substrates
5. To develop a low cost photoelectrochemical cell to degrade various organic species in waste waters and measure the resulting current
6. To develop a simple model for square wave voltammetry
7. To develop a simple model for cyclic voltammetry

Chapter 2 involves characterisation of novel cathodes. These cathodes involve a redox mediator incorporated into an ink matrix.

1.20 References

[1] http://www.clarecoco.ie/news/Notice_Water_InfoMay08.html accessed on 6/6/08

[2] U. Schröder, J. Nielßen, F. Scholz, *Angewandte Chemie*, **115** (2003) 2986 – 2989

[3] B. Min, S. Cheng, B.E. Logan, *Water Research*, **39**, 9 (2005) 1675 – 1686

[4] I.A. Ieropoulos, J. Greenman, C. Melhuish, J. Hart, *Enzyme and Microbial Technology*, **37** (2005) 238 – 245

[5] S.E. Oh, B.E. Logan, *Water Research*, **39** (2005) 4673 – 4682

[6] B. Min, J.R. Kim, S.E. Oh, J.M. Regan, B.E. Logan, *Water Research*, **39** (2005) 4961 – 4968

[7] I. Ihara, K. Umetsu, K. Kanamura, T. Watanabe, *Bioresource Technology*, **97**, 12 (2006) 1360 – 1364

[8] B.E. Logan, *Membrane Technology*, **2006**, 9 (2006) 10 – 17

[9] B.E. Logan, C. Murano, K. Scott, N.D. Gray, I.M. Head, *Water Research*, **39** (2005) 942 – 952

[10] H. Liu, R. Ramnarayanan, B.E. Logan, *Environmental Science and Technology*, **38** (2004) 2281 – 2285

[11] http://www.fuelcells.org/basics/how.html accessed on 19/4/05

[12] C.G. Hamann, A. Hamnett, W. Vielstich, "Galvanic Cells" in *Electrochemistry*, 2nd edition, C.G. Hamann, A. Hamnett & W. Vielstich ed., Wiley, Weinheim Germany, 1998, 370 – 373

[13] C.M.A. Brett, A.M.O. Brett, "Non-electrochemical probes of electrodes and electrode processes" in *Electrochemistry – principles, methods and applications*, 5th edition, C.M.A. Brett & A.M.O. Brett ed., Oxford Science Publications, New York, 2000, 280

[14] A.J. Bard, L.R. Faulkner, "Spectrometric and Photochemical experiments" in *Electrochemical Methods – Fundamentals and Applications,* 1st edition, A.J. Bard & L.R. Faulkner Ed., John Wiley & Sons, New York, 1980, 631

[15] A.J. Bard, L.R. Faulkner, "Spectrometric and Photochemical experiments" in *Electrochemical Methods – Fundamentals and Applications,* 1st edition, A.J. Bard & L.R. Faulkner Ed., John Wiley & Sons, New York, 1980, 641

[16] H. Gerischer, F. Hein, M. Lübke, E. Mayer, B. Pettinger, H.R. Schöppel, *Ber. Bunsenges. Phys. Chem.,* **77** (1973) 284

[17] W.K. Choy, W. Chu, *Chemical Engineering Journal* **136** (2008) 180 – 187

[18] W. Chu, W.K. Choy, T.Y. So, *Journal of Hazardous Materials* **141** (2007) 86 – 91

[19] W.K. Choy, W. Chu, *Chemosphere* **66** (2007) 2106–2113

[20] M. Grätzel, Heterogeneous Photochemical Electron Transfer, CRC Press: Baton Rouge, FL, (1988)

[21] M. Barbeni, E. Pramauro, E. Pelizzetti, E. Borgarello, M. Grätzel, N. Serpone, *Nouv. J. Chim.*, **8** (1984) 547

[22] R.W. Matthews, *Journal of the Chemical Society Faraday Transactions*, **80**, (1984), 457

[23] C.S. Turchi, D.F. Ollis, *Journal of Catalysis*, **122**, (1990), 178

[24] C. Minero, V. Maurino, E. Pelizzetti, *Res. Chem. Intermed.*, **23** (1997) 291

[25] I. Texier, J. Ouzzani, J. Delaire, C. Gianotti, *Tetrahedron*, **55** (1999) 3401

[26] A. Mills, S. Le Hunte, *Journal of Photochemistry and Photobiology A: Chemistry*, **108**, (1997), 1-35

[27] D. Bahnemann, *Solar Energy* **77** (2004) 445-459

[28] K. Vinodgopal, U. Stafford, K.A. Gray, P.V. Kamat, *Journal of Catalysis*, **167**, **1** (1997) 25-32

[29] C. E. Mortimer, *Chemistry*, **5**, (1983), 450

[30] D.F. Ollis, E. Pelizzetti, N. Serpone, *Ibid*, **25**, (1991), 1523

[31] S.I. Nishimoto, B. Ohtani, T. Kagiya, *Journal of the Chemical Society, Faraday Transactions 1*, **81** (1985) 2467 – 2474

[32] A.L. Linsbigler, G.Q. Yu, J.T. Yates Jr., *Chem. Rev.*, **95** (1995) 735

[33] K. Tanaka, M.F.V. Capule, T. Hisanaga, *Chem. Phys. Lett.*, **187** (1991) 73

[34] R.R. Basca, J. Kiwi, *Applied Catalysis B: Environmental*, **16** (1998) 19

[35] D.S. Muggli, L. Ding, *Applied Catalysis B: Environmental*, **32** (2001) 181

[36] T. Ohno, K. Sarukawa, K. Tokieda, M. Matsumura, *Journal of Catalysis*, **203** (2001) 82

[37] H. Gerischer, A. Heller, *Journal of the Electrochemical Society*, **139** (1992) 113

[38] H. Zhang, J.F. Banfield, *Journal of Physical Chemistry B*, **104** (2000) 3481

[39] J.M. Monteagudo, A. Durán, J. Guerra, F. García-Pena, P. Coca, *Chemosphere*, **71** (2008) 161 – 167

[40] D.M. Blake, *Journal of Catalysis*, **157**, **1** (1995), 87-96

[41] B. Kraeutler, A.J. Bard, *Journal of the American Chemical Society*, **100**, (1978), 5985

[42] E. Borgarello, J. Kiwi, M. Grätzel, E. Pelizzetti, M. Visca, *Ibid*, **104**, (1982), 2996

[43] A. Fujishima, K. Honda, *Nature*, **238** (1972) 37 - 38

[44] A. Fujishima, T.N. Rao, D.A. Tryk, *Journal of Photochemistry and Photobiology C: Photochemistry Reviews,* **1**, (2000), 1 – 21

[45] A. Fujishima, X. Zhang, D.A. Tryk, *Surface Science Reports*, **63** (2008) 515 – 582

[46] S.N. Frank, A.J. Bard, *Journal of the American Chemical Society*, **99** (1977) 4667 – 4675

[47] S.N. Frank, A.J. Bard, *Journal of the American Chemical Society*, **99** (1977) 303 - 304

[48] S.N. Frank, A.J. Bard, *Journal of Physical Chemistry*, **81** No. 15 (1977) 1484 - 1488

[49] J.A. Byrne, A. Davidson, P.S.M. Dunlop, B.R. Eggins, *Journal of Photochemistry and Photobiology A: Chemistry,* **148** (2002) 365-374

[50] F. Palmer, B.R. Eggins, H. Coleman, *Journal of Photochemistry and Photobiology A: Chemistry,* **148** (2002) 137-143.

[51] J.A. Byrne, B.R. Eggins, W. Byers, N.M.D. Brown, *Applied Catalysis B, Environmental*, **20** (1999) L85-L89.

[52] Wang Yizhong, *Water Research*, **34**, 3 (2000) 990-994

[53] F. Harrelkas, A. Paulo, M.M. Alves, L. El Khadir, O. Zahraa, M.N. Pons, F.P. van der Zee, *Chemosphere*, **72** (2008) 1816 – 1822

[54] A. Alinsafi, F. Evenou, E.M. Abdulkarim, M.N. Pons, O. Zahraa, A. Benhammou, A. Yaacoubi, A. Nejmeddine, *Dyes and Pigments*, **74** (2007) 439 – 445

[55] C. Hachem, F. Bocquillon, O. Zahraa, M. Bouchy, *Dyes and Pigments*, **49** (2001) 117 – 125

[56] M. Noorjahan, M. Pratap Reddy, V. Durga Kumari, B. Lavecrine, P. Boule, M. Subrahmanyam, *Journal of Photochemistry and Photobiology A: Chemistry*, **156** 1-3 (2003) 179 – 187

[57] L. Zhang, Y. Zhu, Y. He, W. Li, H. Sun, *Applied Catalysis B Environmental*, **40** (2003), 287- 292

[58] J. Shang, W. Li, Y. Zhu, *Journal of Molecular Catalysis A: Chemical*, **202** (2003) 187 – 195

[59] C. Adán, A. Bahamonde, A. Martínez-Arias, M. Fernández-García, L.A. Pérez-Estrada, S. Malato, *Catálisis Today*, **129** (2007) 79 – 85

[60] D. Robert, A. Piscopo, J.V. Weber, *Solar Energy*, **77** (2004) 553 – 558

[61] S. Cho, W. Choi, *Journal of Photochemistry and Photobiology A: Chemistry*, **143** (2001) 221 – 228

[62] C.H. King, E.B. Shotts, R.E. Wooley, K.G. Porter, *Applied Environmental Microbiology*, **545** (1988) 3023

[63] E.F. Duffy, F. Al Touati, S.C. Kehoe, O.A. McLoughlin, L.W.Gill, W. Gernjak, I. Oller, M.I. Maldonado, S. Malato, J. Cassidy, R.H. Reed, K.G. McGuigan, *Solar Energy*, **77** (2004) 649-655.

[64] I.M. Butterfield, P.A. Christensen, T.P. Curtis, J. Gunlazuardi, *Water Research*, **31** (1997) 675

[65] P.S.M. Dunlop, J.A. Byrne, N. Manga, B.R. Eggins, *Journal of Photochemistry and Photobiology A: Chemistry*, **148** (2002) 355 – 363

[66] A. Kumar, N. Mathur, *Applied Catalysis A: General*, **275** (2004) 189 – 197

[67] A.H.C. Chan, J.F. Porter, J.P. Barford, C.K. Chan, *Journal of Materials Research*, **17**, 7 (2002) 1758 – 1765

[68] J.A. Herrera-Melian, J.M. Dona-Rodriguez, E. Tello-Rendon, A. Soler Vila, M. Brunet Quetglas, A. Alvera Azcarate, L. Pascuel Pariente, *Journal of Chemistry Education,* **78** (2001) 775-777.

[69] A. Piscopo, D. Robert, J.V. Weber, *Applied Catalysis B: Environmental*, **35** (2001) 117 – 124

[70] A. Lebrn-Paler, J.E. Pemberton, B.A. Becker, W.H. Otto, C.K. Larive, R.M. Maier, *Analytical Chemistry*, **78** No. 22 (2006), 7649-7658

[71] O. Carp, C.L. Huisman, A. Reller, *Progress in Solid State Chemistry*, **32** (2004) 33 - 177

[72] N. Serpone, *Journal of Photochemistry and Photobiology A: Chemistry*, **104** (1997) 1

[73] M. Grätzel, *Nature,* **414** (2001) 338 – 344

[74] H. Gerischer, *Journal of the Electrochemical Society*, **113** (1966) 1174 – 1182

[75] M.D. Ward, J.M. White, A.J. Bard, *Journal of the American Chemical Society*, **105** (1983) 27

[76] N. Doucet, O. Zahraa, M. Bouchy, *Catalysis Today*, **122** (2007) 168 – 177

[77] G.R. Dey, A.D. Belapurkar, K. Kishore, *Journal of Photochemistry and Photobiology A: Chemistry* **163** (2004) 503–508

[78] R. Dholam, N. Patel, M. Adami, A. Miotello, *International Journal of Hydrogen Energy*, **33** (2008) 6896 – 6903

[79] M. Kaneko, J. Nemoto, H. Ueno, N. Gokan, K. Ohnuki, M. Horikawa, R. Saito, T. Shibata, *Electrochemistry Communications*, **8** (2006) 336 – 340

[80] M. Kaneko, H. Ueno, K. Ohnuki, M. Horikawa, R. Saito, J. Nemoto, *Biosensors and Bioelectronics*, 23 (2007) 140 – 143

[81] K. Hirano, E. Suzuki, A. Ishikawa, T. Moroi, H. Shiroishi, M. Kaneko, *Journal of Photochemistry and Photobiology A: Chemistry*, **136** (2000) 157 – 161

[82] M. Kaneko, T. Hoshi, Y. Kaburagi, H. Ueno, *Journal of Electroanalytical Chemistry*, **572** (2004) 21 – 27

[83] J. Nemoto, M. Sakata, T. Hoshi, H. Ueno, M. Kaneko, *Journal of Electroanalytical Chemistry*, **599** (2007) 23 – 30

[84] J. Nemoto, N. Gokan, H. Ueno, M. Kaneko, *Journal of Photochemistry and Photobiology A: Chemistry*, **185** (2007) 295 – 300

Chapter 2

Characterisation of non-precious metal catalytic electrodes for O_2 reduction

Chapter 2 - Characterisation of non-precious metal catalytic electrodes for O_2 reduction

2.1 Introduction

2.1.1 O_2 reduction and its use in fuel cells

Many fuel cells invariably use O_2 reduction as the cathodic reaction. It is an essential reaction in most fuel cells, and in the novel photochemical fuel cell it is vital regardless of the organic component digested at the anode. Among the energy feedstocks used for such fuel cells are hydrogen, sodium borohydride, formic acid, methanol & formaldehyde. Efforts are required to speed up O_2 reduction so that the fuel cell current is not limited by the cathodic half of the cell. Precious metals (such as Pt) are excellent catalysts for O_2 reduction but are impractical commercially mainly due to their cost.

Therefore since some cobalt macrocyclic complexes based on biological systems [1 - 3, 7 - 9, 16] have shown some promise for catalysing this reaction, the aim here is to characterise the effect of the following towards O_2 reduction:

1. Cobalt complex/organic polymer layers on standard glassy carbon electrodes
2. Mixing the complex with commercial conducting ink & coating the mixture onto transparent acetate sheets

Such cobalt complexes are inexpensive, easily deposited and have a large surface area.

2.1.2 Effect of cobalt phthalocyanine (CoPc) structure on oxygen reduction

While CoPc has a square planar structure, co-ordination of any axial ligands to the cobalt above or below the plane has a major influence on the redox properties of the

metal – macrocycle complex [1, 2]. This is significant as binding sites for oxygen are in the axial direction. The macrocyclic skeleton only contributes a secondary influence to the catalysis compared to the effects of changing the central metal atom [3]. Reduction of cobalt complexed to tetraazamacrocycles increases the distances of only the axially bound ligands [4].

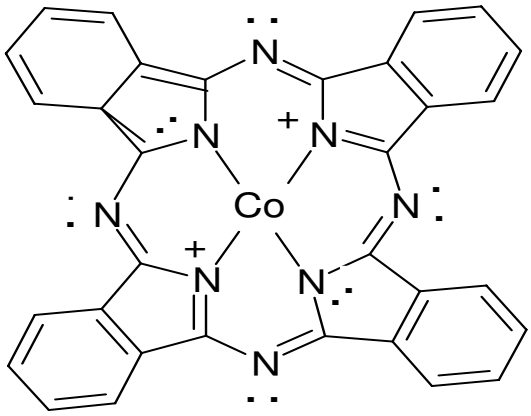

Figure 2.1.1: Structure of cobalt (II) phthalocyanine

2.1.3 Mechanism of oxygen reduction

At a low negative potential, hydrogen peroxide is the main product of oxygen reduction and only at more negative potentials is water formed [5]. Indeed Coutanceau *et al* proved that this 4 electron water forming oxygen reduction reaction happened at potentials less than 0.4 V (NHE) [6]. This group reported current densities for the CoPc catalysed oxygen reduction in a polypyrrole matrix in the order of 2 - 6 mA cm^{-2}.

While many authors agree that the catalytic activities of cobalt macrocycles depends on the Co (III) / Co (II) couple [7 - 9]; the Co (II) / Co (0) redox couple was reported to promote the redox catalysis for the oxidation of hydrazine [10 - 15]. It is thought that the latter redox couple is involved in the catalytic oxygen reduction reaction.

Van Den Brink *et al* found that when used in alkaline fuel cells cobalt (II) phthalocyanine (CoPc) catalyses only the reduction of oxygen to hydrogen peroxide, which not only poses safety hazards but also means that only half of the available power can be created [16]. Upon reduction to hydrogen peroxide, the diffusion-limited current corresponds to the transfer of 2 electrons [17]:

$$O=O + 2\,H^{+} + 2\,e^{-} \rightarrow H\text{-}O\text{-}O\text{-}H \qquad 2.1$$

Only at high negative overpotentials does the reduction of oxygen to water occur in a second step, while this readily happens in one step at iron (II) phthalocyanine (FePc) coated electrodes. The main differences between CoPc and FePc are the potentials at which they form their di and trications. In CoPc, the Co (II) / Co (III) redox couple is well away from where mediation of the catalyst happens, but in FePc this transition occurs where oxygen reduction starts [18 - 20]. Modified electrodes containing FePc were found to be more active in the catalysis of oxygen reduction than CoPc coatings but less adherent to electrode surfaces [21].

Van Den Brink *et al* proposed the following mechanism for the catalysis of oxygen reduction by CoPc starting with initial electron transfer [16]:

$$CoPc^{0} + e^{-} \leftrightarrow CoPc^{-} \qquad 2.2$$

Slow adsorption of oxygen onto to the film then happens as follows:

$$CoPc^{-} + O=O \leftrightarrow CoPc\text{-}O_2^{-} \qquad 2.3$$

In the final step the already partially reduced oxygen is further reduced to hydrogen peroxide while the electrocatalyst is recycled.

$$CoPc\text{-}O_2^{-} + H_2O + e\text{-} \rightarrow CoPc + H\text{-}O\text{-}O^{-} + {}^{-}O\text{-}H \qquad 2.4$$

The partially dissociated hydrogen peroxide created then reacts with reduced CoPc. For the reduction of hydrogen peroxide to $^{-}$O-H, the following mechanism was proposed:

$$CoPc^{-} + H\text{-}O\text{-}O^{-} + H_2O \leftrightarrow CoPc\text{-}O\text{-}H + 2\ {}^{-}O\text{-}H \quad 2.5$$

Adsorption of H-O-O^{-} to the reduced cobalt was shown to be fast. Following this is bond breaking, causing a hydroxyl radical to become adsorbed and this is quickly reduced to hydroxide. This is likely to happen as the entire reduction must happen on one electrocatalytic site (as the sites are 1.2 nm apart [22]), and hydrogen peroxide is too small to have a 2 site interaction.

$$CoPc\text{-}O\text{-}H + e^{-} \leftrightarrow CoPc\text{-}O\text{-}H^{-} \quad 2.6$$

$$CoPc\text{-}O\text{-}H^{-} \leftrightarrow CoPc + O\text{-}H^{-} \quad 2.7$$

$$CoPc^{0} + e^{-} \leftrightarrow CoPc^{-} \quad 2.8$$

The interaction of oxygen with the Co (II) centre is necessary but not sufficient for the electroreduction of oxygen to occur, as Co (III) is reduced to Co (II) at a more positive potential than where oxygen is reduced [23].

The products formed when oxygen is reduced depends largely on the pH of the aqueous solution. Equation 2.9 (a) shows the reduction of oxygen at low pH at 0.68 V while equation 2.9 (b) shows the same reaction at 1.23 V (both vs NHE) [24].

$$O{=}O + 2\ H^{+} + 2\ e^{-} \rightarrow H_2O_2 \qquad E^{\circ} = 0.68\ V \quad 2.9\ (a)$$

$$O{=}O + 4\ H^{+} + 4\ e^{-} \rightarrow 2\ H_2O \qquad E^{\circ} = 1.23\ V \quad 2.9\ (b)$$

The same reaction at high pH at 0.87 V (vs NHE) is shown in equation 2.10.

$$O{=}O + 2\ H_2O + 4\ e^{-} \rightarrow 4\ {}^{-}O\text{-}H \quad 2.10$$

Cycling the voltage negatively starting from 0 V, CoPc is the first compound to be reduced which happens easily at carbon ink (CI) loaded with CoPc:

$$CoPc^0 + e^- \leftrightarrow CoPc^- \qquad 2.2$$

Continuing the negative cycle, low valent cobalt can then combine with dissolved oxygen in solution. The transition metal mediates reduction of the gas and in doing so it is oxidised back to cobalt (II):

$$CoPc^- + O{=}O + 2\,H^+ \rightarrow H_2O_2 + CoPc \qquad 2.11$$

The re-cycled cobalt (II) gets reduced as shown in equation 2.11. This can complete the oxygen reduction process (conversion to water) by interacting with the peroxides created in equation 2.11.

$$CoPc^- + H_2O_2 + 2\,H^+ + 2\,e^- \rightarrow 2\,H_2O + CoPc^0 \qquad 2.12$$

The presence of reduced CoPc has been detected spectrophotometrically [25].

2.1.4 Voltammetry of oxygen reduction

If there are a large number of catalytically active sites on the electrode surface, two peaks for oxygen reduction can be seen (firstly O=O to H-O-O-H and then from H-O-O-H to H_2O) [26]. In cyclic voltammetric studies of CoPc, the reversible couples of Co (III) / Co (II) and of Co (II) / Co (0) have been observed [27].

2.1.5 Cyclic voltammetry

Cyclic voltammetry (CV) is a very popular technique for initial electrochemical studies of systems. It has proven very useful in obtaining kinetic and diffusion parameters along with other information about electrode reactions. It is an extension of linear sweep

voltammetry (LSV) except the voltage is cycled from one preset potential to another and back again cycled as many times as is desired. For a simple one electron transfers where only the analyte O is present in solution (equation 2.13), the potential will be swept negatively to create R (reduced species) electrochemically.

$$O + ne^- \rightarrow R \qquad 2.13$$

In order to form R, voltage is swept negatively in order for the reduction to take place. The standard potential at which this reaction happens at is denoted by E°. This describes the potential of the electrochemical cell when the ratio of the concentration of oxidised species equals that of reduced ones. For a reversible reaction, this potential can be expressed by the Nernst equation (2.14).

$$E = E^\circ + \frac{(RT)}{(nF)} \ln \frac{[O]}{[R]} \qquad 2.14$$

Where:

E	=	Potential / V
E°	=	Standard potential / V
R	=	Universal gas constant 8.314 J mol^{-1} K^{-1}
T	=	Temperature / K
n	=	number of electrons transferred
F	=	Faraday's constant = 96485 J V^{-1} mol^{-1}

Transport of electroactive species is predominantly by diffusion, and this along with the heterogenous kinetics of the reaction determines the current. This current produced is directly proportional to the concentration of the analyte present in solution, so CV is an important analytical method used by industry for qualitative analysis.

When a potentiostat applies a positive bias to the WE where the reaction of interest occurs, it increases the oxidising power of the WE and so it is increases the chances that electroactive species present in solution will be oxidised. The contrary is

true for applying a negative potential, as that reduces an electroactive compound. Upon application of a ramp voltage, the current increases at the potential where the electrode reaction begins (also known as the redox potential). Consumption and subsequent depletion of the electroactive species means that the current decays linearly with $t^{-1/2}$ where t is time in seconds.

Figure 2.1.2 shows how the potential in CV is applied with time. It is cycled from one potential to the next. The current is measured at each point, it is monitored as a function of the applied potential, and an i vs E curve is produced. During the quiet time (typically 2 seconds in this work), the WE gets accustomed to its redox environment before any bias is applied to it. Here, the WE is maintained at the base potential which ideally is a potential where no current flows.

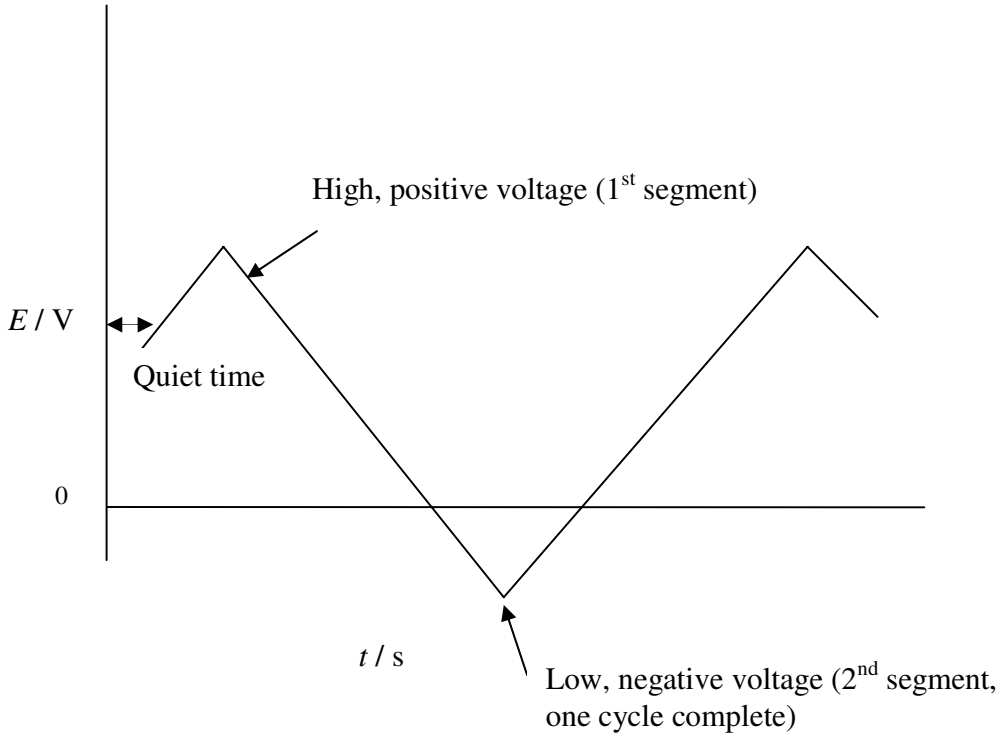

Figure 2.1.2: Waveform applied in cyclic voltammetry

As soon as the potential is applied, it is necessary for the concentrations of O and R to change in order for the Nernst equation (2.15) to be obeyed. The concentration of O at the WE decreases until it reaches zero at which point the current reaches its maximum value.

2.1.6 Working Electrodes (WE)

For the three electrode configuration that is used in this work, the redox process takes place at the WE. The potential applied to the WE determines the availability of the electrons inside the WE. Its surface defines the interface where the electrochemical reaction being studied is taking place. Materials used for the construction of WE normally include inert, conducting and catalytic elements such as Pt, Au and C. Glassy carbon is highly conducting, impermeable to gas and resistant to chemical attack.

As it is the most important electrode to examine the reaction under study, the WE requires some pre-treatment to remove any surface contaminants. The WE is polished with inert compounds with a very fine particle size. As the reactions studied in this work are in aqueous media, sub micron sized aluminium oxide (Al_2O_3) serves as an excellent compound to polish electrodes with.

2.1.7 Reference Electrodes (RE)

For controlled potential experiments in the past, the counter electrode was also the RE in what was a two electrode cell. So while doing its job as acting as a reference potential relative to that of the working electrode, it also passed current through it. This had the effect of causing a change of the redox potential of the active species, and more

so when currents were large. The potential of the RE should not change when small currents pass through it.

The potential of a given RE can be related to by groups worldwide when performing laboratory research in a similar field. As its voltage is fixed, the potential applied is through the WE.

Most REs are at a fixed potential relative to where the reduction of hydrogen takes place at platinum and this is commonly known as the normal hydrogen electrode (NHE) and set to 0 V. All other REs are relative to this. REs used in this work include mercurous chloride in aqueous saturated potassium chloride (also known as saturated calomel, SCE, this is used in this chapter) and mercurous sulphate in aqueous saturated sodium sulphate. For the latter RE, a non – potassium based filling solution is required. Sodium perchlorate is often used in aqueous solutions to maintain a high ionic strength, but if the mercurous sulphate RE is used in aqueous KCl or any potassium – based electrolyte then potassium perchlorate (solubility product 1.05×10^{-2} mol^2 L^{-2}) may precipitate in the junction and block it (equation 2.15).

$$NaClO_4\,(aq) + KCl\,(s) \rightarrow KClO_4\,(s) + NaCl\,(aq) \qquad 2.15$$

Table 2.1.1 shows how the potentials of the different reference electrodes are related to each other [28].

Table 2.1.1: How the potentials of the various REs used in this work relate to the internationally accepted NHE (temperature = 298 K)

RE	*E* vs NHE / V	*E* vs SCE / V
Hg | Aqueous saturated K_2SO_4 | Hg_2SO_4	0.64	0.40
Hg | Aqueous saturated KCl | Hg_2Cl_2	0.24	0
NHE	0	-0.24

2.1.8 Auxiliary / Counter Electrodes (CE)

These are normally made of Pt foil and this is the case in this work where a Pt crescent is the CE. For electrochemical experiments, it is necessary that the area of the CE is much larger than that of the WE. That way, any ensuing current is limited at the WE.

2.1.9 Supporting Electrolyte

In order to minimise migration of electroactive ions caused by the electric field, a high concentration of inert supporting electrolyte is necessary. It is necessary to have the concentration of the supporting electrolyte at least 100 times more concentrated than the active species. Throughout all of this work, the concentration of supporting electrolyte was 0.1 M, while the concentration of electroactive species was much less (typically sub millimolar levels).

Solvents used must be chemically inert and dissolve the supporting electrolyte as well as the compound under study. They must also not provide much inherent resistance, not produce toxic vapours and remain liquid at the working room temperature. Therefore water is an excellent solvent in electrochemistry and it is used throughout this work.

2.1.10 Electrode Preparation

The method in which the electrode is prepared has an influence on the electrocatalysis of O_2 reduction. Catalysts may be attached to the electrode by adsorption [29], vacuum deposition [26], impregnation of porous carbon [30], incorporation into a conducting polymer and solvent evaporation.

The number of active sites for O_2 reduction can differ widely from the anticipated number depending on which technique allows the largest amount of catalyst present on the surface. Thick CoPc layers were prepared by vacuum deposition or incorporated into polypyrrole (PP); with the latter being far more active [31]. This is due to the greater conductivity of PP and O_2 diffusion speed through the CoPc/PP than its vacuum deposited counterpart; allowing all attached molecules to take part in the electrocatalysis. [32].

An effective electrode modification has been carried out by pyrolysis of carbon and metal phthalocyanines allowing the formation of a bond between the metal and the carbon support increasing conductivity [33, 34].

2.2 Experimental

2.2.1 Materials

- De-ionised water (l)
- Potassium chloride (s, KCl, Merck, 99.5+ %)
- Cobalt (II) phthalocyanine (s, CoPc, Eastman, ≥97 %)
- Polystyrene (s, PS, Aldrich, average M_w ~ 45,000, 99 %)
- Poly(vinyl chloride) (s, PVC, Aldrich, average M_w ~ 95,000, 98+ %)
- Poly(4-vinylpyridine) (s, PVP, Fluka, average M_w ~ 70,000)
- Tetrahydrofuran (l, THF, Aldrich, 99+ %)
- Electrodag 423 SS graphite-based P.T.F Ink (s, CI, Acheson Colloids, 1600 Washington Avenue Port Huron , Michigan 48060 USA)
- Oxygen free nitrogen (g, N_2, BOC Gasses, >99.999 %)
- Aluminium oxide 41 μm 600 grit (s, Varian) and 0.3 μm (s, CH Instruments)

- Type J colour inkjet transparencies removable stripe (Xerox)
- Nail varnish
- Felt
- P1000 Pipetman microsyringe (Gilson)

2.2.2 Equipment

- DMV-5800L ultrasonic cleaner (Delta)
- Platinum crescent sheet counter electrode (Pt AE, approx area = 12 cm^2)
- CHI104 glassy carbon working electrode (GCE, CH Instruments, approx area = 0.071 cm^2)
- Ref 401 mercury (I) chloride in saturated potassium chloride reference electrode, potential at 298 K 0.241 V (NHE) [28] (SCE, Radiometer Analytical)
- CHI620A electrochemical analyzer (CH Instruments, 3700 Tennison Hill Drive Austin, TX 78738 USA)

2.2.3 Methodology

2.2.3.1 Preparation of CoPc Catalysts

All catalysts were made up in a 10 mM CoPc & 1 mM polymer (with respect to the monomer) mixture, and were dissolved and made up in 10 ml volumetric flasks with THF to give dark, jade-coloured solutions. The polymers used were PS, PVC and PVP. The purpose of the polymers was to act as supports and to stabilise the catalyst on the electrode surface.

3 μL of each solution was coated onto the clamped GCE facing upwards using the microsyringe. The small volume of the volatile solution quickly evaporated leaving behind a thin CoPc / polymer layer on the GCE surface.

2.2.3.2 Polymer modifications

It was found that PVP layers were insoluble in salt water. Should the layer be soluble, then crosslinking with 1,6-dibromohexane is a possibility. Figure 2.2.1 shows the reaction that takes place in order to keep PVP from diffusing away from the electrode.

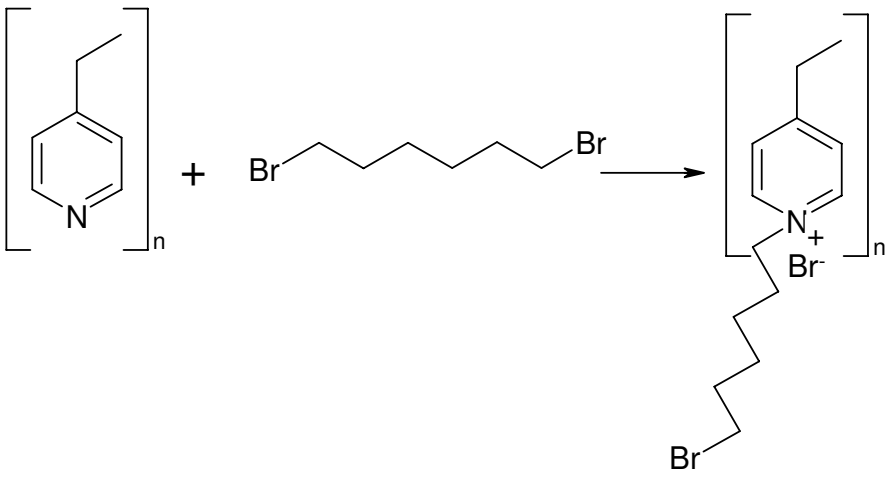

Figure 2.2.1: N alkylation of PVP to form a bromide salt

Insertion of the water soluble tetra sulphonated metal phthalocyanine into the matrix of a conducting polymer can increase the stability of the macrocyclic catalyst [35 – 37]. Skotheim *et al* showed that 35% of cobalt (II) tetrasulphonated phthalocyanine (CoTsPc) was eliminated from the polypyrrole matrix on repeated cycling (after 100 cycles) [38]. However electron-withdrawing substituents (such as the sulphonate group) on the phthalocyanine ring make the reduction of cobalt easier [17].

2.2.3.3 Carbon ink electrode preparation

Reduction of oxygen was done by cyclic voltammetry using a 3 electrode system consisting of conducting carbon (CI) on acetate sheets as working electrode, Pt foil auxiliary electrode and a SCE reference electrode. Aqueous 0.1 M KCl was used as electrolyte in all examples. All were cycled negatively from 0 → – 0.7 V versus SCE. 1 % w/w, 3 % w/w and 5 % w/w solid / gel mixtures of CoPc were mixed into the CI and spread across acetate sheets using a 75 μm cube applicator. The sheets were left to dry overnight in a fume hood at room temperature, where the solvent in which the CI was made in (2-butoxyethylacetate) evaporated.

The next day 5 cm × 1cm strips were cut out of the sheets with a scissors to make the electrodes. Within these strips, 2.5 mm × 2.5 mm sections were pencil-drawn out at the bottom of each electrode (to serve as the working area of 0.063 cm^2, a similar size area of the GCEs). 0.5 cm × 1 cm areas were pencil - drawn out at the top of each electrode to make room for the crocodile clip to attach to it, and this part of the electrode was kept above the solution. The rest of it was masked off with a thick coating of nail varnish to insulate the remaining area of each electrode.

2.2.3.4 Reduction of Oxygen

The same experiment as in section 2.2.3.2 was carried out but using a working GCE as part of the otherwise the same 3-electrode cell. The GCE was polished using 41 μm grit alumina, rinsed with water and then sonicated (to remove excess alumina) for 2 minutes prior to use.

Samples were run using the bare GCE and with 3 μL coatings of each of the catalysts in both ambient and de-aerated (N_2) conditions.

2.2.3.5 Removal of O_2 from supporting electrolyte

The reactions featured in equations 2.1, 2.9, 2.10 and many others can contribute to current measurement. From a chemical point of view, O_2, H_2O_2 and any ensuing radicals can react with the electroactive species under study. Oxygen can oxidise the electrode surface although only to a very small extent.

In this chapter it is necessary to remove O_2 from solution. A lack of O_2 is also desired in order to examine the CoPc redox couple without any interference from the atmospheric gas. The concentration of O_2 was lessened by saturating the solution with oxygen free nitrogen gas. This drives out the majority of any O_2 in solution.

De-aerated solutions were sparged with N_2 for 20 minutes and then the tip of the pipette was placed over the solution on a very low flow rate to maintain a N_2 blanket over the solution.

2.3 Results & Discussion

2.3.1 Characterisation of ink electrodes – bare and incorporating CoPc

Figure 2.3.1 shows the effect of different loadings of the catalyst in the ink on the voltammetric reduction of oxygen in neutral solution. As expected, the heavier the loading of CoPc in the carbon matrix, the greater the current. It can be seen that cobalt catalysts enhance the rate of oxygen reduction over the bare carbon ink. As can be seen, the oxygen reduction wave for the electrode loaded with 1 % CoPc begins at around – 0.4 V while this same process happens at around – 0.25 V for the 5 % loading. This coating produces nearly 3 times the oxygen reduction current than the bare or 1 % CoPc coated electrode does.

While the bare carbon and 1 % CoPc coated electrodes produce similar currents due to oxygen reduction, it can be seen that the catalysis for the electrode containing the catalyst happens earlier and there is a greater area under its peak. There is a better current for this than the bare electrode on the reductive cycle because cobalt is enhancing oxygen reduction.

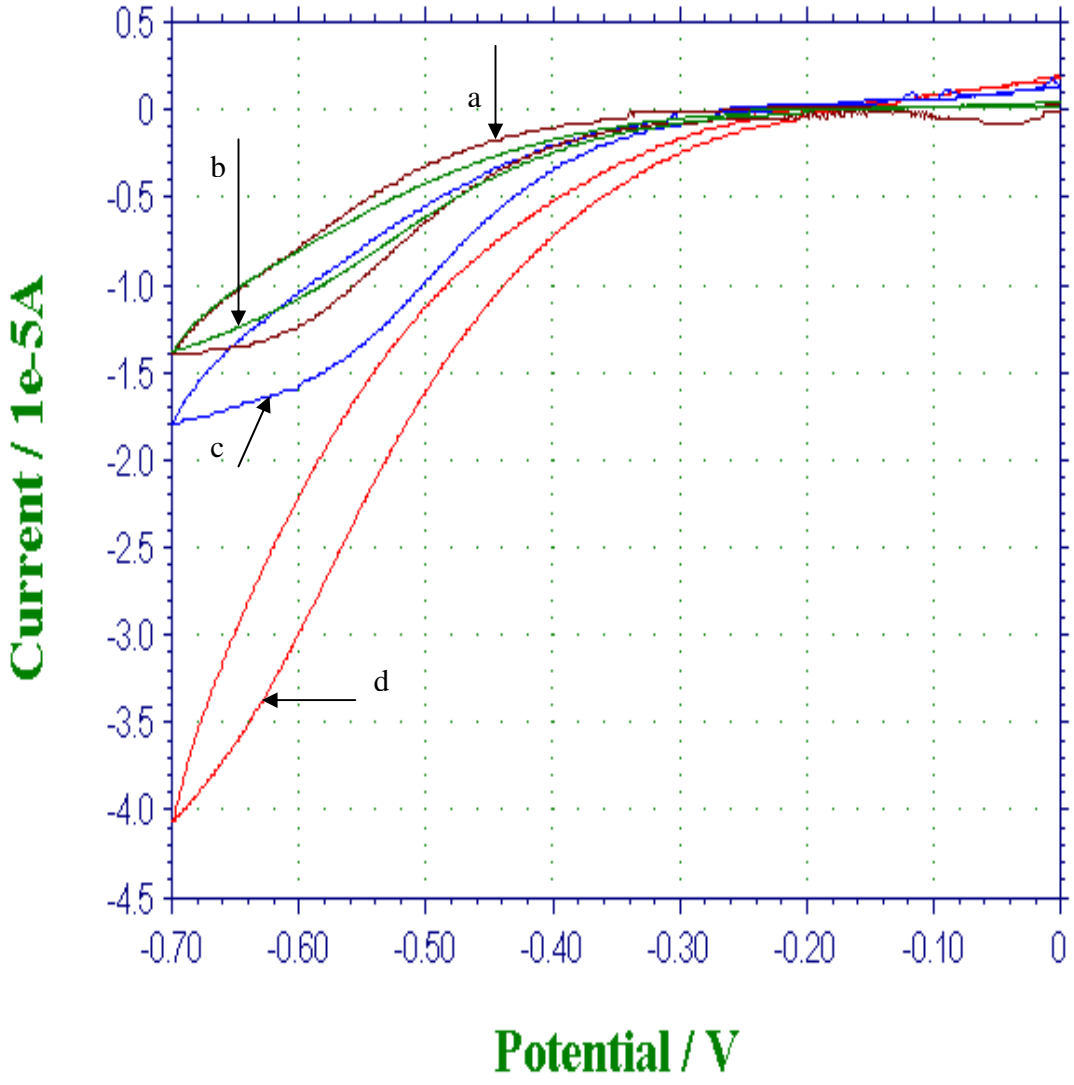

Figure 2.3.1: Cyclic voltammetry at ink electrodes using (a) a bare CI; (b) an electrode containing 1 % w/w CoPc in CI; (c) an electrode containing 3 % w/w CoPc in CI and (d) an electrode containing 5 % w/w CoPc in CI. Electrode area = 0.063 cm^2. Cycled negatively between 0 → - 0.7 V at a scan rate of 50 mV s^{-1} in 0.1 M KCl. All voltages are referred to SCE. Solutions were equilibrated in air.

As all voltammograms shown in figure 2.3.2 were in nitrogen sparged solutions there is no oxygen reduction peak. Therefore any peaks present are due to reduction of the cobalt macrocycle on the initial negative cycle and reformation of cobalt (II) on the

forward cycle. Currents for such catalysts are greater than that of the bare electrode (a), and can be attributed to both double layer charging and electroactivity of the cobalt couple.

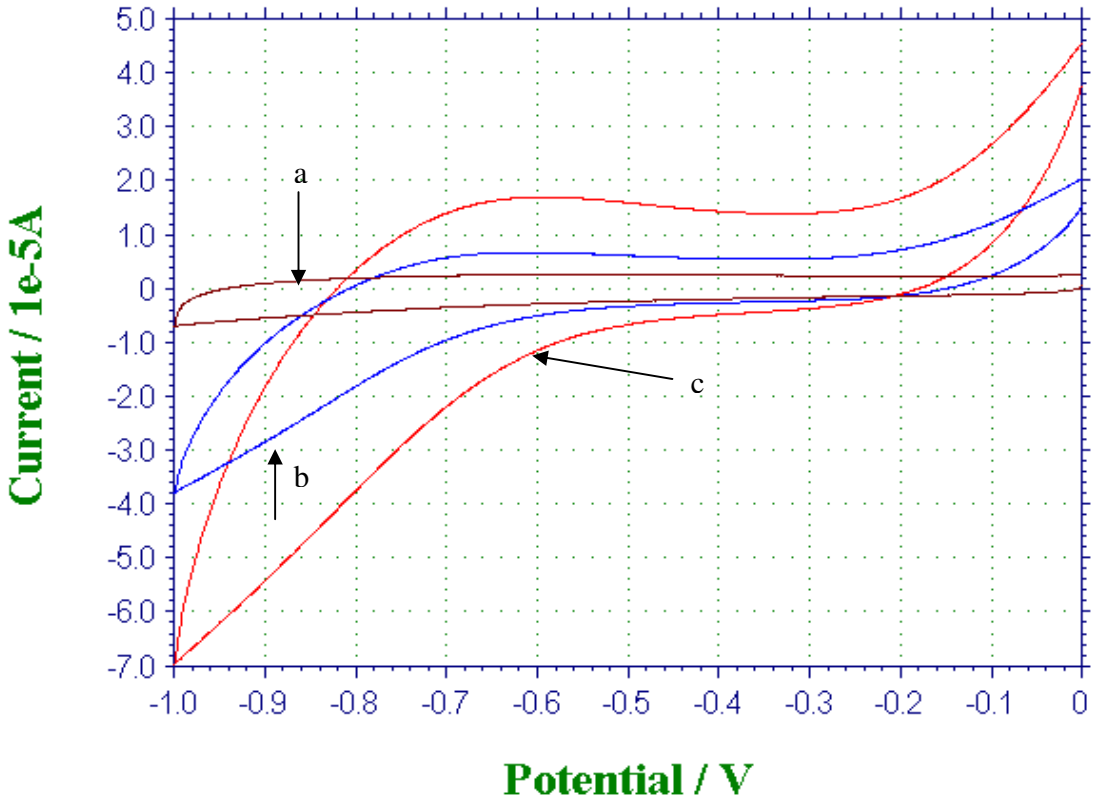

Figure 2.3.2: Cyclic voltammetry in 0.1 M KCl sparged with N_2 using (a) a bare CI; (b) an electrode containing 3 % w/w CoPc in CI and (c) an electrode containing 5 % w/w CoPc in CI. Electrode area = 0.063 cm^2. Cycled negatively between – 0. → - 1 V at a scan rate of 50 mV s^{-1}. All voltages are referred to SCE.

Figure 2.3.3 illustrates the difference between an aerated and a de-aerated solution. A very small current of 2 μA is recorded in nitrogen sparged conditions. In the ambient solution the peak for oxygen reduction begins at around – 0.35 V. There is no positive current for the latter voltammogram because any reduced cobalt has combined

with oxygen on the positive segment and returned to its original state. So when the solution approaches – 0.40 V on the forward cycle there is no cobalt (I) there to oxidise and therefore no current.

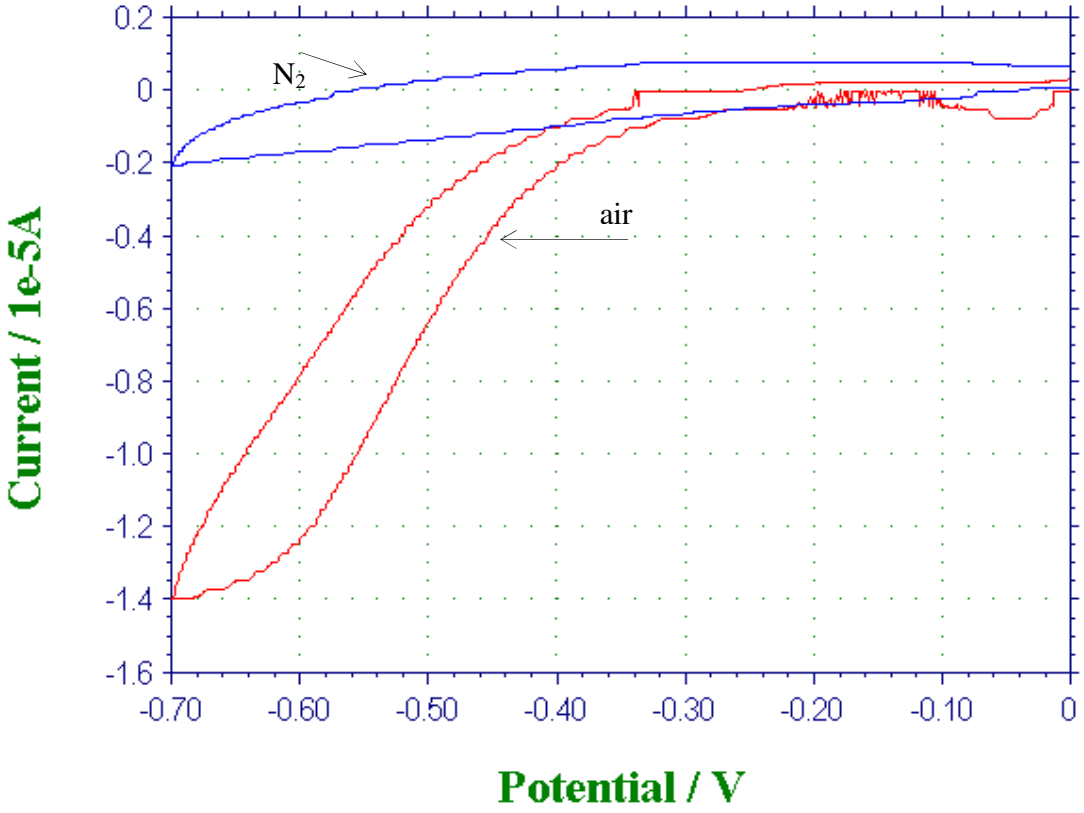

Figure 2.3.3: Voltammetry in 0.1 M KCl using firstly an electrode containing 1 % w/w CoPc in CI in N_2 conditions and secondly the same electrode in ambient conditions. Electrode area = 0.063 cm^2. Cycled negatively between 0 → - 0.7 V at a scan rate of 50 mV s^{-1}. All voltages are referred to SCE.

Similar voltammetry is portrayed in figure 2.3.4 except there is a higher concentration of CoPc present on the electrode. There is a greater current for oxygen reduction using this electrode than the previous one shown in figure 2.3.3 as there is 3 times the amount of cobalt catalyst included this time. Again there is no positive current

displayed on the forward cycle for the reasons stated above. A background current of just over 2 μA is shown in the nitrogen conditions.

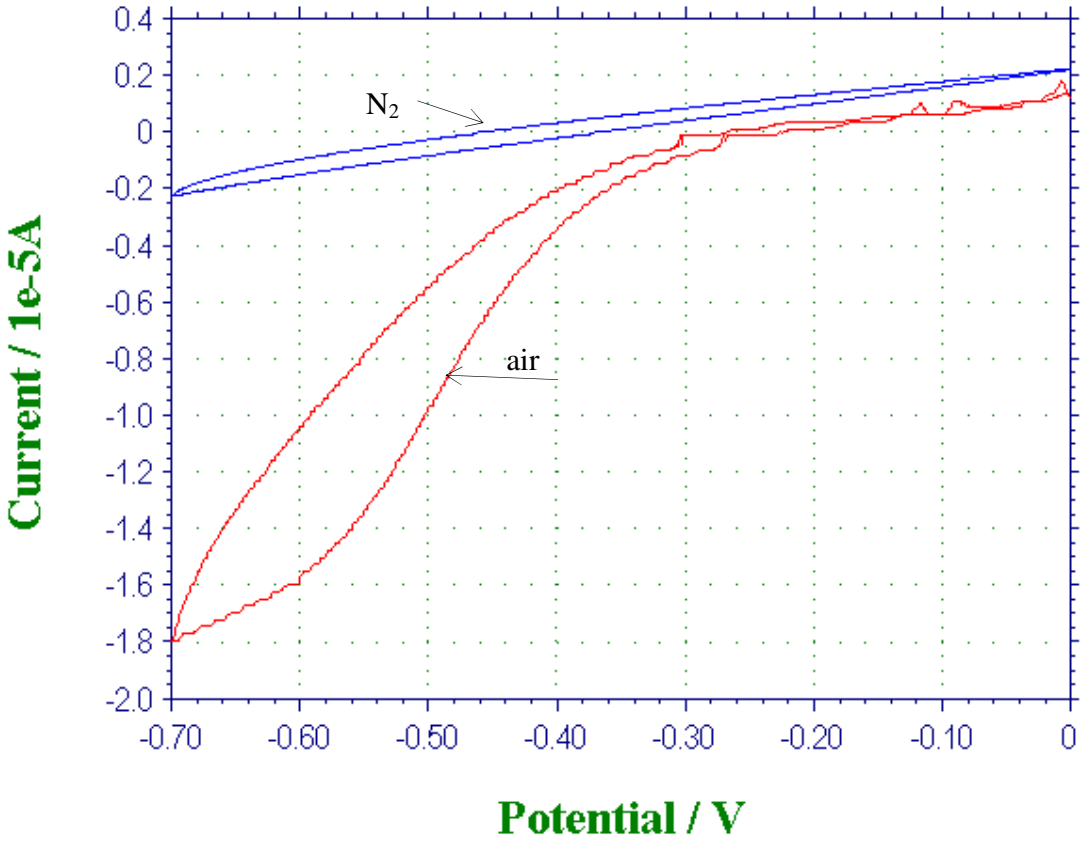

Figure 2.3.4: Cyclic voltammetry in 0.1 M KCl using firstly an electrode containing 3 % w/w CoPc in CI in N_2 conditions and secondly the same electrode in ambient conditions. Electrode area = 0.063 cm^2. Cycled negatively between 0 → - 0.7 V at a scan rate of 50 mV s^{-1}. All voltages are referred to SCE.

In figure 2.3.5 there is 5 % w/w concentration of CoPc in CI. There is a greater current for oxygen reduction again than in figure 2.3.4 as there is more cobalt present. However in order to see the full redox couple for CoPc it is necessary to cycle back to – 1 V (figure 2.3.2) While there is no oxidative current for cobalt in the ambient solution (as

oxygen used up any lower valent cobalt states), this is not the case in the N_2 sparged solution. A positive current is observed representing the re-oxidation of cobalt (0) → cobalt (II). The standard reduction potentials of this couple and of the less important Co^{3+}/Co^{2+} are shown in equations 2.16 (a) and (b) [39].

Co^{3+} + e^- ⇌ Co^{2+} $E° = + 1.92$ V 2.16 (a)

Co^{2+} + $2\ e^-$ ⇌ Co^0 $E° = - 0.28$ V 2.16 (b)

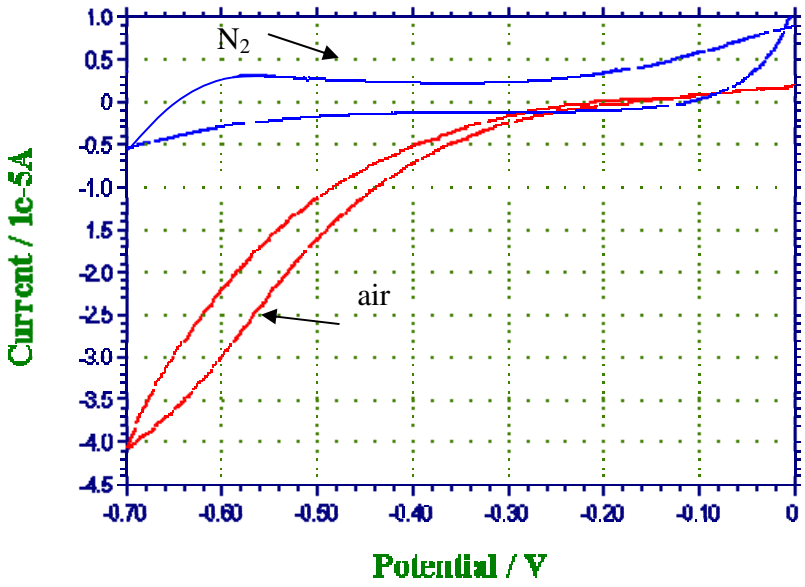

Figure 2.3.5: Cyclic voltammetry in 0.1 M KCl using firstly an electrode containing 5 % w/w CoPc in CI in N_2 conditions and secondly the same electrode in ambient conditions. Electrode area = 0.063 cm^2. Cycled negatively between 0 → - 0.7 V at a scan rate of 50 mV s^{-1}. All voltages are referred to SCE.

The differences in voltammetry of a bare CI electrode in air and nitrogen conditions are shown in figure 2.3.6. In de-oxygenated conditions a residual current of only 2 μA is again displayed (N_2). There no oxidative current this time as there is no species there to be oxidised.

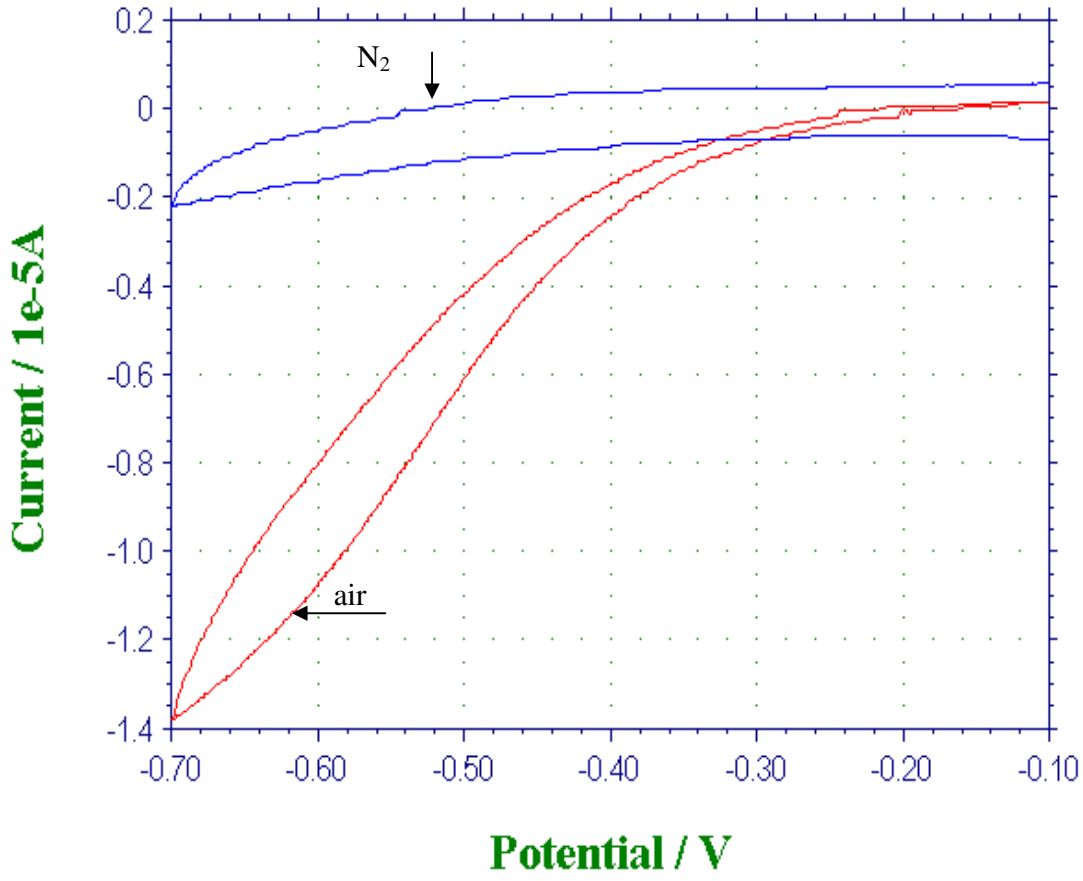

Figure 2.3.6: Cyclic voltammetry in 0.1 M KCl using firstly a bare CI in N_2 conditions and secondly the same electrode in ambient conditions. Electrode area = 0.063 cm^2. Cycled negatively between – 0.1 → - 0.7 V at a scan rate of 50 mV s^{-1}. All voltages are referred to SCE.

Comparing figures 2.3.3, 4, 5 & 6, it can be seen that the 5 % w/w loading of CoPc yields an appreciably greater current for O_2 reduction compared to the other 3 electrodes. This is as expected as there is a greater amount of CoPc present.

2.3.2 Oxygen reduction using GCE – bare and coated with solvent cast CoPc

In the voltammograms obtained on GCE (bare and coated with CoPc) in figure 2.3.7, the O_2 reduction peak occurs at earlier potentials than at the CI electrodes. As

expected, the bare electrode provides the least cathodic current (< 11 μA). This figure is slightly less than the bare CI produced even though its area is 13 % bigger.

The electrode coated with 3 μL of 10: 1×10^{-3} M CoPc: PS produces the greatest current as a result of cobalt and oxygen reduction. There is no real difference between the PVC and the PVP impregnated electrodes.

The peak for cobalt reduction is clearly highlighted when compared to the voltammogram of the bare electrode. In all cases this reduction begins at – 0.2 V and ends at around – 0.35 V. Interestingly, the Co (II) / Co (I) redox couple is much closer to zero volts using GCEs than CIs because of the latters highly resistive behaviour. Also, the magnitude of the current for O_2 reduction is around the same using a bare GCE (figure 2.3.7) and using a bare CI (figure 2.3.6). This is because of the formers superior conductivity and quality.

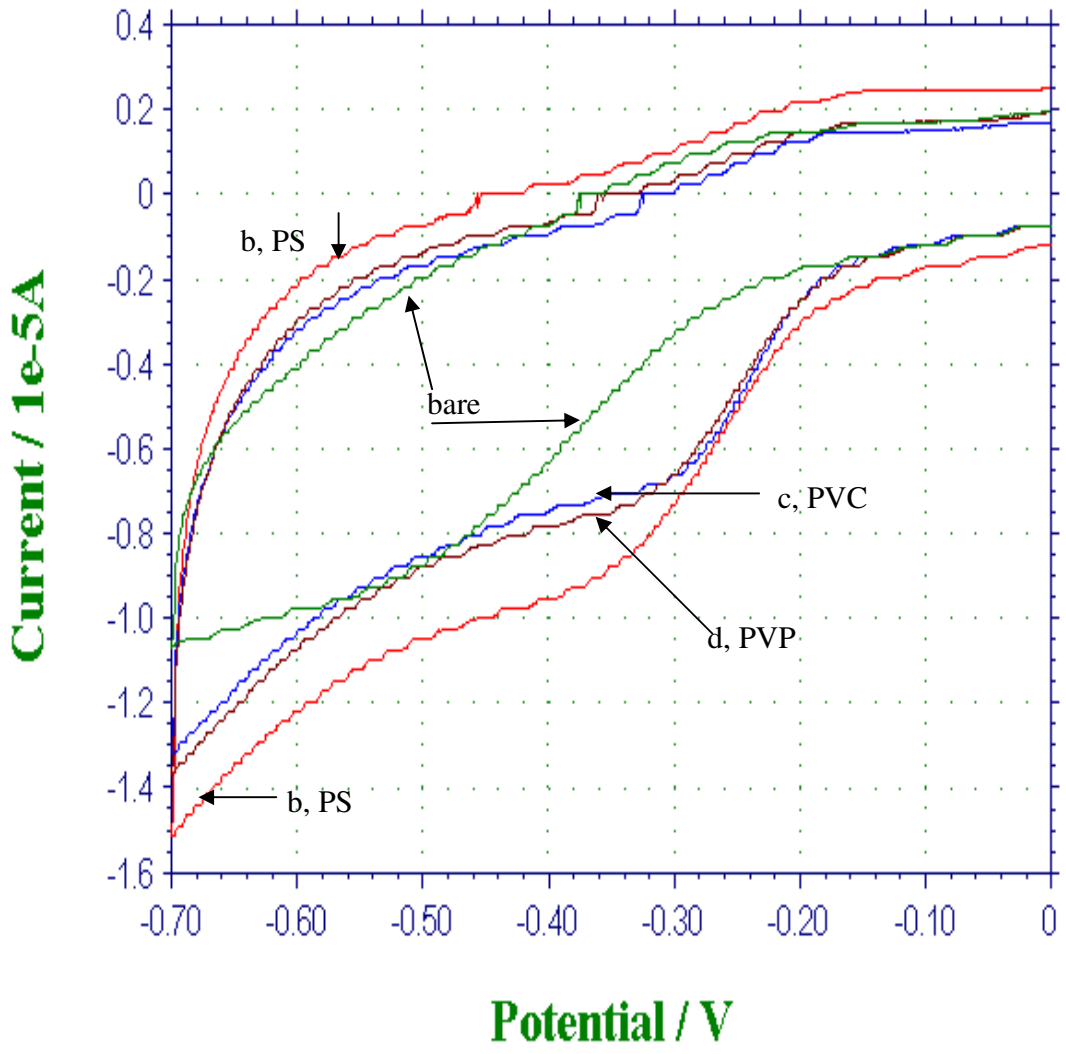

Figure 2.3.7: Voltammetry in 0.1 M KCl equilibrated in air using (a, green) a bare GCE; (b, red) a GCE coated with 3 μL of 10: 1 × 10^{-3} M CoPc: PS; (c, blue) a GCE coated with 3 μL of 10: 1 × 10^{-3} M CoPc: PVC and (d, brown) a GCE coated with 3 μL of 10: 1 × 10^{-3} M CoPc: PVP. Geometric area = 0.071 cm^2. Cycled negatively between 0 → - 0.7 V at 50 mV s^{-1}. All voltages are referred to SCE.

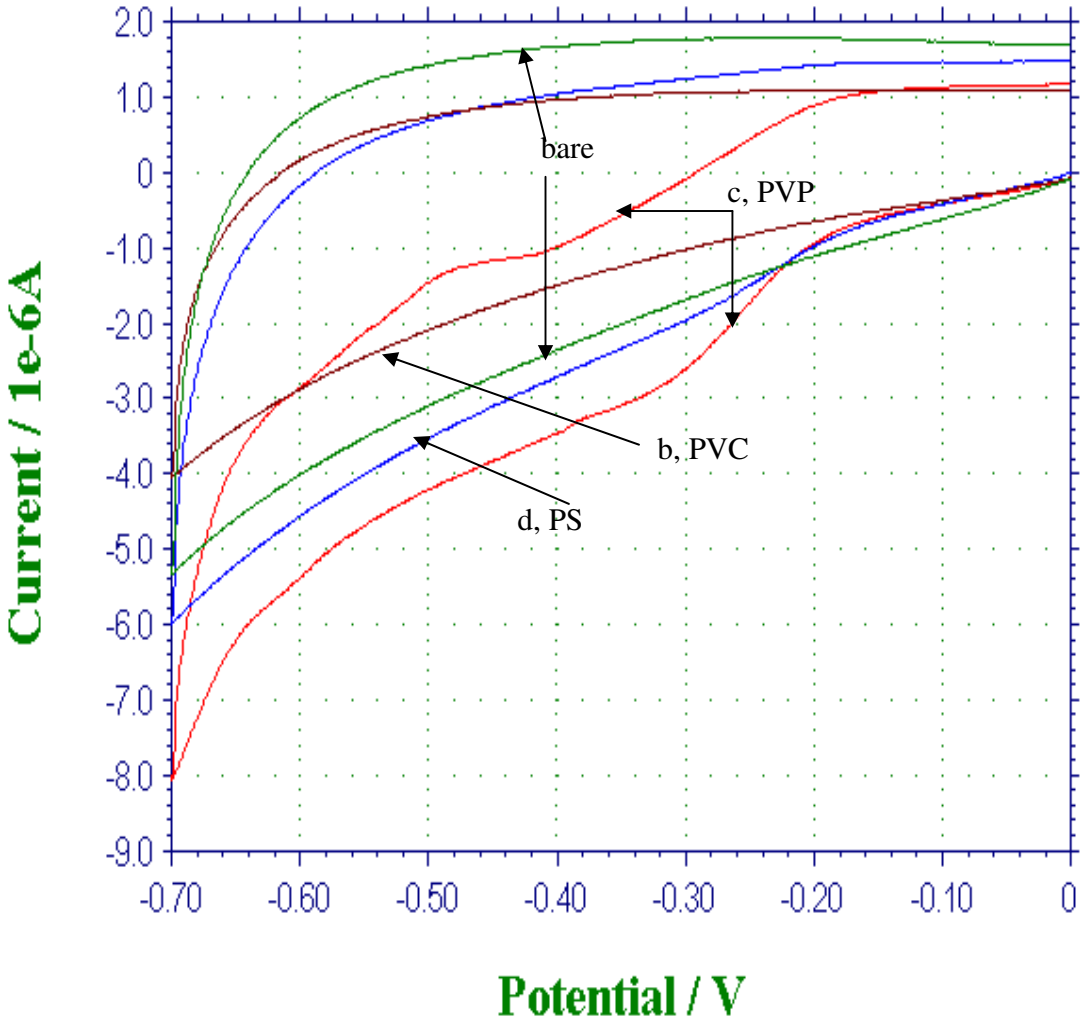

Figure 2.3.8: Voltammetry in 0.1 M KCl using (a, green) a bare GCE in N_2; (b, brown) a GCE coated with 3 μL of 10: 1 × 10^{-3} M CoPc: PVC in N_2; (c, red) a GCE coated with 3 μL of 10: 1 × 10^{-3} M CoPc: PVP in N_2 and (d, blue) a GCE coated with 3 μL of 10: 1 × 10^{-3} M CoPc: PS in N_2. Geometric area = 0.071 cm^2. Cycled negatively between 0 → - 0.7 V at a scan rate of 50 mV s^{-1}. All voltages are referred to SCE.

All coated electrodes have a similar anodic current (around 1 μA). For PVP and PS the results are consistent with a direct oxidation from Co (I) → Co (II). The PS based catalyst may not have adhered well to the electrode as there is a smaller current for Co

reduction compared to the bare electrode. The coating involving PVP provides the greatest cathodic current but because it is in a nitrogen - containing solution this is 5 μA less than the current achieved for the same polymer under oxygenated conditions.

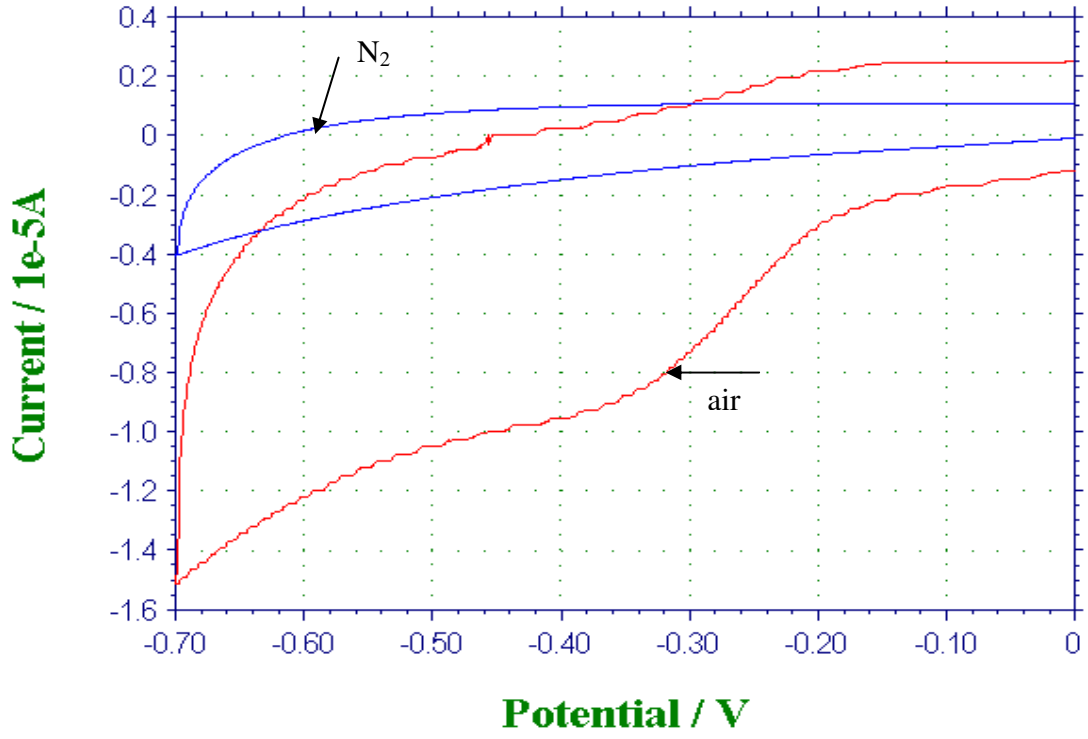

Figure 2.3.9: Voltammetry in 0.1 M KCl using firstly a GCE coated with 3 μL of 10: 1 × 10^{-3} M CoPc: PS in ambient conditions and secondly the same electrode in N_2. Geometric area = 0.071 cm^2. Cycled negatively between 0 → - 0.7 V at a scan rate of 50 mV s^{-1}. All voltages are referred to SCE.

In nitrogen environment there is a much smaller current (1 – 4 μA) for cobalt's redox cycle than in ambient conditions. Twice the anodic and nearly four times the cathodic currents are shown for the electrode in ambient conditions than under nitrogen,

mainly because of oxygen reduction. The peak for cobalt reduction is not very visible under nitrogen conditions because of its low concentration.

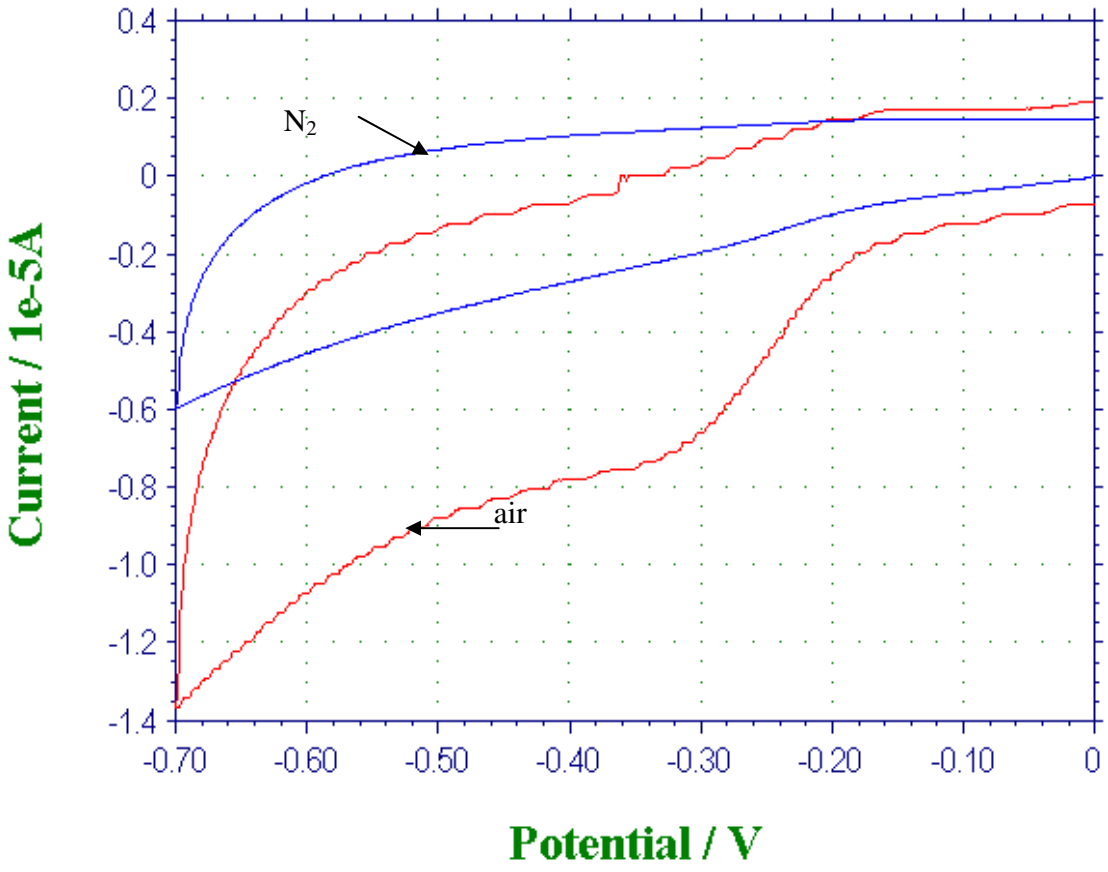

Figure 2.3.10: Voltammetry in 0.1 M KCl using firstly a GCE coated with 3 μL of 10 : 1 × 10^{-3} M CoPc: PVC in ambient conditions and secondly the same electrode in N_2. Geometric area = 0.071 cm^2. Cycled negatively between 0 → - 0.7 V at a scan rate of 50 mV s^{-1}. All voltages are referred to SCE.

The presence of oxygen makes a big difference to the shape of the voltammograms. It takes a much longer length of time to reform cobalt (II) in aerated conditions as most of the oxygen around it has been reduced at that point. In nitrogen the peak for cobalt reduction is slightly more visible than in figure 2.3.9 using PS.

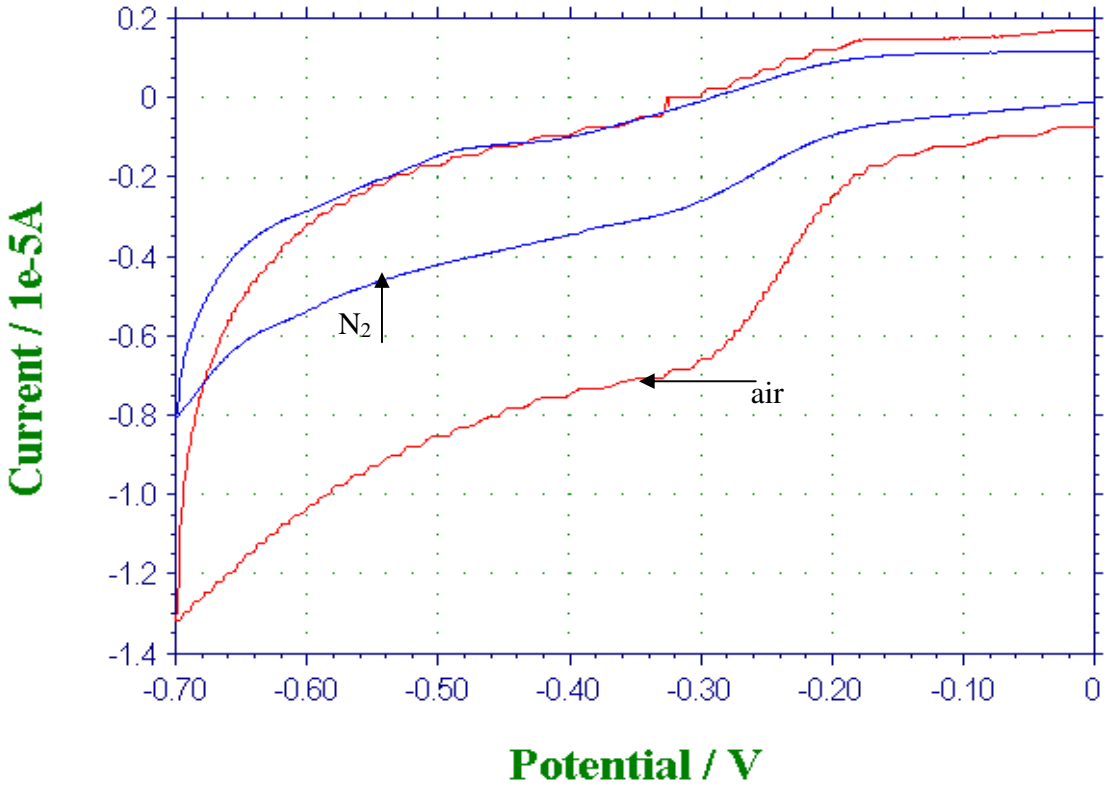

Figure 2.3.11: Voltammetry in 0.1 M KCl using firstly a GCE coated with 3 μL of 10: 1 × 10^{-3} M CoPc: PVP in ambient conditions and secondly the same electrode in N_2. Geometric area = 0.071 cm^2. Cycled negatively between 0 → - 0.7 V at a scan rate of 50 mV s^{-1}. All voltages are referred to SCE.

The only electroactive behaviour for the cobalt complex is using PVP as the polymer in N_2 (above). There is no evidence of electroactivity when using PS or PVC figures 2.3.9 & 10. On one hand this is to be expected as a very conducting GCE was coated with what is really an insulating layer.

When voltammetry is carried out at these electrodes in the presence of oxygen, there is a clear catalysis visible since oxygen reduction occurs at an earlier potential than at the bare electrode (figure 2.3.7). Reduction peaks for oxygen and CoPc are co incident when PVP is the polymer (figure 2.3.11).

2.4 Conclusion

It can be seen from figures 2.3.9 - 11 that there is little electrochemical activity of the cobalt complex seen in nitrogen (except for the latter voltammogram where there is a small couple seen). But in aerated solutions the current is enhanced and oxygen reduction occurs earlier than at the bare electrode (figure 2.3.7).

Comparing figure 2.3.1 & 2.3.7, even though the catalytic reduction of oxygen at CI occurs at a later potential; the resulting currents are greater for 3 % & 5 % loadings than at the coated GCEs. This is particularly seen for the latter loading where the current is 40 μA (figure 2.3.1) compared to 15 μA (figure 2.3.7) at the GCE/PS electrode. This is an especially good result since GCEs are 11 % greater in area than CIs.

It can be seen that a current of 40 μA at – 0.7 V was obtained with 5 % w/w CoPc in CI. There is little evidence of the Co couple in CI electrodes under N_2. Thus, even in the 5 % w/w CoPc in CI mixture, there is little electrical connection between the ink and the catalyst indicating that the catalyst was insulated in the ink binder resin. So in many cases the Co catalyst was not 'seen' in the ink matrix, explaining the low currents recorded from the Co redox couple. However, the presence of the catalyst can be clearly seen in aerated solutions.

In order to obtain large area, cheap flexible electrodes that can be used as cathodes in fuel cells, CI electrodes are an ideal alternative to glassy carbon. In previous work CI electrodes have been used for O_2 reduction with heat treated iron (III) tetramethoxyphenyl porphyrin chloride to study both the kinetics of the reaction [40] and the detection of H_2O_2 [41]. CoPc loaded CI electrodes were employed for the electrocatalysed oxidation of sulphur containing noxious compounds (glutathione and 2-

mercaptoethanol) [42]. In organic solution, the construction of amperometric biosensors based on enzymes (like glucose oxidase) producing oxidizable products such as thiocholine were electrodeposited on the surface of CoPc in CI [43].

CoPc on CI electrodes have also been used for hydrazine oxidation [44]. To the best of this author's knowledge the work described here is the first characterisation of the use of CoPc loaded CI for O_2 reduction. It has been shown that these are far superior than glassy carbon in terms of quality and currents produced.

In chapter 3 there is an investigation of the nature of catalysis of CoPc in confined layers.

2.5 References

[1] F. Beck, *Ber. Bunsenges. Phys. Chem,* **77** (1973) 353

[2] F. Beck, *Journal of Applied Electrochemistry,* **7** (1977) 239

[3] F. Van den Brink, E. Barendrecht, W. Visscher, *Rec. Trav. Chim. Pays Bas*, **99** (1980) 253

[4] P. Zanello, in "The Electrochemical Behaviour of Transition Metal Complexes", Chapter 5 in *Inorganic Electrochemistry – theory, practice & application*, Royal Society of Chemistry**,** London, 1993, pages 266-271

[5] F. Van den Brink, W. Visscher, E. Barendrecht, *Journal of Electroanalytical Chemistry*, **157** (1983) 283 – 304

[6] C. Coutanceau, P. Crouigneau, J. M. Léger, C. Lamy, *Journal of Electroanalytical Chemistry*, **379** (1994) 389 – 397

[7] S. Zecevic, B. Simic-Glavaski, F. Yeager, A. Lever, P. Minor, *Journal of Electroanalytical Chemistry*, **196** (1985) 339

[8] J. Zagal, C. Fierro, W. Muñoz, R. Rozas, S. Ureta-Zañartu, *Electrocatalyis* (Edited by W. O Grady, P. Ross Jr and F. Will), Volume 82-2 (1982) The Electrochemical Society 389

[9] J. Zagal, J. Pavez, M. Aguirre, L. Baséez, L. Padilla, A. Toro-Labbé, *Oxygen Electrochemistry* (Edited by F. Anson, R. Adzic, K. Kinoshita), Volume 95-26 (1995) The Electrochemical Society Soft. Bond Symposium Series 89

[10] J. Zagal, *Journal of Electroanalytical Chemistry*, **109** (1980) 389

[11] J. Zagal, S. Ureta-Zañartu, *Journal of The Electrochemical Society*, **129** (1982) 2242

[12] J. Zagal, W. Muñoz, S. Ureta-Zañartu, *Electrochimica Acta,* **27** (1982) 1373

[13] J. Zagal, S. Lira, S. Ureta-Zañartu, *Journal of Electroanalytical Chemistry,* **210** (1986) 95

[14] Q. Peng, T. Guarr, *Electrochimica Acta*, **39** (1994) 2629

[15] J. Zhang, Y. Tse, W. Pietro, A. Lever, *Journal of Electroanalytical Chemistry*, **406** (1996) 203

[16] F. Van den Brink, W. Visscher, E. Barendrecht, *Journal of Electroanalytical Chemistry*, **157** (1983) 305 – 318

[17] M. Isaacs, M. Aguirre, A. Toro-Labbé, J. Costamagna, M. Páez, J. Zagal, *Electrochimica Acta*, **43**, 12 - 13 (1998) 1821 – 1827

[18] J. Zagal, *Co-ord. Chem. Rev.*, **119** (1992) 89

[19] A. Van Den Putten, B. Elzing, W. Visscher, E. Barendrecht, *Journal of Electroanalytical Chemistry*, **221** (1987) 95

[20] J. Zagal, M. Paez, A. Tanaka, J. R. dos Santos, C. Linkous, *Journal of Electroanalytical Chemistry*, **339** (1992) 13 - 30

[21] C. Coutanceau, A. El Hourch, P. Crouigneau, J. M. Léger, C. Lamy, *Electrochimica Acta*, **40,** 17 (1995) 2739 – 2748

[22] R. D. Rocklin, R. W. Murray, *Journal of Electroanalytical Chemistry,* **100** (1979) 271

[23] R. Durand, F. Anson, *Journal of Electroanalytical Chemistry*, **134** (1982) 273

[24] The Southampton Group in "Electrocatalysis", Chapter 7 in *Instrumental Methods in Electrochemistry,* Ellis Horwood, Prof T.J. Kemp Ed., 1985, page 242

[25] V. E. Kazarimov, M. R. Terasevich, K. A. Radyushkina, V. Andreev, *Bioelectrochemical Bioenergy*, **4** (1977) 18

[26] A. Elzing, A. Ven Der Putten, W. Visscher, E. Barendrecht, *Journal of Electroanalytical Chemistry*, **200** (1986) 313 – 322

[27] W. Nevin, W. Liu, M. Melnik, A. Lever, *Journal of Electroanalytical Chemistry*, **213** (1986) 217

[28] D. J. G. Ives, G. J. Janz, "The Calomel Electrode and Other Mercury-Mercurous Salt Electrodes" in *Reference Electrodes – Theory & Practice*, Volume 1, D. J. G. Ives & G. J. Janz, ed., Academic Press, New York & London, 1961, 160

[29] J. Zagal, R. K. Sen, E. Yeager, *Journal of Electroanalytical Chemistry*, **200** (1986) 283

[30] L. Kreja, A. Plewka, *Electrochimica Acta*, **27** (1982) 251

[31] M. I. Florit, W. E. O Grady, C. A. Linkous, T. Skotheim, M. Rosenthal, Ext. Abstr. , Volume 84- 1, The Electrochemical Society, Princeton, 1984, Abstract No. 415, R. A. Bull, F. R. Fan, A. J. Bard, *Journal of the Electrochemical Society,* **131** (1984) 687

[32] C. P. Andrieux, J. M. Dumas–Bouchiat, J. M. Savéant, *Journal of Electroanalytical Chemistry,* **131** (1982) 1

[33] A. Van Den Putten, B. Elzing, W. Visscher, E. Barendrecht, *Journal of Electroanalytical Chemistry*, **205** (1986) 233

[34] A. Biloul, F. Coowar, O. Contamin, G. Scarbeck, M. Savy, D. Van Den Ham, J. Riga, J. J. Verbist, *Journal of Electroanalytical Chemistry*, **289** (1990) 189

[35] M. Velazquez–Rosenthal, T. A. Skotheim, C. A. Linkous, *Synthetic Metals,* **15** (1986) 219

[36] R. Jiang, S. Dong, *Journal of Electroanalytical Chemistry*, **246** (1988) 101 - 117

[37] A. El Hourch, A. Rakotondrainibe, B. Beden, P. Crouigneau, J. M. Léger, C. Lamy, A. A. Tanaka, E. R. Gonzalez, *Electrochimica Acta*, **39** (1984) 889

[38] T. Skotheim, M. Velazquez–Rosenthal, C. A. Linkous, *Journal of the Chemical Society – Chemical Communications,* **612** (1985) 5

[39] C. E. Housecroft, E. C. Constable, "Electrochemistry" in *Chemistry*, 3rd edition, C. E. Housecroft & E. C. Constable ed., Pearson Education Ltd, 2006, 581

[40] S. Lj. Gojkovic, S. Gupta, R. F. Savinell, *Electrochimica Acta,* **462, 1** (1999) 63-72

[41] S. Lj. Gojkovic, S. Gupta, R. F. Savinell, *Electrochimica Acta,* **45, 6** (1999) 889-897

[42] N. Sehlotho, S. Griveau, N. Ruille, M. Boujtita, T. Nyokong, F. Bedioui, *Material Science and Engineering: C,* **28, 5-6** (2008) 606-612

[43] N. A. Pchelintsev, P. A. Millner, *Analytica Chimica Acta,* **612, 2** (2008) 190-197

[44] J. Wang, P. V. A. Pamidi, *Talanta,* **42, 3** (1995) 463-467

Chapter 4

Use of ink based visible light active photoelectrochemical cells with organic substrates

Chapter 4 - Use of ink based visible light active photoelectrochemical cells with organic substrates

4.1 Introduction

4.1.1 Fuel cells and energy production

Fuel cells come in all shapes and sizes and some of the more efficient versions run at molten salt temperatures [1]. Others operate with well defined fuels based on hydrocarbon feed stocks that have been purified to remove sulphur by cracking. They are similar to a battery but have a distinct advantage as there is a continuous supply of reagents. For a non-rechargeable battery, whenever its fuel runs out (e.g. lead, nickel, manganese, lithium etc) it is no longer capable of operation.

Typically for fuel cells a fuel such as hydrogen, methane, methanol or other organic compounds are oxidized and are used in tandem with a species capable of being reduced; oxygen is the compound of choice due to its ready availability. The most ideal system from an environmental standpoint is that of a hydrogen/oxygen fuel cell where the product is water which avoids the production of CO_2 (scheme 4.1).

<u>Anode:</u> $2\ H_2\ (g) \rightarrow 4H^+ + 4e^-$

<u>Cathode</u>: $O_2\ (g) + 4H^+ + 4e^- \rightarrow 2\ H_2O\ (g)$

<u>Overall</u>: $2\ H_2\ (g) + O_2\ (g) \rightarrow 2\ H_2O\ (g)$

$\Delta G = -\ 474.2\ kJ\ mol^{-1}$

$$E_{cell} = E_{O2} - E_{H2}$$

$$E_{cell} = 1.229\ V - 0\ V$$

$$E_{cell} = 1.229\ V$$

Scheme 4.1: Sum of half reactions involved at a typical hydrogen fuel cell

There are many problems, however, associated with using hydrogen as a fuel such as storage and its low energy density (only 2 electrons are produced per mole during the oxidation). This is in stark contrast to some organic compounds where 6 or 8 electrons can be produced using acetic acid (scheme 4.2) or even 100 in the case of octane (an ingredient of petrol).

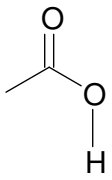

$$+ 2\ H_2O \rightarrow 2\ CO_2 + 8\ H^+ + 8\ e^-$$

$$2\ O_2 + 8\ H^+ + 8\ e^- \rightarrow 4\ H_2O$$

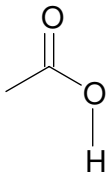

$$+ 2\ O_2 \rightarrow 2\ CO_2 + 2\ H_2O$$

$\Delta G = -873.1\ kJ\ mol^{-1}$, $E^\circ = 1.131\ V$

Scheme 4.2: Fuel cell involving acetic acid as the substrate

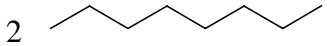

$$2 \quad + \ 32\ H_2O \rightarrow 16\ CO_2 + 100\ H^+ + 100\ e^-$$

$$25\ O_2 + 100\ H^+ + 100\ e^- \rightarrow 50\ H_2O$$

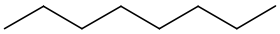

$$2 \quad + 25\ O_2 \rightarrow 16\ CO_2 + 18\ H_2O$$

$\Delta G = -10{,}611\ kJ\ mol^{-1}$, $E° = 1.100\ V$

Scheme 4.3: Complete combustion of octane

4.1.2 Photocatalysis of TiO_2

During a photocatalytic process, light activates the photocatalyst. The semiconductor photocatalyst absorbs impinging photons with energies higher (lower wavelength) than the bandgap or threshold energy and generates oxidation sites on the surface. These oxidation sites react with adsorbed water molecules or hydroxyl ions (OH^-) and produce hydroxyl radicals ($OH^\bullet$, scheme 4.4), very strong oxidants capable of oxidising virtually any organic compound [2, 3].

$$TiO_2 + h\nu \rightarrow TiO_2 + e^- + h^+$$

$$h^+ + OH^- \rightarrow OH^\bullet$$

Scheme 4.4: Absorption of light energy by TiO_2 and subsequent combination with anions to form radicals

4.1.3 Development and characterisation of a photo assisted fuel cell for the removal of organic compounds from waste water

Work in photoelectrochemistry peaked in the 1980's where there was the prospect of using sunlight shining on suspensions of titanium dioxide in order to catalytically cleave water into hydrogen and oxygen [4 - 8]. In this way a clean and efficient method of producing

hydrogen as a fuel was envisaged. However, there was a requirement to use a rather high energy light to achieve the splitting and it was not as efficient with visible light [8].

Since then suspensions of TiO_2 or immobilised TiO_2 have been used successfully to oxidise organic contaminants in waste waters when exposed to light [9 - 12]. These compounds have included propanol [12].

The aim of this fuel cell was to show that it is indeed feasible to use TiO_2 illuminated by natural daylight to mineralise organic compounds (formic acid & starch are presented as examples here) while at the same time using a non precious metal based cathode for oxygen reduction.

4.2 Experimental

4.2.1 Materials

- De-ionised water (l)
- Potassium chloride (s, KCl, Merck, 99.5+ %)
- Cobalt (II) phthalocyanine (s, CoPc, Eastman, ≥97 %)
- TiO_2 (s, TITANDIOXID P25, Degussa AG GB AC D-60287 Frankfurt)
- Poly(4-vinylpyridine) (s, PVP, Fluka, average M_w ~ 70,000)
- Sodium hydroxide (s, Merck, 98 %)
- Methanol (l, MeOH, Aldrich, 99+ %)
- Formic acid (l, FA, Aldrich, 95 – 97 %)
- Starch (s, BioChemika, from potato, 98 %)
- Electrodag 423 SS graphite-based P.T.F Ink (s, CI, Acheson Colloids, 1600 Washington Avenue Port Huron , Michigan 48060 USA)
- Oxygen free nitrogen (g, N_2, BOC Gasses, >99.999 %)
- Aluminium oxide 41 μm 600 Grit (s, Varian)

- Type J colour inkjet transparencies removable stripe (Xerox)
- Cube applicator

4.2.2 Equipment

- DMV-5800L ultrasonic cleaner (Delta)
- Platinum crescent sheet counter electrode (PtAE, approx area = 12 cm^2)
- CHI104 glassy carbon working electrode (GCE, CH Instruments, approx area = 0.071 cm^2)
- Ref 321 silver - silver (I) chloride in saturated potassium chloride reference electrode, potential at 298 K = 0.197 V (NHE) [13] (Ag/AgCl, Radiometer Analytical)
- Ref 601 mercury - mercury (I) sulphate in saturated potassium sulphate reference electrode, potential at 298 K = 0.638 V (NHE) [13] (MSE, Radiometer Analytical)
- CHI620A electrochemical analyzer (CH Instruments, 3700 Tennison Hill Drive Austin, TX 78738 USA)
- 60 W tungsten incandescent standard household light bulb
- Keithley 616 digital electrometer (figure 4.2.1) linked to a PC; data acquisition was by means of Pico Technology (figure 4.2.2) (Cambridgeshire, UK), with an ADC 16 analog to digital converter.
- Q-Sun xenon test chamber (Q-Panel laboratory Products)

The following figures show some of the instrumentation used in this work, including a data collector and an electrometer.

Figure 4.2.1 Keithley 616 digital electrometer

Figure 4.2.2 Pico Technology 16 bit 8 channel data logger

4.2.3 Methodology

4.2.3.1 Electrode preparation

A bare carbon electrode was made by coating a projector transparency with a thin film of graphite-based polymer thick film (P.T.F.) ink (Acheson Colloids , 1600 Washington Ave, Port Huron, Mi, 48060) using a cube applicator. Cobalt phthalocyanine (CoPc) electrodes were prepared by mixing graphite-based P.T.F. ink (10 g) with a known amount of cobalt phthalocyanine powder (320 mg) (Aldrich). A thin film (approximately 75 μm) of this paste was coated onto a transparency and dried at room temperature.

For the anode, the method involved using a layer of carbon ink as above (approximately 37 μm in thickness) followed by a 75 μm thick layer of a suspension of 2 g TiO_2 (Degussa P-25) and 0.007 g poly (4- vinyl-pyridine) suspended in methanol (10 cm^3). This electrode will be termed a bi-layer electrode. Electrodes of several breadths were cut out and nail polish was used to mask off a defined active area of 1, 3 & 6 cm^2. All of these

electrodes were prepared by using a cube film applicator that allows thin films of either 37 μm or 75 μm to be produced.

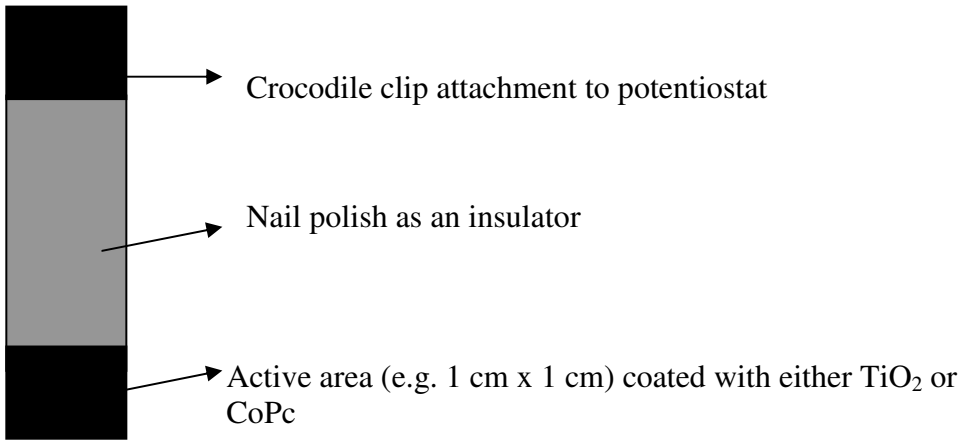

Figure 4.2.3 Typical electrode used

4.2.3.2 Characterisation of CoPc by cyclic voltammetry

A three electrode, single compartment cell was employed for the cyclic voltammetric characterisation of CoPc and its role in enhancing O_2 reduction was examined. An Ag/AgCl electrode was used as a reference and a platinum wire was used as an auxiliary electrode and the cobalt phthalocyanine electrode was used as working electrode. Cyclic voltammetry, potential control and charge and current measurement were performed using a CHI620A Electrochemical Analyzer (CH Instruments, 3700 Tennison Hill Drive Austin, TX 78738 USA), which was linked to a computer.

4.2.3.3 Logging of current transients

A TiO_2 electrode was used as photoanode and a CoPc electrode was used as cathode for current - time analysis. Formic acid (FA, 0.01 mol L^{-1}) was used as substrate with KCl as electrolyte. The light source was a standard 60 W tungsten spot light. The cell was connected to a Keithley, 616 digital electrometer and linked to a PC and data acquisition was by means of Pico Technology, with a ADC 42 or a ADC 16 analog to digital converter. All experiments

were conducted at room temperature. Chemicals were all reagent grade quality and solutions were prepared in deionised water.

4.2.3.4 Influence of pH on current and FA depletion

FA (25 cm^3 of 10 mM) in aqueous KCl (0.1 M) was placed in a one compartment cell with a bi-layer TiO_2 and CI anode and a 3.1 % CoPc in CI cathode. The pH of the solution was increased by the addition of aqueous NaOH (10 mM).

4.2.3.5 Simulation of daylight conditions

In order to model sunlight, a Q-Sun test chamber was used (Q-Panel laboratory Products). This contains a xenon pulsed light source. In the experiments the Q-Sun was programmed at maximum irradiance (0.68 W m^{-2} at 340 nm), because this would give a spectrum similar to that of sunlight. In order to maximise the voltage or currents of the cell, two TiO_2 electrodes and two CoPc electrodes were placed in series or parallel in the Q-Sun testing chamber. The electrodes for the fuel cell had nominal areas of 3 cm^2 or else 6 cm^2. Current and potential were measured using a Keithley electrometer.

The substrate used for the cells was FA (10 mM) in a Petri dish, which was used as a cell and the electrodes were placed facing upward toward the light. Five different arrangements were constructed as shown in figures 4.2.4 - 8. The white electrodes represent the bi-layer TiO_2 electrodes while the black electrodes present the 3.1 % CoPc electrodes on which O_2 reduction occurs.

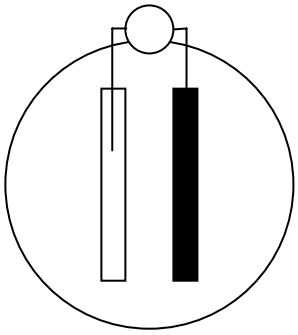

Figure 4.2.4 10 mM FA in aqueous 0.1 M KCl in a one compartment cell (Petri dish) with a bi-layer TiO_2 anode and a 3.1 % CoPc cathode connected through a 100 kΩ resistor

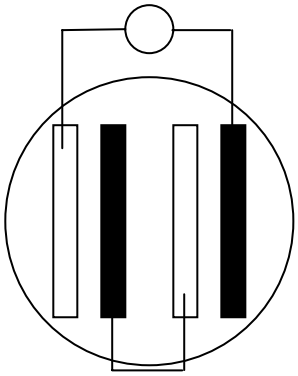

Figure 4.2.5: 10 mM FA in aqueous 0.1 M KCl in a one compartment cell (Petri dish) with 2 bi-layer TiO_2 anodes and two 3.1 % CoPc cathodes in series connected through a 100 kΩ resistor

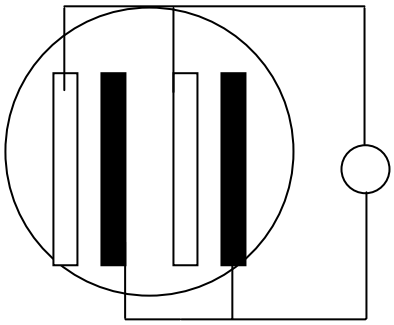

Figure 4.2.6: 10 mM FA in aqueous 0.1 M KCl in a one compartment cell (Petri dish) with 2 bi-layer TiO_2 anodes and two 3.1 % CoPc cathodes in parallel in a one compartment cell connected through a 100 kΩ resistor

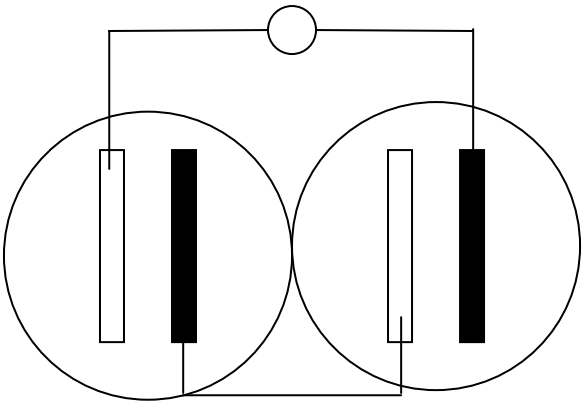

Figure 4.2.7: 10 mM FA in aqueous 0.1 M KCl in a two compartment cell (Petri dish) with 2 bi-layer TiO_2 anodes and two 3.1 % CoPc cathodes in series connected through a 100 kΩ resistor

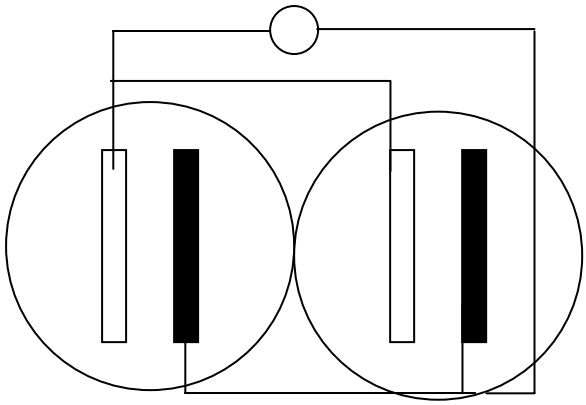

Figure 4.2.8: 10mM FA in aqueous 0.1 M KCl in a two compartment cell (Petri dish) with 2 bi-layer TiO_2 anodes and two 3.1 % CoPc cathodes in parallel connected through a 100 kΩ resistor

4.2.3.6 Q Sun testing chamber

Semiconductors absorb light below a threshold wavelength λ_g, the fundamental absorption edge, which is related to the band gap energy via: [14]

$$\lambda_g \text{ (nm)} = \frac{1240}{E_g \text{ (eV)}} \qquad 4.1$$

The threshold energy of the TiO_2 photocatalyst is 3.2 eV, so it can only be activated by solar irradiation with wavelengths less than 387.5 nm. At the ground level, solar irradiation starts at about 300 nm, and only a mere 4 % of the total solar spectrum can activate TiO_2.

For some experiments in this chapter a Q-sun, xenon test chamber was used. The Q-sun allows accelerated testing and it can be programmed to expose the cell to the equivalent of noon summer sunlight for 24 hours a day.

For the experiments the Q-sun was programmed at an irradiance of 680 mW m^{-2} at 340 nm, because this would give a very comparable spectrum to that of real sunlight as can be seen overleaf.

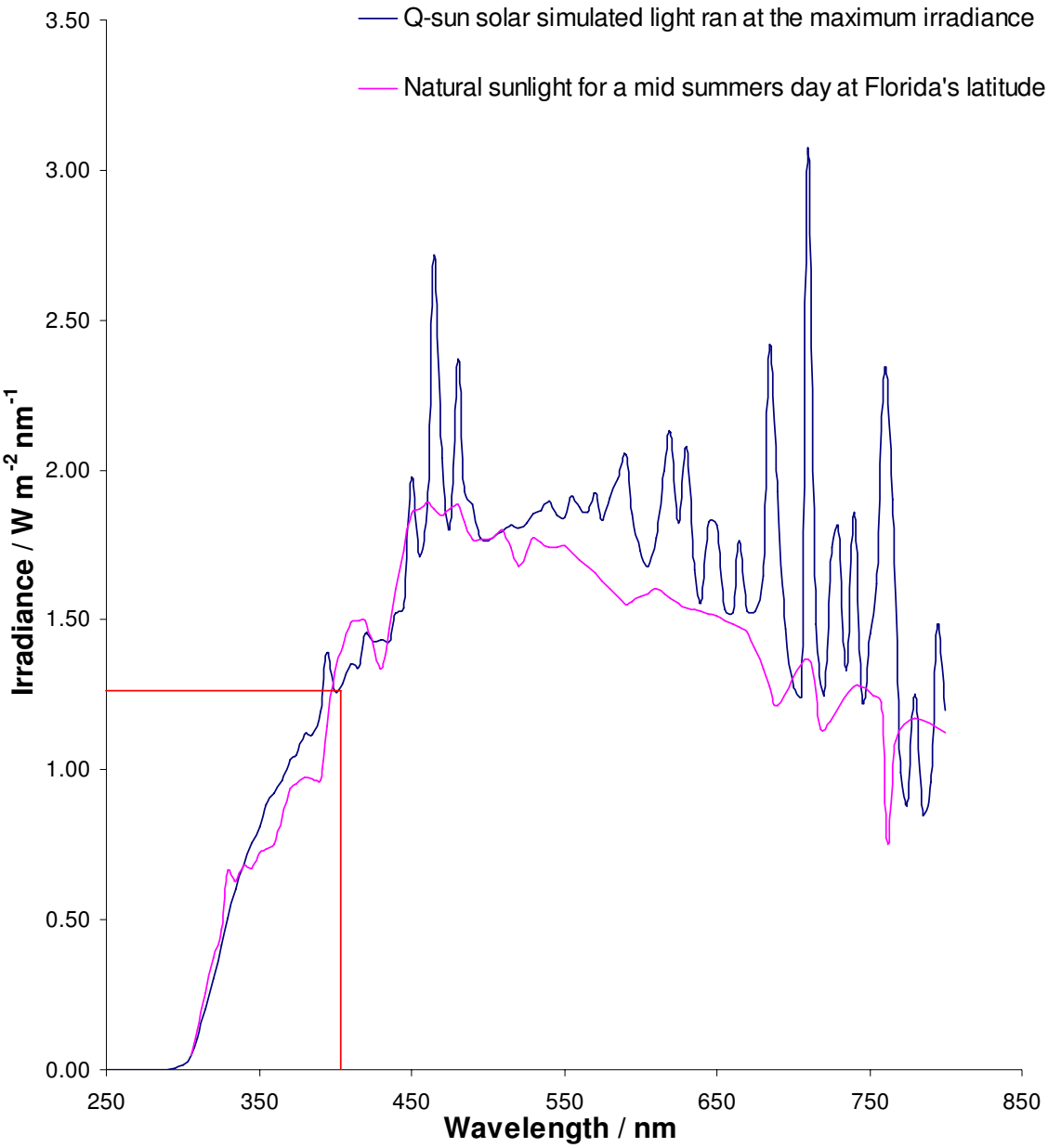

Figure 4.2.9: Spectral distributions of natural daylight and solar simulated light from the Q-sun machine. The machine was operated at the maximum irradiance value (0.68 W m^{-2} at 340 nm). The minimum irradiance the instrument can run at for a light cycle is 0.25 W m^{-2} at 340 nm at this same wavelength. This data was obtained courtesy of correspondence with Q-Panel [15].

4.2.3.7 Effect of the concentrations of organic compounds on current

Again using the Q-Sun solar simulator, the current was measured as a function of FA concentration in a one compartment cell as in figure 4.2.5 above. Starting with 1 mM FA, incremental additions of FA were made to the cell and the current was measured using a Pico technology data logger interfaced to a laptop.

A similar experiment was carried out, but instead of using simple organics like FA, the glucose polymer starch was used. Starting at 100 ppm, again additions of known concentrations were made in order to increase the concentration and study the resulting current.

4.3 Results and Discussion

4.3.1 Characterisation of CoPc & CI electrodes by cyclic voltammetry

Figure 4.3.1 shows the cyclic voltammogram of bare CI in air and nitrogen conditions. A reduction current is seen at potentials more negative than – 0.7 V due to the reduction of oxygen.

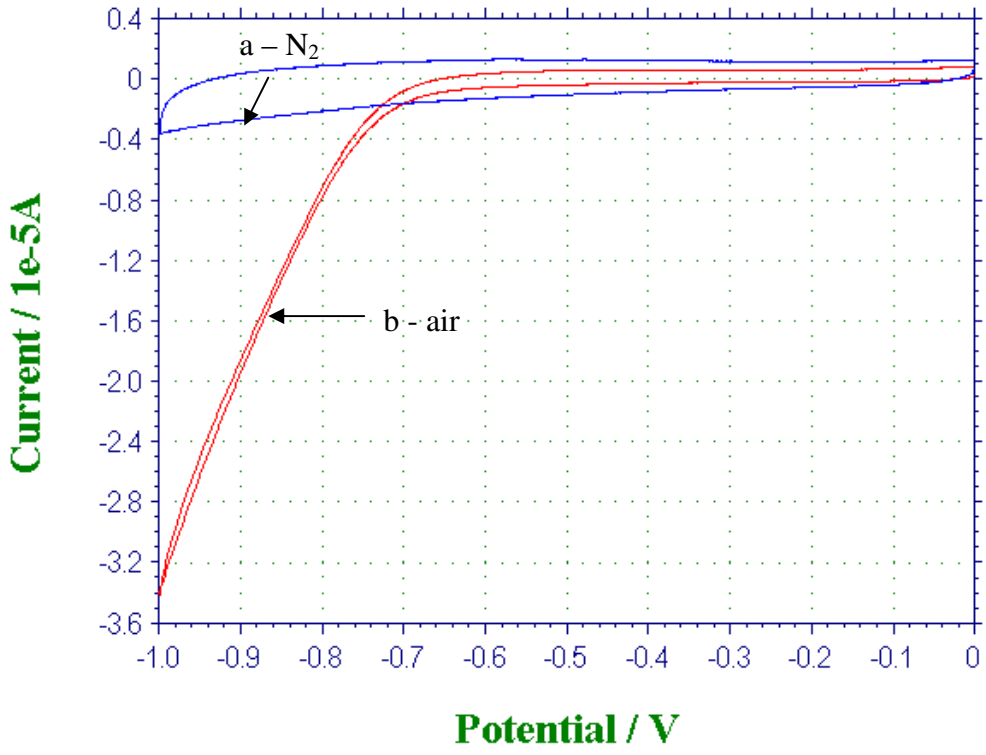

Figure 4.3.1: Oxygen reduction at ink electrodes using (a) bare CI in N_2 (g) and (b) bare CI in ambient conditions. Electrode area = 1 cm^2. Cycled negatively between 0 → - 1 V at a scan rate of 20 mV s^{-1} in 0.1 M KCl. All voltages are referred to Ag/AgCl.

When looking at the voltammetry of coated electrodes (figure 4.3.2) it can be seen that there is a reduction current at – 650 mV while there is a re-oxidation of Co. The reduction current is due to two reactions; the reduction of oxygen and the reduction of cobalt. The reduction current in nitrogen environment is much smaller than its aerated counterpart as the main reducible species is Co (II). The reversible reaction that takes place may be:

$$Co\ (II) + e^- \rightarrow Co\ (I) \qquad 4.2$$

$$Co\ (I) + O{=}O + 2\ H^+ \rightarrow Co\ (II) + H_2O_2 \qquad 4.3$$

This is reduction of Co and re-oxidation by O_2. On comparing figure 4.3.1 with figure 4.3.2, a bigger reduction current can be noted at the 3.1 % CoPc electrode than its bare counterpart at – 1.0 V; this implies the higher catalytic efficiency of CoPc reduction in which a greater number of catalytic sites are available for dissolved oxygen.

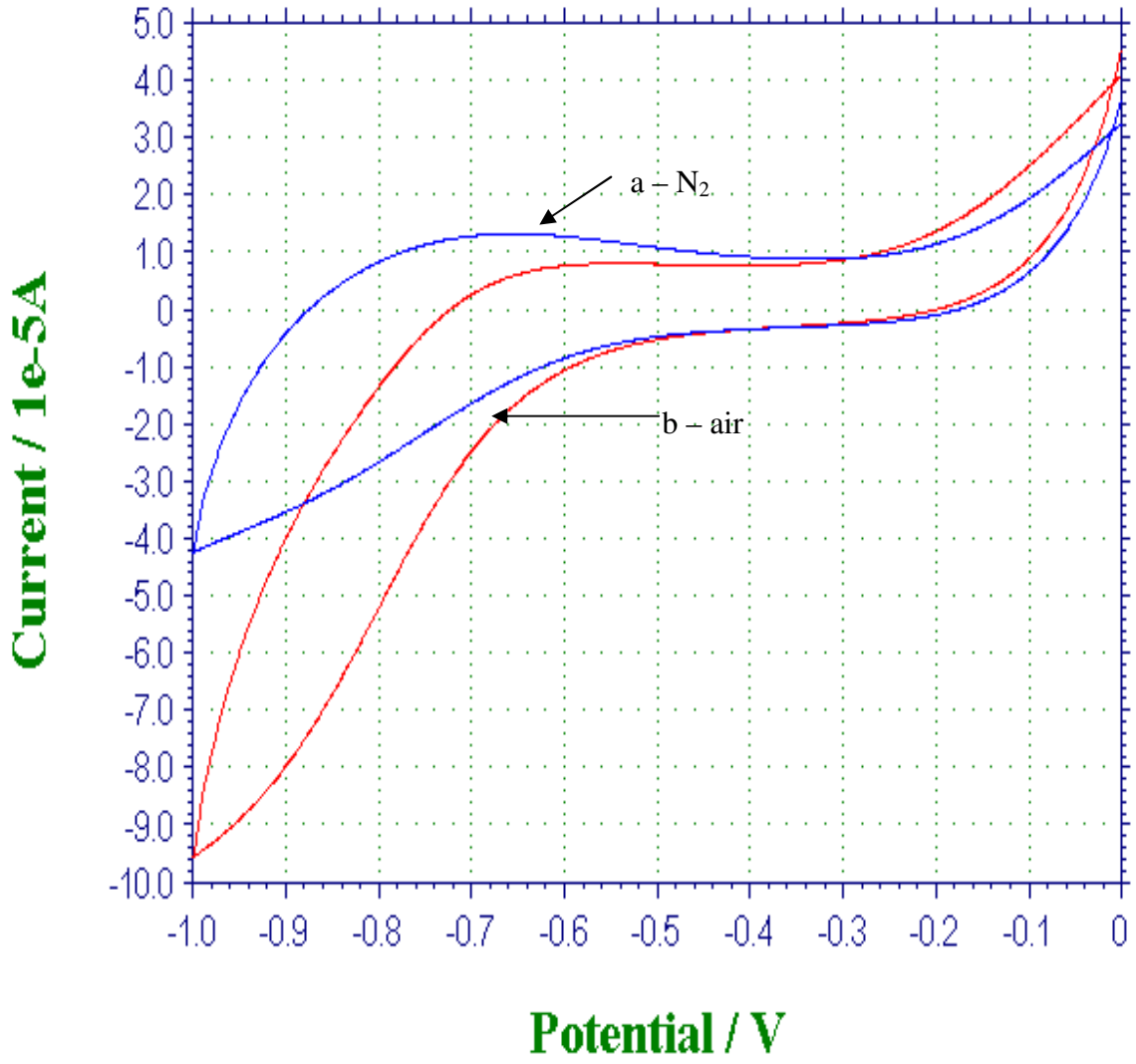

Figure 4.3.2: Oxygen reduction at ink electrodes using (a) an electrode containing 3.1 % w/w CoPc in CI in N_2 and (b) the same electrode in ambient conditions. Electrode area = 1 cm^2. Cycled negatively between 0 → - 1 V at a scan rate of 20 mV s^{-1} in 0.1 M KCl. All voltages are referred to MSE.

4.3.2 Current – time analysis

Titanium dioxide is a photoactive semi-conductor, so current versus time analyses were made of the cell in the dark and when the cell was exposed to light. The current of a two electrode photoelectrochemical cell was measured. Initially when the light (60 W tungsten bulb) was switched on the current increased. After the current

was stabilised (illustrated), the light was switched off and the current dropped as can be seen in figure 4.3.3.

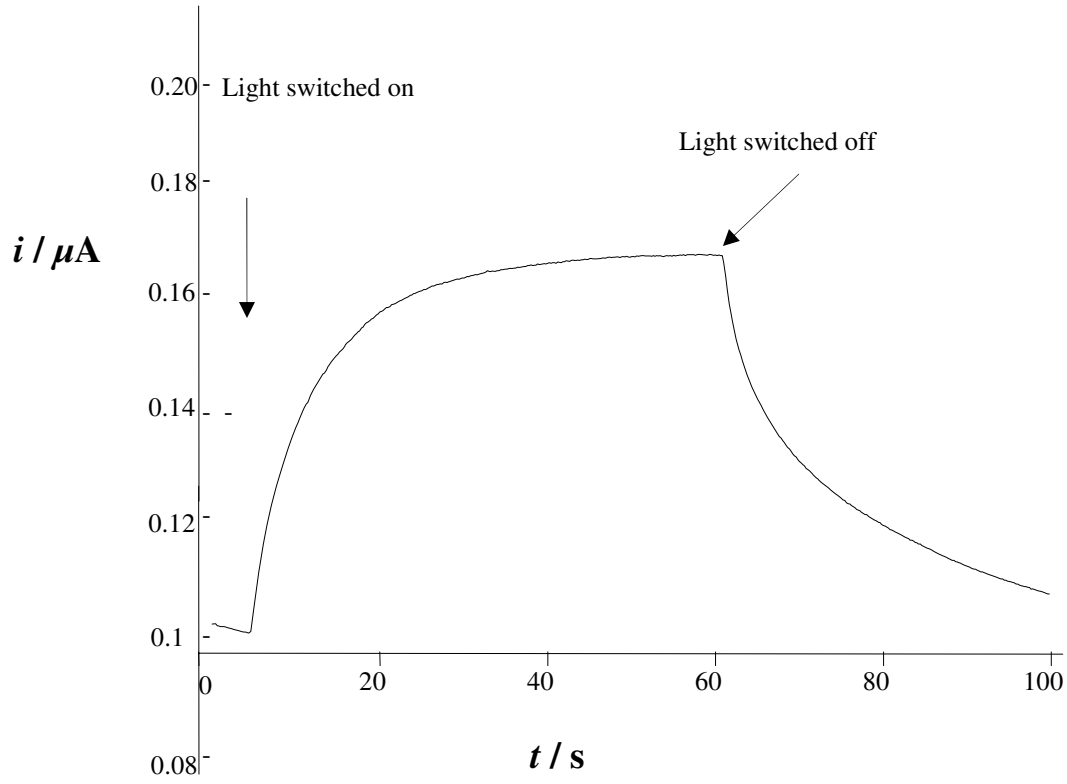

Figure 4.3.3: Influence of light (60 W tungsten incandescent visible bulb) on the current of a two compartment cell (1 mM FA in aqueous 0.1 M KCl) with a TiO_2 coated CI anode and a 3.1 % CoPc coated CI cathode, electrode area = 1 cm^2

While running the experiments featured in figures 4.3.3 and 4, stirring the beaker showed no change in the current. This indicates that the speed of the reactions in the cell are not affected by mass-transport and were thus only kinetically limited. Figure 4.3.4 features a similar experiment in a one compartment cell. Here the current is more responsive and sharper because of the lack of resistance of ions through a porous frit.

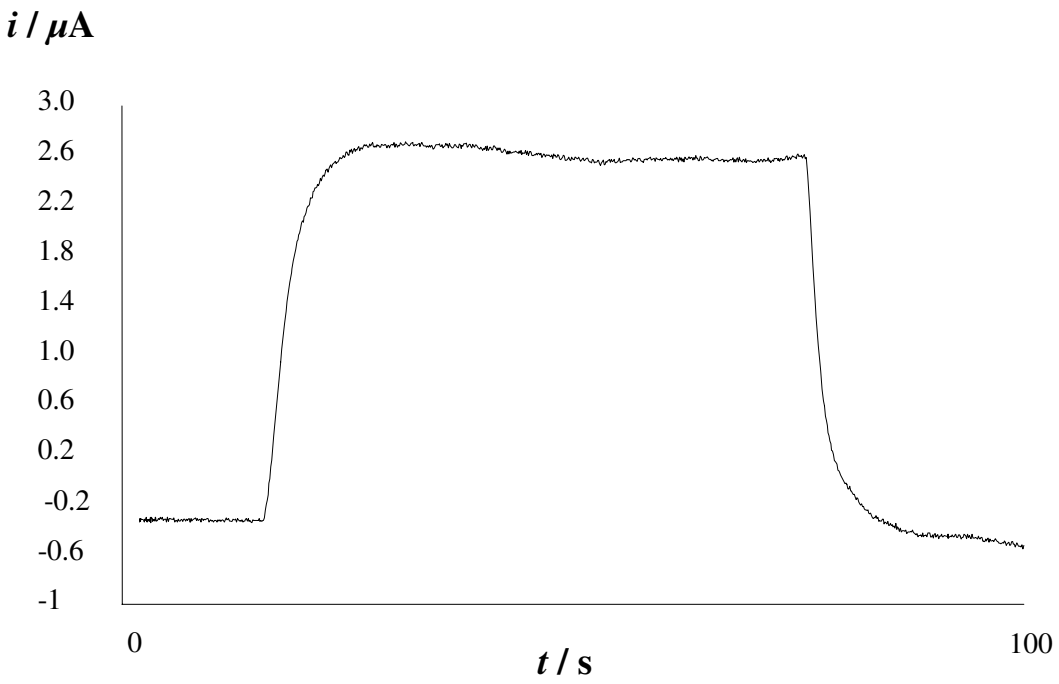

Figure 4.3.4: Influence of light (60 W tungsten visible household bulb) on the current of a cell (10 mM FA in aqueous 0.1 M KCl) with a TiO_2 coated CI anode and a 3.1 % CoPc coated CI cathode in a one compartment cell, electrode areas = 3 cm^2

4.3.3 Influence of pH on current

A dilute solution of sodium hydroxide was prepared and added dropwise to the 10 mM solution of FA and stirred before transients were recorded. Figure 4.3.5 shows the influence of pH on current transients achieved. The current decreases with increasing pH, which increases the amount of formate while lessening the acid concentrations. It should be remembered that these processes are spontaneous.

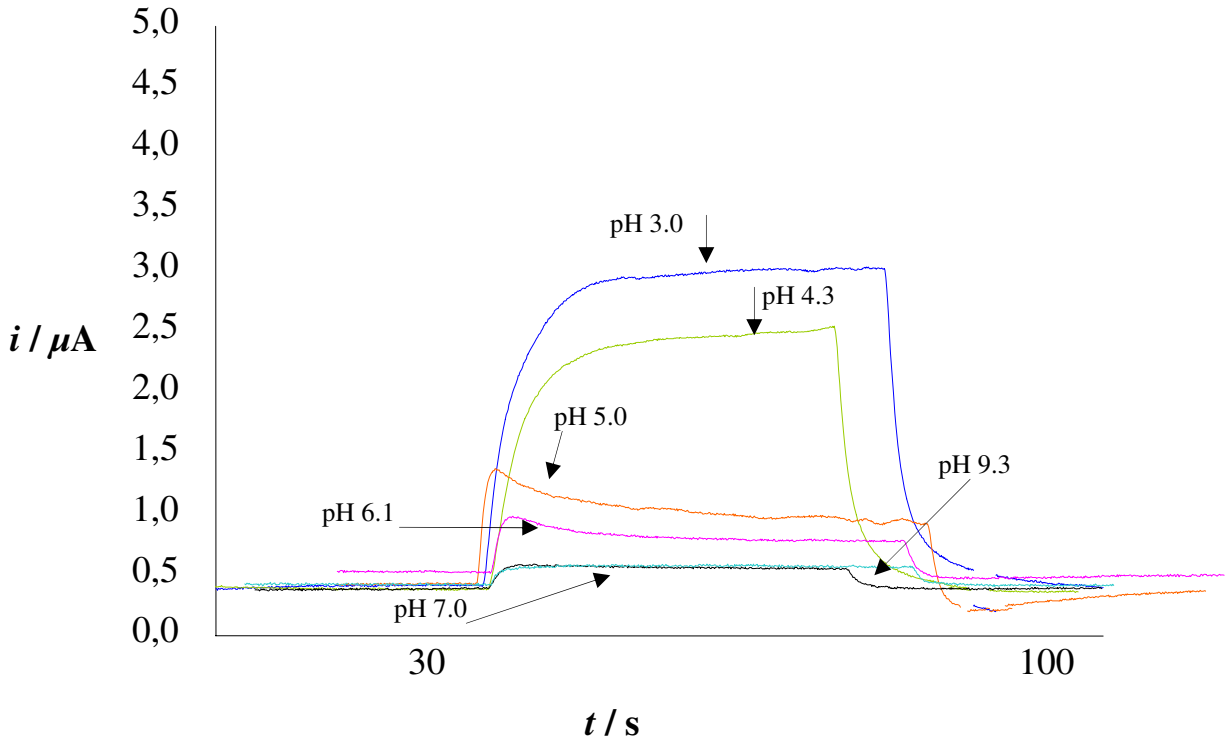

Figure 4.3.5 (a): Influence of pH on the current of a cell (10 mM FA in aqueous 0.1 M KCl) with a TiO_2 coated CI anode and a 3.1 % CoPc coated CI cathode, 60 W tungsten visible incandescent household bulb, electrode area = 3 cm^2

Figure 4.3.5 (a) shows that FA adsorbs strongly onto TiO_2, which is consistent with what was found by Villarreal *et al* [16]. This data is plotted in figure 4.3.5 (b).

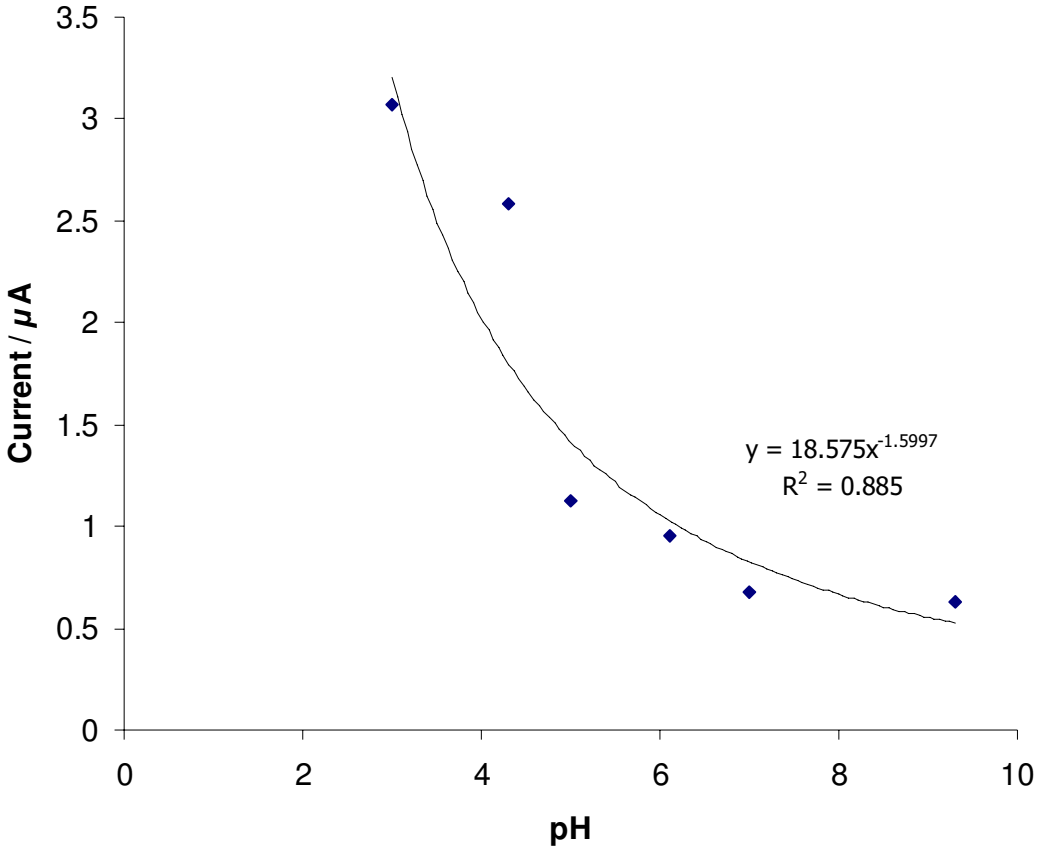

Figure 4.3.5 (b): Influence of pH on the current of a cell (10 mM FA in aqueous 0.1 M KCl) with a TiO_2 coated CI anode and a 3.1 % CoPc coated CI cathode, 60 W tungsten visible incandescent household bulb, electrode area = 3 cm^2

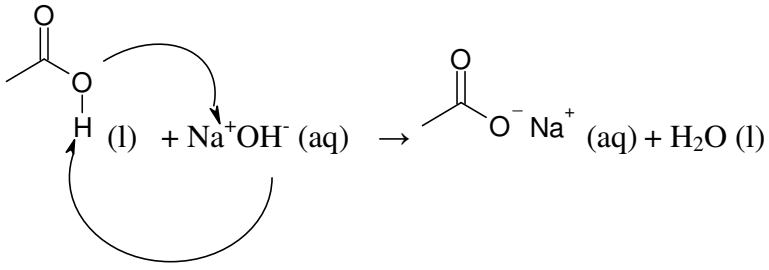

Figure 4.3.6: Mechanism of representation of the neutralisation of FA

As the pH increases, more formate is created. As can be seen in the two previous figures, in acidic conditions FA adsorbs quite well to TiO_2. But in alkaline solution, the formate anion finds it difficult to attach to the negatively charged TiO_2 surface, for electrostatic reasons.

In recent work it was found that when near UV light is shone on TiO_2 when oxidising formate, the efficiency peaks at around pH 5 – 6 [17]. Formate repels the negatively charged TiO_2 surface at more neutral pH, while in acidic conditions adsorption of formate to the catalyst is lessened as TiO_2 agglomerates at low pH.

4.3.4 Electrode stability

A one compartment cell consisting of a TiO_2 coated CI anode along with a 3.1% CoPc on CI cathode was constructed. Both WE and CE had an area of 6 cm^2. With a FA concentration of 0.1 M and a 60 W tungsten light source, the cell was placed in a black box to prevent interference from daylight. It can be seen from figure 4.3.7 that the current is stable over this period of time, and this is evidence of the high quality of the fabricated electrodes.

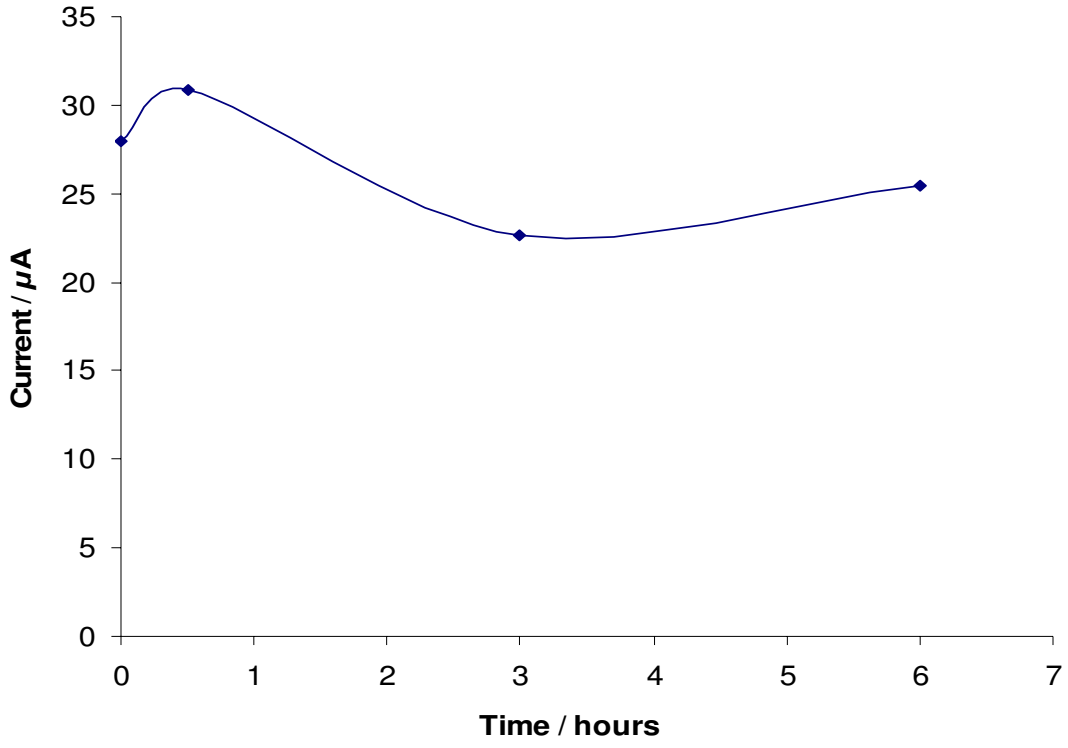

Figure 4.3.7: Variation of current response over time for a one compartment photoelectrochemical cell containing 0.1 M FA, 60 W tungsten visible household light bulb.

4.3.5 Degradation of organics using simulated solar light

With the Q Sun instrument, summer daylight conditions can be achieved and accurately reproduced. So in many ways it is better than daylight as a light source given its reproducibility.

Figure 4.3.8: Q Sun test chamber

Cells were placed in series or parallel in order to investigate if there was an enhancement of current when the positioning of the electrodes was switched. Five different arrangements were constructed as shown earlier in figures 4.2.5 - 9. Section 4.2.3.6 detailed the experimental set up. In order to increase the voltage or currents of the cell, two TiO_2 electrodes and two CoPc electrodes were placed in series or parallel. These experiments were run in the Q-Sun testing chamber. Typically the electrodes for the fuel cell had nominal areas of 3 cm^2. The substrate used for the cells was FA (1 M), a Petri dish was used as a cell and the electrodes were placed facing upward towards the light. Tables 4.3.1 - 3 detail some of the results.

Table 4.3.1: Current and voltage responses for both one and two compartment photoelectrochemical cells containing 1 M FA in different configurations, Q Sun light source. Anode and cathode areas were 3 cm^2. Measurements were also made in dark conditions.

Cell configuration	One compartment cell *(Figure 4.2.4)*	One compartment cell in series *(Figure 4.2.5)*	One compartment cell in parallel *(Figure 4.2.6)*	Two compartment cell in series *(Figure 4.2.7)*	Two compartment cell in parallel *(Figure 4.2.8)*
i / μA, dark	0.2	0.2	0.1	0.1	0.2
i / μA, light	33.1	31.2	71.5	27.1	53.5
E / V, dark	0.056	0.056	0.027	0.077	0.072
E / V, light	0.646	0.726	0.606	1.241	0.627

Table 4.3.2: Current and voltage responses for both one and two compartment photoelectrochemical cells containing 1 M FA in different configurations, Q Sun light source. Anode and cathode areas were 6 cm^2. Measurements were also made in dark conditions.

Cell configuration	One compartment cell *(Figure 4.2.4)*	Two compartment cell in series *(Figure 4.2.7)*	Two compartment cell in parallel *(Figure 4.2.8)*
i / μA, dark	0.3	0.1	0.5
i / μA, light	38.6	58.5	79.4
E / V, dark	0.119	0.053	0.044
E / V, light	0.727	1.435	0.713

Current increases but open circuit potential remains the same when electrodes are in parallel with each other. The one compartment cell in parallel is probably the best set up, as it gives twice the current of any other system examined here, and at a lower potential. When the area of both electrodes was 6 cm^2 in series, the potential is 1.435 V which is not far from to the 1.5 V required for recharging a normal household rechargeable battery.

When you double the electrode area:

1. Dark potential triples for a one compartment cell
2. Current doubles for a two compartment cell in series

As power is the product of current and voltage and as all electrode areas were known, power density values were calculated and these are displayed in table 4.3.3.

Table 4.3.3: Power density values for both one and two compartment photoelectrochemical cells containing 1 M FA in different configurations, Q Sun light source.

Cell Configuration	Electrode area / cm^2	Power density / mW m^{-2}
One compartment cell	3	66
One compartment cell in series	3	38
One compartment cell in parallel	3	72
Two compartment cell in series	3	56
Two compartment cell in parallel	3	55
One compartment cell	6	47
Two compartment cell in series	6	84
Two compartment cell in parallel	6	94

For producing the optimum power density, it is best that the electrodes are placed in parallel.

4.3.6 Two compartment cells

O_2 can be reduced at TiO_2 on CI electrodes and can also be reduced at a CoPc on CI electrode, both at – 0.6 V (Vs MSE). So an experiment was set up whereby two TiO_2 on CI electrodes were placed in the cell, and again transients were measured by Pico Technology data logging. This experiment was run in a two compartment cell that prevents the mixing of the two solutions but permits the passage of ions between the two compartments.

To be able to compare the results in a two compartment cell with the results in a single compartment cell, the test was firstly run with the two electrodes (either both TiO_2 on CI or else one of these along with a CoPc on CI electrode) in compartment A

and secondly with one electrode in each compartment. So four situations were covered in total and the cathode varied each time along with whether it was a single or two compartment cell. The electrodes in the twin cell were of the same area.

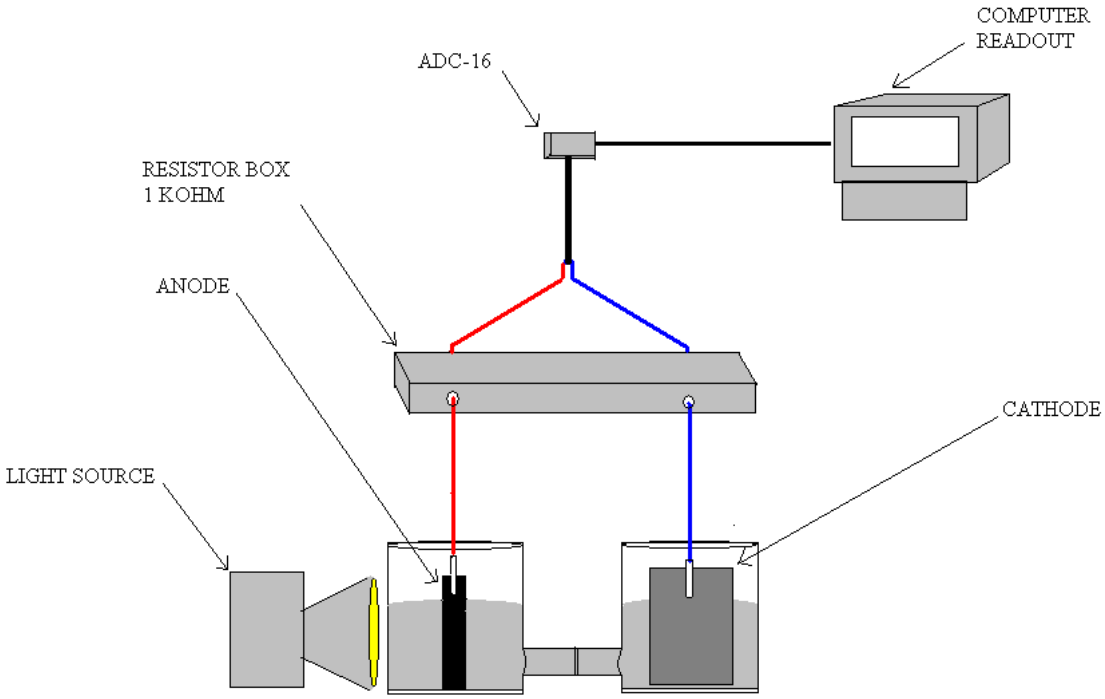

Figure 4.3.9: Block diagram of the experimental set up in a two compartment cell (10 mM FA in aqueous 0.1 M KCl). TiO_2 coated CI anode and either the same cathode or else a 3.1 % w/w CoPc coated CI cathode, 60 W tungsten visible incandescent household light bulb. All electrode areas were equal (3 cm^2).

Some of the results achieved using different configurations of the twin cell are described in figure 4.3.10.

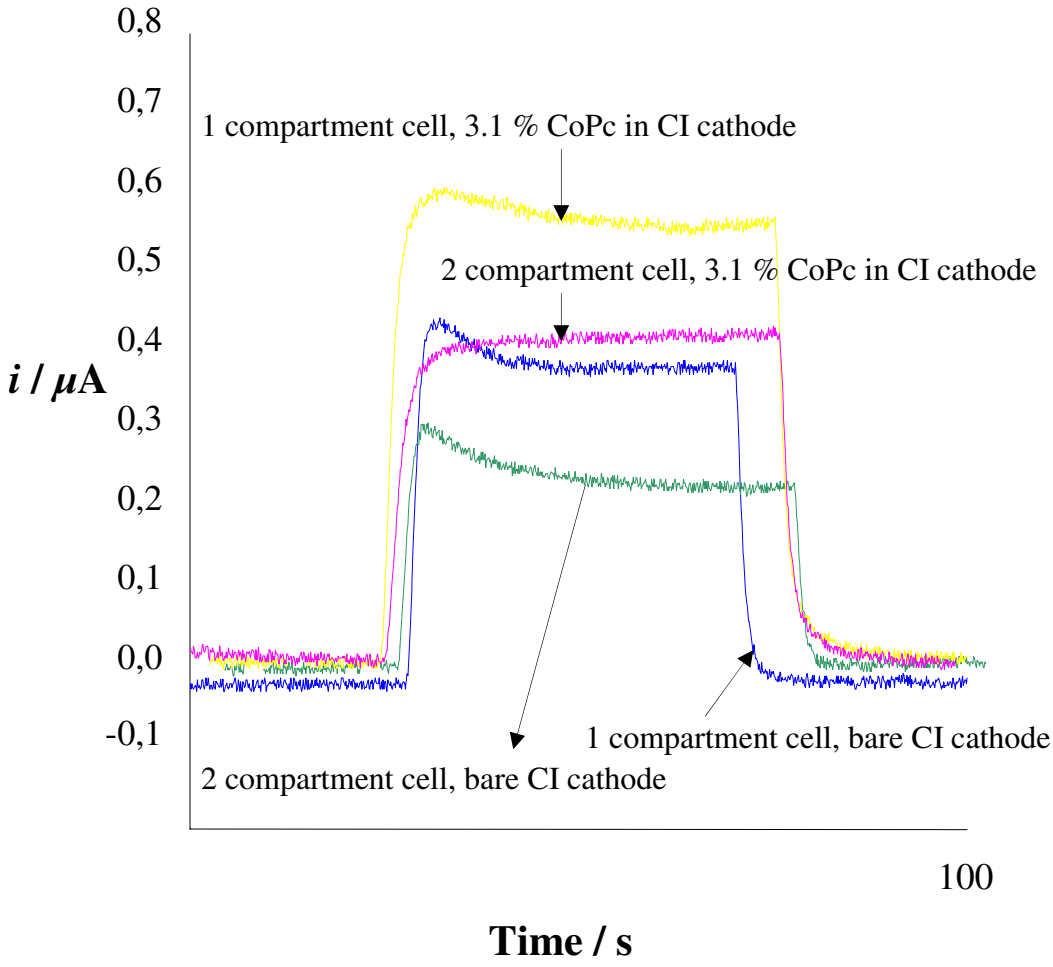

Figure 4.3.10: Comparison of the current transients received from a number of fuel cells, some with two compartments and some single compartment. 10 mM FA was the substrate in aqueous 0.1 M KCl. TiO_2 coated CI anode in all cases and either the same cathode or else a 3.1 % w/w CoPc coated CI cathode, 60 W tungsten visible incandescent household light bulb. All electrode areas were equal (3 cm^2). Resistance = 100 kΩ.

In all cases for a single compartment cell, the current is higher than for its double compartment counterpart. This shows that single compartment cells are a better configuration. In a two compartment cell, the frit between the two compartments introduces a resistance which reduces the current. When the lamp shines on the TiO_2 coated CI anode, electrons are created from the oxidation of formic acid. Also, a much better fuel cell is produced when a 3.1 % CoPc in CI cathode is used instead of a bare CI one.

In figure 4.3.11 the relationship between concentration of FA and the current produced is evaluated. There is a dramatic increase in current from zero current when the cell is exposed to light.

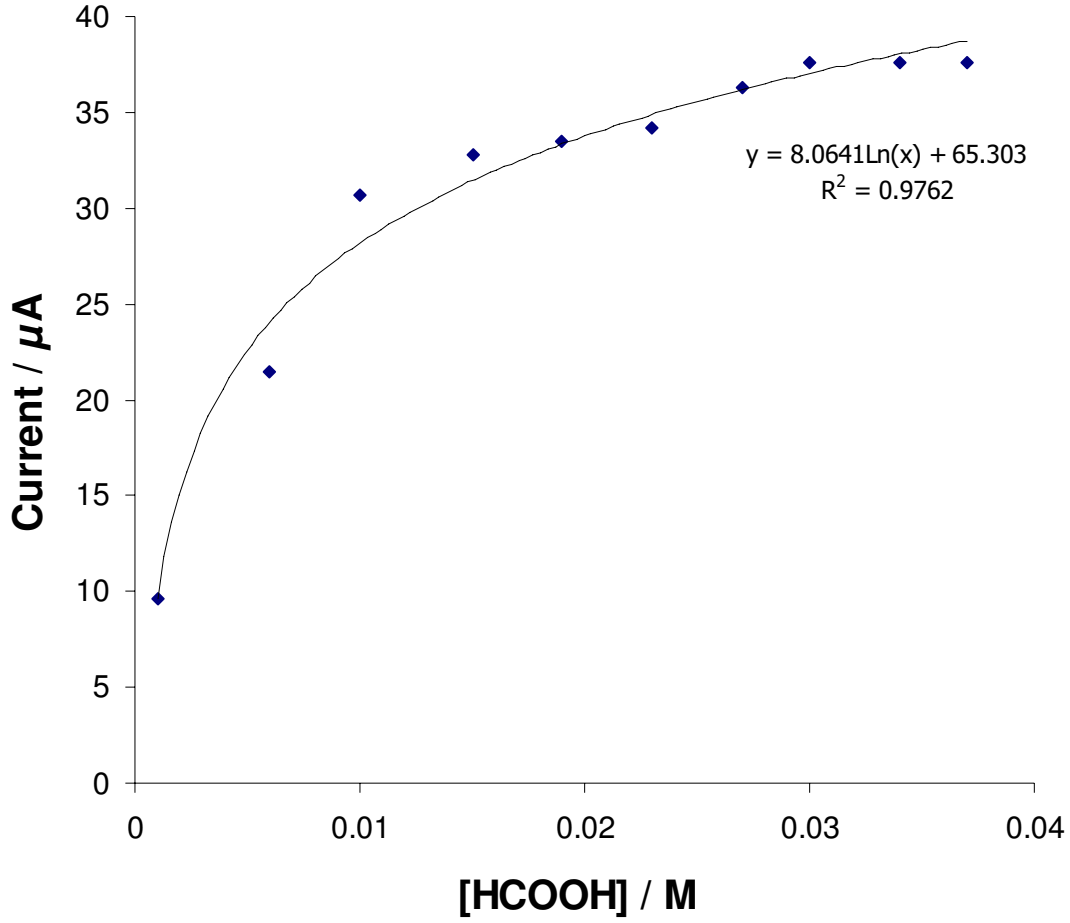

Figure 4.3.11: Influence of degradation of FA on the current recorded using solar simulated light from the Q-sun machine. The machine was operated at maximum irradiance (0.68 W m^{-2} at 340 nm). FA in 0.1 M KCl was used as the substrate in a one compartment cell, TiO_2 on CI anode, 3.1 % w/w CoPc on CI cathode. Both electrode areas were 1 cm^2.

As can be seen in figure 4.3.11, there is not a linear relation between the concentration of FA and the current produced, as the latter levels off at higher concentrations of FA. The current obtained in the Q-sun testing chamber is higher than the current obtained using a 60 W tungsten lamp.

FA is a molecule that is easily decomposed, however in waste water there are many long chained molecules that are not so easy to decompose. In order to investigate if the photoelectrochemical cell is able to decompose more complicated molecules, FA was replaced by starch, a polysaccharide and complex carbohydrate which is often a component in waste water streams and again the current was measured using transient techniques. The results are displayed in figure 4.3.12.

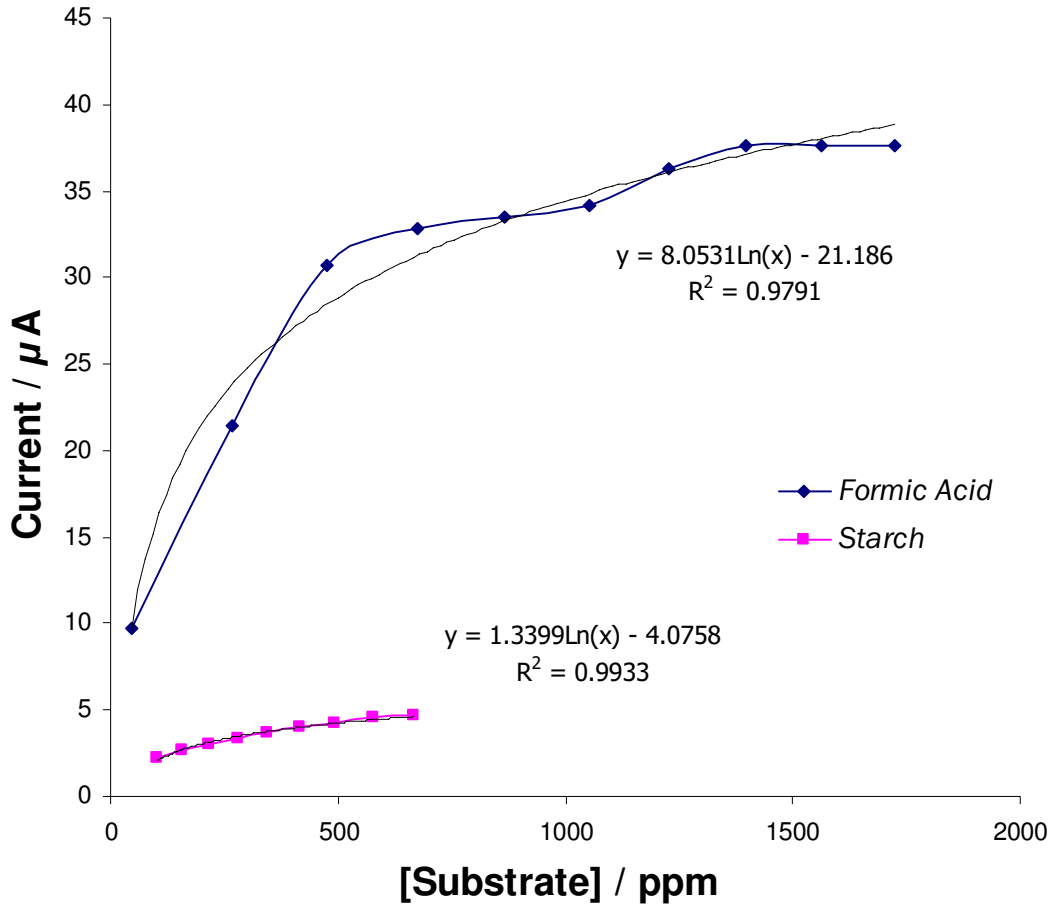

Figure 4.3.12: Influence of degradation of starch on the current recorded using solar simulated light from a Q-sun machine. The machine was operated at maximum irradiance (0.68 W m^{-2} at 340 nm). Starch in 0.1 M KCl was used as the substrate in a one compartment cell, TiO_2 on CI anode, 3.1 % w/w CoPc on CI cathode. Both electrode areas were 1 cm^2.

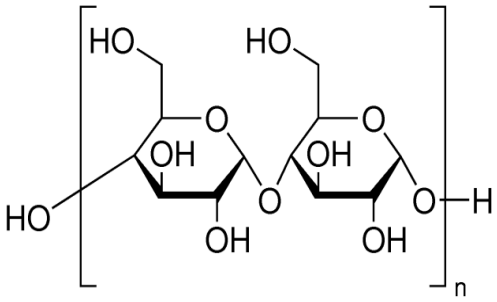

Figure 4.3.13: Chemical structure of starch.

When comparing figure 4.3.11 with figure 4.3.12, one can see that the current obtained for the starch is much smaller. But there is some current, so that means that the cell is also able to decompose long chained molecules that are hard to decompose. The two are overlayed in figure 4.3.14.

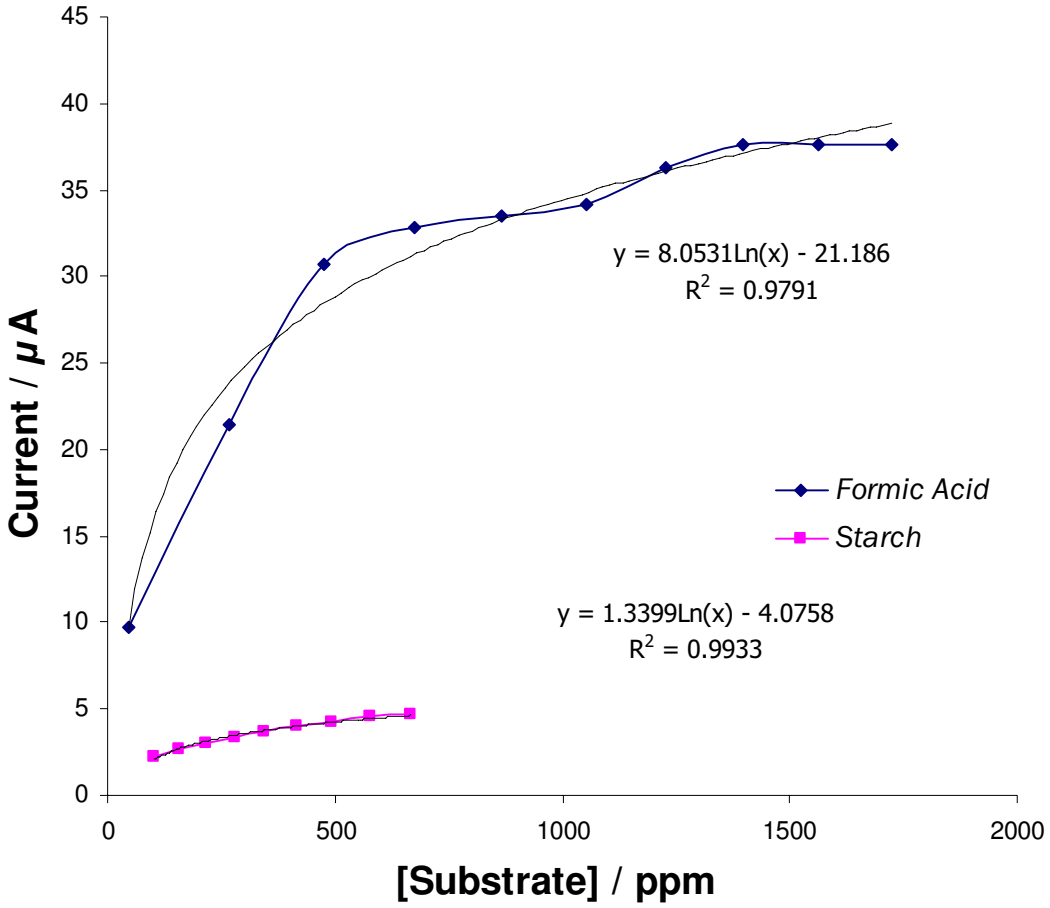

Figure 4.3.14: Figures 4.3.11 and 12 overlayed. This time concentration is expressed as ppm for both organics.

4.4 Conclusion

In this work it was demonstrated that:

- Current may be obtained from flexible, planar electrodes
- Current increases with increasing concentration of substrate
- Photoelectrochemical cells can be combined in series or parallel; so in this respect they behave like batteries
- Photoelectrochemical cells can operate very well under ambient conditions with the assistance of simulated solar irradiation due to TiO_2 photocatalysis
- Such cells can only operate to a small extent in the dark
- Cells can operate successfully for a number of hours continuously without any major decrease in quality or power output
- When FA is the substrate, there is an increase in current with increasing acidity
- Current increases, not linearly however, with increasing concentration of FA or starch

Far more organic compounds can be digested in such photoelectrochemical cells. However, there is a limited concentration of oxygen in aqueous solutions, determined by its solubility in water (around 9 mg L^{-1}). To allow a practical device, using wastewater with low oxygen content and high COD, a different cathode is required, which are provided by air electrodes. These are used in the next chapter and can use atmospheric oxygen and make use of the far more abundant supply of oxygen in the atmosphere (around 21 %).

4.5 References

[1] S. Srinivasan, *Journal of the Electrochemical Society*, **136**, (1989), 41 C

[2] R.W. Matthews, *Journal of the Chemical Society Faraday Transactions*, **80**, (1984), 457

[3] C.S. Turchi, D.F. Ollis, *Journal of Catalysis*, **122**, (1990), 178

[4] M. Gratzel, J.K. Thomas, *Journal of the American Chemical Society*, **95** (1973), 6885

[5] W.E. Ford, J.W. Otvos, M. Calvin, *Nature*, **273** (1978), 507

[6] M. Calvin, *Acc. Chem. Res*, **11** (1978), 369

[7] E. Yesodharan, M. Gratzel, *Helv. Chim. Acta*, **64** (1981), 362

[8] K. Kalyanasandaram, E. Borgarello, M. Gratzel, *Helv. Chim. Acta*, **64** (1981), 362

[9] Y. Zhang, J.C. Critterden, D.W. Hand, *Chem. Industry*, (1994), 714

[10] S. Malato, J. Blanco, A. Vidal, C. Richter, *Applied Catálisis B: Environmental*, **37**, (2002), 1

[11] C. Nasr, K. Vinodgopal, L. Fisher, S. Hotchandani, A.K. Chattopadhyay, P.V. Kamat, *Journal of Physical Chemistry*, **100**, (1996), 8436

[12] E.F. Duffy, F. Touati, S.C. Kehoe, O.A. McLoughlin, L. Gill, W. Gernjak, I. Oller, M.I. Maldonado, S. Malato, J. Cassidy, R.H. Reed, K.G. McGuigan, *Solar Energy*, **77** (2004) 649-655

[13] D. J. G. Ives, G. J. Janz, "The Calomel Electrode and Other Mercury-Mercuorous Salt Electrodes" in *Reference Electrodes – Theory & Practice*, Volume 1, D. J. G. Ives & G. J. Janz, ed., Academic Press, New York & London, 1961, 160

[14] M. Grätzel, Heterogeneous Photochemical Electron Transfer, CRC Press: Baton Rouge, FL, (1988)

[15] http://www.q-panel.com/html/q-sun.html, date accessed 21/10/08

[16] T.L. Villarreal, R. Gomez, M. Neumann-Spallart, N. Alonso-Vante, P. Salvador, *Journal of Physical Chemistry B*, **108** (2004) 15172 - 15181

[17] J.M. Monteagudo, A. Durán, J. Guerra, F. Garcia-Peña, P. Coca, *Chemosphere*, **71** (2008) 161 – 167

Chapter 5

Degradation of organic compounds using visible light

Chapter 5 – Degradation of organics using visible light

5.1 Introduction

5.1.1 Organic wastes in water

From an aquatic point of view, there is a need to de-toxify organic waste, break down these molecules and convert them to less harmful ones and possibly convert them into a different phase. Many organics are toxic to ecosystems in water.

The behaviour of organic compounds is dependent upon their molecular structure, size, shape and the presence of functional groups that are important determinants of toxicity. It is important to know the structure of organic compounds, in order to predict their fate in living organisms and the environment. There are many different types of organic pollutants that can be persistent in water, often due to their use in industry.

5.1.1.1 Detergents

Detergents are very harmful for the environment. Soaps for washing contain a non – polar hydrocarbon end to dissolve the grease and dirt, and the molecule is made water soluble by the addition of a polar group at the end (figure 5.1.1). These are commonly known as surfactants, or surface acting agents as they lessen the surface tension of water. But the composition of detergents is not as simple as this.

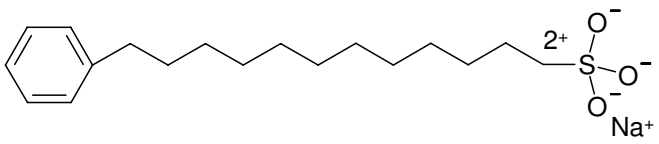

Figure 5.1.1: Sodium dodecylbenzenesulphonate, a typical surfactant used in detergents. The molecule is mainly lipophylic but is made water soluble by the presence of the polar sulphonate group at the end.

Detergents contain a large number of additives, many of which are harmful for the environment. Surfactants (figure 5.1.1) are often a necessity in detergents. Antiseptic items like phenols have been used to kill bacteria off clothes. Hard water (water naturally containing a large number of minerals such as calcium and magnesium) became a problem in the detergent industry as such ions bound to surfactants to leave a scum present on clothes. This is evident when 'bath rings' form. To counteract this, manufacturers added phosphates to their detergents (to bind Ca^{2+} and Mg^{2+}). An oversupply of phosphate (also used in agricultural fertilisers) in water can lead to algal blooms which deplete dissolved oxygen levels within the water, destroying the water's ecosystem.

Even many phosphate – free detergents are harmful. Some of them contain alkyl phenols which are oestrogen mimics that can have serious detrimental effects on populations of aquatic animals, such as decreasing their ability to reproduce [1]**.** Other softeners include zeolites and EDTA. Detergents are made more acidic for descaling, or caustic may be added to break down organics. Both of these processes alter water pH. Abrasives are added to loosen up dirt and enzymes are added to break up foodstuffs.

Dyes, optical brighteners such as coumarins and azoles, fabric softeners, colors, and perfumes are also present in many detergents. Many of these are used to create a perceived "whitening" effect, making materials look less yellow by increasing the overall amount of blue light reflected. The clothing industry is often guilty of releasing many dyes into rivers. Solar - activated aqueous suspensions of TiO_2 have been used to decolourise and mineralise many commercial dyes used in the clothing industry [2].

5.1.1.2 Sewage treatment

When an organic polluting load is discharged into a river it is gradually eliminated by the activities of micro organisms in a way very similar to the processes in the sewage treatment works [3]. This self-purification requires sufficient concentrations of oxygen, and involves the breakdown of complex organic molecules into simple inorganic molecules. Dilution, sedimentation and sunlight also play a part in the process.

Organic effluents also frequently contain large quantities of suspended solids which reduce the light available for photosynthetic organisms. When these suspended solids settle out, the characteristics of the river bed are altered, rendering it an unsuitable habitat for many invertebrates. Toxic ammonia is often present.

5.1.1.3 Presence of chlorinated organics

Some man made chemicals synthesised are not only harmful for the environment but they persist for a long time due to their stability. Polychlorinated biphenyls (PCB's, figure 5.1.2) are examples of such chemicals. PCBs were mainly synthesised to be used in the electrical industry as coolants and insulating fluids for transformers and capacitors and as stabilizing additives in flexible PVC coatings of electrical wiring and electronic components.

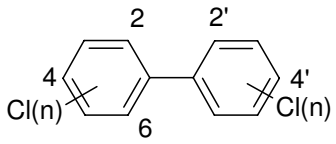

Figure 5.1.2: General structure and numbering system of a PCB

Other reasons why they were created were to be used as flame retardants, hydraulic fluids, sealants (used in caulking, etc) and in adhesives. Production blossomed because everyone assumed that these compounds were harmless. Less than a nanogram of a typical PCB such as Aroclor 1260 (a sticky yellow resin) will dissolve in a litre of water. Not only are they insoluble in water, but extremely resistant to most known chemical reactions such as oxidation, reduction, addition, elimination, and electrophilic aromatic substitution. Due to their lack of water solubility, they dissolve in the skin of most animals, and this has been a cause of many bird and fish kills. In the US, General Electric released 600 tonnes of PCBs into the Hudson river over a 30 year period. Studies have shown that they cause liver cancer in mammals [4 - 9]. In fact they have been found in the atmosphere, soil and water all over the world even in the most remote areas. PCBs are classified as persistent organic pollutants which bioaccumulate in animals' fatty tissues and then enter the food chain.

Due to their lack of reactivity; breaking down, removal and clean up of PCBs is a very difficult operation. There is the risk of creating extremely toxic dibenzodioxins and dibenzofurans through partial oxidation. Incineration in the presence of excess fuel and oxygen is an option, but if there is a lack of oxygen present the intermediates such as the latter two compounds may form due to incomplete combustion. One of the best ways to degrade such harmful compounds is through the use of TiO_2 photocatalysis.

5.1.2 Degradation of organics

There has been much work done worldwide on clean up of organic and biological wastes in water using TiO_2 irradiated with visible or UVA light. The percentage viability

of *Escherichia coli* was reduced to < 5 % within a half an hour using TiO_2 enhanced by daylight in sun kissed areas [10]. A similar type of solar photocatalysis was also used to lessen the COD (from 85 % to 20 % in three hours) of wastewater from olive mills in Portugal and Spain [11]. *P*-nitrophenol concentrations were decreased from 55 ppm to < 5 ppm in an hour using a low intensity 18 W UV lamp (300 μW cm^{-2}, 30 % UVA, 5 % UVB) [12].

TiO_2 photocatalysis has found use in the removal of trace organics from water [13]. Many compounds from the pharmaceutical industry, such as hormones, preservatives and anaesthetics have been identified in drinking water and have been traditionally treated by ozonolysis [14]. Reyes *et al* found a 40 % removal of the antibiotic tetracycline using a Philips 160 W black light (λ_{max} = 365 nm), and a 100 % degradation of the water soluble four - fused - rings containing compound was achieved with a commercial solarium used for cosmetic treatment (6 × 20 W lamps) [15]. Both experiments were effective in removing the organic within an hour.

Tamoxifen concentrations were decreased by 15 ppm in 15 minutes and Gemfibrozil dropped from 50 ppm to 5 ppm in 2 hours using a medium pressure 125 W Hg lamp peaking at 360 nm in the presence of TiO_2 [16]. Both pharmaceuticals have been found in mud and soil samples at the outlet of water treatment plants. Using the same make and model lamp to irradiate TiO_2, Coleman *et al* managed to halve the estrogenic efficiency of steroids within 10 minutes [17].

Aside from such complex and industry–specific molecules, normal reagents and common solvents have been degraded using TiO_2 and UVA light or natural sunlight. Formic acid was oxidised using an annealed coated ITO soda lime anode irradiated by a

Philips 18 W UVA lamp, and the electrons produced were put to good use where they reduced cupric sulphate to copper metal [18]. The very stable polar aprotic solvent acetonitrile was mineralised as a function of sunlight intensity in the Mediterranean again using TiO_2 [19]. Recent work has seen anionic textile dyes like erythrosine decolourised in solution with a low pressure 125 W Hg lamp [20].

5.1.3 Photolytic degradation of chlorinated aromatics

Titanium dioxide suspensions have been employed for mineralisation of organic species such as chlorobenzoic acid by photolytic degradation [21], while immobilised layers have been used to remove paraquat from aqueous solutions [22]. Coupling of TiO_2 coatings in electrochemical cells by Vinodgopal *et al* (1993, 1994) [23, 24] involved three electrode cells to enhance the oxidation of the stable 4 – chlorophenol (4CP). Alhakimi *et al* compared the use of natural and artificial UV light on the degradation of 4CP, and found that sunlight gave 6 times better degradation than a Phillips 100 W Hg lamp [25]. Using a 75 W Hg high pressure lamp with a low irradiance of less than 1 mW cm^{-2}, Horikoshi *et al* monitored the influence of halide addition on 4CP degradation by FT-IR [26].

Halides have also been oxidised using light activated TiO_2, including iodide [27] and bromide [28]. More simple halogenated aromatics like TCMs and dichloromethane have been broken down using daylight assisted photocatalysis of TiO_2 in a homogenised suspension [29].

5.1.4 Photolytic degradation of 2-propanol (IPA)

As IPA has been previously reported to degrade to acetone [30], it was decided to investigate this further. Using a 150 W Xe lamp (100 mW cm^{-2}) to irradiate TiO_2 immobilised onto acetate sheets, Duffy *et al* found a complete degradation of 100 ppm IPA within 24 hours of irradiation and a corresponding increase in acetone levels [31].

In this work common solvents like 2-propanol (IPA) were degraded using UVA light and TiO_2. In recent work at a surface confined TiO_2 layer, acetone (ACE) was photodegraded [32]. During ACE photoxidation, the progress was followed by GCMS and the workers found bigger molecules in the effluents such as IPA, mesityl oxide (from the self-aldol condensation of acetone), diacetone alcohol, methyl ethyl ketone, acetic acid, acetaldehyde and ethyl acetate.

5.1.5 Photolytic degradation of phenols and their derivatives

TiO_2 was annealed and immobilised by different methods on electrodes and irradiated with a 150 W Xe lamp for phenol remediation [33]. Degradation of phenols in aqueous suspensions in the presence of oxygen can often yield the disinfection by-product precursor catechol [34], and Tryba *et al* found that as this phenol oxidation happened in the TiO_2 suspension, increasing amounts of catechol, hydroquinone and benzoquinone were formed [35].

However the presence of catechol as a disinfection by product in water (resulting from humic acid degradation) may not necessarily be a bad thing. Using TiO_2 irradiated by solar simulated light (80 mW cm^{-2}), Rincon *et al* were able to show a correlation of the photoreactivity of dihydroxybenzene isomers and photocatalytic *E. coli* disinfection [36], and hypothesised that the reason for the toxic effect on *E. coli* was because of the

high concentrations (2 mM) of the aromatics. Benzaldehyde (Bz), along with similar aromatics like potassium hydrogen phthalate and ascorbic acid are degraded in a similar fashion and are presented in this chapter.

5.1.6 Photoelectrochemical cell design

Frequently in electrochemical experiments, counter electrodes are placed in a compartment separated from the rest of the solution often by a porous frit. One of the reasons for this is to avoid contamination of products and ions arising from the reaction that is happening at the working electrode. If the reaction happening at the working electrode (WE) is oxidation of an organic compound, it is possible to use a different compartment for the cathodic reaction (O_2 reduction) if the products of O_2 reduction interfered with oxidation of the organic compound.

The protons donated from protic solvents (water in this work) can react with electrochemical intermediates such as radical anions. So use of water as the solvent can stabilise any intermediates involved in O_2 reduction.

5.1.7 The aim of this work

In this work simple alcohols, chlorinated aromatics, dihydroxybenzenes and diesterifiedbenzenes were placed in different arrangements of a photoelectrochemical cell, all containing TiO_2 immobilised on a surface modified electrode. Such compounds were all degraded using a variety or light sources and experimental conditions.

5.2 Experimental

5.2.1 Materials

- De-ionised water (l)
- Potassium chloride (s, KCl, Merck, 99.5+ %)
- TiO_2 (s, TITANDIOXID P-25, Degussa AG GB AC D-60287 Frankfurt), BET specific surface area = 50 m^2 g^{-1}, 80 % anatase, 20 % rutile
- Methanol (l, MeOH, Aldrich, 99+ %)
- Tetrahydrofuran (l, THF, Fluka, ≥ 99.5 %)
- Electrodag 423 SS Graphite-based P.T.F Ink (s, CI, Acheson Colloids, 1600 Washington Avenue Port Huron , Michigan 48060 USA)
- Type J colour inkjet transparencies removable stripe (Xerox)
- Cube applicator
- Two compartment (twin) electrochemical cell
- Air electrode made from a sheet of MnO_2/carbon paper/Ni mesh/Teflon dispersion [37] (produced by Electro-Chem-Technic)
- Potassium hydrogen phthalate (s, KHP, SigmaUltra, ≥ 99.95 %)
- Ascorbic acid (s, AA, SigmaUltra, ≥ 99.0 %)
- Benzaldehyde (s, Bz, Aldrich ReagentPlus®, ≥99 %)
- 2-propanol (l, IPA, Aldrich, ≥99 %)
- Acetone (l, ACE, Aldrich, 99.5 %)
- 2-butanol (l, IBA, Aldrich, 99 %)
- Pyrocatechol (s, CAT, Sigma-Aldrich, 99 %)
- 4-chlorophenol (s, 4CP, Fluka puriss., ≥ 99.0 % (GC))

5.2.2 *Equipment*

- Platinised titanium sheet (approx area = 20 cm^2)
- Carbon ink working electrode coated with TiO_2 (CI/TiO_2, Acheson/Degussa, area = 25 cm^2)
- 60 W tungsten incandescent standard household light bulb
- Mastech M-830B voltmeter
- Pico Technology (Cambridgeshire, UK) data acquirer with an ADC 16 analog to digital converter.
- Shimadzu GC-8A linked to a Shimadzu Chromatopac C-R8A chart recorder
- Shimadzu UV-160 spectrophotometer
- Photochemical Reactors Ltd 400 W Hg medium pressure lamp type PW 135 powered by a Photochemical Reactors Ltd 3140 source, peak emission at 365 nm
- Oriel 6253 150 W Xe arc lamp powered by an Oriel 69907 source with a peak emission at 850 nm
- Ocean Optics software linked to CPU with P – 100 - 2 UV/Vis 100 μm optical fibre, USB2G15808 spectrometer

5.2.3 *Methodology*

5.2.3.1 Electrode preparation

Details of how CI anodes were made were listed in 4.2.3.1.When dry, 25.0 cm^2 areas along with a 5 cm × 1 cm attachment were drawn off with a pencil and cut out of

the acetate sheets with a scissors (figure 5.2.1). Drying was important, and only electrodes with no dust spots or voids in their conduction pathways were used.

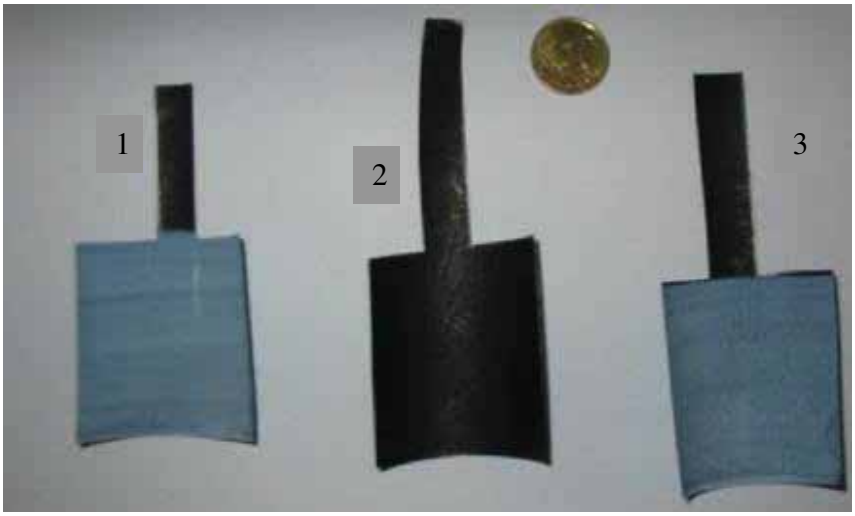

Figure 5.2.1: Working anodes used. All are made from CI coated onto acetate sheets and dried at room temperature. Electrical connection was via the 'tail' to allow a working area of 25 cm^2. Electrode number 2 is bare. Electrodes 1 and 3 were dip coated in a TiO_2 suspension.

2 g of TiO_2 (Degussa P-25), 35 mg of poly (4- vinyl-pyridine) (PVP) and 35 mg of polyvinylchloride were suspended in 50 ml of MeOH and 50 ml of THF and placed in a 100 ml volumetric flask. Once the carbon ink was dry, anodes were dip coated (by hand) into a 100 ml beaker of a THF suspension of TiO_2.

A reasonably reproducible method of dip coating was followed. A 100 ml volumetric flask containing TiO_2 was shaken and poured into a 100 ml beaker. Anodes were dip coated in such a way that would allow 25 cm^2 areas to be coated at an approximate rate of 24 mm per second into the beaker, and withdrawn at the same rate. This is a fast rate of dip coating and leads to a thicker layer than if the dip coating had been done slowly. These were then left to dry at room temperature overnight and a

second coating was applied the following day in the same manner and a third coating the day after that.

The resistance of many bare CI electrodes were measured using a Mastech M-830B voltmeter. One crocodile clip was attached to one end of the electrode and its corresponding one to the other. This formed a 5 cm circuit. The results are tabulated in table 5.2.1.

Table 5.2.1: Resistance & average conductivity of CI electrodes

R / Ω	R / Ω	R / Ω	R / Ω	R / Ω	Average Resistance / Ω	10^3 Average Conductivity / Ω^{-1}
67.6	47.8	65.4	45.2	53.9	60.8	16.4
82.3	105.8	115.9	90.7	55.4		
80.7	54.7	42.1	53.6	62.6		
87.2	57.5	63.2	56.8	66.2		
63.2	66.2	64.5	50.2	55.9		
60.8	55.6	68.5	52.3	56.7		
51.3	46.2	34.9	44.7	52.0		
56.9	52.7	51.4	39.5	38.1		
39.3	69.2	68.2	88.2	55.7		

As can be seen, resistance of the electrodes is quite small and so this leads to a conducting electrode. Resistances of CI anodes that were dip coated in the TiO_2 suspension were also measured when dried. These results are presented in table 5.2.2.

Table 5.2.2: Resistance & average conductivity of CI electrodes coated with TiO_2

R / Ω	R / Ω	R / Ω	R / Ω	R / Ω	Average Resistance / Ω	Average Conductivity / × 10^{-3} Ω^{-1}
82.3	105.8	115.9	90.7	55.4	98.9	10.1
57.4	166.7	168.2	87.8	68.2		

As can be seen from table 5.2.2, coating the CI electrodes with TiO_2 slightly decreases their conductivity. This is because TiO_2 is essentially an insulator (until activated by light).

5.2.3.2 Cell arrangements

5.2.3.2.1 Two compartment (twin) cell

The diagram below shows the setup of the two compartment photo-assisted fuel cell employed in this work. In this arrangement a two-compartment cell was used which employed a carbon ink (Source: Acheson colloids, Plymouth, UK) anode which was covered with the photo-excitable substance titanium dioxide.

The cathode used in most cases (figure 5.2.3) was an air electrode (produced by Electro-Chem-Technic) attached to the bottom of a 2 cm diameter plastic tube that was 10 cm long. During the analysis the air electrode was dipped at the solution air interface. Here there was an interaction of all three phases – solid (MnO_2 on carbon), liquid (aqueous solution of 0.1 M KCl) and gas (atmospheric air). Use of an air electrode allowed an increase in concentration of oxygen during the reduction process.

In other cases (figure 5.2.2) such as during 2-propanol oxidation a platinised titanium sheet was used as a solution based cathode (area = 20 cm^2).

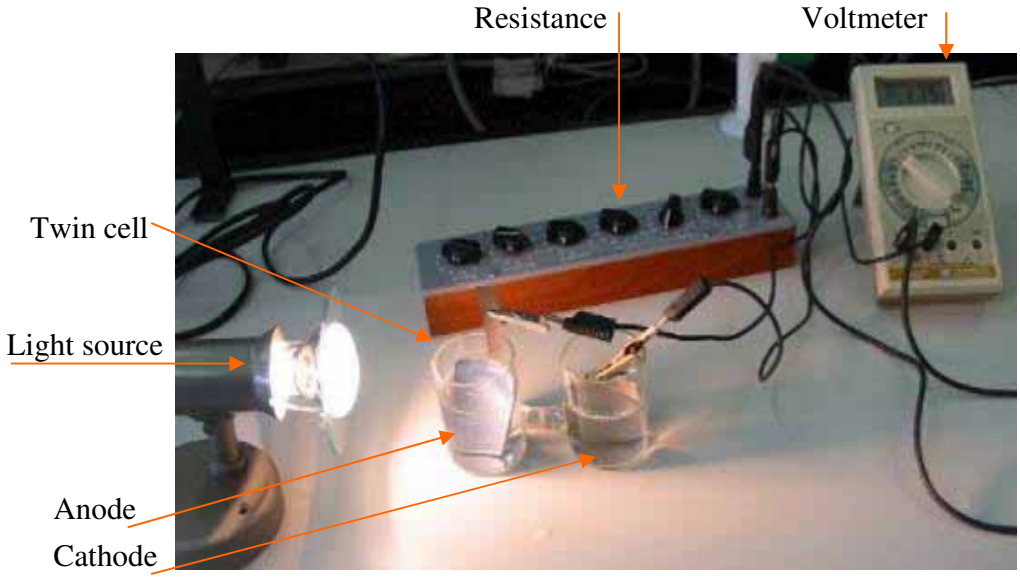

Figure 5.2.2: Two compartment photo-assisted fuel cell using platinised titanium sheet as cathode

5.2.3.2.2 One compartment photoelectrochemical cell

The diagram below represents the configuration of the single compartment photo-assisted fuel cell. It works on the same principle as the two compartment cell, except for the fact that both the anode and the cathode are not separated resulting in the oxidation and reduction processes occurring within the one compartment. As the test solution is prepared with aqueous 0.1 M KCl, it acts as its own electrolyte allowing transport of ions.

As in figure 5.2.2 for the twin compartment photo-assisted electrochemical cell, the current is passed across a 1 kΩ resistance and measured with either the voltmeter or the data logger. Using the one compartment cell configuration essentially removes

variations in results caused by the movement of solution through the frit as present in the two compartment cell configuration.

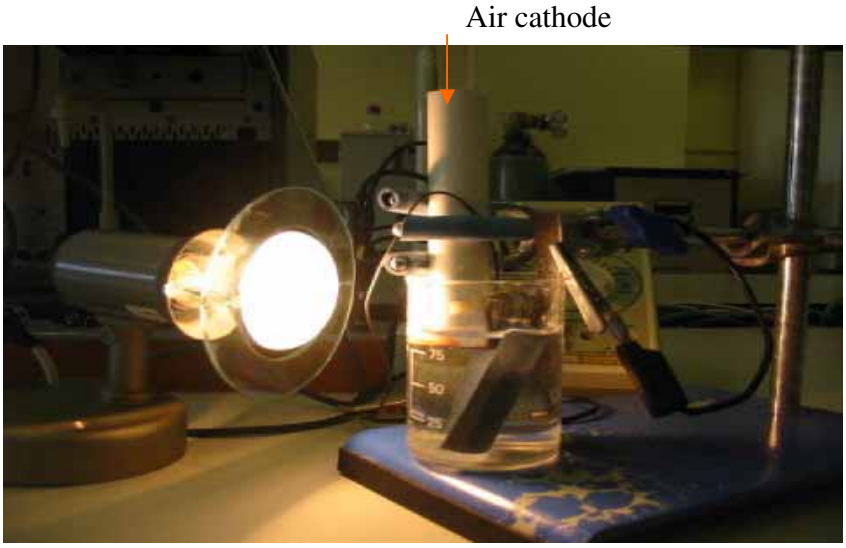

Figure 5.2.3: One compartment light assisted photoelectrochemical twin cell. 25 cm^2 TiO_2/carbon ink anode and platinised cathode linked through a 1 kΩ resistor. Irradiated by a 60 W tungsten lamp

5.2.3.2.3 Two compartment cell for 2-propanol degradation

When 2-propanol (IPA) was used as the fuel, a two compartment cell was used as shown in figure 5.2.2. However an air electrode was not used. Instead a platinised titanium sheet was employed as the cathode. When this was set up, there is far less oxygen available for reduction at the cathode.

5.2.3.3 Light sources used

5.2.3.3.1 Visible light

A 60 W tungsten incandescent bulb was used and this emitted mainly in the visible region of the electromagnetic spectrum but had a very small percentage of UV (as

can be seen in figure 5.2.4). The problem with this is that not only is the light collimated, but in addition to emitting light it also emits a lot of heat. This is what makes incandescent bulbs so energy inefficient, and they emit primarily in the infrared.

The small percentage of UV light in a standard household bulb is one of the reasons why P-25 is active in the visible region.

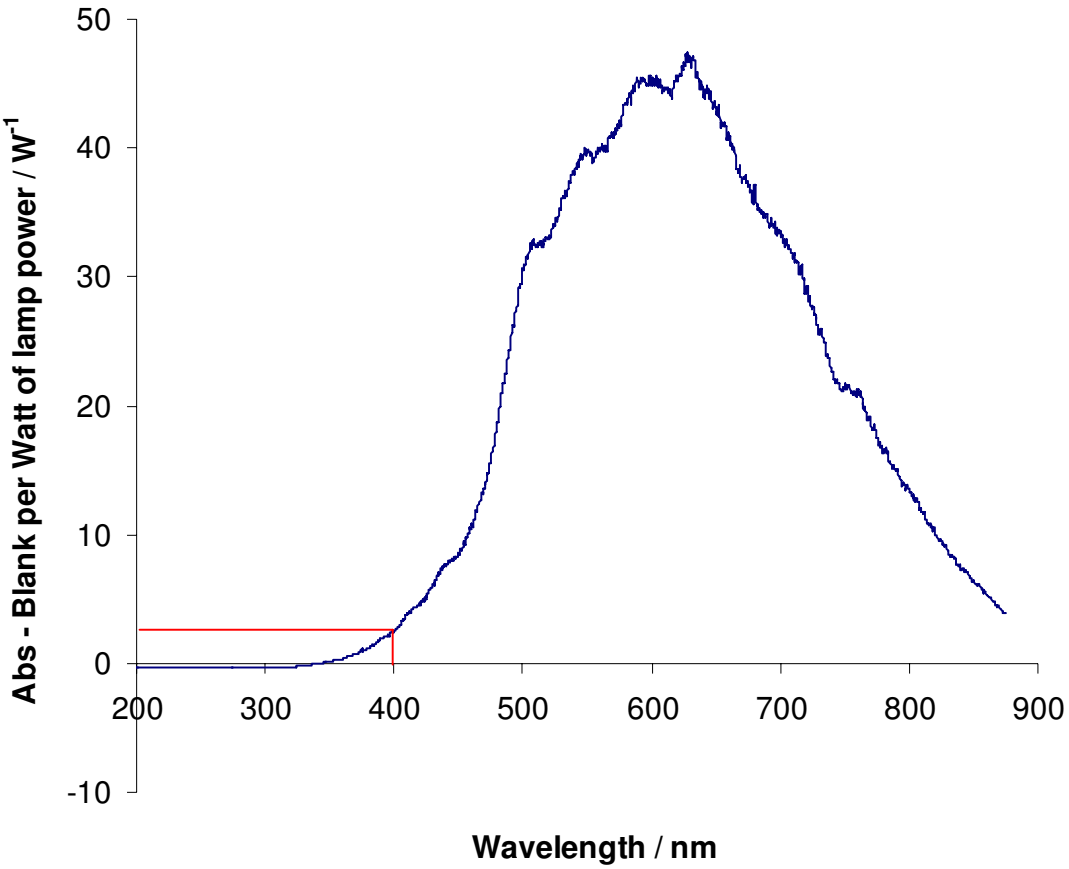

Figure 5.2.4: Emission spectra of a 60 W incandescent household bulb using an Ocean Optics spectrometer in scope mode. Dark absorbance value were taken in a black box (as are all measurements) and subtracted. Number of pixels in processed spectrum = 2048, integration time = 50 msec, spectra averaged = 100 (therefore one sample every 5 seconds). Graph was normalised to being a distance of 10.0 cm away from the source via a distance correction factor. Absorbance recorded was then divided by the wattage of the bulb (60 W).

This small amount of UV present (perhaps less than 5 %) is important as it's enough to activate photocatalysis on a TiO_2 surface, and explains the results later on in this chapter in figures 5.3.4 and 5. This is also important as TiO_2 is often used as a self-cleaning agent in windows and as an anti-bacterial agent paints, specifically for use in hospital walls. The semiconductor can therefore be easily activated when using these energy inefficient 'old fashioned' light bulbs (which are being phased out of use shortly to reduce electricity bills and carbon emissions).

Interestingly, non-visibly active (un-doped) titania would struggle to work as a hygienic coating when painted on to walls of modern buildings, including most offices, factories and workplaces. This is because there is no UV in fluorescent glow tubes (figure 5.2.5).

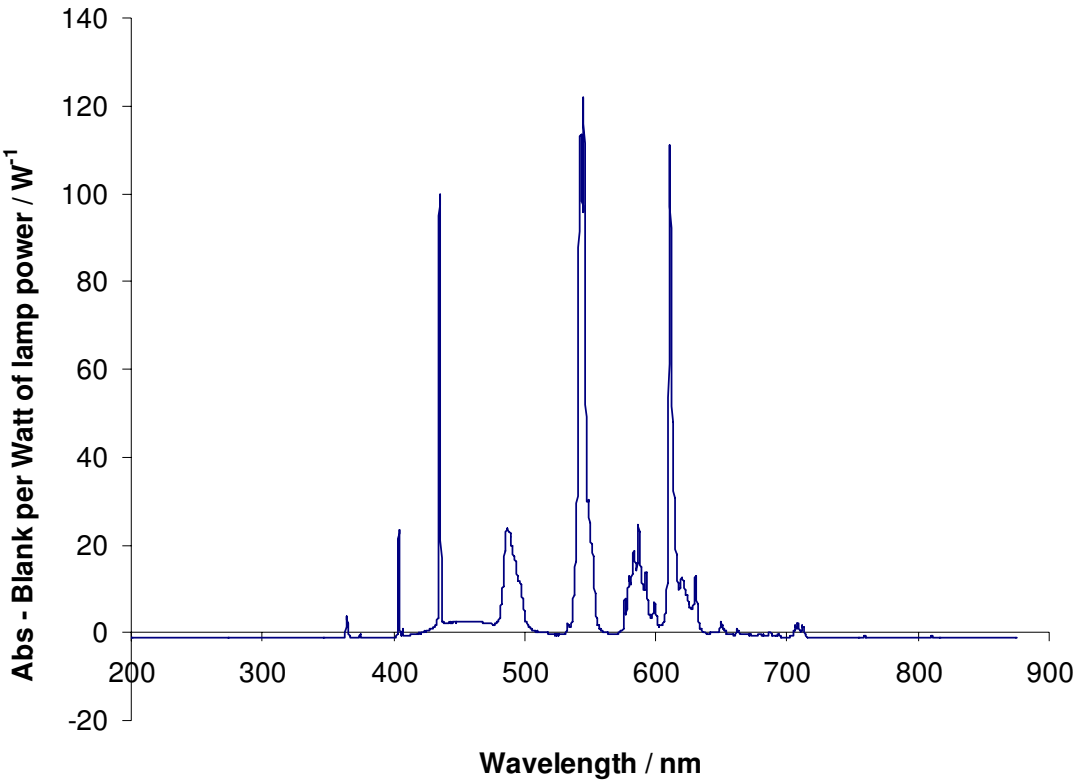

Figure 5.2.5: Emission spectra of a Polylux XL Cool White 835 36 W fluorescent glow tube (power of 3350 lumens) using an Ocean Optics spectrometer in scope mode. Dark absorbance value were taken in a black box (as are all measurements) and subtracted. Number of pixels in processed spectrum = 2048, integration time = 50 msec, spectra averaged = 100 (therefore one sample every 5 seconds). Graph was normalised to being a distance of 10.0 cm away from the source via a distance correction factor. Absorbance recorded was then divided by the wattage of the bulb (36 W × 2).

5.2.3.3.2 UV light sources used - 400 W Hg

As was shown in the introduction, anatase TiO_2 needs to be irradiated with light of a wavelength less than 387.5 nm (section 1.5). In this work a 400 W Hg medium pressure lamp was used (Photochemical Reactors Ltd).

The lamp has an output of 5×10^{19} photons per second and is primarily aimed at catalyzing organic reactions that are light induced (e.g. pericyclic Diels – Alder concerted

reactions). It contains immersion wells which are double-walled vessels made of quartz glass which houses the irradiation lamp. Inlet and outlet tubes provide for air or water cooling. A PTFE tube extends to the bottom of the annular space to allow coolant liquid to flow upwards from the bottom of the well. Thus a reflux style of system was set up.

A reflux condenser jacket of water surrounded the long vertical lamp at all times to keep the temperature to a minimum. In order to take out samples the lamp had to be switched off. A space between the walls allows filtering of certain wavelengths to lessen the occurrence of secondary photochemical reactions. The outer reaction flasks are made of borosilicate glass and are fitted with one central ground socket to take an immersion well and other smaller sockets for a reflux condenser or drop-in funnel, sampling port etc. The flasks was supported by a laboratory retort stand and clamp and housed in a black UV box for safety reasons.

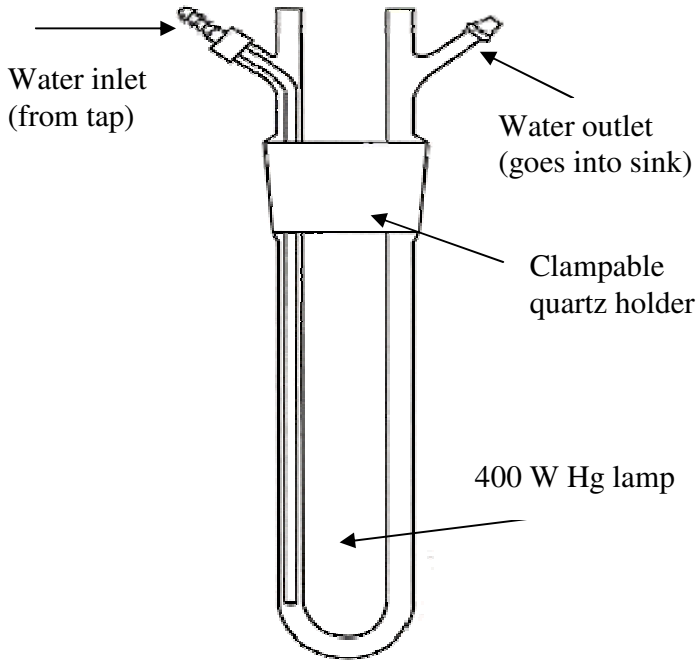

Figure 5.2.6: Housing for 400 W Hg lamp

The emission spectra of this lamp is shown in figure 5.2.7.

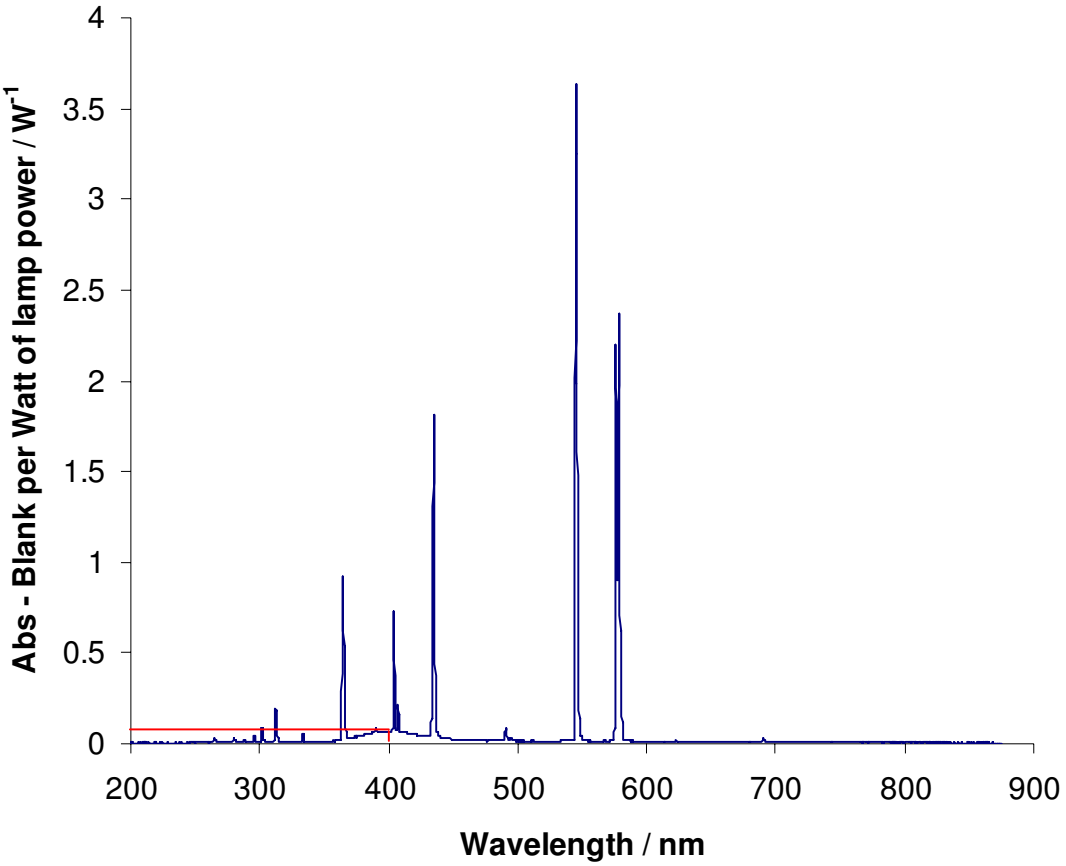

Figure 5.2.7: Emission spectra of a Photochemical Reactors Ltd 400 W Hg medium pressure lamp using an Ocean Optics spectrometer in scope mode. Dark absorbance value were taken in a black box (as are all measurements) and subtracted. Number of pixels in processed spectrum = 2048, integration time = 50 msec, spectra averaged = 100 (therefore one sample every 5 seconds). Graph was normalised to being a distance of 10.0 cm away from the source via a distance correction factor. Absorbance recorded was then divided by the wattage of the bulb (400 W).

As can be seen from figure 5.2.7, λ_{max} is at around 550 nm but the main UV peak emission is at 365 nm. There is a lot of UV in this diffuse lamp.

5.2.3.3.3 UV light sources used – 150 W Xe

The next light source was an Oriel 6253 150 W Xe arc lamp. In contrast to the 400 W Hg UV lamp, this was a very focused light source. Figure 5.2.8 shows its emission spectrum.

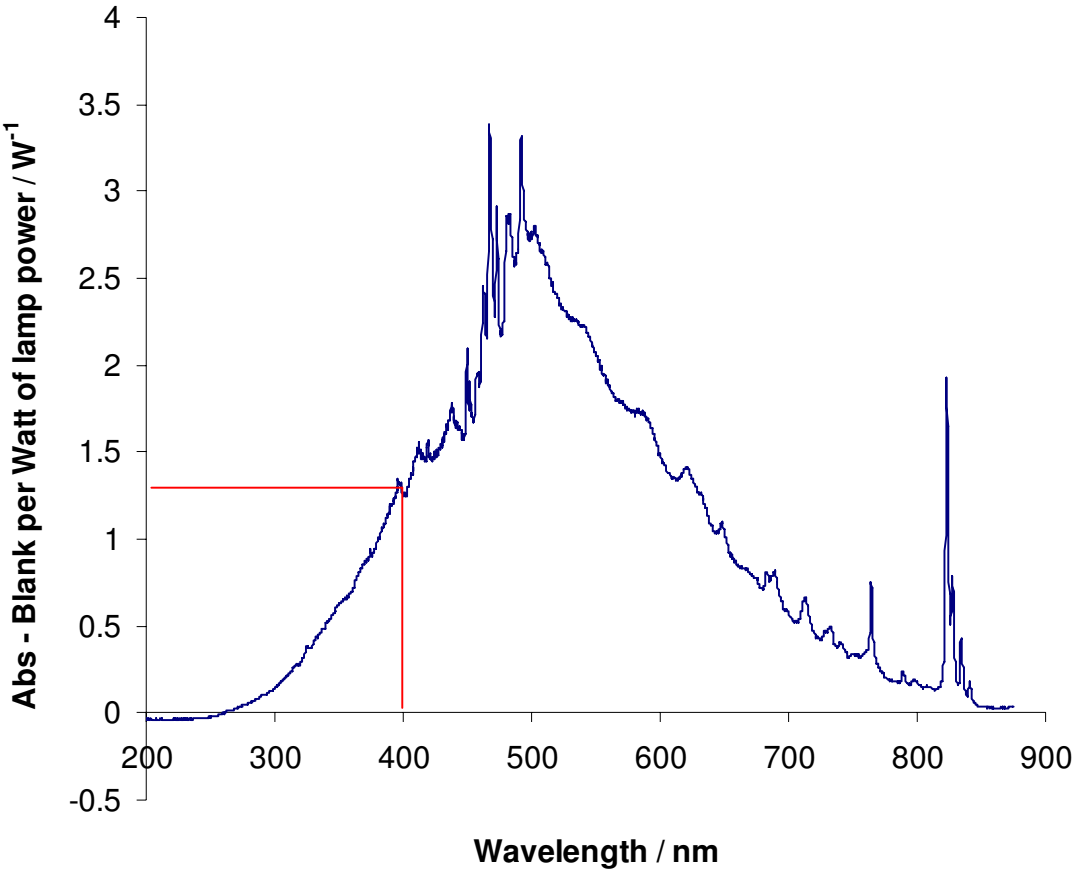

Figure 5.2.8: Emission spectra of an Oriel 6253 150 W Xe arc lamp using an Ocean Optics spectrometer in scope mode. Dark absorbance value were taken in a black box (as are all measurements) and subtracted. Number of pixels in processed spectrum = 2048, integration time = 50 msec, spectra averaged = 100 (therefore one sample every 5 seconds). Graphs was normalised to being a distance of 10.0 cm away from the source via a distance correction factor. Absorbance recorded was then divided by the wattage of the bulb (150 W).

5.2.3.4 Detection methods to monitor the degradation of organic compounds

5.2.3.4.1 Ultraviolet/visible spectroscopy

The rate of degradation of potassium hydrogen phthalate (KHP, figure 5.2.9) as a function of time was monitored by UV absorption.

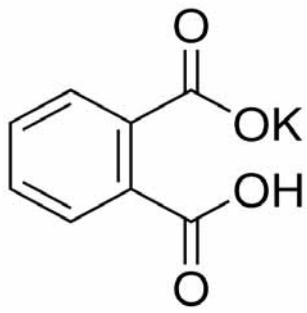

Figure 5.2.9: Chemical structure of KHP, a white powder

The same technique was used to follow photocatalytic degradations of 4-chlorophenol, benzaldehyde and catechol.

5.2.3.4.2 Gas Chromatography

The rate of degradation of 2 - propanol (IPA, figure 5.2.10) as a function of time was monitored by gas chromatography.

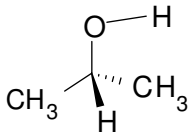

Figure 5.2.10: Chemical structure of IPA, a clear organic solvent

IPA (40 cm^3, 150 ppm) made up in aqueous 0.1 M KCl was degraded at the anode using a light assisted TiO_2 catalyst on carbon ink on acetate sheets. Each anode was a

5cm * 5cm sheet of approximately 75 μm thick carbon ink on acetate; with a nib on the top so that the crocodile clip could attach to it without being dipped in solution.

The whole circuit was put through a 1 kΩ resistor and onto a voltmeter which measured the ensuing voltage at various times. 0.4 ml aliquots were taken from the anodic jar and added to 0.1 ml of 500 ppm 2-butanol (IBA). The latter served as an internal standard. Shortly after each aliquot was collected they were analysed by gas chromatography featuring an OV-17 packed column. The separation conditions are detailed in table 5.2.3.

Table 5.2.3: Experimental conditions used during gas chromatography

Column	OV-17
Injection volume	1 μL
Primary gas pressure (N_2)	2 kg cm^{-2}
Carrier gas 2 (N_2) pressure	1 kg cm^{-2}
Hydrogen pressure	0.5 kg cm^{-2}
Air pressure	0.5 kg cm^{-2}
Injector temperature	120° C
Column temperature	80° C
Attenuation	- 2

Solutions of IPA, acetone (ACE), butanol and isobutanol (IBA) were made up in aqueous 0.1 M KCl in the concentration range of 100 - 1000 ppm. From this it was found that ACE was the first compound off the column at a retention time of ~ 1.5 mins, IPA was the next organic at 2.2 – 2.3 mins and IBA was next to elute at 3.7 mins. Retention times vary slightly for every experiment and even within an experiment as the gas pressures change all the time.

All of these compounds gave sharp, well resolved peaks on the packed column, however there was a low, broad peak at 5 – 6.5 mins which represented water and so each injection had to be ran for this length of time in order to get this out of the system, otherwise this peak would be present at the start of the next injection (figure 5.2.11). Butanol was the last organic compound off the column, eluting at 7.6 – 7.7 mins.

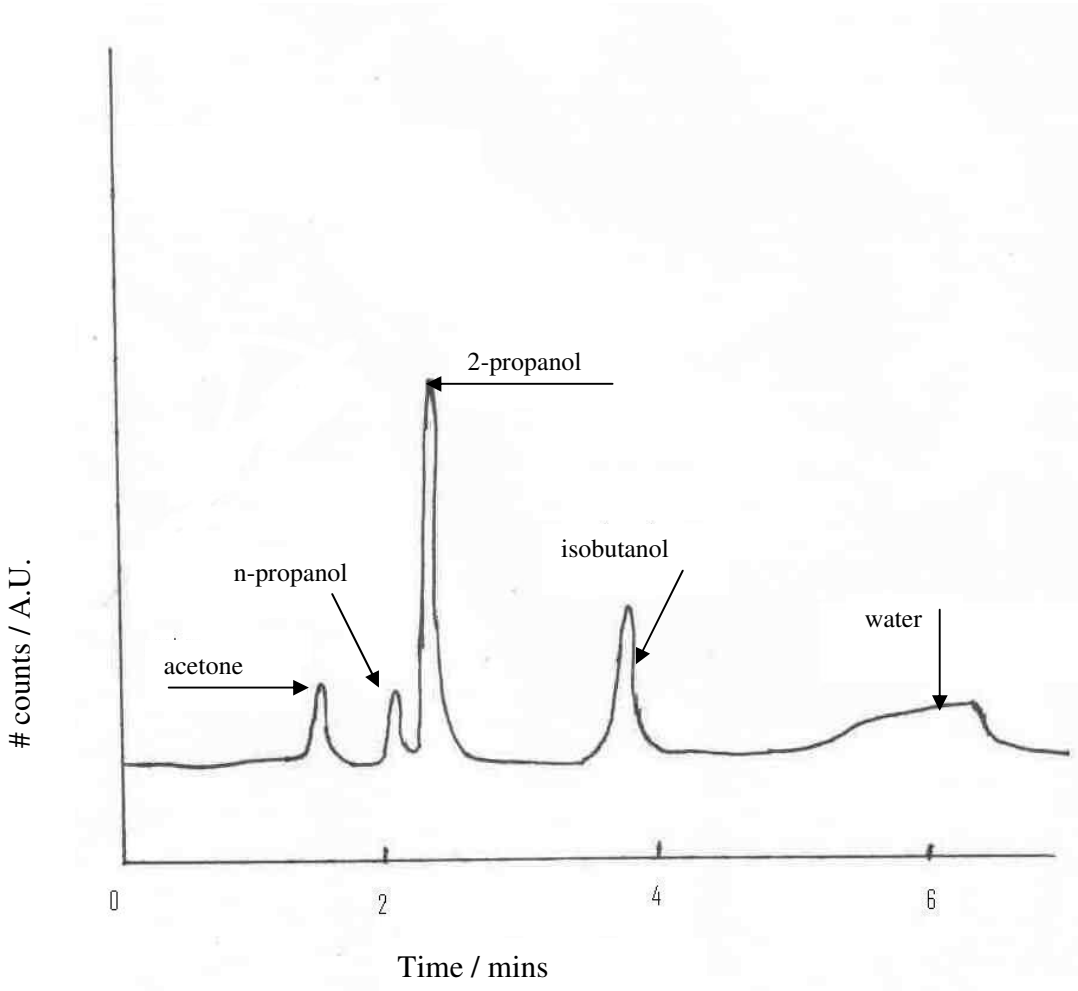

Figure 5.2.11: A typical chromatogram obtained showing peak identification and retention time

5.3 Results and Discussion

5.3.1.1 Degradation of potassium hydrogen phthalate (KHP) in a one compartment cell using predominantly visible light

A one compartment cell was used as outlined in figure 5.2.2. The single compartment cell removes the possibility of the fuel being diluted by the electrolyte, as can happen in a twin cell if the electrolyte diffuses across the porous frit.

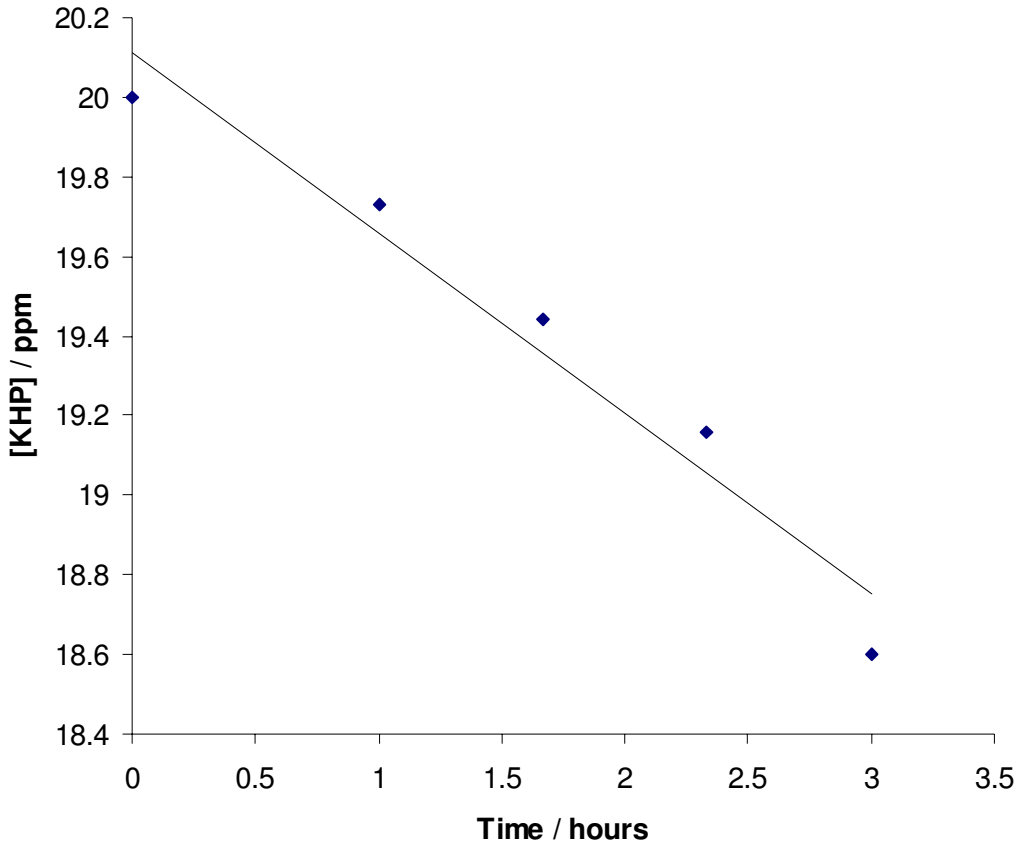

Figure 5.3.1: Degradation of KHP (20 ppm) in aqueous 0.1 M KCl with time (hours) in a one compartment cell. 25 cm^2 TiO_2/CI anode and 1.3 cm^2 air cathode connected through a 1 kΩ resistor. 60 W tungsten visible lamp.

As can be seen in figure 5.3.1, the degree to which KHP is degraded over three hours is small. A decrease in current produced was noted as a function of time. From this result it appears that potassium hydrogen phthalate is very stable and difficult to break down using visible light sources. The small decrease in absorbance was accompanied by an equally small current increase over the three hour period. Therefore there was very little degradation of aqueous KHP in this time period using a visible light source.

5.3.1.2 Degradation of KHP using a 400 W Hg lamp

An aqueous KHP solution (16 ppm) was exposed to a 400 W Hg lamp for 90 minutes. The original absorbance of the solution was 1.044, after exposure the absorbance was 1.043, showing that potassium hydrogen phthalate was very stable even when exposed to a UV light source.

While there were no calculations made, it is plausible that not many photons of light were impinged on the TiO_2 coated anode. Neutral KHP is very stable, and the negative charge on its anionic oxygen (figure 5.2.5) is stabilised through the carbonyl ester, the benzene ring and by the potassium cation.

5.3.2 Degradation of phthalic acid (HHP) using a 400 W Hg lamp

Reduction in pH has a positive effect on the current produced when trying to degrade many organic compounds, and KHP was investigated to see if it was one of such compounds. This is because at low pH values (< 6), the TiO_2 surface is positively charged, and KHP is present at this pH as phthalic acid (HHP), capable of adsorbing onto the catalyst surface [38]. In this work the pH is dropped to 3.0.

A control was added to support the results. Two solutions of potassium hydrogen phthalate (100 cm^3, 10 ppm) where prepared and both acidified using hydrochloric acid (0.1 M). Both samples were exposed to a 400 W lamp. One sample was a single compartment photoelectrochemical cell (as in figure 5.2.2), while the other acted as a reference with a non-connected TiO_2 anode submerged in the pollutant. In doing this it was possible to see the influence the cell set-up had on the degradation process. The experimental procedure was run for a period of 2 hours with UV absorbance measured every 10 minutes. The findings are shown in figure 5.3.2.

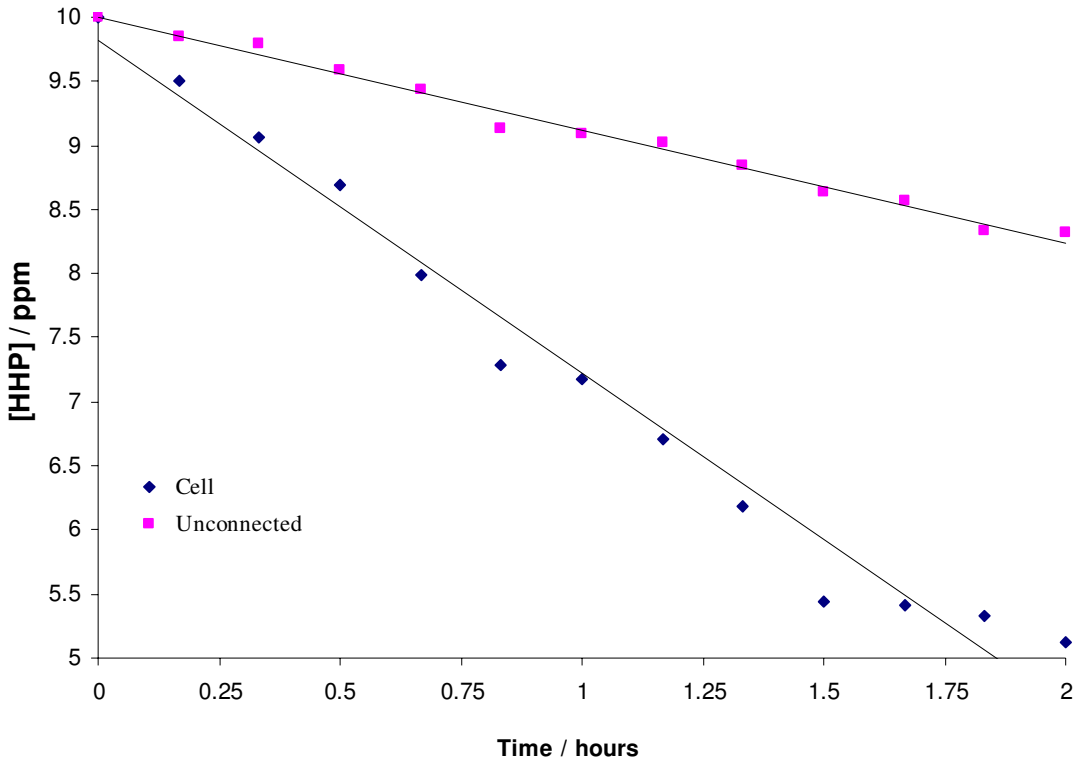

Figure 5.3.2: Degradation of HHP (10 ppm) in aqueous 0.1 M KCl with time (hours) in a one compartment cell. 25 cm^2 TiO_2/CI anode and air cathode connected through a 1 kΩ resistor. Unconnected cell also included. Irradiated by a 400 W Hg lamp.

This was a vast improvement on any reduction in concentration of KHP prior to this. The findings under acidic conditions with potassium hydrogen phthalate were promising as a strong adsorption at the catalyst surface may have taken place.

From the graph displayed in figure 5.3.2 above it can be seen that the connected cell undergoes a much more significant reduction in concentration in relation to the sample where the cell set-up is absent. This highlights the fact that the cell comprising of the TiO_2 anode and air cathode has a major positive effect on the reduction in concentration of organic species.

There is a 49 % reduction in the concentration of acidified KHP for the cell, while the reference only has a reduction of just 13 %. From this result it can be concluded that the cell does in fact increase the efficiency of the degradation process of potassium hydrogen phthalate when under acidic conditions.

During this experiment current was also monitored using a voltmeter every 10 minutes, and it averaged out at 37 μA. From the measurements of current taken during the known experimental time, the number of moles of electrons in the reaction could be calculated for potassium hydrogen phthalate oxidation, and using the UV absorbance readings the reduction in concentration could be calculated. The findings are depicted in the table below.

Table 5.3.1: Number of moles of electrons –Vs- moles/l of sample degraded

	Initial number of moles of KHP	Final number of moles of KHP (after 2 hours irradiation)	Number of moles of electrons consumed	[KHP] degraded / moles
KHP (10 ppm)	4.9×10^{-6} moles	2.35×10^{-6} moles	2.8×10^{-6}	2.55×10^{-6}

From the results depicted in the table above, it can be seen that the moles of electrons produced by the cell (2.8×10^{-6}) and moles of KHP reduced during this experimental run (2.55×10^{-6}) are of the same magnitude. This correlation of figures highlights the relationship between the current produced and the concentration of the fuel degraded, as it would be expected that the higher the current produced by the cell, the higher the reduction in concentration of fuel.

5.3.3 Degradation of ascorbic acid (AA) using predominantly visible light

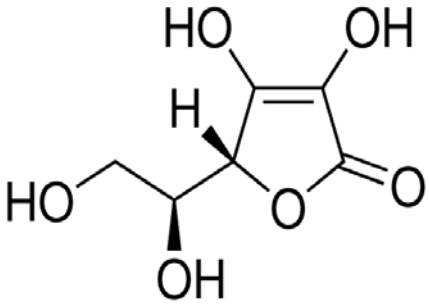

Figure 5.3.3: Chemical structure of AA (vitamin C), a white powder and an important antioxidant.

Ascorbic acid is known to be readily oxidized so it was an obvious compound of choice to see if an improvement in the rate of degradation of the organic fuel could be obtained. AA absorbs UV light which again allowed the degradation to be monitored using UV analysis, allowing for fast accurate reading to be taken with little preparation time.

An aqueous AA sample (10 ppm) was monitored by UV spectroscopy over a 4 hour period using a one compartment cell, and the results are presented in figure 5.3.4. Almost total degradation took place in this period of time and the AA sample had much of its conjugation broken.

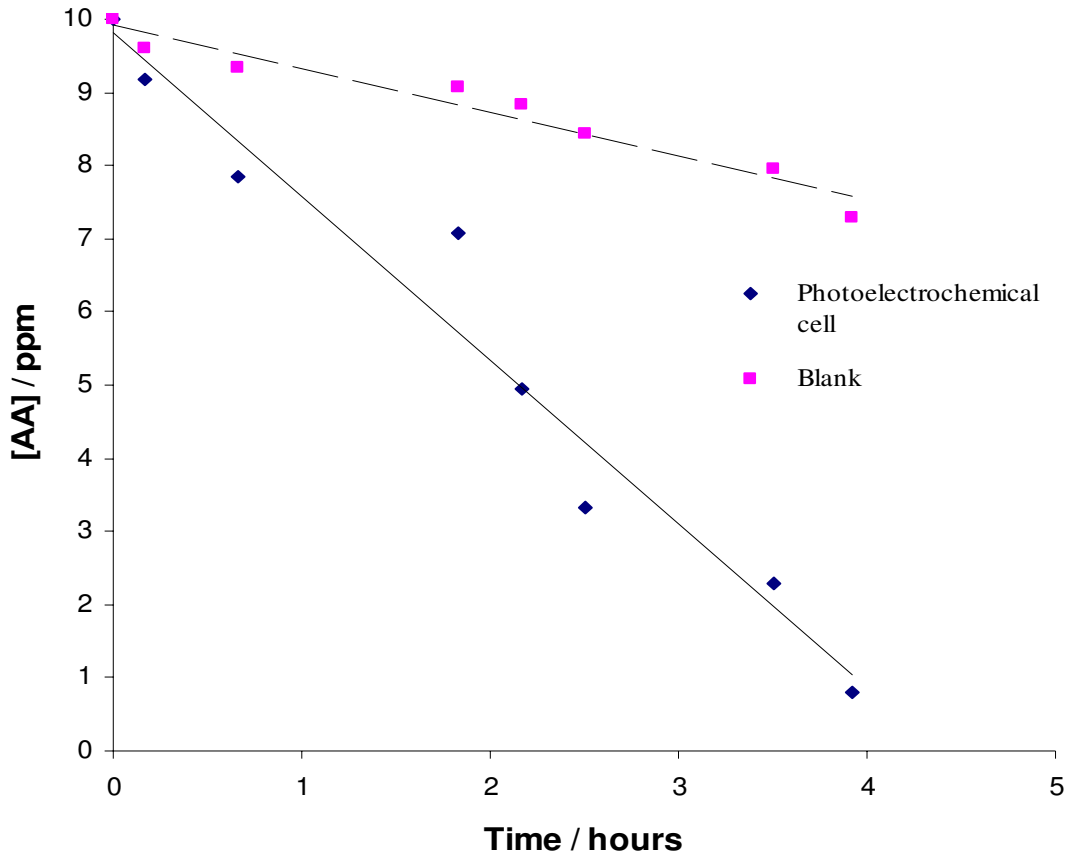

Figure 5.3.4: Degradation of AA (10 ppm) in aqueous 0.1 M KCl with time (hours) in a one compartment cell. 25 cm^2 TiO_2/CI anode and 1.3 cm^2 air cathode connected through a 1 kΩ resistor. 60 W tungsten visible lamp.

The graph above shows that over the three hour period ascorbic acid concentration steadily decreased as a function of time when exposed to the light source and the cell set-up. Also during this experiment a reference ascorbic acid (also 10 ppm) solution was prepared to assess the degradation taking place at normal room conditions. This allows one to see what proportion of the degradation could be attributed to the cell if any, since it was known that ascorbic acid undergoes simple oxidation from oxygen in air. The result is shown above.

The linear decrease in concentration with respect to time indicates zero order degradation. This ties in well with the literature when using surface confined TiO_2 [31]. This plot demonstrates that while AA is known to be quite prone to open air oxidation [39], the photoelectrochemical cell greatly accelerates this process.

5.3.4 Degradation of benzaldehyde (Bz) using predominantly visible light

For this analysis the experimental run was extended to 4 hours. The configurations and set-up was the same as shown in figure 5.2.3. The results obtained are as shown in figure 5.3.5.

From the graph it can be seen that a significant drop in absorbance was obtained over the 4 hour period while deploying the 60 watt visible light source. However it was found that the disconnected Bz concentration decreased with the cell unconnected. There was a 27 % reduction of the Bz sample in the photoelectrochemical cell, and for the unconnected reference there was a 16 % reduction. This suggests that Bz is also prone to simple open air oxidation; but the photoelectrochemical cell had a positive impact on the degradation of the organic compounds in relation to the disconnected reference sample.

An 11 % increase in degradation was obtained from the sample where the photoelectrochemical cell was deployed. During this run the current reading obtained averaged out at 13 μA.

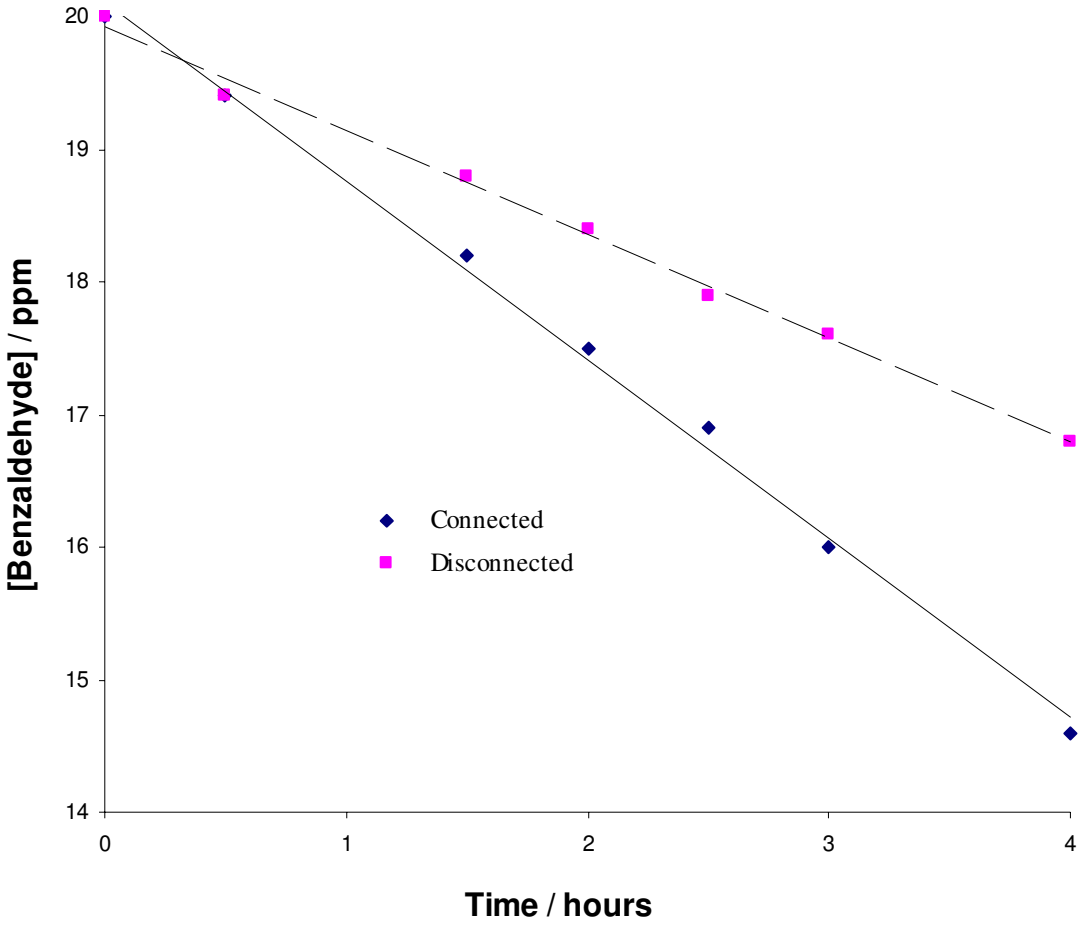

Figure 5.3.5: Degradation of Bz (20 ppm) in aqueous 0.1 M KCl with time (hours) in a one compartment cell. 25 cm^2 TiO_2/CI anode and 1.3 cm^2 air cathode connected through a 1 kΩ resistor. 60 W tungsten visible lamp.

5.3.4.1 pH effects on the degradation of bz

The pH of Bz was reduced from its neutral reading to an acidic state of approximately pH 3.0 (with dilute hydrochloric acid) to see if this could lead to a more efficient degradation of the organic species The sample was again exposed to a 60 W tungsten light source (figure 5.3.6). Current of 21 μA was obtained during this experimental run.

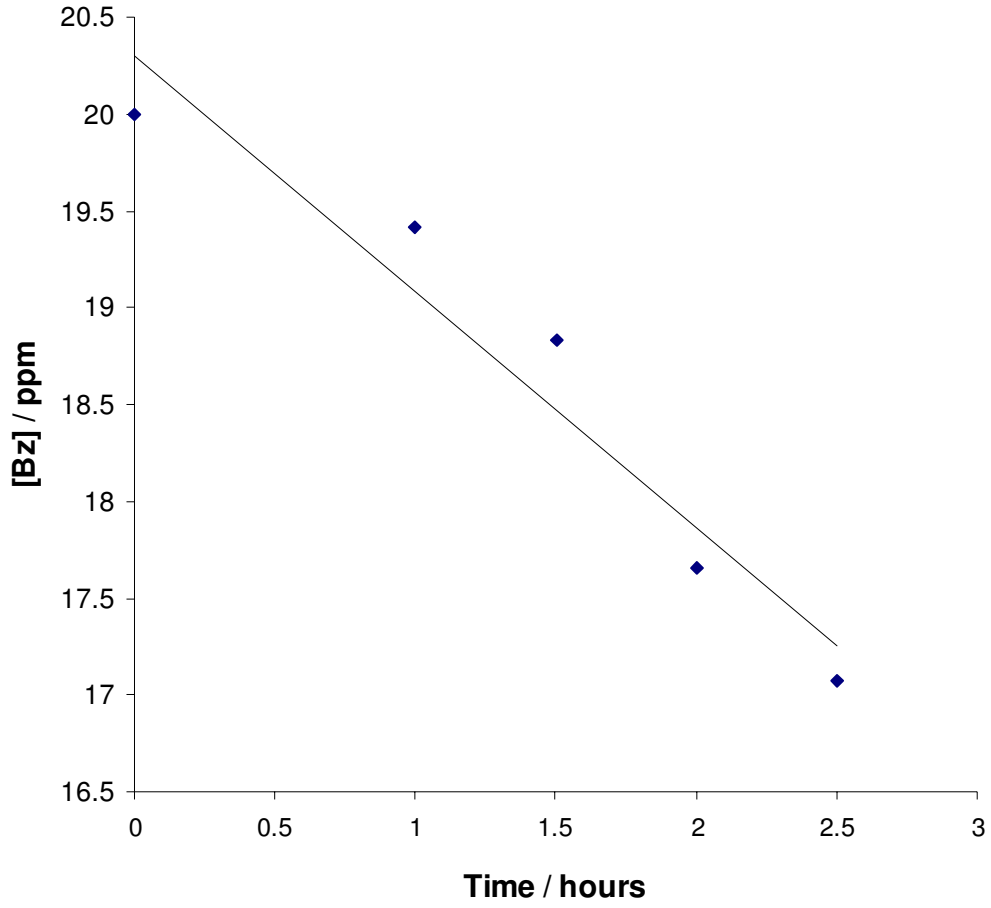

Figure 5.3.6: Degradation of pH 3 Bz (20 ppm) in aqueous 0.1 M KCl with time (hours) in a one compartment cell. 25 cm^2 TiO_2 anode and 1.3 cm^2 air cathode connected through a 1 kΩ resistor. 60 W tungsten visible lamp.

Although a higher current was obtained during degradation of pH 3 Bz than its neutral counterpart, there was no significant impact on the rate of degradation. In the 150 minutes timeframe there was a concentration reduction of 15 %, while the non-acidified solution had a reduction of 39 % after 120 minutes under similar conditions when analyzed previously (figure 5.3.5).

Acidifying Bz therefore does not improve its degradation. Figure 5.3.7 shows some current transients collected for aqueous 20 ppm Bz with the light source alternating between on and off.

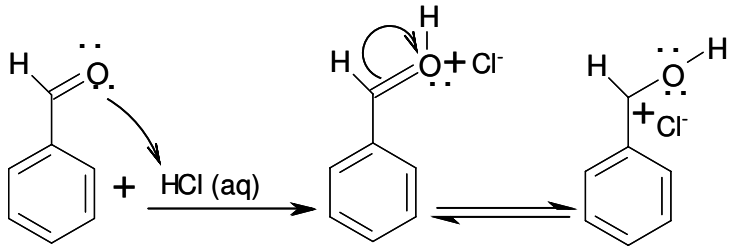

Figure 5.3.7: Chemical structure of Bz (left). Acidification leads to protonation of the oxygen atom which can make it more electrophilic.

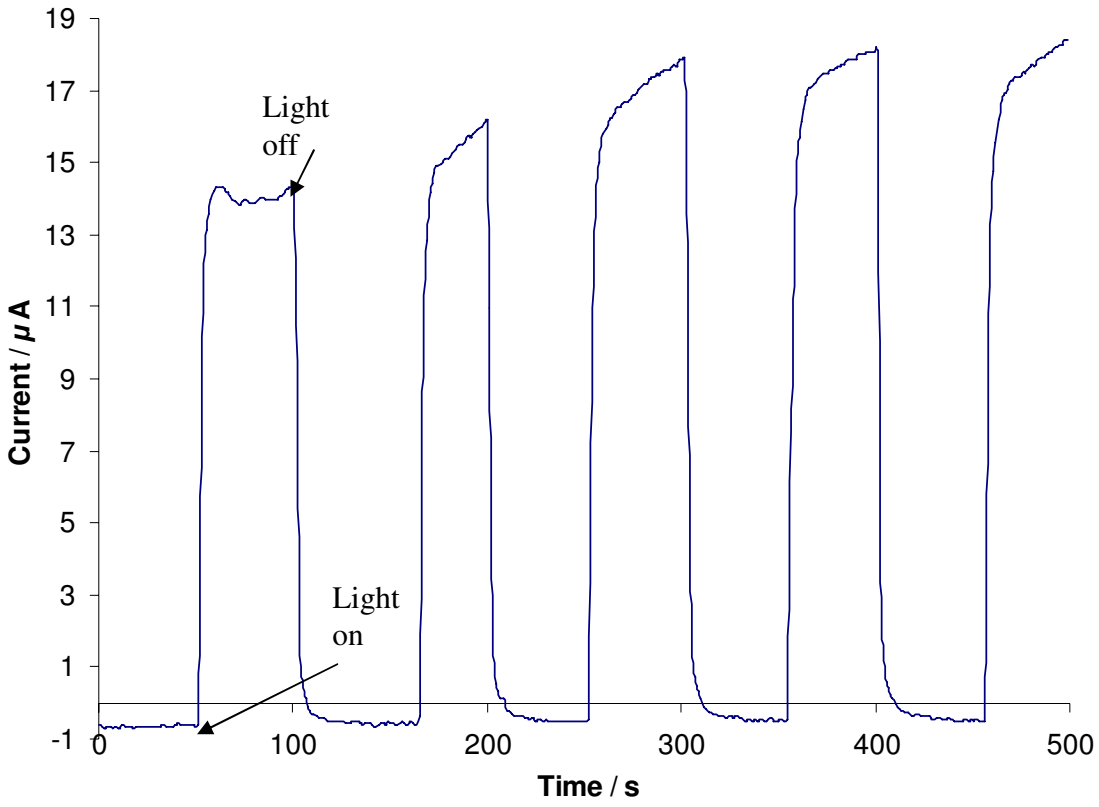

Figure 5.3.8: Open circuit photocurrents for benzaldehyde (20 ppm) in aqueous 0.1 M KCl with time (seconds) in a one compartment cell. 25 cm^2 TiO_2/CI anode and 1.3 cm^2 air cathode connected through a 1 kΩ resistor. 60 W tungsten visible household light bulb.

It can be seen that when the light is switched on, the semiconductor catalyst is activated and there is a large increase in current. When there is no longer any illumination, there is a steep and immediate drop in the current accordingly.

5.3.4.2 Degradation of Bz using a 400 W Hg lamp

A single compartment photoelectrochemical cell was used with an air cathode and 400 W Hg lamp. A reference sample was also exposed to the light source. The samples where exposed to the light source for 2 hours with UV readings taken every 30 minutes. The results are shown in figure 5.3.9.

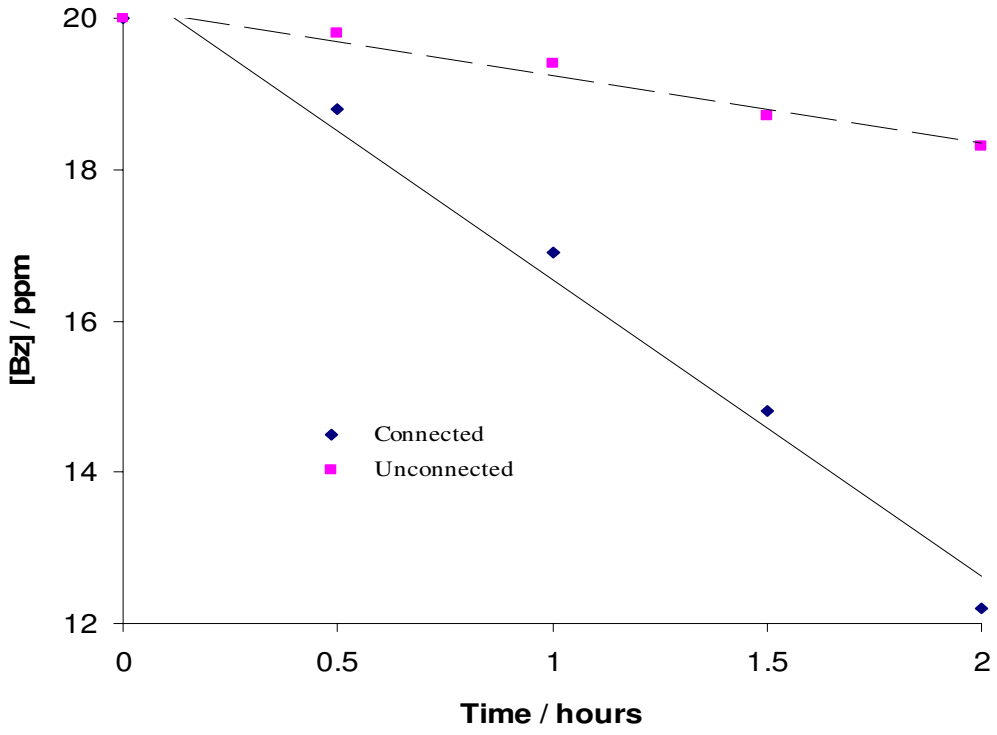

Figure 5.3.9: Degradation of Bz (20 ppm) in aqueous 0.1 M KCl with time (hours) in a one compartment cell. 25 cm^2 TiO_2/CI anode and air cathode connected through a 1 kΩ resistor. Unconnected cell also included. Irradiated by a 400 W Hg lamp.

From the graph it can be seen that Bz (20 ppm) in the photoelectrochemical connected cell exposed to the light source underwent a more significant drop in absorbance as opposed to the reference sample. This is consistent with the result obtained for HHP, showing that the cell increases the degradation efficiency of various organic compounds. The sample solution had a 39 % decrease in concentration, while the reference showed an 8.5 % decrease in concentration. The current obtained during this experimental run averaged at 25 μA, the moles of electrons reacting was 1.85 x 10^{-6} corresponding to the moles of benzaldehyde reduced 7.32 x 10^{-6}.

5.3.5.1 Degradation of IPA

IPA was used as the fuel in a one compartment cell using a visible light source. An exponential style of decay was observed. Such types of degradation are more typical for TiO_2 suspensions in the fuel irradiated by light. Given the linear style of decay found for this surface confined system, it is possible that the TiO_2 layers in this work were a little too thick and therefore stripped off the electrode surface and into solution. If this was the case, the light was only activating the TiO_2 at the edge of the layer and was less likely to do so for TiO_2 adsorbed to the underlying carbon ink surface.

An interesting aspect of IPA degradation is that it may form acetone (ACE) as a primary oxidation product (figure 5.3.10).

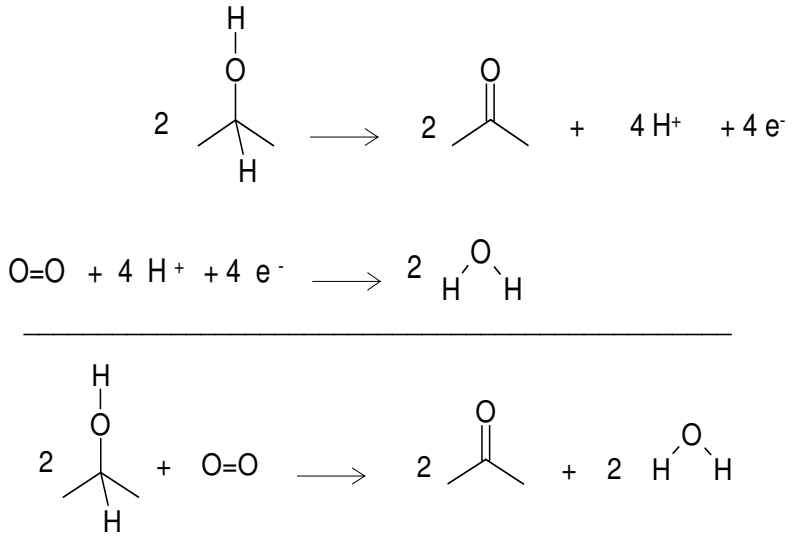

Figure 5.3.10: Oxidation of IPA, reduction of oxygen

As ACE is a by product of IPA oxidation, an interesting experiment was constructed in order to investigate the amounts of ACE produced upon IPA oxidation. Both compounds were compatible with the column used. However determination of acetone is unreliable as there is much evaporative loss from the samples as the storage time is prolonged [40].

Because of the extreme heat produced by the lamp a lot of the acetone that was created by the oxidation of IPA evaporated before injection time. Samples were stored in vials and it is possible that much of the created acetone may have evaporated into and dissolved in the rubber seals of the vials. For these reasons, the results of the degradation or formation of either compound are not presented.

The problems associated with ACE determination from IPA consumption accruing from TiO_2 enhanced with near UV light were avoided by Ohtani *et al* [41]. This work involved TiO_2 impregnated with Pt in a suspension. As equimolar amounts of

hydrogen gas as ACE are produced from IPA photodegradation (figure 5.3.10), this group was able to measure amounts of H_2 adsorbed onto the TiO_2/chloroplatinic acid amalgam.

In similar work very small amounts of ACE were produced from photodegraded IPA when using bare TiO_2 [42]. Using a 500 W Hg lamp in an argon atmosphere, samples were analysed using a GC Tenax column at 200° C, and in some cases dimerisation products like acetylacetone were formed. As equal amounts of H_2 were produced as the consumption of ACE, they showed that the photodehydrogenation of IPA proceeds photocatalytically.

Li *et al* proposed a mechanism for IPA oxidation and subsequent acetone production [43].

Photoexcitation:	$TiO_2 + h\nu \rightarrow TiO_2h^+ + TiO_2\ e^-$
Formation of a surface hydroxyl radical:	$H_2O + TiO_2h^+ \rightarrow {}^{\bullet}OH_{surface} + H^+$
Formation of a radical intermediate:	${}^{\bullet}OH_{surface} + (CH_3)_2CHOH \rightarrow (CH_3)_2CHO^{\bullet} + H_2O$
Electron injection by radical intermediate:	$(CH_3)_2CHO^{\bullet} \rightarrow (CH_3)_2CO + H^+ + e^-$
Oxygen reduction:	$O_2 + 2e^- + 2\ H^+ \rightarrow H_2O_2$
Photocatalysed oxidation:	$(CH_3)_2CHOH + O_2 \rightarrow (CH_3)_2CO + H_2O_2$

It is likely that this mechanism is followed in this work, and acetone is produced. Li *et al* were also able to show that for the same TiO_2 film coated onto an electrode, cathodic photogenerated currents increased with increasing pH. This makes the pH of the solution an important issue, and it was neutral in this work.

5.3.5.2 Degradation of IPA using a 150 W Xe lamp

IPA was used photodegraded with the aid of an oriel 6253 150 W Xe arc lamp, and again the experiment was followed by gas chromatography. The results are featured in figure 5.3.11 and consist of three different situations:

1. Connected - 25 cm^2 TiO_2/CI anode & air cathode linked through a 1 kΩ resistor in a beaker of IPA (100 cm^3, 106 ppm) in 0.1 M KCl
2. Unconnected - beaker of IPA (100 cm^3, 106 ppm) in 0.1 M KCl with a 25 cm^2 TiO_2/CI anode
3. Blank - beaker of IPA (100 cm^3, 106 ppm) in 0.1 M KCl

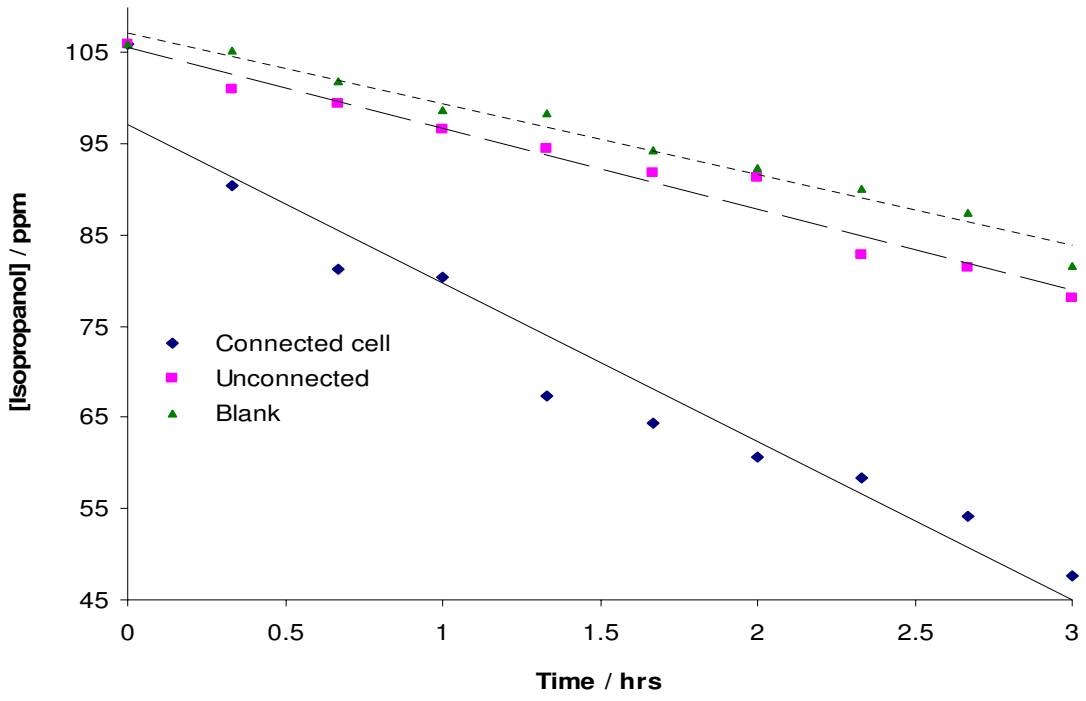

Figure 5.3.11: Degradation of IPA (106 ppm) in aqueous 0.1 M KCl with time (hours) in a one compartment cell. 25 cm^2 TiO_2/CI anode and air cathode connected through a 1 kΩ resistor. Unconnected cell also included. Irradiated by a 150 W Xe lamp.

As can be seen by figure 5.3.11, there is a steady decomposition of IPA within the 3 hour timeframe. For the unconnected cell and the blank the decomposition is less pronounced. For the unconnected cell, there is a small amount of IPA oxidation. This may indicate that oxidation of IPA can be oxidised to CO_2 as there was no real evidence for an acetone intermediate. This could all happen at the TiO_2 particle and there is no real need for O_2 reduction when this happens.

5.3.6.1 Degradation of catechol (CAT) using daylight

Having studied the decomposition of alcohols with many experimental configurations (varying compartments, cathodes and light sources), it was decided to change compounds from simple alcohols to substituted phenols. To begin with, the attention turned to catechol (CAT, figure 5.3.12), a 1,2-dihydroxybenzene. CAT is originally a white to light tan coloured solid but discolours to brown on exposure to air and light.

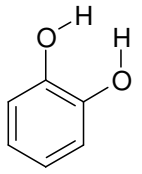

Figure 5.3.12: Chemical structure of catechol

With many reports in the literature of organic degradation at TiO_2 using daylight [9, 10, 18], it was decided to follow suit. 64 ppm CAT was made up in 0.1 M KCl and again the 3 situations were covered, as described previously in section 5.3.5.1 (unconnected, connected and blank). Aliquots were removed with a Pasteur pipette at different time periods (normally morning and evening for seven to fourteen days), placed in a quartz cuvette & analysed with a Shimadzu UV-160 from 200 – 400 nm.

2 distinct sharp peaks appear for the aqueous solution of CAT at 275 and 218 nm. It is the peak at 275 nm that breaks down when the conjugation is broken. Therefore the peak at 218 nm is due to a different transition. The contents of the cuvette were then returned to their respective beakers. Again all photoelectrochemical cells were stirred using a magnetic stirrer at a consistent reproducible rate. Figure 5.3.13 shows how the UV spectrum looked like (a) at the start of the experiment and (b) after 5 days.

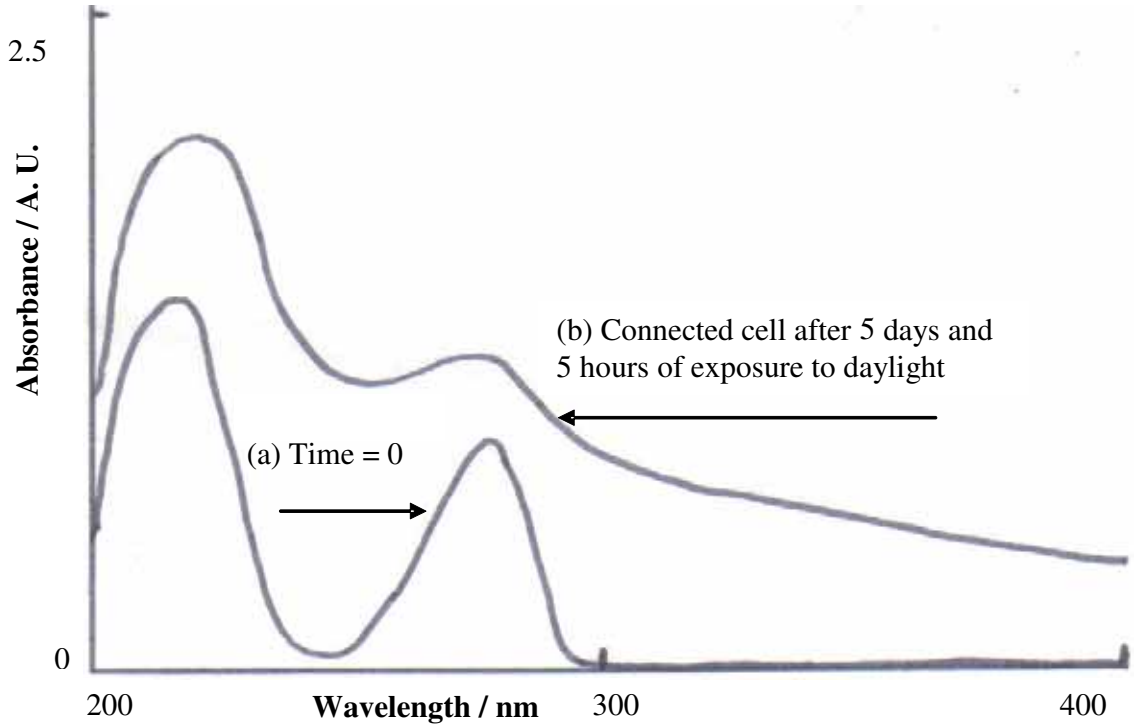

Figure 5.3.13: Initial UV spectra of CAT (a) and (b) after 126 hours. The one compartment cell consisted of an air cathode and a 25 cm^2 TiO_2 on C anode. These were placed in a beaker of 55 ppm CAT (50 cm^3) in 0.1 M KCl and the both terminals were connected through a 1 kΩ resistor

The results of the daylight assisted photoelectrodegradation are detailed in figure 5.3.14.

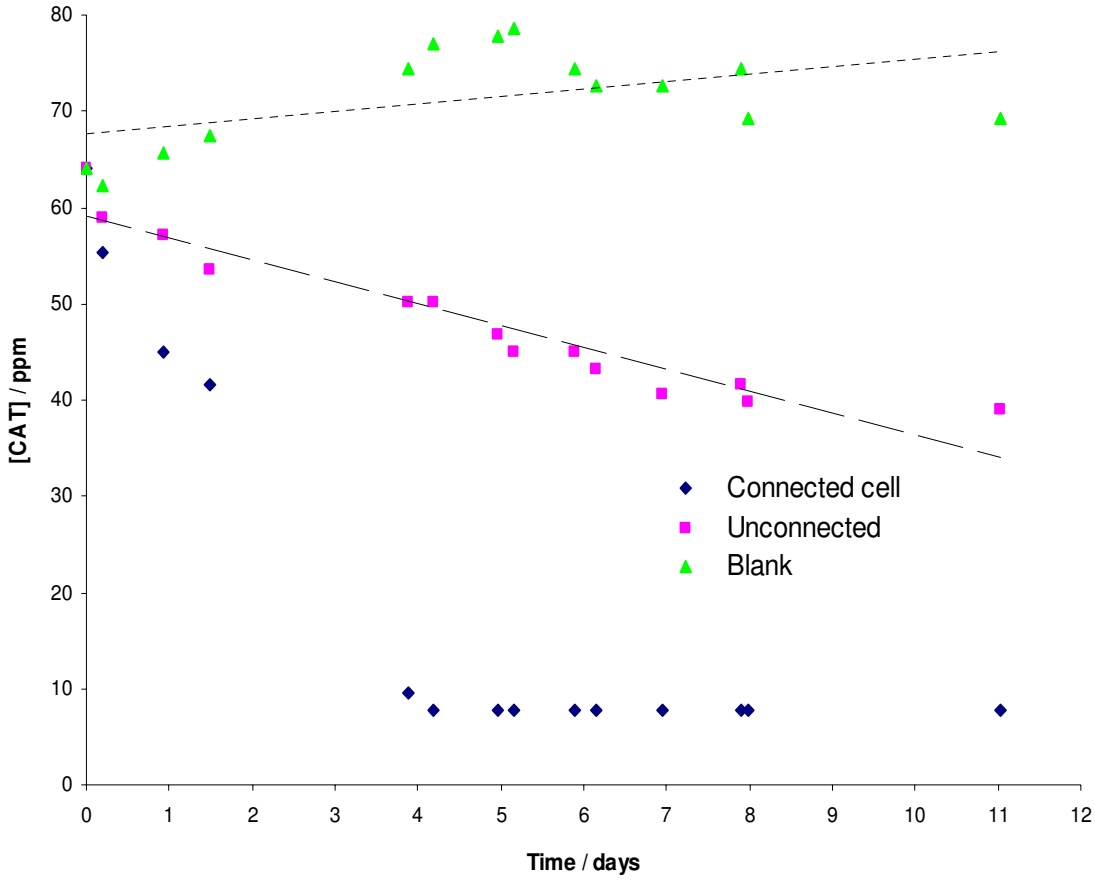

Figure 5.3.14: Degradation of CAT (64 ppm) in aqueous 0.1 M KCl with time (days) in a one compartment cell. 25 cm^2 TiO_2/CI anode and air cathode connected through a 1 kΩ resistor. Unconnected cell and blank are also included. Irradiated by daylight.

For the connected cell using daylight, CAT degraded from 64 to 8 ppm within 4 days (88 % degradation). It's concentration was down to 40 ppm (22 %) and 77 ppm (120 %) for the unconnected cell & control respectively within the same timeframe. Absorbance for the control sample actually increased over these long time periods due to partial evaporation of the aqueous sample over the week, and so leaving the CAT dissolved in less amounts of salt water.

The results reveal that there is no breakdown for the blank, so light or heat alone cannot degrade CAT. It must also be considered that the photoelectrochemical cell was continuously connected throughout this period and so it was acting as a photoelectrochemical cell even at night in the dark. Therefore, not all of the decrease can be due to light activated TiO_2 photocatalysis. Interestingly, for the connected cell there is no further breakdown after 4 days, because all of the sites on the working TiO_2 electrode were used up at that stage. The brown solid CAT could be seen adsorbed to the surface.

It was decided to repeat the same experiment (shown in figure 5.3.15) exposed to natural sunlight with fresh electrodes but in a shorter time frame, again using daylight as the source. There is a fast degradation at the connected photoelectrochemical cell – in 2.5 hours it goes from 55 ppm down to 49 ppm (11 % breakdown) but for the unconnected cell the breakdown goes as far as 51 ppm (7 %) in this time period.

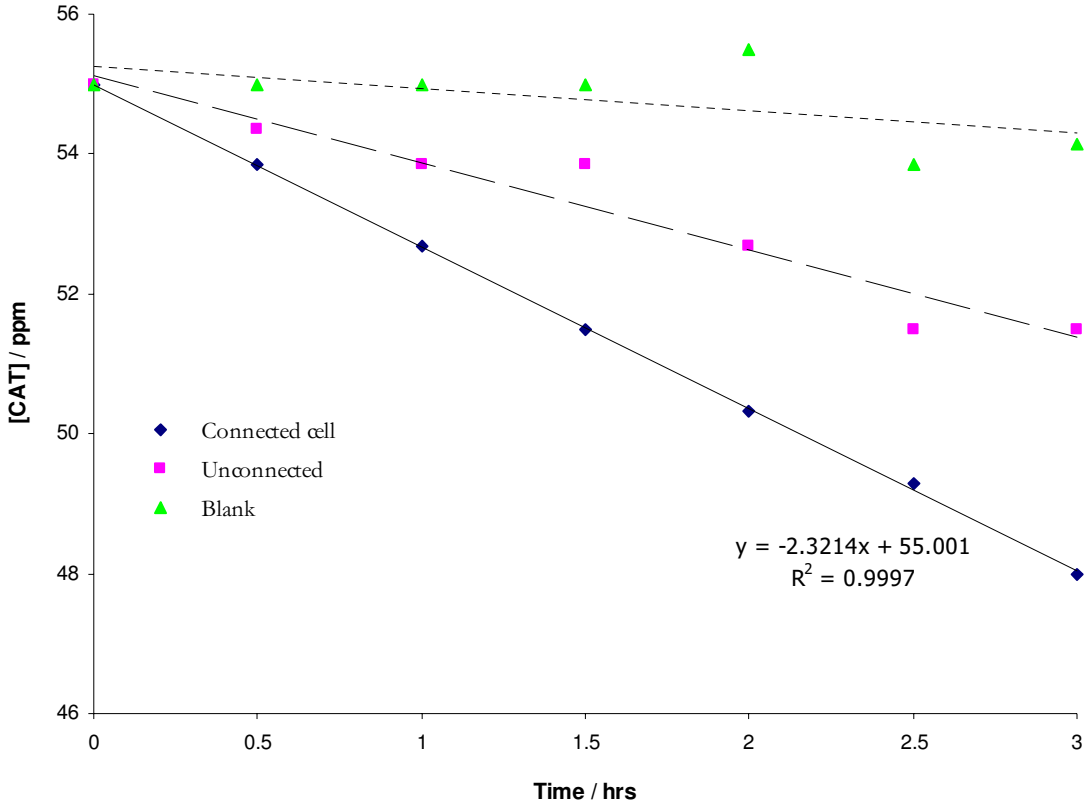

Figure 5.3.15: Degradation of CAT (55 ppm) in aqueous 0.1 M KCl with time (hours) in a one compartment cell. 25 cm^2 TiO_2/CI anode and air cathode connected through a 1 kΩ resistor. Unconnected cell and blank are also included. Irradiated by daylight.

5.3.6.2 Degradation of CAT using a 150 W Xe lamp

A similar experiment was carried out as in section 5.3.6, but instead of using daylight an oriel 6253 150 W Xe arc lamp was used instead. The results are detailed in figure 5.3.16.

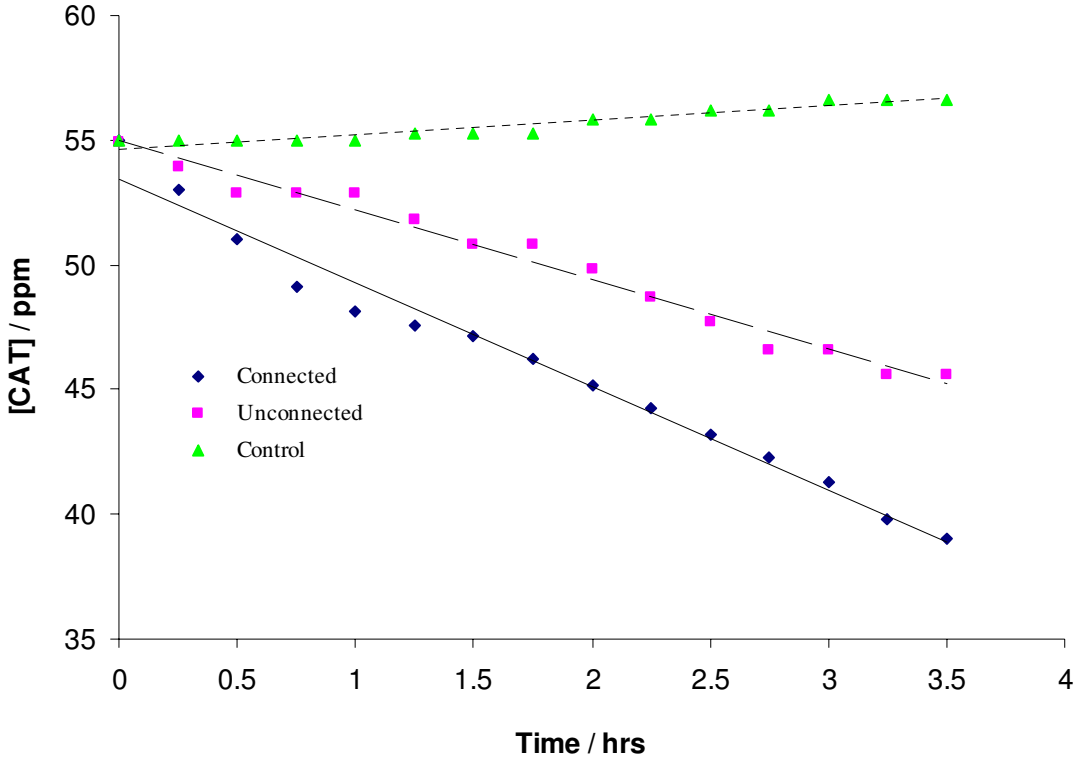

Figure 5.3.16: Degradation of CAT (55 ppm) in aqueous 0.1 M KCl with time (hours) in a one compartment cell. 25 cm^2 TiO_2/CI anode and air cathode connected through a 1 kΩ resistor. Unconnected cell and blank are also included. Irradiated by a 150 W Xe arc lamp.

In 3.5 hours the connected cell had broken CAT down from 55 ppm to 39 ppm (29 % degradation). In 2.5 hours it's down to 43 ppm (22 % breakdown), and in the same timeframe when using daylight there was a CAT decrease in concentration from 55 ppm to 49 ppm (11 % decrease). This means that the 150 W Xe lamp is twice as efficient as sunlight for activating TiO_2 on the electrode and catalysing the photoelectrodegradation. This may be because it is much more focused than daylight and also contains more UV.

During this experiment, the question of what CAT degraded to arose. It may be possible that a 1,2–benzenedione was formed. Oxidation reactions of phenol were found

to yield ring opening products like maleic, formic, acetic, oxalic, malonic, succinic and fumaric acids not only on the solid surface but also in the liquid phase [44].

5.3.7.1 Degradation of 4-chlorophenol (4CP) using daylight

As the results obtained for CAT degradation were promising when using a connected photoelectrochemical cell, an attempt was made to degrade the severe pesticide 4-chlorophenol (4CP) using the same experimental set up as featured in sections 5.3.6. There have been many attempts to degrade 4CP before. In a visible light-driven twin cell, a tungsten trioxide (WO_3) photoanode was adsorbed on a conducting glass slide and used to degrade the 2,4-dichlorophenol (2,4-DCP); while the loss of the parent molecule was determined by HPLC [45]. TiO_2 photoassisted degradation of 4CP was carried out by Serpone *et al* [46], and they discovered that upon addition of 4 other prominent hole acceptors, the excess electrons present on the TiO_2 nanoparticles left a blue colour (confirmed by diffuse reflectance spectra).

The experiment was ran for a week, and again samples were taken out every morning and evening. Even in such small quantities, 4CP leaves a pungent odour. Its UV spectra are shown in figure 5.3.17 (a) at the start of the experiment and (b) after the experiment.

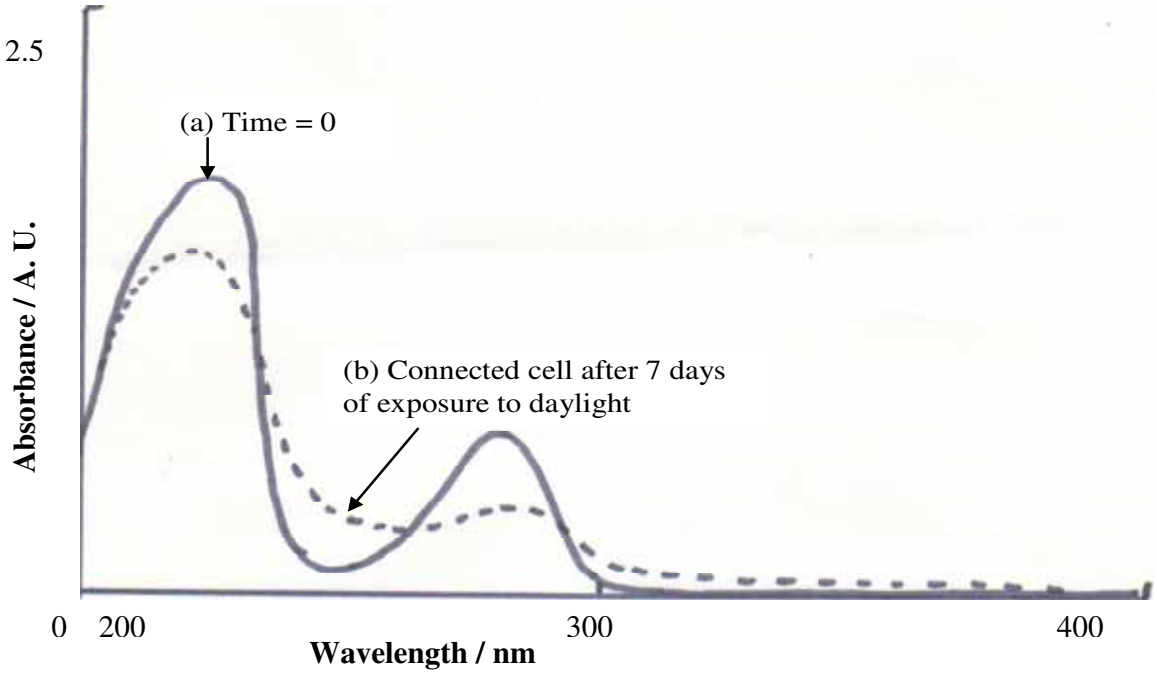

Figure 5.3.17: Initial UV spectra of 4CP (a) and (b) after 7 days. The one compartment cell consisted of an air cathode and a 25 cm^2 TiO_2 on C anode. These were placed in a beaker of 43 ppm 4CP (50 cm^3) in 0.1 M KCl and the both terminals were connected through a 1 kΩ resistor

The results of the photocatalysed degradation are shown in figure 5.3.18.

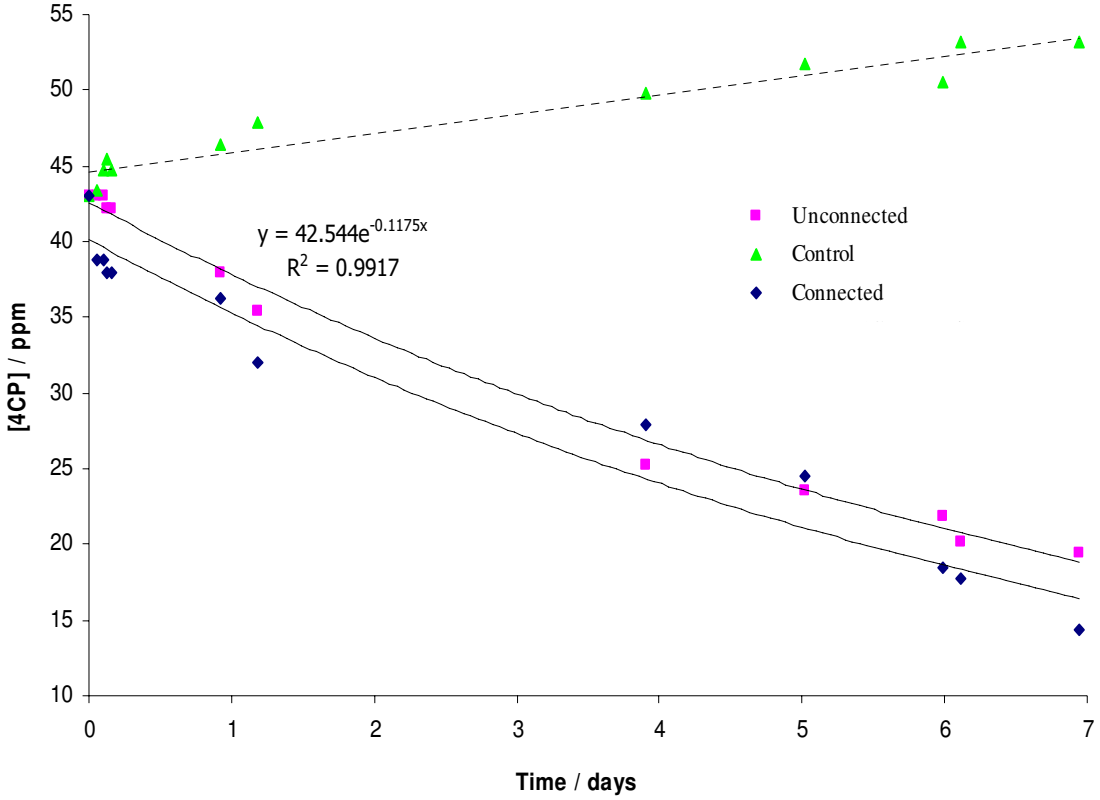

Figure 5.3.18: Degradation of 4CP (43 ppm) in aqueous 0.1 M KCl with time (hours) in a one compartment cell. 25 cm^2 TiO_2/CI anode and air cathode connected through a 1 kΩ resistor. Unconnected cell and blank are also included. Irradiated by daylight.

From the results it appears that 4CP is a far more stable compound than CAT. For the connected cell within four days of using the same light source (daylight), CAT is degraded from 64 to 8 ppm (88 % degradation). Within the same time period and under the same conditions, 4CP goes from 43 to 28 ppm (35 % decrease). So 4CP is over twice as stable as CAT.

5.3.7.2 Degradation of 4CP using a 150 W Xe lamp

The next step was to repeat the experiment using a 150 W Xe lamp as the light source with the same experimental conditions. The results are shown in figure 5.3.19.

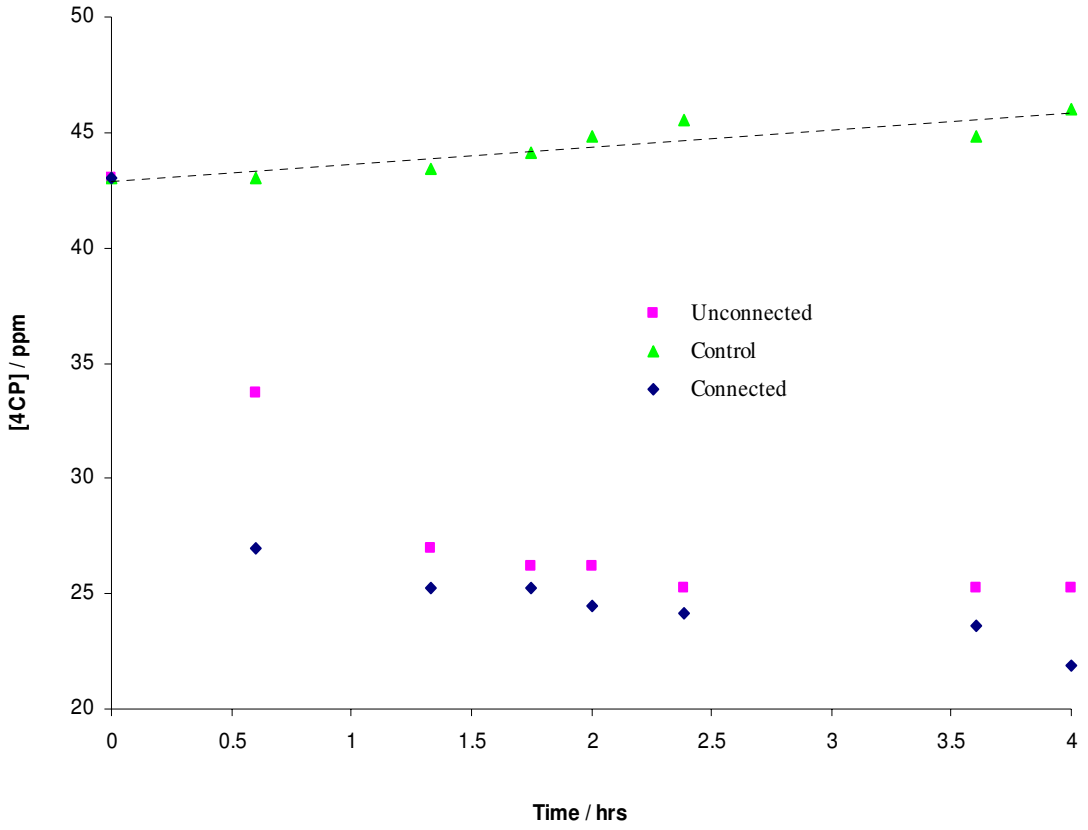

Figure 5.3.19: Degradation of 4CP (43 ppm) in aqueous 0.1 M KCl with time (hours) in a one compartment cell. 25 cm^2 TiO_2/CI anode and air cathode connected through a 1 kΩ resistor. Unconnected cell and blank are also included. Irradiated by a 150 W Xe lamp.

When using daylight as the light source for the connected cell, in 3 hours 4CP is degraded from 43 to 38 ppm (12 %). When using a 150 W Xe lamp for the connected cell there is decrease from 43 to 24 ppm (35 %). So in this instance, the 150 W Xe lamp was 3 times a better light source than daylight.

5.4 Conclusion

In conclusion, although light with very little UV was used; there is some evidence of degradation of organics facilitated by the presence of the electrochemical cell. Benzaldehyde degrades readily with some indication that the cell speeds up the rate of degradation. However the most compelling evidence is that for ascorbic acid, where there is a clear improvement in the rate of degradation in the cell.

As can be seen in the results presented, there is a substantial degradation of many different organic compounds using an irradiated surface bound TiO_2 in various arrangements of photoelectrochemical cells. The aim of the chapter is to validate the theory that the practical photoelectrochemical system operates better than TiO_2 coatings alone. It should be noted that the system comprises of an ink based anode which can be cheaply produced and the air electrode material is readily available.

The stable KHP is degraded faster at the connected electrode than at the unconnected anode when using a 400 W Hg light source. However for some pollutants (catechol and 4-chlorophenol), the advantage of the connected photoelectrochemical cell is not as much over the presence of TiO_2. What are promising are the results obtained for catechol exposed to daylight on the inside of a laboratory window sill. Catechol is degraded readily with the cell compared to the unconnected anode in this example.

5.5 References

[1] M. Lemberg, J. Menendez, C. Koth, M. Freeman, *Abstracts / Journal of Biotechnology* 118S1 (2005) S1–S189.

[2] Yizhong Wang, *Water Research*, **34**, 3 (2000) 990 – 994

[3] http://www.lenntech.com/home.htm accessed on 15/6/08

[4] S. Safe, G. Mason, B. Keys, K. Farrell, B. Zmudzka, T. Sawyer, J. Piskorska-Pliszczynska, L. Safe, M. Romkes, S. Bandiera, *Chemosphere*, **15**, 9 - 12 (1986) 1725-1731

[5] G. Mason, T. Sawyer, B. Keys, S. Bandiera, M. Romkes, J. Piskorska-Pliszczynska, B. Zmudzka, S. Safe, *Toxicology*, **37**, 1-2 (1985) 1-12

[6] S. Safe, T. Sawyer, G. Mason, S. Bandiera, B. Keys, M. Romkes, J. Piskorska-Pliszczynska, B. Zmudzka, L. Safe, *Chemosphere*, **14**, 6-7 (1985) 675-683

[7] S. Bandiera, T. Sawyer, M. Romkes, B. Zmudzka, L. Safe, G. Mason, B. Keys, S. Safe, *Toxicology*, **32**, 2 (1984) 131-144

[8] S. Bandiera, K. Farrell, G. Mason, M. Kelley, M. Romkes, R. Bannister, S. Safe, *Chemosphere*, **13**, 4 (1984) 507-512

[9] J. Andres, I. Lambert, L. Robertson, S. Bandiera, T. Sawyer, S. Lovering, S. Safe, *Toxicology and Applied Pharmacology*, **70**, 2 (1983) 204-215

[10] P. Fernández, J. Blanco, C. Sichel, S. Malato, *Catalysis Today*, **101** (2005) 345 - 352

[11] W. Gernjak, M.I. Maldonado, S. Malato, J. Cáceres, T. Krutzler, A. Glaser, R. Bauer, *Solar Energy*, **77** (2004) 567 – 572

[12] T. Essam, M.A. Amin, O. El Tayeb, B. Mattiasson, B. Guieyesse, *Water Research*, **41** (2007) 1697 – 1704

[13] G. Vincent, P.M. Marquaire, O. Zahraa, *Journal of Photochemistry and Photobiology A: Chemistry* 197 (2008) 177–189.

[14] I.A. Balcioglu, M. Otker, *Chemosphere*, **50** (2003) 85

[15] C. Reyes, J. Fernández, J. Freer, M.A. Mondaca, C. Zaror, S. Malato, H.D. Mansilla, *Journal of Photochemistry and Photobiology A: Chemistry* **184** (2006) 141 – 146

[16] S. Yurdakal, V. Loddo, V. Augugliaro, H. Berber, G. Palmisano, L. Palmisano, *Catalysis Today*, **129** (2007) 9 – 15

[17] H.M. Coleman, E.J. Routledge, J.P. Sumpter, B.R. Eggins, J.A. Byrne, *Water Research*, **38** (2004) 3223 – 3240

[18] J.A. Byrne, A. Davidson, P.S.M. Dunlop, B.R. Eggins, *Journal of Photochemistry and Photobiology A: Chemistry*, **148** (2002) 365 – 374

[19] V. Augugliaro, A. Bianco Prevot, J. Cáceres Vazquez, E. Garcia Lopez, A. Irico, V. Loddo, S. Malato Rodriguez, G. Marci, L. Palmisano, E. Pramauro, *Advances in Environmental Research*, **8** (2004) 329 – 335

[20] M.A. Hasnat, M.M. Uddin, A.J.F. Samed, S.S. Alam, S. Hossain, *Journal of Hazardous Materials*, **147** (2007) 471 – 477

[21] G. Balasubramanian, D. Dionysiou, M.T. Suidan, I. Baudin, J.-M. Laine, *Applied Catalysis B Environmental*, **47** (2004),73-84

[22] J.-C. Lee, M.-S. Kim, B.-W. Kim, *Water Research*, **36** (2002) 1776-1782.

[23] K. Vinodgopal, S. Hotchandani, P.V. Kamat, *Journal of Physical Chemistry,* **97** (1993) 9040-9044.

[24] K. Vinodgopal, U. Stafford, K.A. Gray, P.V. Kamat, *Journal of Physical Chemistry*, **98** (1994) 6797-6803

[25] G. Alhakimi, S. Gebril, L. Studnicki, *Journal of Photochemistry and Photobiology A: Chemistry*, **157** (2003) 103 – 109

[26] S. Horikoshi, T. Miura, M. Kajitani, H. Hidaka, N. Serpone, *Journal of Photochemistry and Photobiology A: Chemistry*, **194** (2008) 189 – 199

[27] G.P. Smested, M. Gratzel, *Journal of Chemistry Education*, **75** (1998) 752-756

[28] C. Bohrman-Linde, M.W. Tausch, *Journal of Chemistry Education*, **80** (2003) 1471-1473.

[29] S. Malato Rodríguez, J. Blanco Gálvez, M. Maldonado Rubio, R. Fernández Ibáñez, W. Gernjak, I. Oller Alberola, *Chemosphere*, **58** (2005) 391 – 398

[30] A. Fujishima, T.N. Rao, D.A. Tryk, *Journal of Photochemistry and Photobiology A: Chemistry*, **1** (2001) 1 – 21

[31] E.F. Duffy, F. Al Touati, S.C. Kehoe, O.A. McLoughlin, L.W.Gill, W. Gernjak, I. Oller, M.I. Maldonado, S. Malato, J. Cassidy, R.H. Reed, K.G. McGuigan, *Solar Energy*, **77** (2004) 649-655

[32] G. Vincent, P.M. Marquaire, O. Zahraa, *Journal of Photochemistry and Photobiology A: Chemistry*, **197** (2008) 177 – 189

[33] J.A. Byrne, B.R. Eggins, N.M.D. Brown, B. McKinney, M. Rouse, *Applied Catalysis B: Environmental*, **17** (1998) 25 – 36

[34] I. Ilisz, A. Dombi, *Applied Catalysis A: General*, **180** (1999) 35

[35] B. Tryba, A.W. Morawski, M. Inagaki, M. Toyoda, *Applied Catalysis B: Environmental*, **63** (2006) 215 – 221

[36] A.G. Rincon, C. Pulgarin, N. Adler, P. Peringer, *Journal of Photochemistry and Photobiology A: Chemistry*, **139** (2001) 233 – 241

[37] A. Verma, S. Basu, *Journal of Power Sources*, **145** (2005) 282 – 285

[38] G. Alhakimi, L.H. Studicki, M. Al-ghazali, *Journal of Photochemistry and Photobiology A: Chemistry*, **154**, Issue 2-3 (2003) 219-228

[39] P.J. O'Connell, C. Gormally, M. Pravda, G. Guilbault, *Analytica Chimica Acta,* **431** (2001) 239 – 274

[40] M.D. Trotter, M.J. Sulway, E. Trotter, *Clinica Chemica Acta*, **35**, 1 (1971) 137 – 143

[41] B. Ohtani, K. Iwai, S. Nishimoto, S. Sato, *Journal of Physical Chemistry B*, **101** (1997) 3349 – 3359

[42] S.I. Nishimoto, B. Ohtani, T. Kagiya, *Journal of the Chemical Society, Faraday Transactions 1*, **81** (1985) 2467 – 2474

[43] J. Li, L.M. Peter, R. Potter, *Journal of Applied Electrochemistry*, **14** (1983) 495 – 504

[44] A. Santos, P. Yustos, A. Quintanilla, S. Rodriguez, F. Garcia-Ochoa, *Applied Catalysis B: Environmental*, **39** (2002) 97

[45] S. Nissen, B.D. Alexander, I. Dawood, M Tillotson, R.P.K. Wells, D.E. Macphee, K. Killham, *Environmental Pollution* **157** (2009) 72–76

[46] N. Serpone, I. Texier, A.V. Emeline, P. Pichat, H. Hidaka, J. Zhao, *Journal of Photochemistry and Photobiology A: Chemistry* **136** (2000) 145 – 155

Chapter 6

Modelling square wave voltammetry at microelectrodes

Chapter 6 – Microelectrode work

6.1 Introduction

6.1.1 Microelectrodes

Microelectrodes are defined as electrodes that have at least one dimension (i.e. length, breadth or height) in the order of between 0.1 to 50 μm [1]. While they exhibit high current densities (A m^{-2}), their very small area leads to a low total current so the percentage electrolysis of a solution is small. Steady state currents are more easily achieved at microelectrodes than at their larger macro counterparts. This is due to the operation of more efficient mass transport mechanisms. After a certain time, a steady state is reached and the current for a disk ultramicroelectrode is given by equation 6.1.

$$i = 4r_0nFDc \qquad 6.1$$

Where:

i	=	current / A
r_0	=	electrode radius / cm
D	=	diffusion co-efficient / cm^2 s^{-1}
n	=	number of electrons transferred
F	=	Faraday's constant = 96485 A s mol^{-1}
C	=	Concentration / mol cm^{-3}

Equation 6.1 allows the calculation of the electrode radius. A nominal size of the radius is given by the manufacturer but this may vary and it is very difficult to make an electrode this size with accuracy. For that reason, the electrode is used and the current measured allows us to measure the radius with more accuracy.

In figure 6.1.1 the diffusion profile at microelectrodes and how it is arrived at is depicted. For planar electrodes linear diffusion predominates while for hemispherical and disk electrodes radial diffusion is possible.

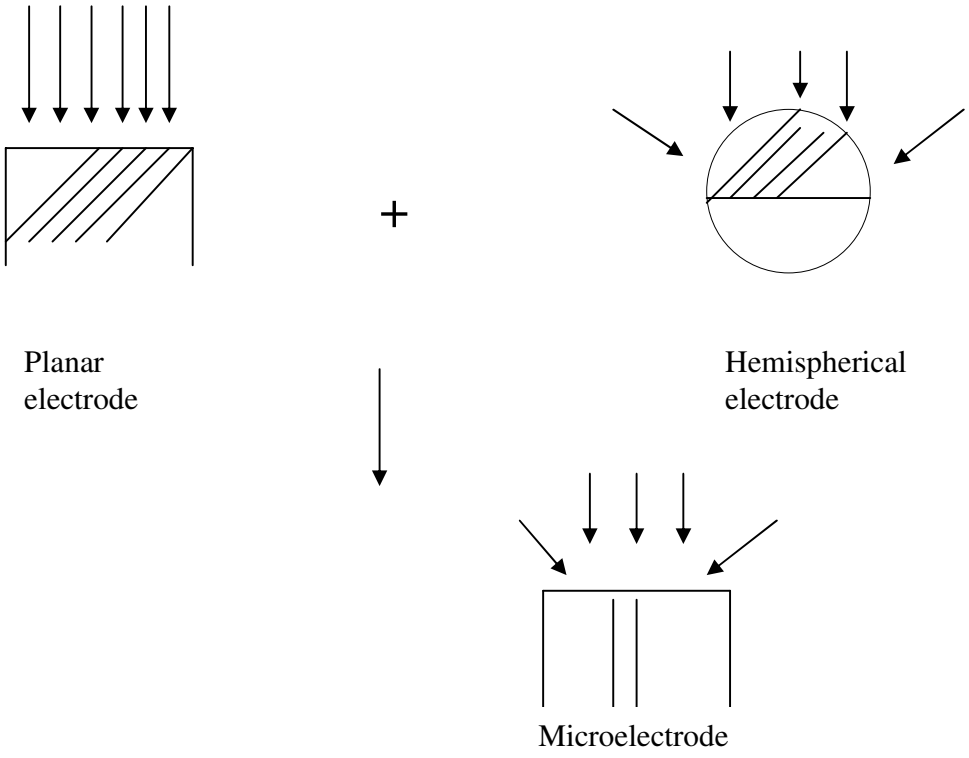

Figure 6.1.1: Diffusion profiles at a microelectrode

Because the microelectode is so accessible to analytes, diffusion rates are high. Their low currents mean that *i*R drop in the solution (ohmic potential and product of Ohm's law, equation 6.2); and interferences from convection are negligible, another bonus. Supporting electrolyte isn't as necessary when using microelectrodes as measurements can be made in resistive media which from an industrial point of view makes microelectrodes economically advantageous.

$$E = iR \qquad 6.2$$

Where: E = Potential / V
i = Current / A
R = Resistance / V A^{-1} = Ω

Microelectrodes small size has enabled their uses in the medical world. They can probe current responses at regions where space is at a premium, such as at nerve synapses and junctions.

For all of the listed advantages that they possess, it stands to reason that microelectrodes must have some disadvantages too. As there is a steady supply of material to the microelectrode (figure 6.1.1), when voltammetry is performed at it a sigmoidal response is obtained (figure 6.3.1).

Because of their small size, their manufacture is more difficult and they are therefore more costly than macroelectrodes. Adsorption of physical or chemical species can inhibit their active working area and lessen the flow of current. Such processes can also delay their response.

In order to rid the electrode surface of such contaminants and impurities, polishing on a soft cloth with a slurry of alumina is necessary. While this is the same routine used for macroelectrodes, the polishing procedure for microelectrodes is a much more delicate ordeal, as rough polishing will diminish the surface area and possibly render the microelectrode useless. Should this happen however, the microelectrode can be restored to working order by paring back the surrounding insulating area and exposing the disc wire.

6.1.2 Square wave voltammetry (SWV)

SWV as an analytical technique is less than 60 years old but with advances in computer processing units and instrumentation such as potentiostats used to apply a bias, it has become a relatively important one. This is mainly because it is possible to operate the method at fast sweep rates. This sweep rate is given by equation 6.3. Typically in

SWV scan rates can run at 200 mV s^{-1} which is much faster than most cyclic voltammetry experiments run at. As a result, the electrode reaction for the species in solution is generally diffusion limited.

$$\nu = Es(f) \qquad 6.3$$

Where: ν = scan rate / V s^{-1}
Es = Incremental base potential / V
f = Frequency / s^{-1}

Pulse techniques are concerned with the measurement of current as a function of time after the application of a potential step, and so it can be said that they are based on chronoamperometry. A useful peaked response is obtained instead of a sigmoidal one. The current is recorded at two points – at the top of the wave (t_1, often referred to as 2tp) and at the bottom (t_2, often referred to as tp), (figure 6.1.2) after the double layer has time to charge and the capacitance current is diminished. The waveform for this pulsed technique is in stark contrast with the linear wave signal in cyclic voltammetry (figure 2.1.2). E_{sw} is the square wave amplitude (half peak to peak). E_{step} (also known as ΔE_{inc} and Es) is the staircase potential step height. The difference between the two currents is then plotted against applied potential to give a peaked voltammogram.

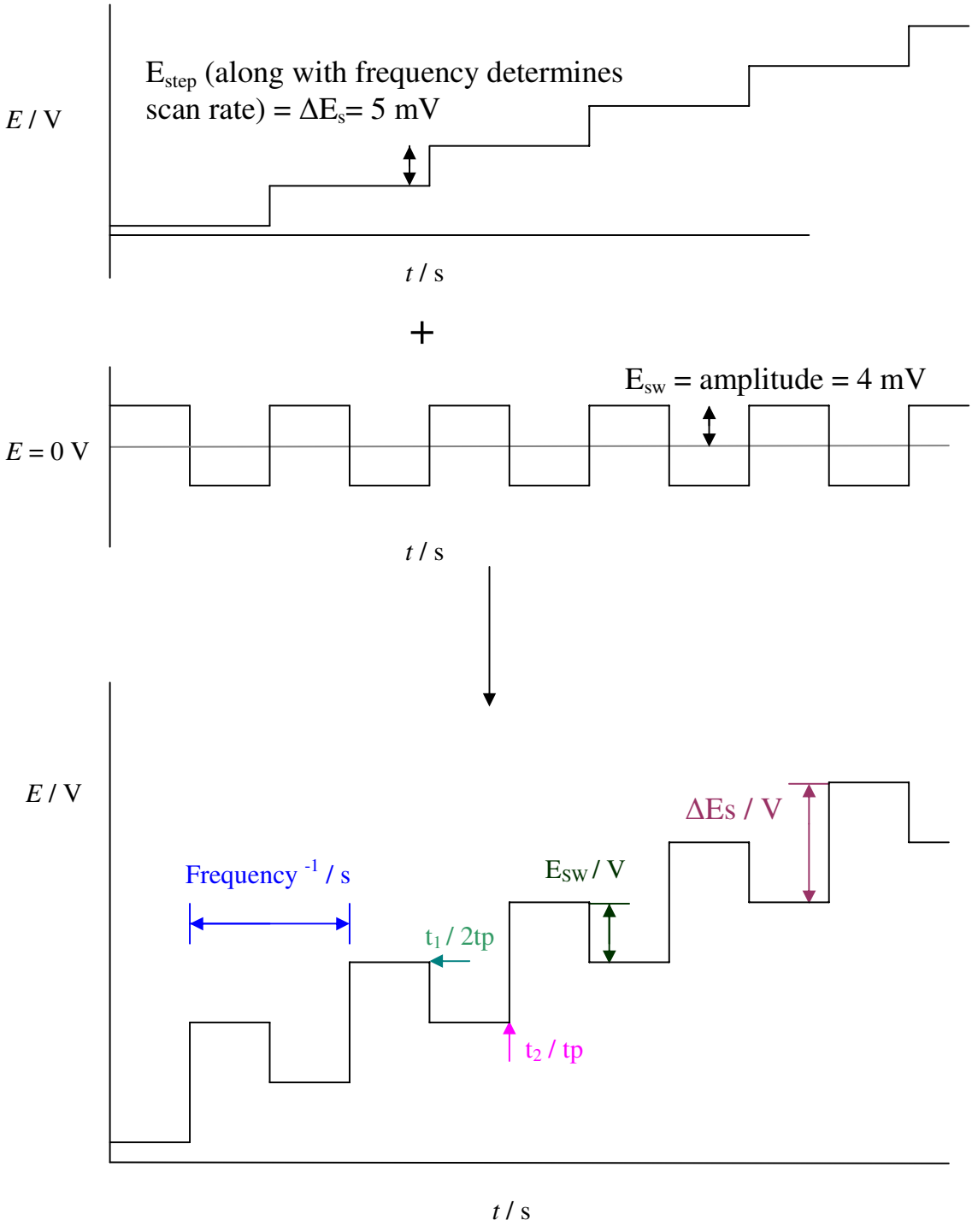

Figure 6.1.2: Potential pulses arising in SWV

As the current is sampled at two different points, a high and a low current value is obtained; and the latter is subtracted from the former (figure 6.1.3). It is peak shaped but consists of a differential curve between the current recorded in the forward half-cycle and the current recorded in the reverse half-cycle. As the reverse scan (current measured at t_2) produces a negative current, when it is subtracted from the current measured at t_1 it produces an absolute value and thus a larger peak. Figure 6.1.3 shows this differentiated current output as plotted against potential to yield a typical square wave voltammogram.

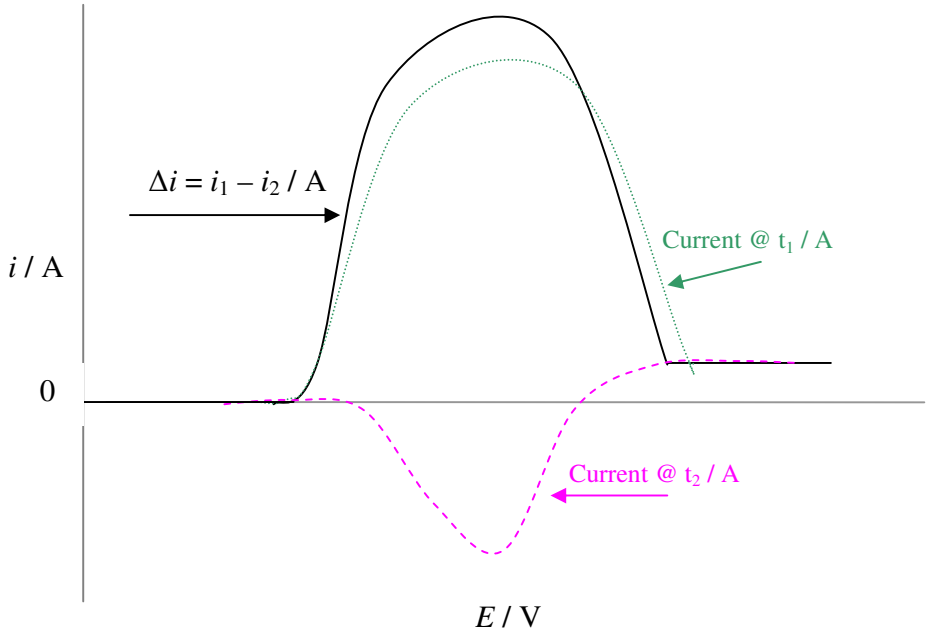

Figure 6.1.3: Current outputs at a microelectrode and how the overall current is calculated

For a reversible process (such as in ferrous cyanide used in this work), the peak width at half height is given by equation 6.4.

$$\Delta E_{phh} = 4900 \text{ mV} \frac{RT}{nF} \quad 6.4$$

Where: ΔE_{phh} = Peak width at half height / V
R = Universal gas constant 8.314 J mol^{-1} K^{-1}
T = Temperature / K
n = number of electrons transferred
F = Faraday's constant = 96485 J V^{-1} mol^{-1}

At a typical room temperature of 20° C, equation 6.4 can be abbreviated to equation 6.5.

$$\Delta E_{phh} = \frac{124 \text{ mV}}{n} \quad 6.5$$

The peak current depends on amplitude, and heights of the wave can be quite large. However, large pulse amplitudes give rise to broadened waves. Current can increase linearly with the square root of frequency, and a linear one of these plots indicates a diffusion controlled process.

Microelectrodes have found many uses in electroanalysis as single disks or arrays. The use of SWV has traditionally been employed for anodic stripping methods, for example in the determination of epinephrine [2] and more commonly for the detection of heavy metals, Cd^{2+}, Pb^{2+} and Cu^{2+} [3 - 5]. However organics such as paraquat [6, 7], chloroamphenicol [8] and vanillin [9] have been determined using SWV at microelectrodes.

6.1.3 Modelling SWV at microelectrodes

There has been work done in modelling SWV at microelectrodes by Whelan *et al* [10]. Furthermore the application of SWV has been modelled at spherical electrodes [11] and spherical microelectrodes [12]. In this work the application of an empirical model is

evaluated, used previously for differential pulse voltammetry at a microelectrode [13] and a rotating disk electrode [14], to SWV at a microelectrode disk.

6.1.4 The steady state model

This model relies on the rapid achievement of a microelectrode steady state current on application of SWV pulses. The square wave voltammetric waveform arises from the superimposition of two waveforms, an incremental staircase potential of amplitude ΔEs, which has a square wave amplitude waveform superimposed on it (as shown in figure 6.1.2) of magnitude E_{sw} [15, 16]. The current is sampled at the lower potential of the E_{sw}, at tp, and then at the higher potential, at 2tp where tp is related to the frequency of the square wave waveform, as f = 1/(2tp), and the difference between these two currents is the output. The pulse of length tp corresponds to half the period of the applied staircase potential. At the lower potential (tp) the current is given by equation 6.6:

$$i_1 = \frac{4nFrDC}{1+\varepsilon_1} \qquad 6.6$$

Where:
- r = microelectrode radius / cm
- D = diffusion co-efficient of the electroactive species in solution / $cm^2\ s^{-1}$
- n = number of electrons transferred
- F = Faraday's constant = 96485 A s mol^{-1}
- C = Concentration / mol cm^{-3}
- ε_1 = a function of the applied potential E_i

$$\varepsilon_1 = \exp\left(\frac{-nF(E_i - E^o)}{RT}\right) \qquad 6.7$$

Where:
- Ei = initial potential / V
- E^o = formal potential of the electroactive couple / V
- R = Universal Gas constant 8.314 J $mol^{-1}\ K^{-1}$
- T = Temperature / K

On application of the pulse E_{sw}, the current sampled at 2tp is given by equation 6.8.

$$i_2 = \frac{4nFrDC}{1+\varepsilon_2} \qquad 6.8$$

where

$$\varepsilon_2 = \exp\left(\frac{-nF(E_i + 2Esw - E^0)}{RT}\right) \qquad 6.9$$

And in the next time increment the base potential E_i will increment by ΔE_s. The output current is given by equation 6.10 (as illustrated in figure 6.1.2).

$$\delta i = i_2 - i_1. \qquad 6.10$$

Typically the current output is plotted against the mid point potential of each square wave cycle [10]. As an approximation, the Taylor series expansion of the exponential function is given by equation 6.11.

$$\left(\frac{1}{1+e^x}\right) \approx 1/2 - x/4 + x^3/48 + O(x^4) \qquad 6.11$$

Equation 6.11 can then be used to obtain an estimate for the current output, δi.

6.2 Experimental

6.2.1 Materials

- De-ionised water (l)
- Potassium chloride (s, KCl, Merck, 99.5+ %)
- Potassium hexacyanoferrate(II)-3-hydrate (s, FeoCN, Riedel-de Haën, 99 %)
- Oxygen free nitrogen (g, N_2, BOC Gas, > 99.999 %)
- Aluminium oxide 41 μm 600 grit (s, Varian)
- Felt

6.2.2 Equipment

- DMV-5800L ultrasonic cleaner (Delta)
- Ref 401 mercury (I) chloride in saturated potassium chloride reference electrode, potential at 298 K 0.241 V (NHE) [17] (SCE, Radiometer Analytical)
- Ref 601 mercury - mercury (I) sulphate in saturated potassium sulphate reference electrode, potential at 298 K = 0.638 V (NHE) [17] (MSE, Radiometer Analytical)
- Platinum crescent sheet counter electrode (PtAE, approx area = 12 cm^2)
- CHI107 Pt disc microelectrode (PtME10, CH Instruments, diameter = 10 μm)
- CHI108 Pt disc microelectrode (PtME25, CH Instruments, diameter = 25 μm)
- CHI620A electrochemical analyser, (CH Instruments, 3700 Tennison Hill Drive Austin, TX 78738 USA)

6.2.3 Methodology

6.2.3.1 Experimental set up

Experiments were carried out at room temperature (20 ± 3^{o}C) using a microelectrode, with a nominal 10 μm or 25 μm diameter Pt disk (source = IJ Cambria Scientific Ltd, 11 Gwscwm Road, Burry Port, Carms, SA16 OBS UK) in a three electrode one compartment cell. The reference electrode was a saturated calomel electrode and the auxiliary electrode was Pt wire. Potentials were controlled using a CHI 620A electrochemical analyser. Chemicals were reagent grade and solutions were prepared in deionised water.

6.2.3.2 SWV studies

SWV was carried out on an unstirred aqueous solution of 5 mM FeoCN in 0.1 M KCl. Three parameters were varied – the incremental staircase (ΔEs); this has a square wave amplitude waveform superimposed on it, (E_{sw}) and frequency (f).

All scans were performed at an initial potential of - 0.2 V to a final potential of 0.6 V. Sensitivity was set at 1×10^{-8} A V^{-1}. Each electrode was lightly polished with alumina between scans.

6.2.3.3 Cyclic voltammetry studies

A cyclic voltammogram (CV) using the same PtME was done in order to more accurately determine the electrode area (quoted as having a diameter of 10 or 25 μm).

CV was done in an unstirred solution cycled for 2 segments positively from – 0.2 → 0.6 V using an SCE reference at a scan rate of 20 mV s^{-1} and sensitivity of 1×10^{-8} A V^{-1}.

6.3 Results & Discussion

6.3.1 Cyclic voltammetry studies

Figure 6.3.1 shows a selection of cyclic voltammograms at microelectrodes. There is a sigmoidal shape obtained due to the absence of mass transfer limitations.

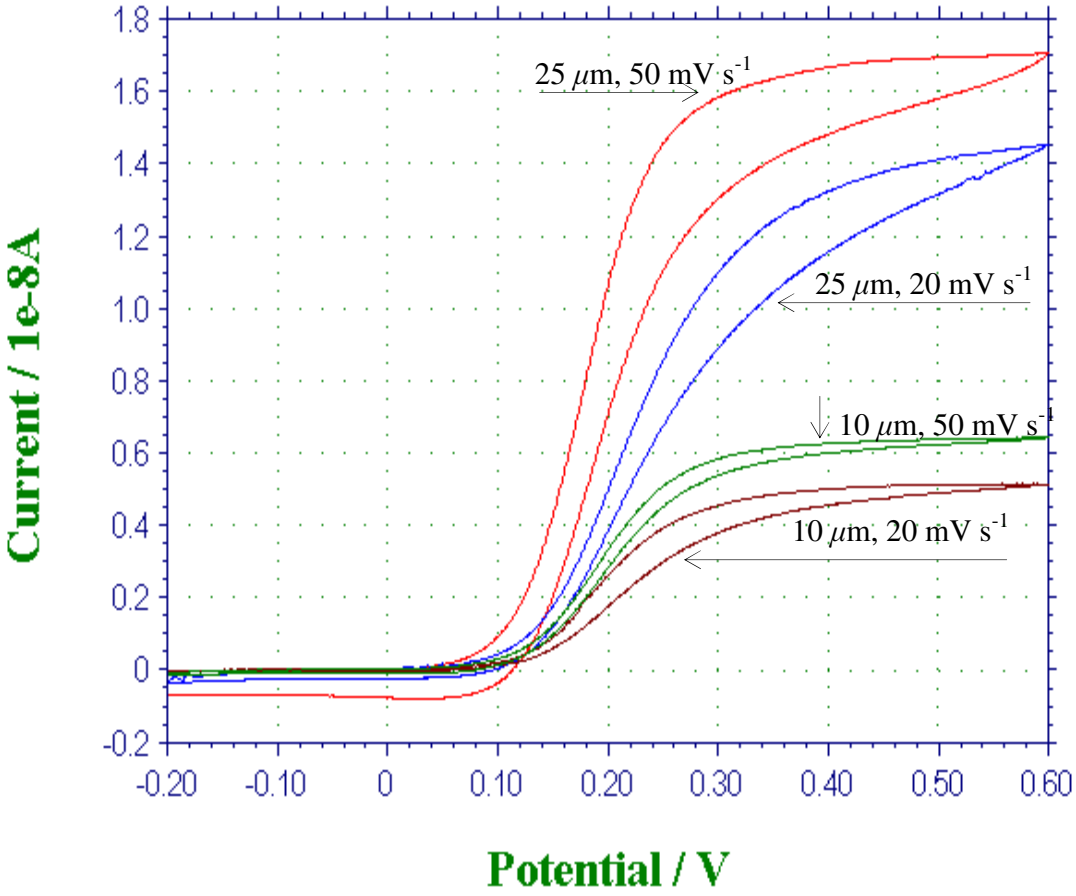

Figure 6.3.1: Cyclic voltammogram of 5 mM FeoCN in aqueous 0.1 M KCl using a 10 μm or 25 μm PtME, Pt crescent AE and a calomel RE. Cycled positively from 0.6 to – 0.2 V at either 20 or 50 mV s^{-1}.

In figure 6.3.2 a more typical cyclic voltammogram is shown, this time using a working macroelectrode.

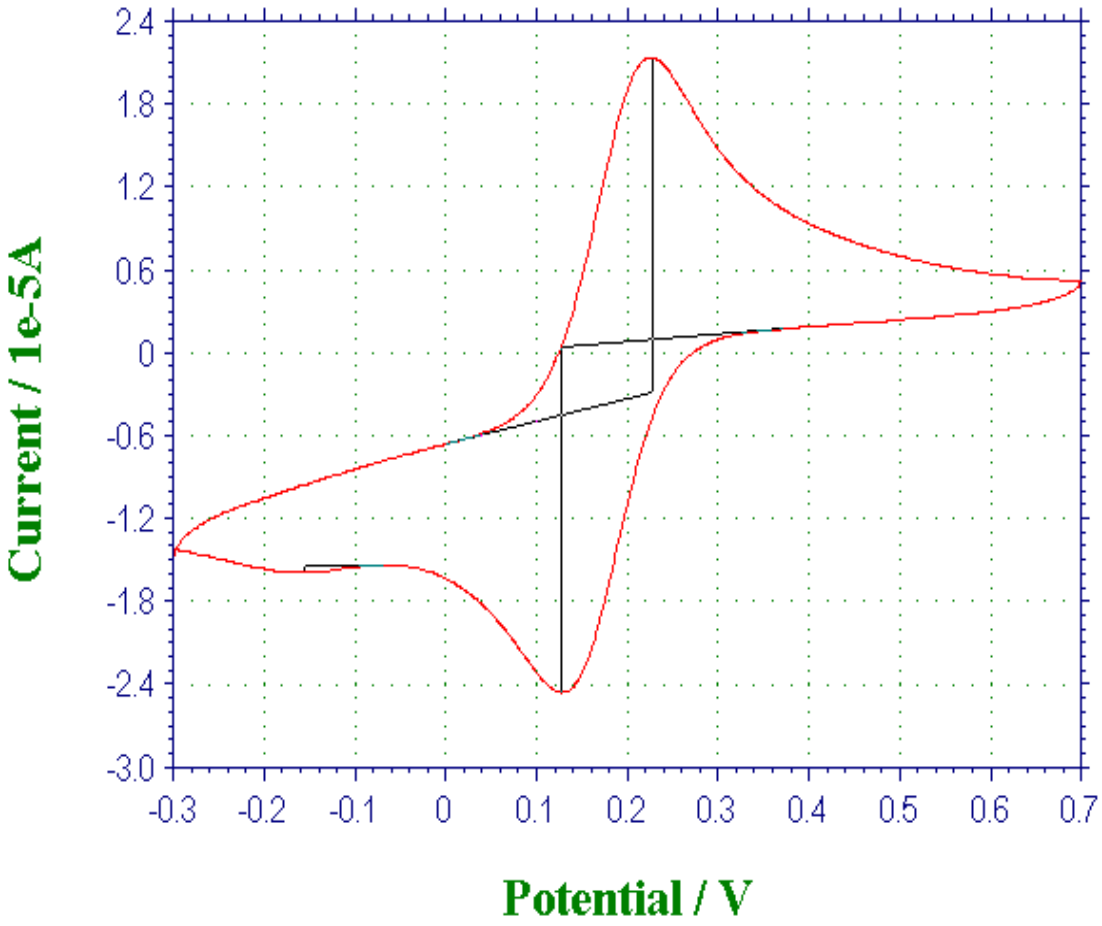

Figure 6.3.2: Cyclic voltammogram of 5 mM ferricyanide in aqueous 0.1 M KCl using a glassy carbon electrode (area = 0.07 cm^2), Pt crescent AE and an MSE reference electrode. Scan rate = 50 mV s^{-1}.

6.3.2 Determination of r for both the 10 µm & 25 µm microelectrodes

As was mentioned previously, the exact electrode areas had to be determined by CV as there is a huge margin for error when dealing with such tiny areas. An interesting point of note is that for both anodic and cathodic cycles at 0 V there is little or no current produced at this applied potential. This indicates a pure solution of ferrocyanide; if there

was current produced without applying any potential then some of the ferrocyanide would have oxidised to ferricyanide, with the solution going from clear to a pale green/yellow. For this reason it was vital to make up solutions freshly.

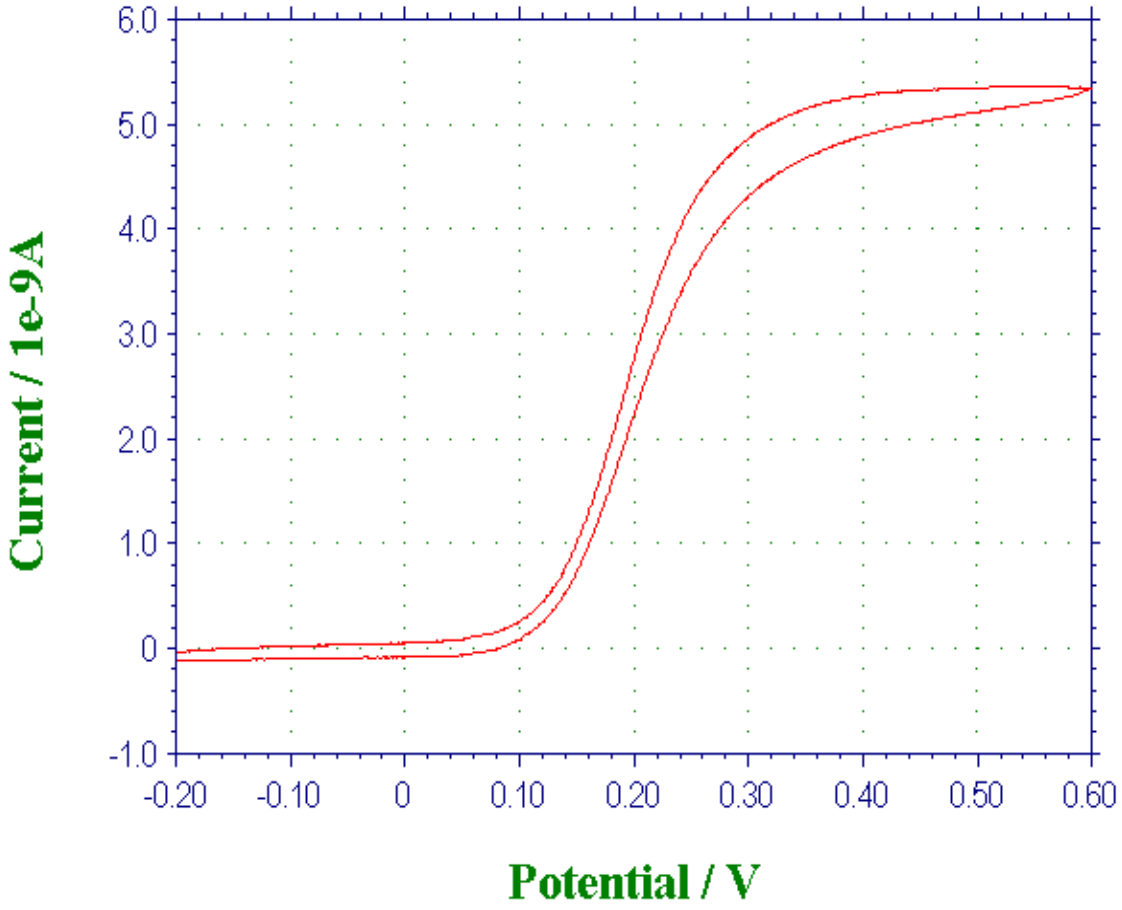

Figure 6.3.3: Cyclic voltammogram of 5 mM ferrocyanide in aqueous 0.1 M KCl using a PtME (nominal diameter = 10 μm), Pt crescent AE and a calomel RE. Cycled positively from – 0.2 to 0.6 V at a rate of 50 mV s^{-1}.

From initial linear sweep voltammetric experiments with the two electrodes in 5 mM $K_4[Fe(CN)_6]$ in 0.1 M KCl, the current was determined to be 5.1 nA and 14.1 nA from which effective radii were calculated to be 4.1 microns and 11.2 microns for 10 and 25 μm electrodes respectively, using a diffusion coefficient of 6.5 x 10^{-6} cm^2s^{-1} [18].

Following this, square wave potential waveforms were applied to determine the nature of the current response.

6.3.3 Variation in amplitude (E_{sw})

6.3.3.1 Effect of E_{sw} on current

The parameters varied for SWV were pulse height E_{sw}, staircase step height ΔEs and frequency f. It was found that the parameter which has the greatest effect on peak current is pulse height E_{sw}. Figure 6.3.4 shows the experimental current profile for a range of E_{sw} values. It can be seen that peak current and peak width at half height increases with E_{sw}.

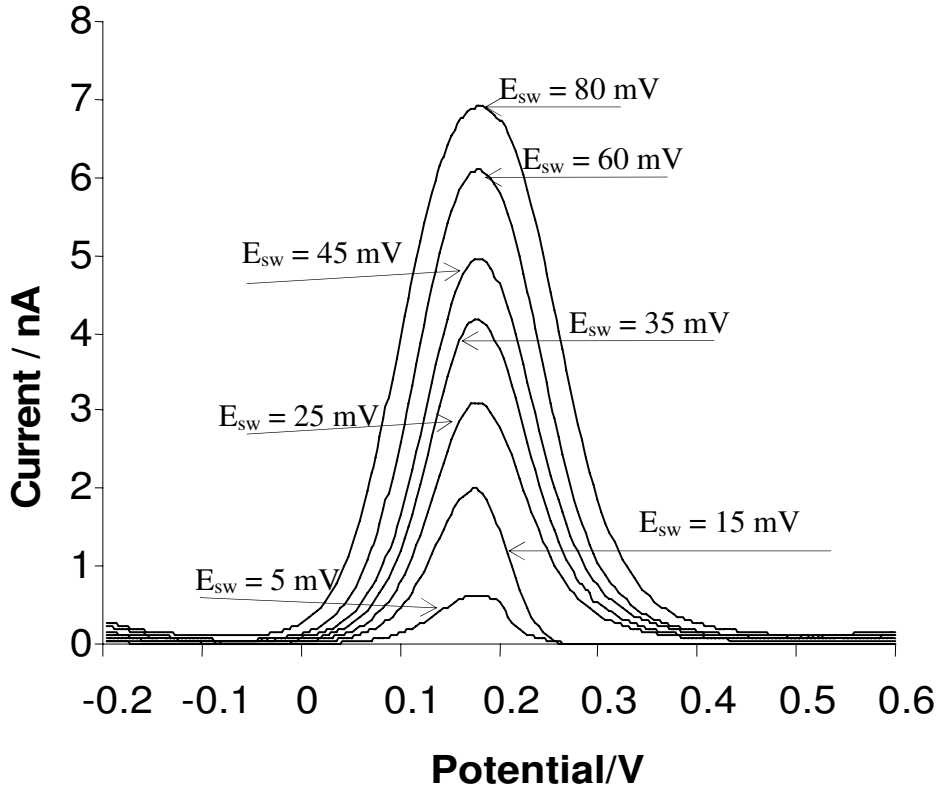

Figure 6.3.4: Square wave voltammograms of 5 mM FeoCN in aqueous 0.1 M KCl using a PtME (nominal diameter = 10 μm), Pt crescent AE and a calomel RE. Cycled positively from – 0.2 to 0.6 V at a rate of 50 mV s^{-1}. ΔEs was 4 mV, f = 5 Hz. E_{sw} was varied.

The peak current magnitude varies linearly with the E_{sw} up to and E_{sw} value approximately 40 mV (figure 6.3.5). At higher E_{sw} values, the magnitude of peak current levels off with increasing E_{sw} (figure 6.3.6).

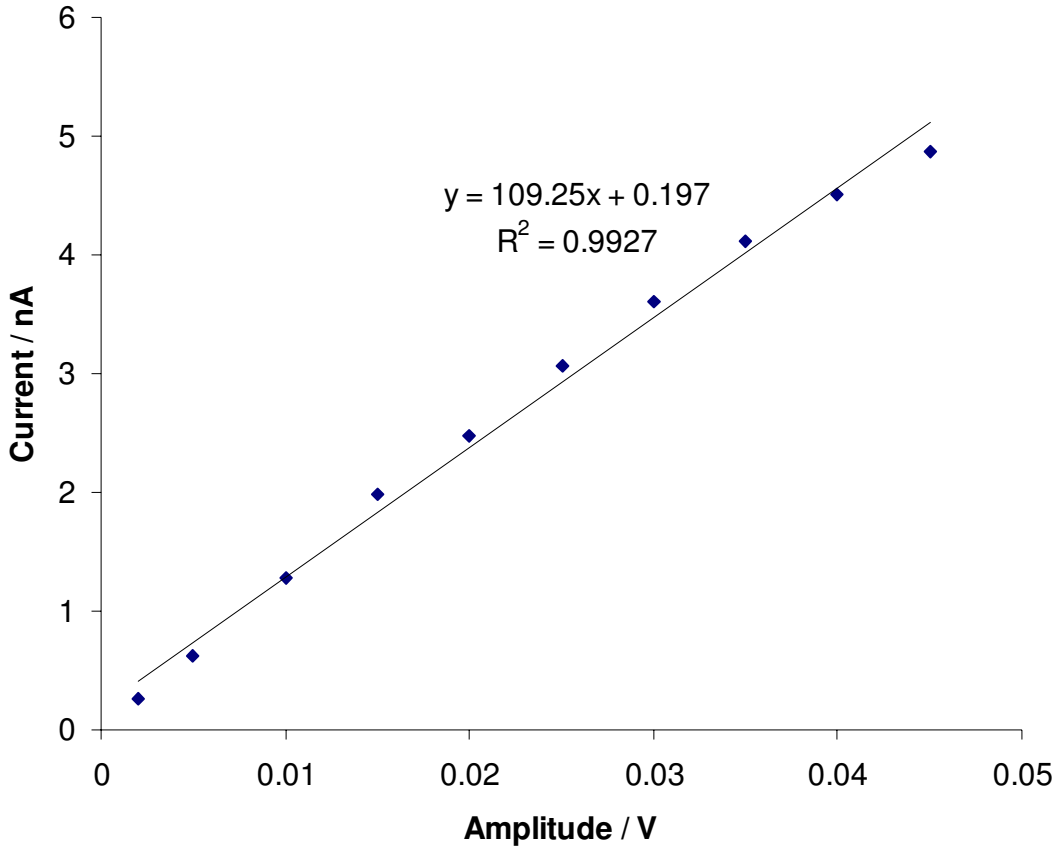

Figure 6.3.5: Variation of current with amplitude (E_{sw})

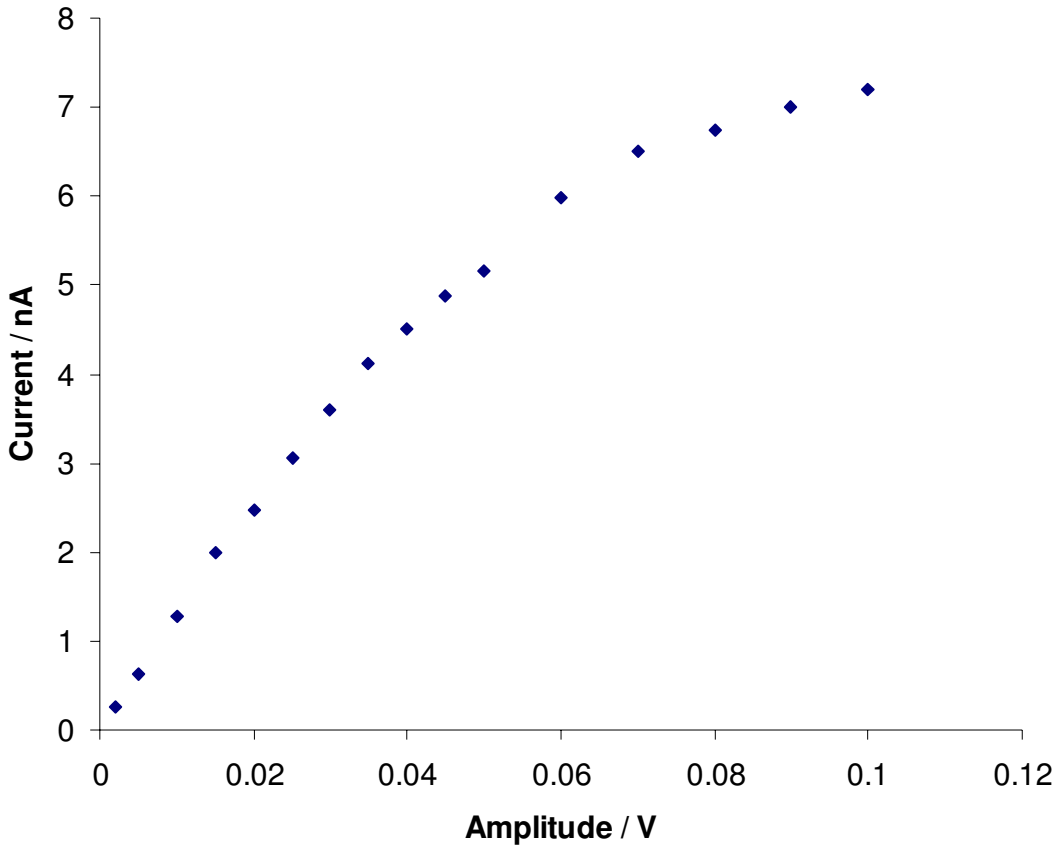

Figure 6.3.6: Variation of current at higher E_{sw} (amplitudes)

When equation 6.11 is substituted into 6.10, the approximation is

$$\delta i \approx \frac{2\, n^2 F^2 r D C E_{sw}}{RT} \qquad 6.12$$

Equation 6.12 predicts a linear behaviour between peak current and E_{sw}. From an analytical viewpoint, changing E_{sw} will increase the sensitivity of the analytical method. Therefore equation 6.12 can explain the data obtained in figures 6.3.4 and 6.3.5.

Figure 6.3.7 shows the modelled profile predicted by the model for the experimental conditions of figure 6.3.4. It can be seen that the current potential profile of figure 6.3.7 mirrors that of figure 6.3.4.

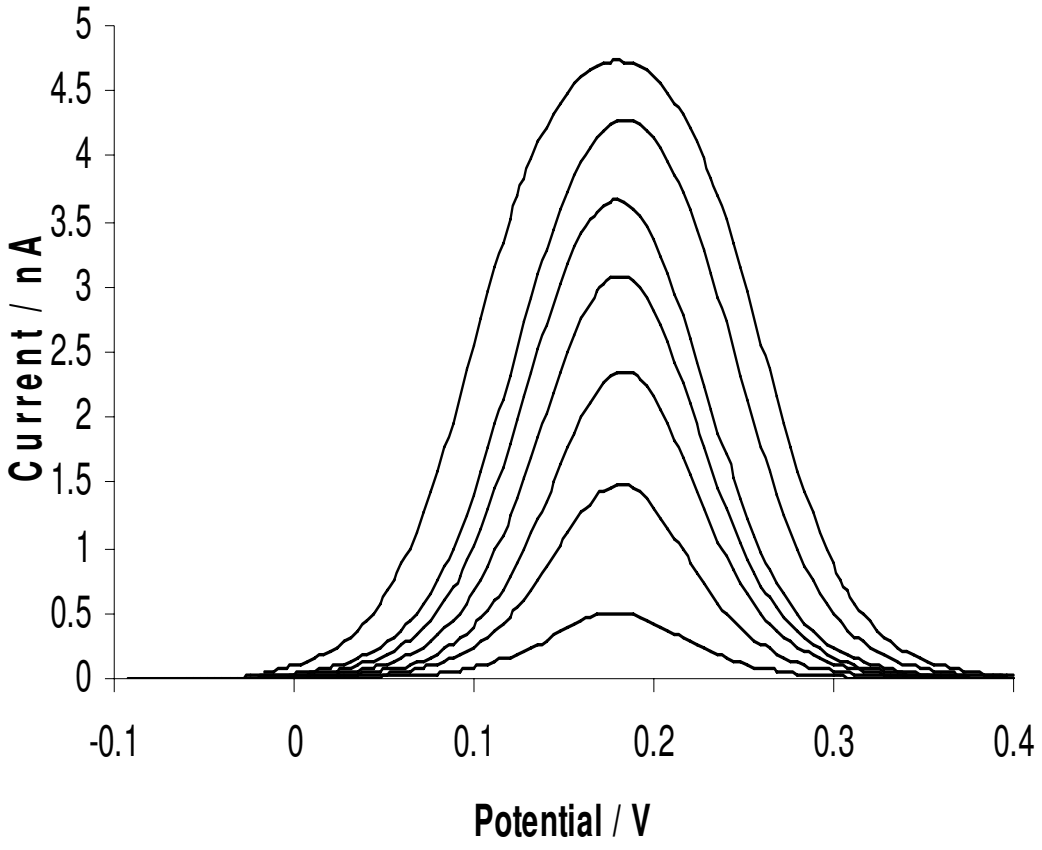

Figure 6.3.7: Simulated output using the model for SWV at a 4.1 μm radius microelectrode. E_{sw} = 5, 15, 25, 35, 45, 60 and 80 mV in order of increasing peak magnitude. Other conditions are as in figure 6.3.4

Table 6.3.1 displays the characteristic parameters of the profiles. It can be seen that there is an increase in δi_p with E_{sw}. The notable difference between the model and experimental results is the peak current magnitude. At low E_{sw} values the difference between theory and experimental is relatively constant. This difference cannot be explained by double layer charging current or residual current since there is not enough residual current in the experimental plots to warrant this assertion. The greater experimental current may be due to a redox cycling effect where the ferricyanide

$[Fe(CN)]^{3-}$ generated on the forward pulse is reduced on the subsequent reverse pulse and *vice versa.*

Table 6.3.1: Experimental and model I simulation outputs. f = 5 Hz, ΔEs = 0.004 V and C = 5 mM. The δ*i* (%) difference is the calculated as 100(experimental – theory) / theory

Electrode radius / μm	E_{sw} / mV	Model		Experimental		
		E_p / V	δi_p / nA	E_p /V	δi_p / nA	δi %
4.1	15	0.179	1.483	0.176	2.00	34
4.1	25	0.181	2.355	0.176	3.11	32
4.1	35	0.179	3.084	0.176	4.17	35
4.1	45	0.181	3.660	0.180	4.96	35
4.1	60	0.180	4.268	0.180	6.09	32
4.1	80	0.180	4.727	0.180	6.91	46
11.2	5	0.181	1.389	0.180	1.99	44
11.2	10	0.178	2.795	0.184	3.97	44
11.2	15	0.179	4.063	0.184	5.92	46
11.2	20	0.180	5.307	0.184	8.20	54
11.2	25	0.181	6.45	0.184	10.10	56
11.2	35	0.179	8.448	0.184	13.34	54
11.2	45	0.181	10.025	0.184	16.93	69
11.2	60	0.180	11.690	0.188	20.13	72

The difference is consistent at low E_{sw} values for both the 10 and 25 μm electrodes. At higher E_{sw} values the percent difference increases as the pulses are larger which means that the currents are deviating from steady state and the current is being sampled during a Cottrell regime.

6.3.3.2 Effect of E_{sw} on peak width at half height (E_{phh})

Figure 6.3.8 shows how much broader the peak current at half height gets when the amplitude of the wave is increased for the 10 μm electrode. Figure 6.3.9 shows that the same trend is followed when using the larger 25 μm electrode.

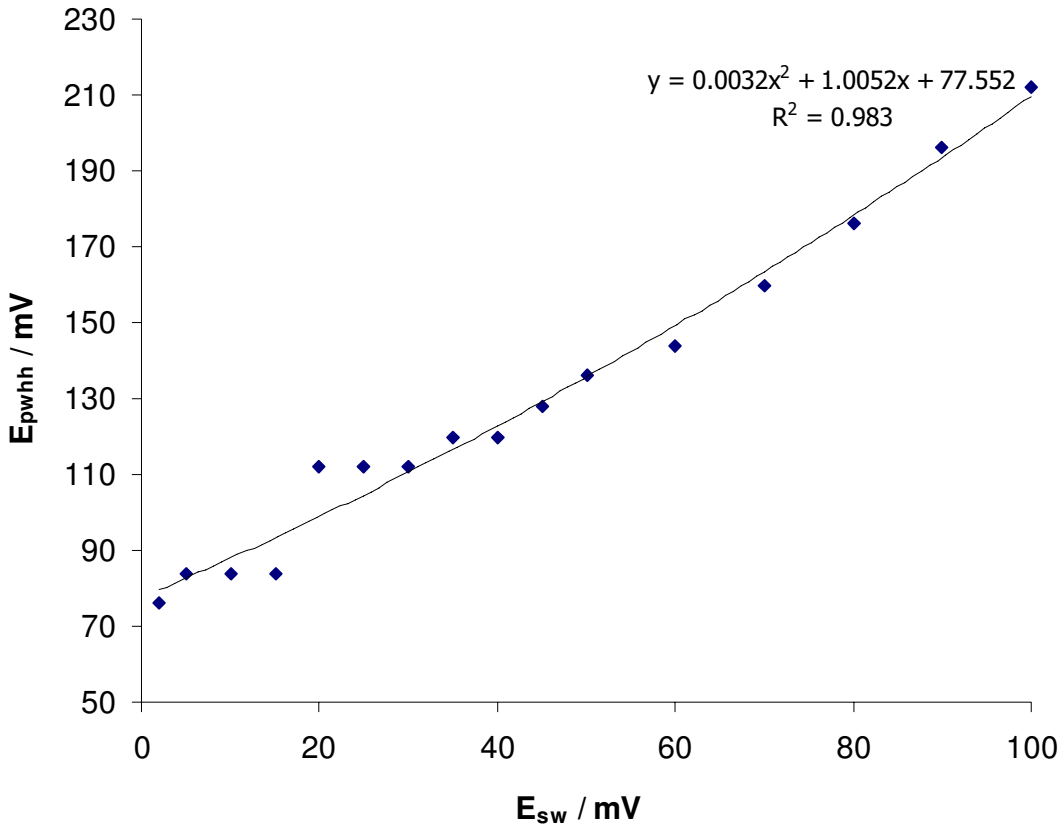

Figure 6.3.8: Experimentally obtained variations in peak width at half height (E_{pwhh}) with amplitude (E_{sw}) for the 10 μm electrode. f = 5 Hz, ΔEs = 0.004 V and C = 5 mM.

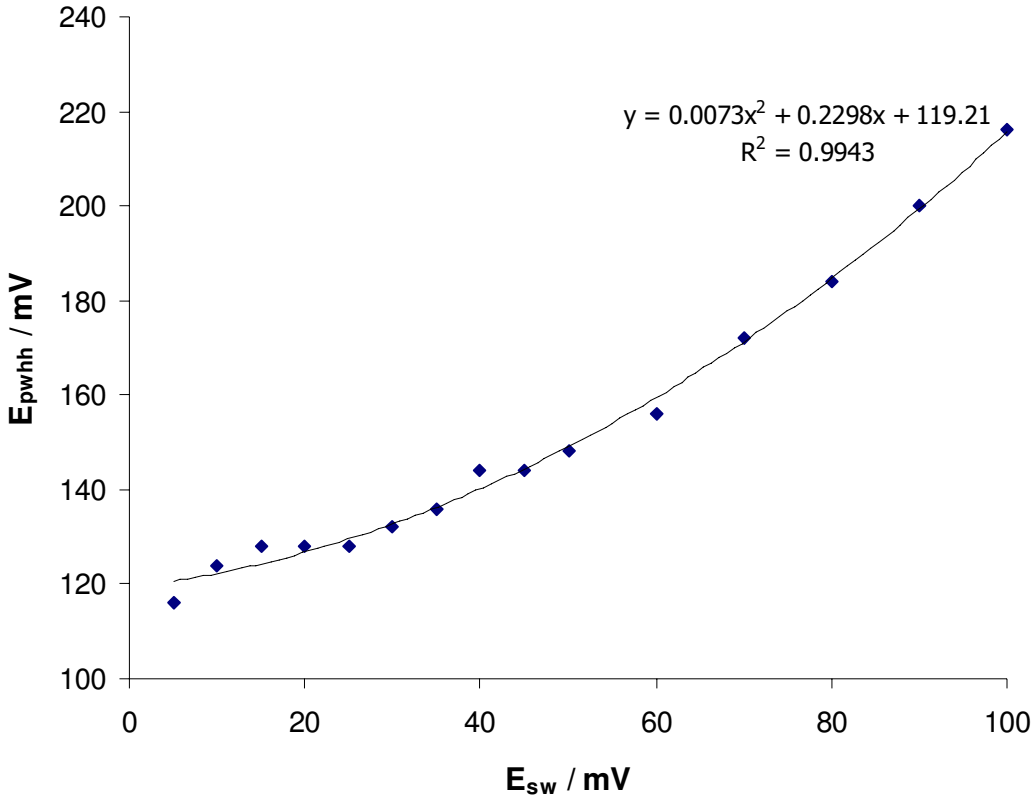

Figure 6.3.9: Experimentally obtained variations in peak width at half height (E_{pwhh}) with amplitude (E_{sw}) for the 25 μm electrode. f = 5 Hz, ΔEs = 0.004 V and C = 5 mM.

In figure 6.3.9 the peak width at half height limits off at approximately 120 mV which is consistent with equation 6.5. Not the same ideal behaviour is seen for the 10 μm electrode in figure 6.3.8 possibly due to passivation. The digital simulation model also predicts peak broadening with amplitude increases as can be seen table 6.3.2. However it predicts a more conservative broadening and not as much as has been observed experimentally.

Table 6.3.2: Experimental and model I simulation outputs showing how peak width at half height increases with increasing amplitude. f = 5 Hz, ΔEs = 0.004 V and C = 5 mM.

Electrode radius / μm	E_{sw} / mV	Model I	Experimental
		E_{pwhh} / mV	E_{pwhh} / mV
4.1	15	92	84
4.1	25	96	112
4.1	35	108	120
4.1	45	116	128
4.1	60	136	144
4.1	80	168	176
11.2	5	92	116
11.2	10	92	124
11.2	15	92	128
11.2	20	96	128
11.2	25	96	128
11.2	35	104	136
11.2	45	112	144
11.2	60	136	156

6.3.3.3 Effect of E_{sw} on position of the peak (E_p)

When the amplitude of the wave is increased, the peak position does not shift.

6.3.4 Variation in staircase potential (ΔEs)

Changing ΔEs from 4 to 15 mV at the 4.1 μm radius microelectrode yielded a peak current of 1.3 nA. The model also predicts no effect of ΔEs on peak current magnitude, and the same behaviour is observed experimentally. Any change in ΔEs also has no bearing on the position of the peak, E_p.

Table 6.3.3 shows that changing the staircase potential height has no bearing on the current produced.

Table 6.3.3: Effect of ΔEs on experimental peak current. E_{sw} = 15 mV, f = 5 Hz for 5 mM FeoCN

r / μm	ΔEs / mV	*i*p / nA
4.1	4	1.38
4.1	8	1.36
4.1	15	1.35
11.2	2	4.02
11.2	6	4.10
11.2	10	4.03

6.3.5 Variation in frequency (f)

At low frequencies (f < 15 Hz), the frequency has no effect on the peak current magnitude; which is also predicted by the model. There is also no effect on the change in sampling frequency on the position of the peak, E_p.

Table 6.3.4 shows that for the 10 μm electrode frequency has no bearing on current. Figure 6.3.8 shows that an increase in sampling frequency results in a marginal increase in current.

Table 6.3.4: Effect of frequency on the experimental peak current using a 10 μm electrode. E_{sw} =15mV, ΔEs = 4 mV, and concentration $K_4[Fe(CN)_6]$ = 5 mM

r / μm	f / Hz	*i*p / nA
4.1	5	1.34
4.1	10	1.27
4.1	15	1.38
4.1	20	1.47
4.1	25	1.55

6.4 Conclusion

This simple model predicts that there is an increase in sensitivity with increasing pulse amplitude, E_{sw}. This is borne out with experimental results. In addition there is no increase in sensitivity with step height, ΔEs or frequency. There is no shift in the peak current position with all three of these parameters. However there is a large discrepancy between the experimental and modelled current. The main difficulty associated with microelectrodes is their small size; it is difficult to remove adsorbed species form the electrode surface.

6.5 References

[1] I. Montenegro, M. A. Queiros, J. L Daschbach (editors), *Microelectrodes: theory and applications,* Proceedings of NATO Advanced Study Institute (1991), Kluwer Academic Publishers, Dordrecht Netherlands, 1991

[2] S.-Y Ly, Y.-H. Kim, I.-K.Han, I.-G.Moon, W.-W.Jung, S.-Y.Jung, H.-J.Sin, T.-K. Hong, M.-H.Kim, *Microchemical Journal*, **82** (2006) 113

[3] P.R.M. Silva, M.A. El Khakani, M. Chaker, A. Dufresne, F. Courchesne, *Sensors and Actuators B: Chemical*, **76 (**2001) 250

[4] P.R.M. Silva, M.A. El Khakani, B. Le Drogoff, M. Chaker, A.K. Vijh, *Sensors and Actuators B: Chemical,* **60** (1999) 161

[5] P.R.M. Silva, M.A. El Khakani, M. Chaker, G.Y. Champagne, J. Chevalet, L. Gastonguay, R. Lacasse, M. Ladouceur, *Analytica Chimica Acta*, **385** (1999) 249

[6] D.De Sousa, S.A.S. Machado, R.C. Pires, *Talanta***, 69** (2006) 1200

[7] D.De Sousa, S.A.S. Machado, *Analytica Chimica Acta*, **546** (2005) 85

[8] L. Agüí, A. Guzmán, P. Yánez - Sedeno, J.M. Pingarrón, *Analytica Chimica Acta*, **461** (2002) 65

[9] L. Agüí, J.E. López - Guzmán, A. González - Cortés, P. Yánez - Sedeno, J.M. Pingarrón, *Analytica Chimica Acta*, **385** (1999) 241

[10] D.P. Whelan, J.J. O'Dea, J. Osteryoung, K. Aoki, *Journal of Electroanalytical Chemistry*, **202** (1986) 23

[11] A. Molina, C. Serna, F. Martínez - Ortez, *Journal of Electroanalytical Chemistry,* **486** (2000) 9

[12] F. Garay, M. Lovrič, *Journal of Electroanalytical Chemistry*, **527** (2002) 85

[13] E. Howard, J. Cassidy, J. O'Gorman, *Electroanalysis*, **10** (1998) 1208

[14] E. Howard, J. O'Gorman, J. Cassidy, *Electroanalysis*, **11** (1999) 23

[15] J. Osteryoung, J.J. O'Dea, in A.J.Bard, ed. Electroanalytical Chemistry, Volume 14, M.Dekker, New York, 1986, 209.

[16] J. Osteryoung, in M.I.Montenegro *et al* (eds.) *Microelectrodes, Theory and Applications*, Kluwer, Dordrecht, 1991, 139.

[17] D. J. G. Ives, G. J. Janz, "The Calomel Electrode and Other Mercury-Mercuorous Salt Electrodes" in *Reference Electrodes – Theory & Practice*, Volume 1, D. J. G. Ives & G. J. Janz, ed., Academic Press, New York & London, 1961, 160

[18] D.T. Sawyer, J.L. Roberts, "Indicator Electrodes" in Experimental Electrochemistry for Chemists, Volume 1, D.T. Sawyer & J.L. Roberts Ed., Wiley, New York, 1974, 77.

Chapter 7

A model for cyclic voltammetry with a Langmuir Hinshelwood pre step applied to the formic acid system

Chapter 7 – A model for cyclic voltammetry with a Langmuir Hinshelwood pre step applied to the formic acid system

7.1 Introduction

7.1.1 Cyclic voltammetry with a Langmuir Hinshelwood model

Langmuir Hinshelwood adsorption has been implicated in TiO_2 photocatalysis previously [1 - 5] using 4-chlorophenol [2], benzoic acid [3], erythrosine (a synthetic dye) [4] and oxalic acid [5] as test compounds. Formic acid is a molecule that is easily decomposed whose decomposition follows a CE mechanism, and so it was an ideal test molecule. During its photoassisted degradation on a TiO_2 surface, Langmuir Hinshelwood models have been fitted to its decomposition before [5]. Diffusion models (explicit finite difference methods) have previously been applied to chemicals with reversible adsorption/desorption equilibria adsorbed on TiO_2 films [6].

For immobilised irradiated TiO_2, Byrne *et al* measured the photocurrent response of a number of simple organics [7]. They found that oxalate bound more tightly to the TiO_2 surface than acetate and formate, but adsorption was not as good at higher concentrations of solute. Negligible background currents due to the aqueous electrolyte (KCl) on its own were also recorded.

The model consists of a CE mechanism (homogenous chemical process preceding heterogeneous electron transfer) where the C step is governed by Langmuir Hinshelwood kinetics.

$$B \rightarrow R \qquad 7.1$$

$$R \rightarrow O + ne^- \qquad 7.2$$

The term involved along with the diffusion equation is

$$\text{Rate} = \frac{k'KC}{1 + KC} \qquad 7.3$$

where *k*' has units of mol L^{-1} s^{-1} (RKL) and units of K are L mol^{-1} (RKB1). [B] = C and c = C. Thus the diffusion equations to be solved simultaneously are:

$$\frac{\partial c_B}{\partial t} = D\frac{\partial^2 c_B}{\partial x^2} - \frac{k'KC_B}{1+KC_B} \qquad 7.4$$

$$\frac{\partial c_R}{\partial t} = D\frac{\partial^2 c_R}{\partial x^2} + \frac{k'KC_B}{1+KC_B} \qquad 7.5$$

$$\frac{\partial c_O}{\partial t} = D\frac{\partial^2 c_O}{\partial x^2} \qquad 7.6$$

Where: *D* = diffusion coefficient / cm^2 s^{-1}
x = distance from the electrode surface / m
c = concentration / mol L^{-1}

With the initial condition that the concentrations of O and R are zero and that there is an initial concentration of B equal to C_B^0, the boundary conditions are as follows:

$$\left.\frac{dC_B}{dx}\right|_{x=0} = 0 \qquad 7.7$$

And

$$\left.\frac{dC_R}{dx}\right|_{x=0} = -\left.\frac{dC_O}{dx}\right|_{x=0} \qquad 7.8$$

RKT is the time interval, *k* (sec), the total time /2000 and C_B^o is used to make the concentration dimensionless as $C^* = C/C_B^o$.

RH is the distance interval, *h* (cm), estimated by the diffusion layer /9 dimensionless diffusion coefficient

$$D_m = \frac{D_k}{[(h^{**}2)^*2]}$$

$$D_m = \frac{D^*RKT}{[(RH^{**}2)^*2]}$$

$$RKDD = \frac{RKL^*RKT}{C_B^0}$$

$$RKD = RKB1^*C_B^0$$

$$\frac{C_{i,j+1}-C_{i,j}}{k}=\frac{D}{2}\left[\frac{C_{i+1,j+1}+C_{i-1,j+1}-2C_{i,j+1}}{h^2}+\frac{C_{i+1,j}+C_{i-1,j}-2C_{i,j}}{h^2}\right]+\frac{k'KC_{i,j}}{1+KC_{i,j}} \qquad 7.9$$

Applying dimensionless parameters: $C^* = \frac{C}{C_B^o}$ to equation 7.9:

$$\frac{(C^*_{i,j+1}-C^*_{i,j})C_B^o}{}=\frac{Dk C_B^o}{2h^2}\left[\frac{C^*_{i+1,j+1}+C^*_{i-1,j+1}-2C^*_{i,j+1}}{}+\frac{C^*_{i+1,j}+C^*_{i-1,j}-2C^*_{i,j}}{}\right]+\frac{kk'KC^*_{i,j}C_B^o}{1+KC_{i,j}}$$

……..7.10

Where the dimensionless terms are:

$$k'' = \frac{kk'}{C_B^o} \qquad \text{(RKDD)}$$

$$K' = KC_B^o \qquad \text{(RKD)}$$

Where k is the step length and C_B^o is the initial concentration on substitution we get:

$$\frac{(C^*_{i,j+1}-C^*_{i,j})}{}=\frac{Dk}{2h^2}\left[\frac{C^*_{i+1,j+1}+C^*_{i-1,j+1}-2C^*_{i,j+1}}{}+\frac{C^*_{i+1,j}+C^*_{i-1,j}-2C^*_{i,j}}{}\right]+\frac{k''K'C^*_{i,j}}{1+K'C^*_{i,j}}$$

…….... 7.11

These equations were solved using FORCE software on a pc and the typical run time was 15 seconds.

7.1.2 Applications of the model

Model results are obtained as the FORTRAN software is applied through Microsoft Excel. By varying some figures and parameters, different voltammetric outputs are obtained. Model results were then compared with experimental ones obtained using UV light.

7.1.3 Use of visible light

Later on in this chapter, results are presented for a similar system when using visible light although a Langmuir model was not fit to it. In addition, an area study was performed, and the effect of electrode distance from the lamp was also evaluated.

7.2 Experimental

7.2.1 Materials

- De-ionised water (l)
- Potassium chloride (s, KCl, Merck, 99.5+ %)
- Cobalt (II) phthalocyanine (s, CoPc, Eastman, ≥97 %)
- TiO_2 (s, TITANDIOXID P25, Degussa AG GB AC D-60287 Frankfurt)
- Formic acid (l, FA, Aldrich, 95 – 97 %)
- Poly(4-vinylpyridine) (s, PVP, Fluka, average M_w ~ 70,000)
- Methanol (l, MeOH, Aldrich, 99+ %)
- Electrodag 423 SS graphite-based P.T.F Ink (s, CI, Acheson Colloids, 1600 Washington Avenue Port Huron , Michigan 48060 USA)
- Type J colour inkjet transparencies removable stripe (Xerox)
- Cube applicator

7.2.2 Equipment

- CHI620A electrochemical analyzer (CH Instruments, 3700 Tennison Hill Drive Austin, TX 78738 USA)
- Air electrode made from a sheet of MnO_2/carbon paper/Ni mesh/Teflon dispersion [8] (produced by Electro-Chem-Technic)
- Platinum crescent sheet counter electrode (PtAE, approx area = 12 cm^2)
- 60 W tungsten incandescent standard household light bulb
- Data acquisition was by means of Pico Technology (Cambridgeshire, UK), with an ADC 16 analog to digital converter.
- Oriel 6253 150 W Xe arc lamp powered by an Oriel 69907 source with a peak emission at 850 nm

7.2.3 Methodology

7.2.3.1 Electrode preparation

Details of how the electrodes were prepared were described in section 4.2.3.1. Anodic electrode areas were typically 25 cm^2 unless otherwise stated.

7.2.3.2 Effect of concentration on current

Using either a 60 W visible of 150 W UV lamp, current was measured as a function of FA concentration in a one compartment cell. Starting with 0.1 M KCl, incremental additions of 0.5 M FA were added to the cell and the current was measured using Pico technology interfaced to a laptop.

7.2.3.3 Logging of current transients

Details of how the current transients were collected were described in section 4.2.3.3. However, there was no digital electrometer needed. All experiments were conducted at room temperature. Chemicals were all reagent grade quality and solutions were prepared in deionised water.

7.3 Results and Discussion

7.3.1 Theoretical results obtained using FORTRAN software

Initially the program was run under conditions where the rates *k*' and K are very fast. In that way the preceding step for the formation of R is invisible and the slow step is the cyclic voltammetry of the R/O redox couple. Figure 7.3.1 shows the output. Here, *k*' and K are equally fast.

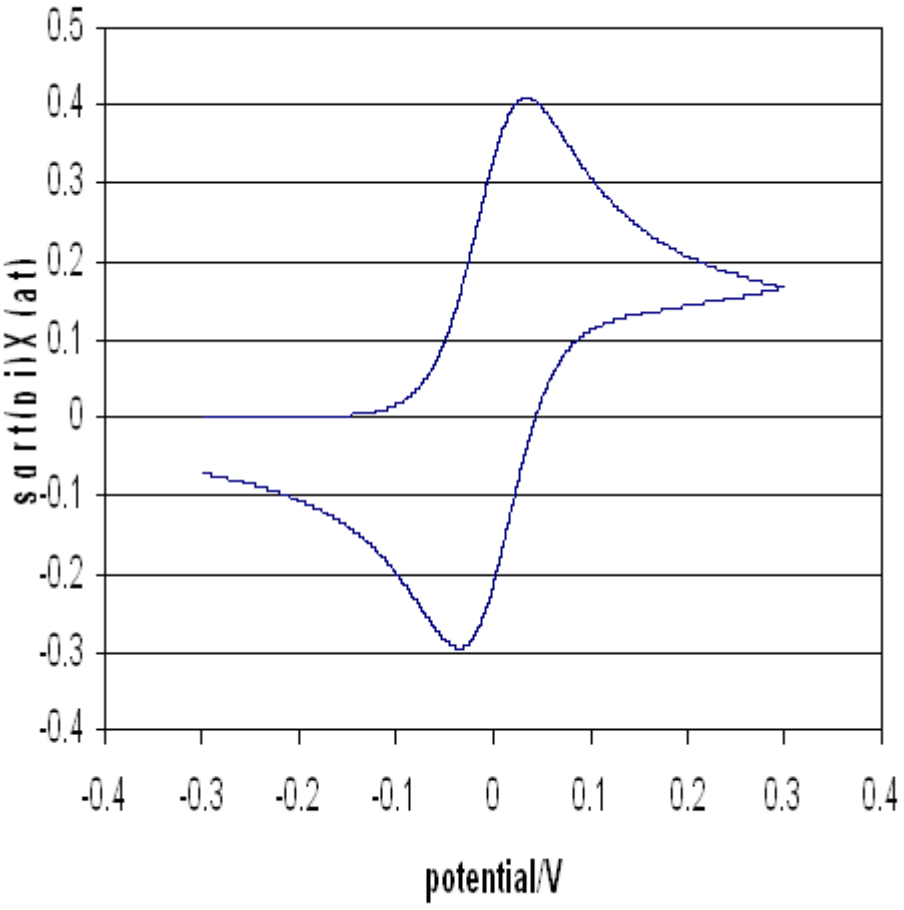

Figure 7.3.1: Simulated cyclic voltammogram. L = 9999, s = 0.001 mV s^{-1}, C = 10^{-2} M, RKL = 2, RKB1 = 2.

The data was read into an EXCEL file and plotted. The peak to peak separation ΔE_p of 70 mV which is a little bigger that the 57/n mV predicted by Nicholson and Shain [9]. In addition the dimensionless current is smaller than 0.4463 also predicted by Nicholson and Shain. This is due to the limited number of time interval steps used. As the number of time interval steps increases the peak current tends to 0.4463. However in order to fit the plot in EXCEL, a maximum of 32,000 points is allowed and so the peak current is 0.41. Taking this to be the ideal reversible situation, *k*' and K were varied and the model outputs are presented in figures 7.3.2 - 5.

In figure 7.3.2, *k*' (RKL) was varied while K (RKB1) was kept constant. It can be seen that a steady state current underlies the reversible cyclic voltammetry. This steady state current increases with increasing *k*'. This is reasonable looking at the term added to the diffusion equation. With increasing *k*', the quantity of R increases yielding an increase in current. However after the voltammetric peak, a steady state current is obtained which depends on the kinetics. This current is smaller than the diffusion controlled current in figure 7.3.1. In figure 7.3.2, a peak would normally be observed for this, but instead a steady state is obtained.

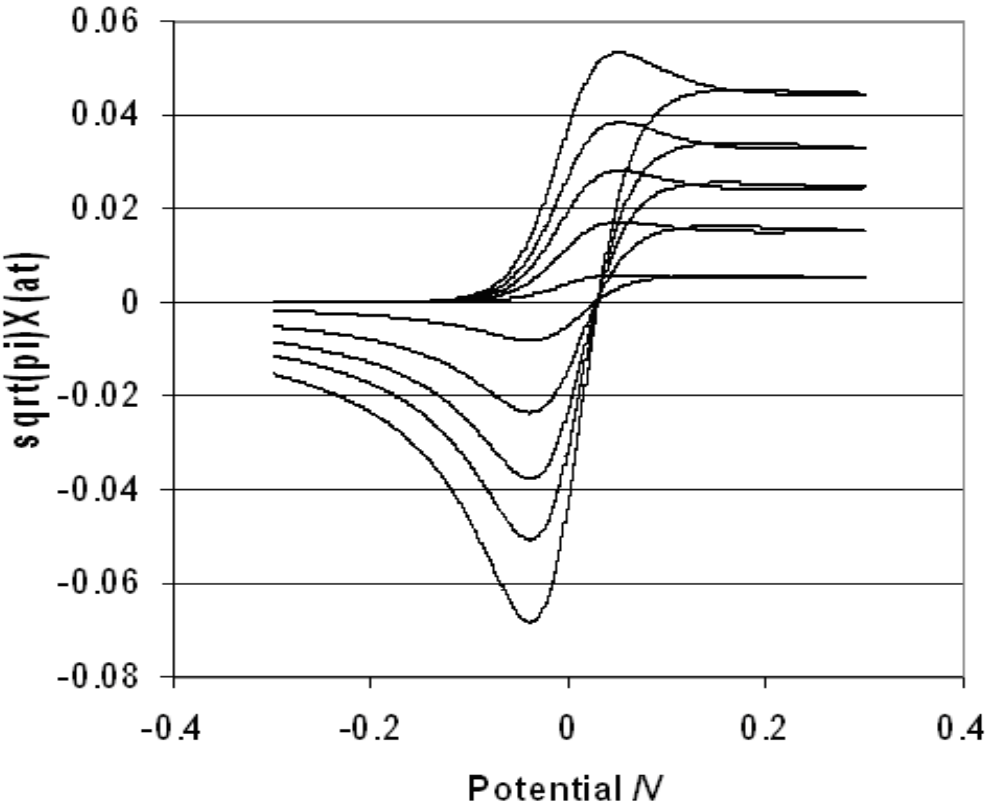

Figure 7.3.2: This figure has the same conditions as figure 7.3.1 except RKB1 = 1 x 10^{-2} and RKL = 1, 3, 5, 7 and 10 x 10^{-3} in order of increasing current magnitude. It can be seen that there is a steady state current as a response that increases with the value of RKL.

When RKL is small (in this case for example 1 or 3 mol L^{-1} s^{-1}), a steady state current is observed as the redox species R is being slowly and constantly produced. When the polarity of the cycle is switched to negative (having been originally positive), the current doubles back along itself as there is still a small amount of R present.

On the other extreme, at higher RKL values (e.g. 10 mol L^{-1} s^{-1}), a peaked output is obtained. This is because there is a large amount of R produced at a very fast rate in a short length of time, and before the cycle reaches 50 mV the amount of R

available drops off significantly. This results in a reduction of current and therefore a peak.

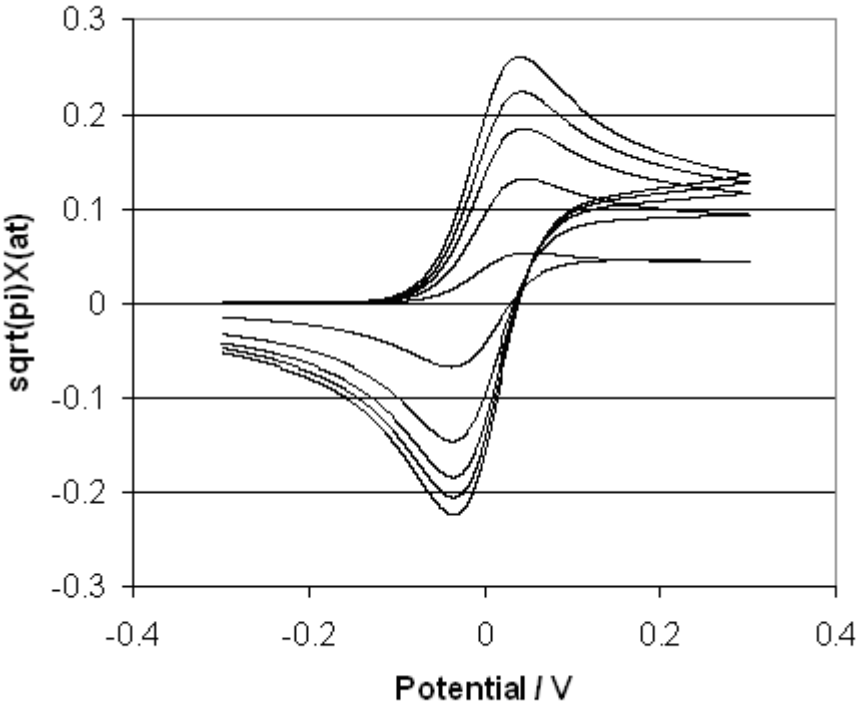

Figure 7.3.3: The figure has the same conditions as figure 7.3.1 except that RKL = 10^{-1} and RKB1 = 1, 3, 5, 7 and 10 x 10^{-3} values. There is a transition from a steady state situation to a diffusion controlled situation.

Figures 7.3.3 - 5 show the effect of changing K for different values of *k*'. Within each voltammogram RKB1 (K) is changed, while over the 3 figures the rate of reaction (RKL) gets 10 times smaller in each plot. While lessening RKL, the current decreases 5 fold and then almost 10 fold when going from figure 7.3.4 to 5.

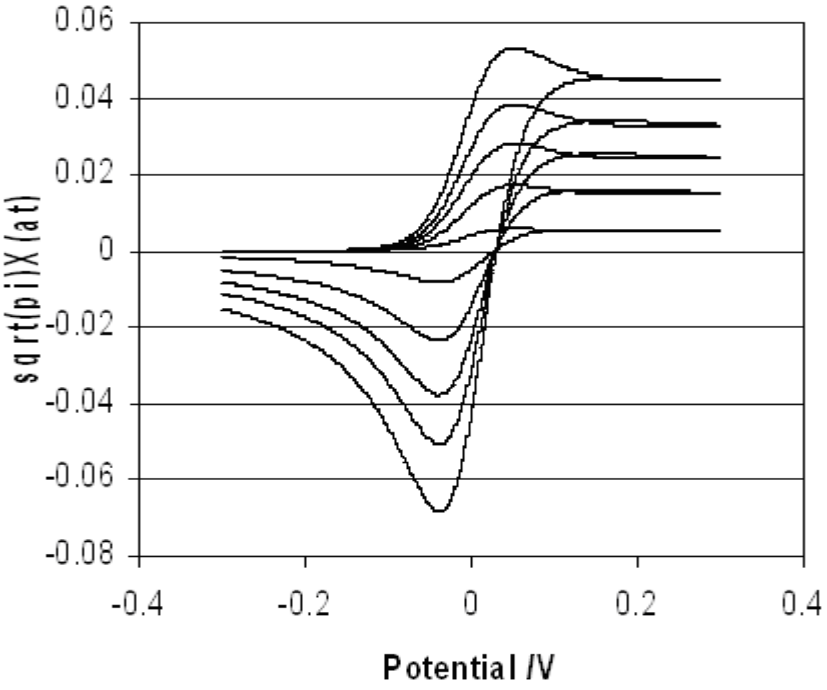

Figure 7.3.4: Simulated cyclic voltammogram with RKL = 10^{-2} and RKB1 = 1, 3, 5, 7 and 10 x 10^{-3}. It can be seen that there is a greater contribution toward steady state with lower RKL values.

Figure 7.3.5 displays an anodic current over 40 times less than that in figure 7.3.3; as the rate of reaction (k' / mol L^{-1} s^{-1}), was make 100 times smaller.

Table 7.3.1: Decreasing current with decreasing rate of reaction

k' / mol L^{-1} s^{-1}	i / A	K / L mol^{-1}
10^{-1}	0.25	10^{-3}
10^{-2}	0.045	10^{-3}
10^{-3}	0.006	10^{-3}

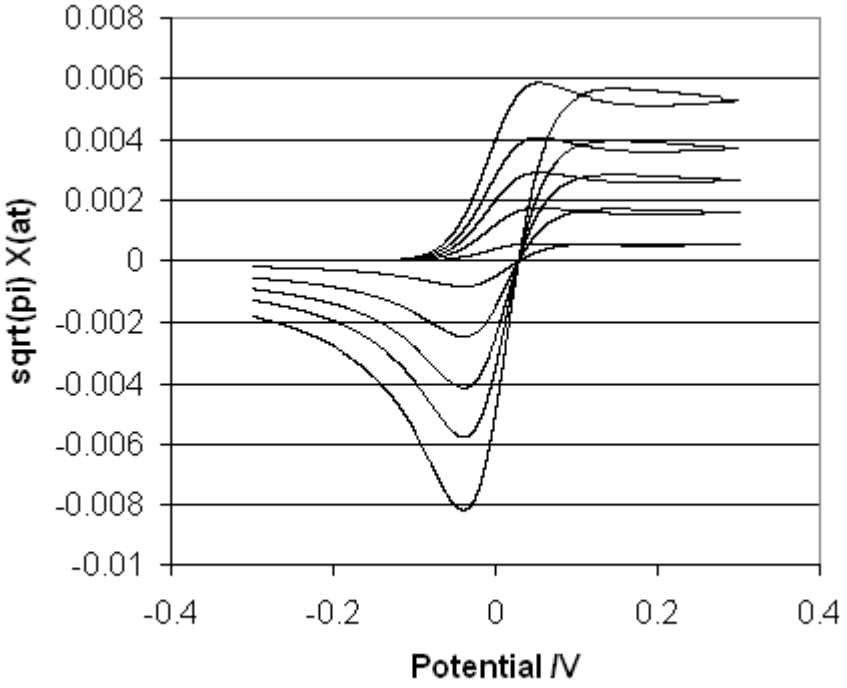

Figure 7.3.5: Simulated cyclic voltammogram with (*k*') RKL = 1 x 10^{-3} and (K) RKB1 = 1, 3, 5, 7 and 10 x 10^{-3}. Other conditions the same as figure 7.3.1.

When *k*' (RKL) is very small there is a greater appearance of steady state current. However K (RKB1) can be seen to directly influence the increase in current. In figure 7.3.4, increasing K does increase the degree of reversibility of the system. Both constants directly affect the magnitude of the steady state current.

In all of these cases when the concentration of B is changed it has no effect on the voltammetry. This is because the output is a dimensionless current [2]:

$$\sqrt{\pi}\chi(at) = \frac{i}{nFAC_B^{o}(aD)^{1/2}} \qquad 7.13$$

Where: $a = \frac{nF\nu}{RT}$

ν = scan rate / V s^{-1}
n = number of electrons
F = Faraday's constant / C mol^{-1}
A = electrode area / cm^2

R = universal gas constant / V C mol^{-1} K^{-1}
T = temperature / K
i = current / A
C_B^o = initial [formic acid] / mol L^{-1}
D = diffusion coefficient / cm^2 s^{-1}

Based on equation 7.13, there is a linear relationship between current and concentration. Thus for previous curves current is not influenced by changing A, C_B^o, ν or *D*. And since all the parameters are made dimensionless sometimes with respect to the initial concentration of the only species present, namely B, varying the concentration of B has no effect. Thus peak current increases linearly with concentration of B.

In the case of formic acid, it can be seen that there is a similar steady state voltammetric output. This is due to the pre reaction of formic acid at the TiO_2 surface (chemisorption) in the presence of UV light, producing species that are subsequently electrolysed. Thus there is a pre adsorption / reaction step, which is simplified in the above model as a single step.

7.3.2 Results obtained experimentally

It can be seen in figure 7.3.6 that steady state current in cyclic voltammograms for formic acid (FA) increases with formic acid concentration.

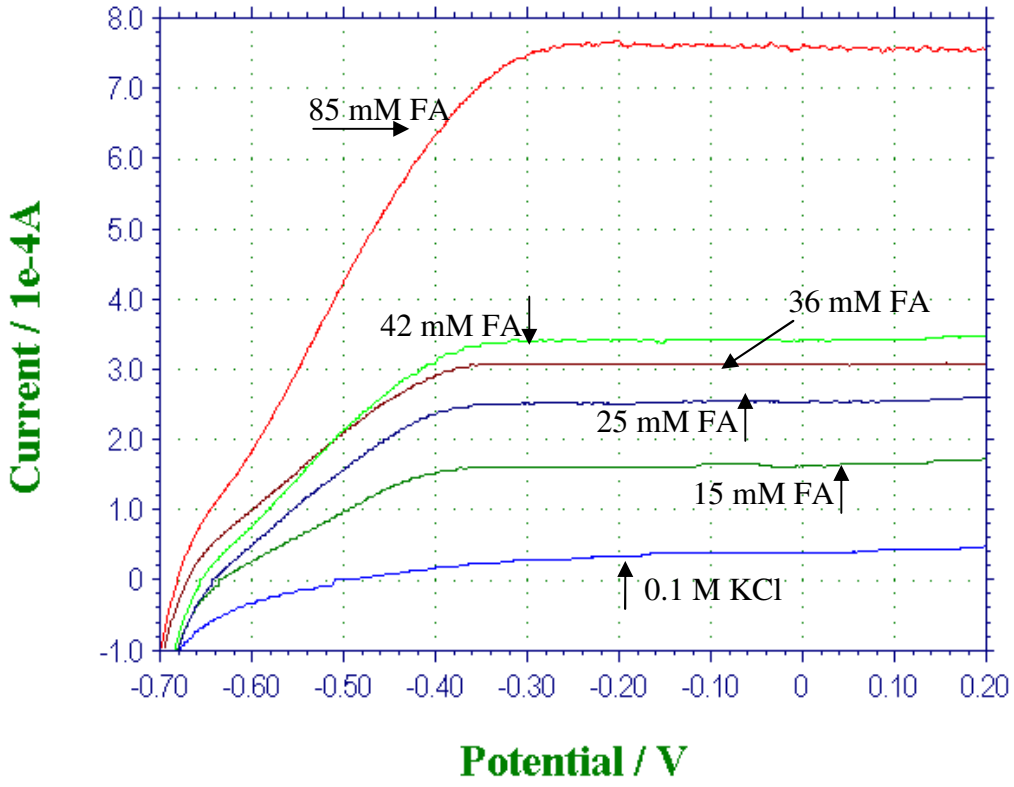

Figure 7.3.6: Cyclic voltammetry of aqueous 0.1 M KCl with incremental amounts of FA added (50+ cm^3) in an unstirred solution. A 1 cm^2 TiO_2/CI WE and 12 cm^2 PtAE were used; powered by a CHI 620A potentiostat. 150 W oriel Xe lamp. Cycled positively from – 0.7 to 0.2 V (SCE) at 50 mV s^{-1}, however only the first (positive) segment is shown.

In the case of FA there is no reverse peak as seen in the model, this is illustrated in figure 7.3.7, and more steady state voltammetry is produced rather than a peaked output. This is because the oxidation of FA is kinetically slow, while the model is based on a reversible system with fast kinetics (such as ferrocene).

Voltammetry of formic acid in the dark yields little or no current at the TiO_2 coated ink electrode indicating that there is little oxidation of formic acid at the

underlying carbon (figure 7.3.7). This is in stark contrast to the current produced upon exposure to light.

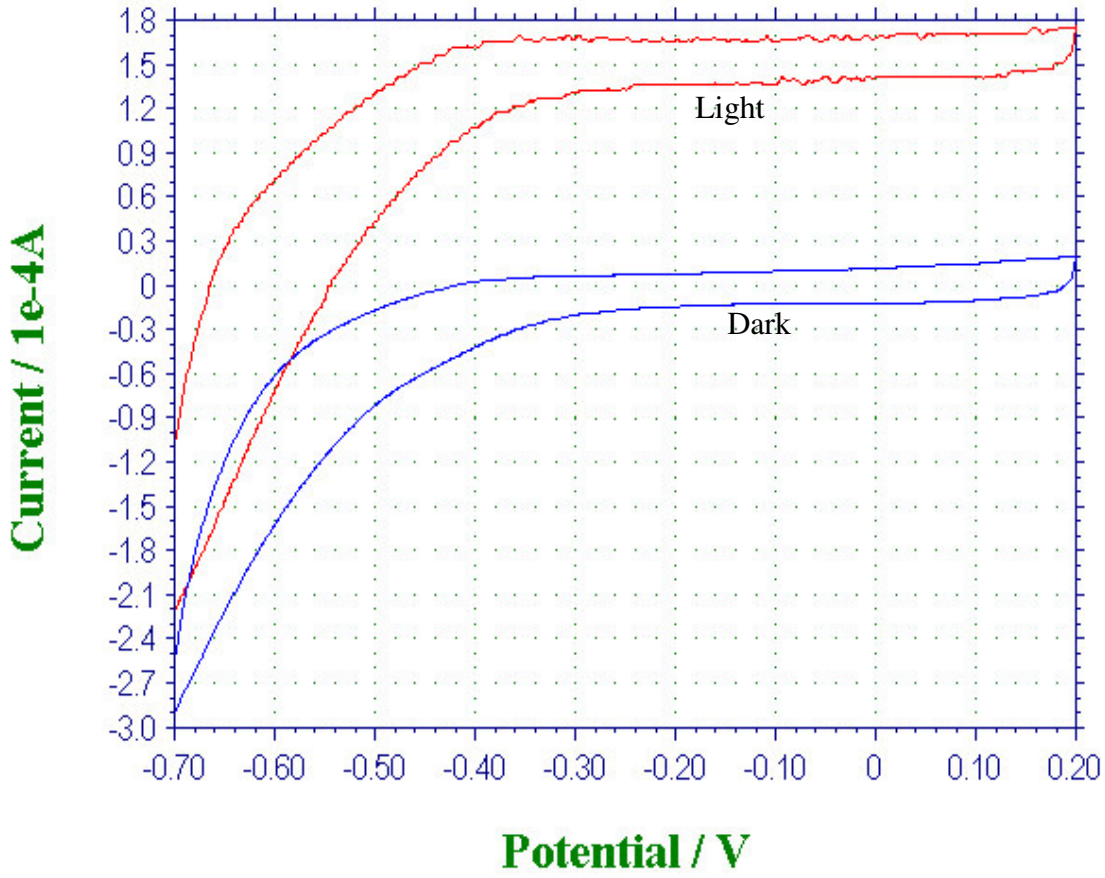

Figure 7.3.7: Cyclic voltammetry of aqueous formic acid (16 mM in 0.1 M KCl, 50.5 cm^3) in an unstirred solution. A 1 cm^2 TiO_2/CI WE and 12 cm^2 PtAE were used; powered by a CHI 620A potentiostat. 150 W oriel Xe lamp. Cycled positively from –0.7 to 0.2 V (SCE) at 50 mV s^{-1}

It is evident from figure 7.3.7 that formic acid oxidation depends on TiO_2 photocatalysis. This is because of the difference of current magnitudes received for dark results and light. It is also evident that current is limited at the anode. Thus on exposure to light, in the presence of TiO_2, formic acid is converted to a species that has a facile electrochemistry. The apparent steady state current during voltammetry (and also during light transients in section 4.3.2 and 4.3.6) indicates that there is a kinetic step which limits current flow.

In following with the theoretical results, looking at figure 7.3.7 it is as if *k*' and K are relatively small, as a steady state current is observed. Comparing this with the modelled current in figure 7.3.2, each has a steady state current. In the model, the steady state current is due to the slow steps or small values of *k*' and K in equation 7.3. *k*' is related to the rate of production of the electroactive species R, and this determines the constant current. Such a pre – electrochemical step is proposed for formic acid, which has a constant current (figure 7.3.7) for the same reason.

In addition to the results presented above when using UV light sources, it was found that currents increased with concentration of formic acid. The results are presented in figure 7.3.8.

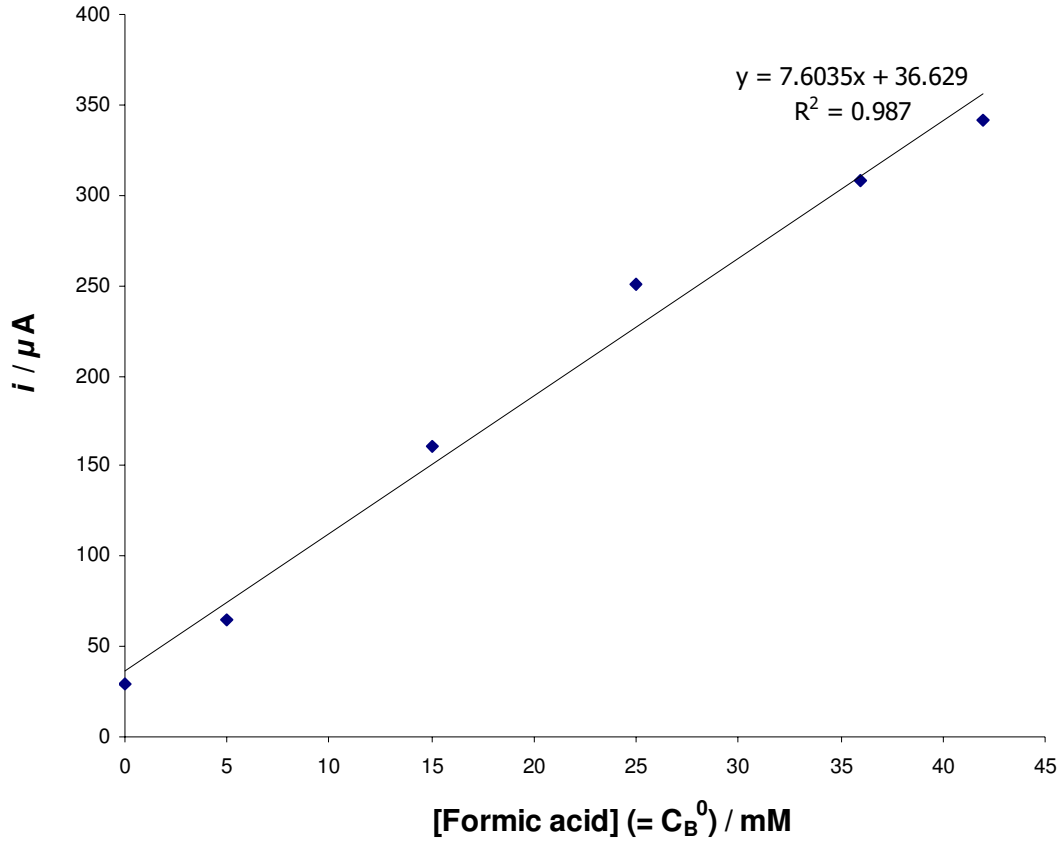

Figure 7.3.8: Current obtained (by cyclic voltammetry, conditions are as listed in figures 7.3.6 and 7) from aqueous formic acid oxidation.

There is a linear relationship between current and concentration experimentally, which is consistent with the model results.

7.3.3 Use of visible light to collect transients

In chapter 4 there was much work done using formic acid as a substrate. Sections 4.3.2 and 4.3.6 saw some current – time analysis carried out, and while the anode was the same as the work presented above, the cathode consisted of carbon ink containing cobalt phthalocyanine. Electrode areas were also 3 times bigger at 3 cm^2 and a visible 60 W tungsten light source was used. Figure 4.3.3 showed a current transient for 1 mM FA in 0.1 M KCl while figures 4.3.4 and 5 (a) showed transients for 10 mM FA in 0.1 M KCl.

This work was repeated using the same light source but 1 cm^2 electrode areas along with an air cathode. Known amounts of 0.5 M FA were added and current transients like in figures 4.3.3, 4 and 5 (a) were built up and overlayed. The current was collected using pico technology and the results are displayed in figure 7.3.9.

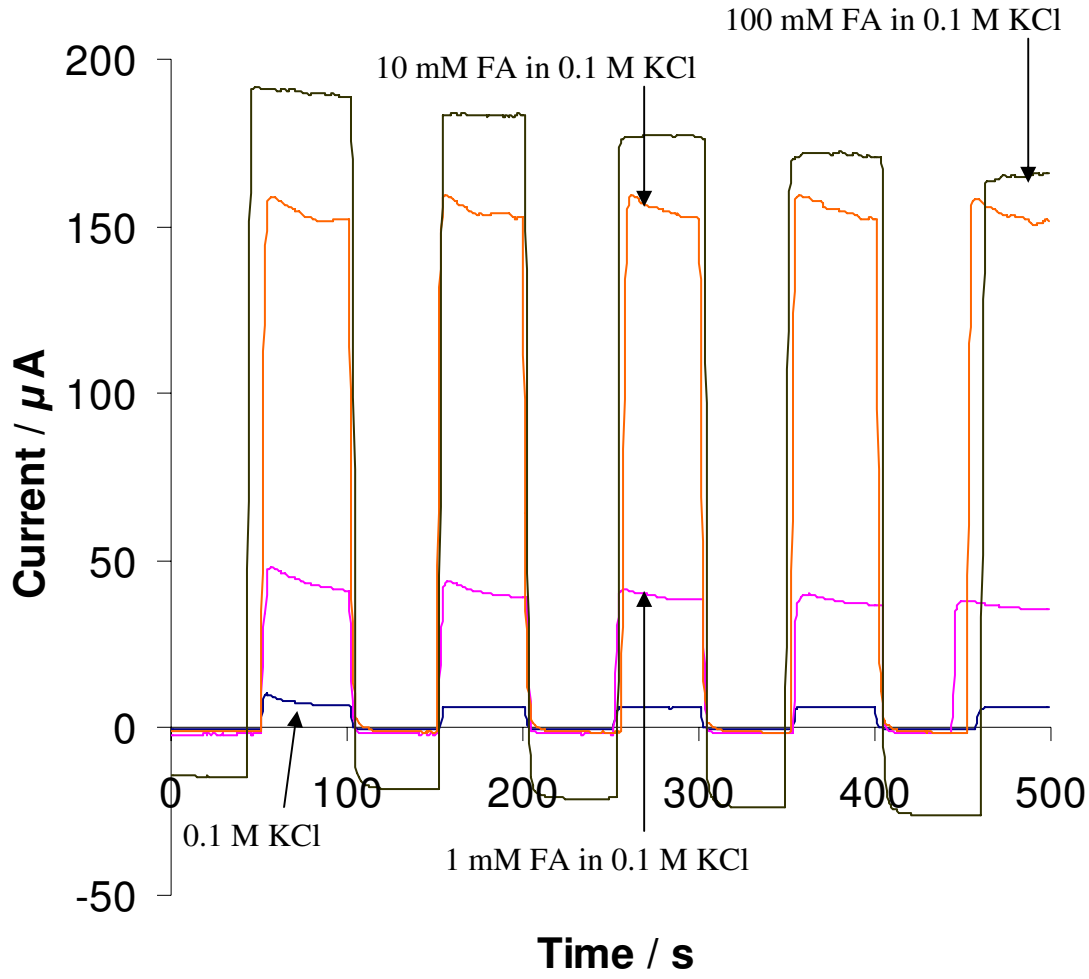

Figure 7.3.9: Photocurrents of aqueous formic acid (1, 10 and 100 mM in 0.1 M KCl, 50 cm^3) in an unstirred solution. 25 cm^2 TiO_2/CI anode and 1.3 cm^2 air cathode were used. Current was collected for 500 seconds with Pico technology across a 1 kΩ resistor. 60 W tungsten lamp. The lamp was switched on and off every 50 seconds.

A negative dark current of around 15 μA can be seen for 0.1 M FA, and around 1 or 2 μA for the others. As this current is recorded before the light is switched on, this indicates a dark reaction, and because its polarity is negative, it is typical of FA oxidation at the air cathode. When the light is switched on, the oxidation is limited at the TiO_2 coated anode as the current increases upon exposure to light.

7.3.4 Current concentration profiles using visible light

As can be seen in figure 7.3.9**,** current increases with concentration. Referring back to chapter 4 again, this relationship between current and concentration was explored again using cobalt and ink based cathodes. Using the Q-sun as a light source, currents were found to increase but level off (figure 4.3.11). Figure 7.3.10 shows standard additions of FA and how the current responds accordingly to give a similar shape to the curve recorded in figure 7.3.11.

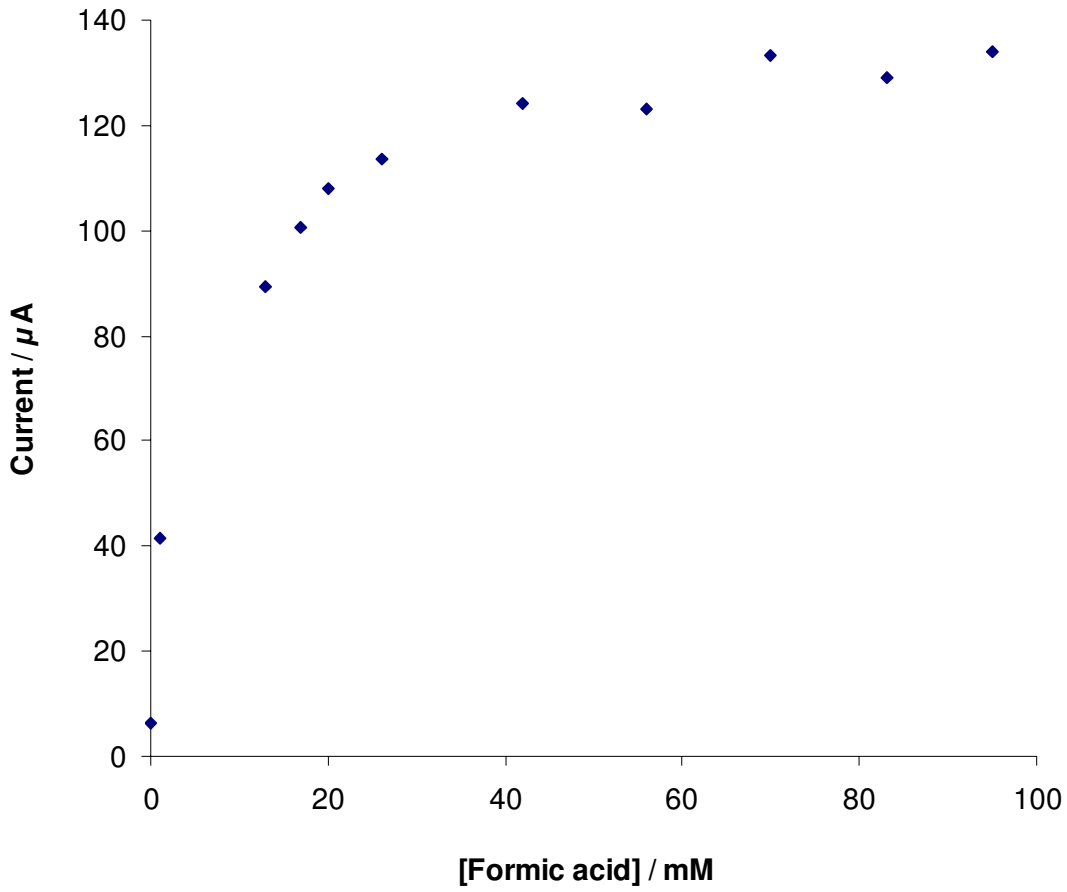

Figure 7.3.10: Current versus concentration for formic acid for aqueous 0.1 M KCl in an unstirred solution. Current was collected for 500 seconds with Pico technology across a 1 kΩ resistor. 60 W tungsten lamp. Experimental is as detailed in figure 7.3.9.

7.3.5 Area study

An experiment was constructed to evaluate the effect of electrode area on the currents received. Experimental conditions were as above with an air cathode for 10 mM FA, but the size of the ink based TiO_2 coated anode varied. The results are displayed in figure 7.3.11.

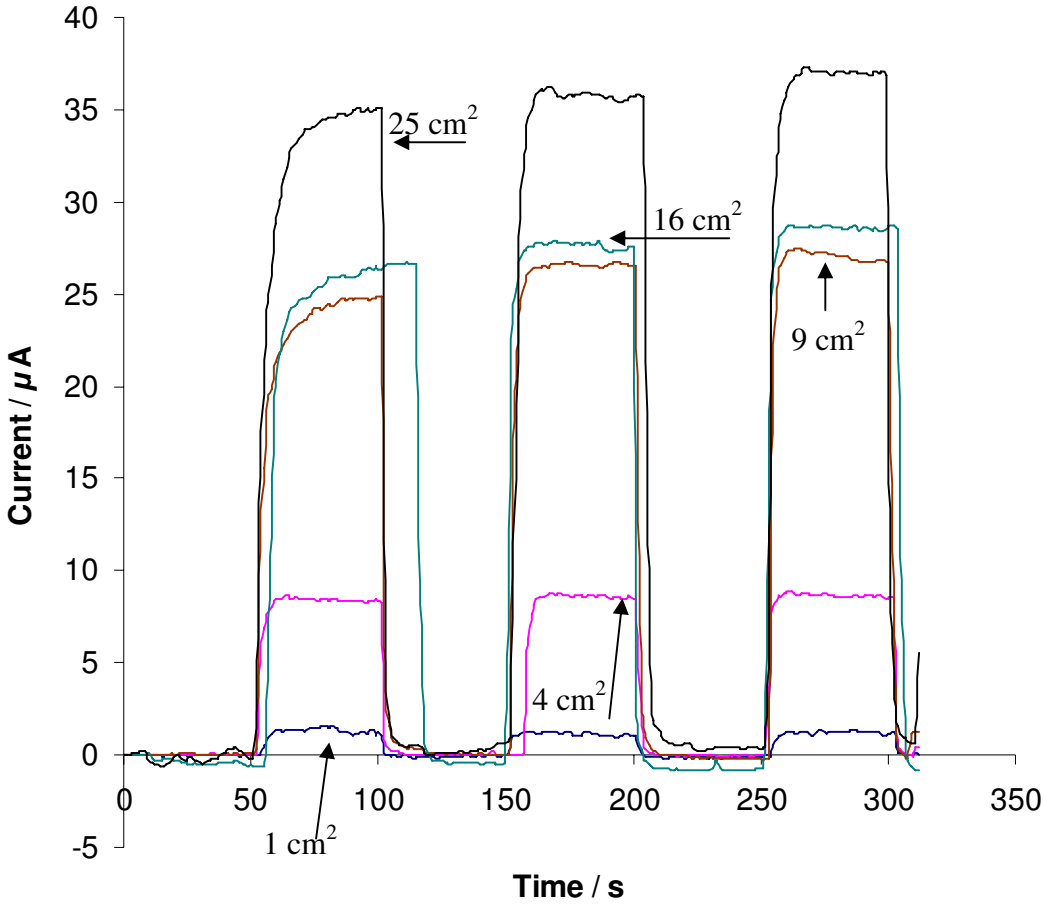

Figure 7.3.11: Photocurrent transients of aqueous formic acid (1 mM in 0.1 M KCl, 50 cm^3) in an unstirred solution. 1, 4, 9, 16 & 25 cm^2 TiO_2/CI anode and 1.3 cm^2 air cathode were used. Current was collected for 300 seconds with Pico technology across a 1 kΩ resistor. 60 W tungsten lamp. The lamp was switched on and off every 50 seconds.

An interesting point of note is that there is also a negative dark current for the results obtained in figure 7.3.11 (maximum of 6 μA but typically < 1 μA). However

the results are presented as 'absolute' values, with all currents presented as starting at a current of 0 μA.

It stands to reason that the larger the electrode area, the larger the current magnitude. However a more interesting take on things was how current output behaved per unit of electrode area.

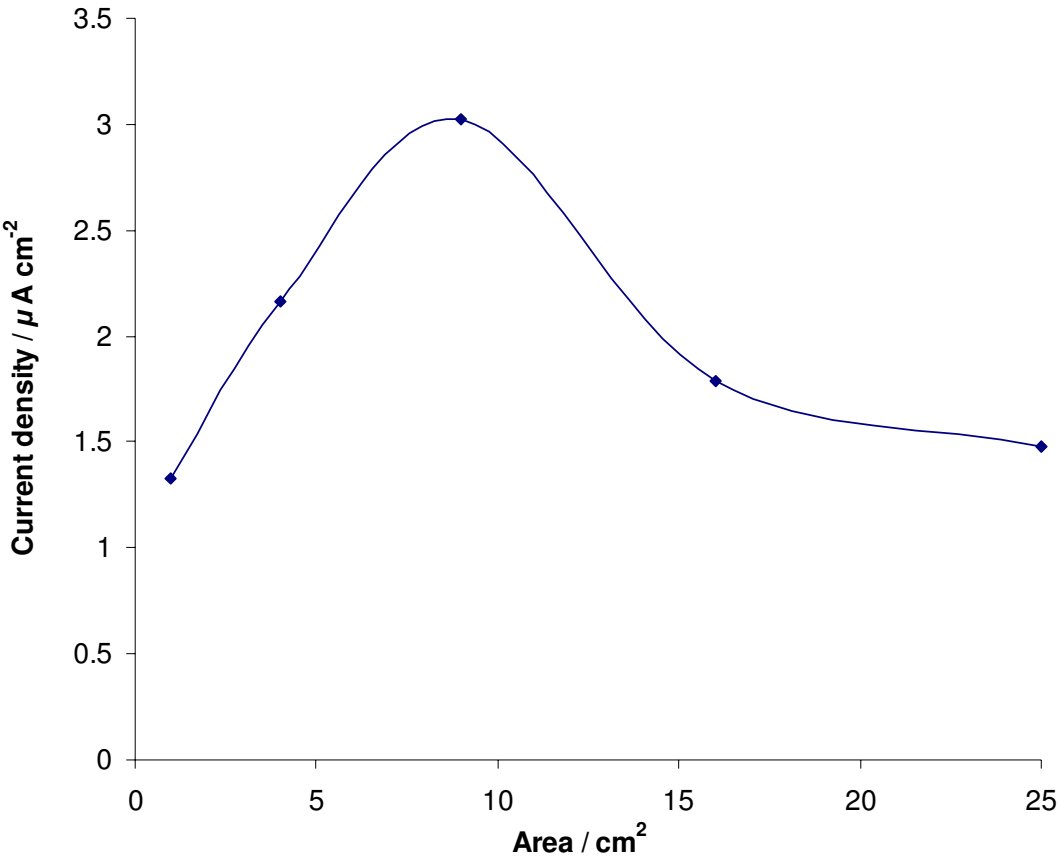

Figure 7.3.12: Current density of aqueous formic acid (10 mM in 0.1 M KCl, 50 cm^3) in an unstirred solution for different electrode areas. Currents were recorded at 275 seconds and experimental is as in figure 7.3.11.

As can be seen above, the optimal electrode area was 9 cm^2. At this size of an electrode, light is put to its best use; with more electron - hole pairs created per unit area than at larger electrodes.

7.3.6 Effect of distance

The effect of distance of the TiO_2 coated anode from the light (measured with a ruler) on current was evaluated, and the results are displayed in figure 7.3.13.

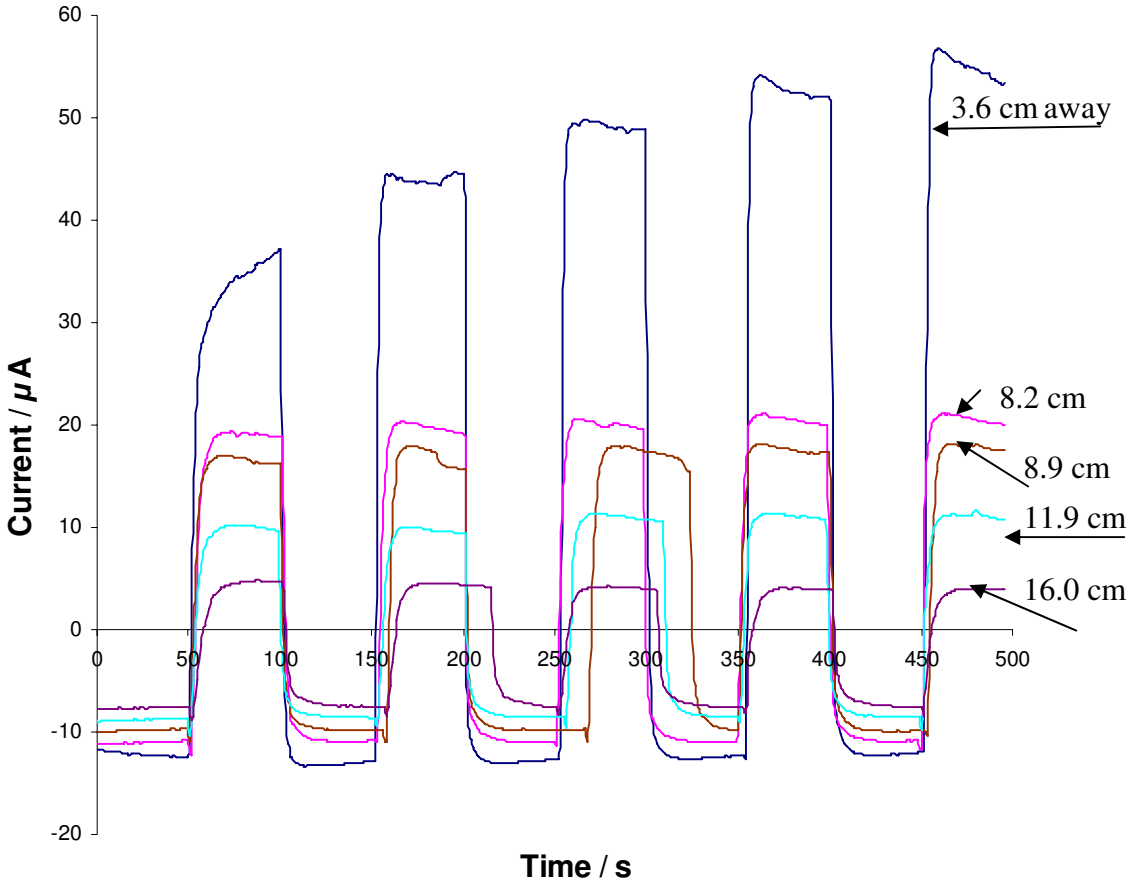

Figure 7.3.13: Current transients of aqueous formic acid (10 mM in 0.1 M KCl, 50 cm^3) in an unstirred solution. 25 cm^2 TiO_2/CI anode and 1.3 cm^2 air cathode were used. Current was collected for 500 seconds with Pico technology across a 1 kΩ resistor. A 60 W tungsten lamp varied in distance from the electrode. The lamp was switched on and off every 50 seconds.

As can be seen above, lower currents are obtained the further the anode is away from the light source. This is more evidence that FA oxidation is limited at the TiO_2 anode, and is further illustrated in figure 7.3.14.

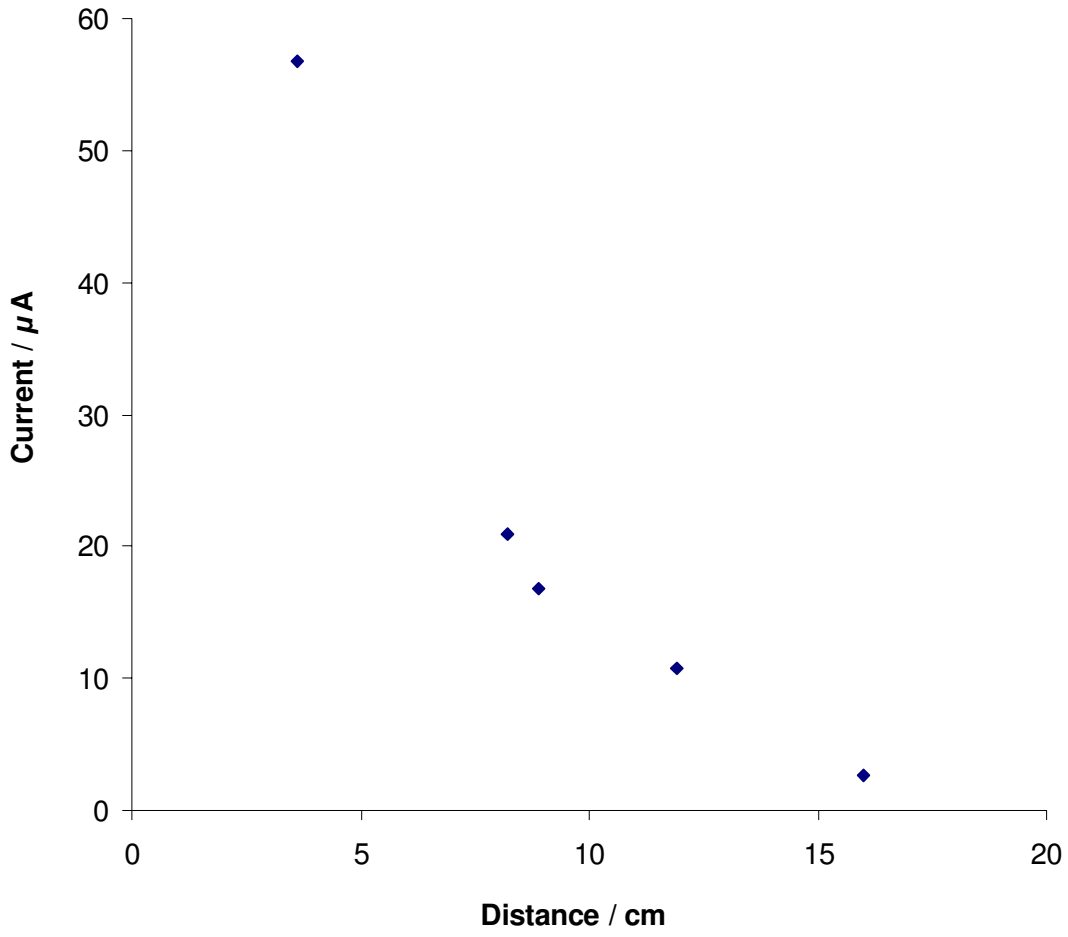

Figure 7.3.14: Effect of distance from the light source on currents produced, which were collected after 460 seconds. Experimental conditions are as in figure 7.3.13.

7.4 Conclusion

From the work done in chapter 7, it is possible to make some conclusions. The data received from the model was not comparable with the experimental, and such 'beautiful' voltammetry was not observed. This is because the FORTRAN software model was written for reversible systems rather than the steady state results in figure 7.3.6.

It was also shown that in this work, FA degradation depends on light assisted photocatalysis. Polynomial regression lines fit current concentration profiles and Langmuir Hinshelwood plots display correlation coefficients close to unity, but linear

regression relationships did not. Current increased and 'levelled off' with increasing FA concentration, in agreement with the results achieved experimentally in chapter 4 but again not in agreement with the model. This is because the computerised model predicts that the current increases linearly and infinitely with increasing concentration, and does not take into account depletion of TiO_2 sites available on the electrode surface, electrode fouling, passivation and many other natural experimental variables that may be encountered.

A similar 'levelling off' process was obtained when using a less powerful visible light source. On more minor notes, current was naturally found to increase with increasing electrode area, and it also increased the closer a distance the electrode was from the light source. An electrode area of 9 cm^2 provided the greatest current density.

7.5 References

[1] K. Vasanth Kumar, K. Porkodi, F. Rocha, *Catalysis Communications*, **9** (2008) 82 – 84

[2] H. Ted Chang, Nan-Min Wu, Faqing Zhu, *Water Research*, **34**, 2 (2000) 407 – 416

[3] T. Velegraki, D. Mantzavinos, *Chemical Engineering Journal* **140**, Issues 1-3, (2008) 15 - 21 doi:10.1016/j.cej.2007.08.026

[4] M.A. Hasnat, M.M. Uddin, A.J.F. Samed, S.S. Alam, S. Hossain, *Journal of Hazardous Materials*, **147** (2007) 471 – 477

[5] T.A. McMurray, J.A. Byrne, P.S.M. Dunlop, J.G.M. Winkelman, B.R. Eggins, E.T. McAdams, *Applied Catalysis*, *A, General*, **262**, (2004), 105

[6] K.J. McKenzie, P.M. King, F. Marken, C.E. Gardner, J.V. Macpherson, *Journal of Electroanalytical Chemistry* **579** (2005) 267 – 275

[7] J.A. Byrne, B.R. Eggins, S. Linquette-Mailley, P.S.M. Dunlop, *Analyst*, **123** (1998) 2007 - 2012

[8] A. Verma, S. Basu, *Journal of Power Sources*, **145** (2005) 282 – 285

[9] R.S. Nicholson, I. Shain, *Analytical Chemistry*, **36** (1964) 706

Chapter 8

Conclusions and further work

Chapter 8 – Conclusions and further work

8.1 Initial characterisation

There have been a number of conclusions associated with this work. In chapter 2 it has been shown that the presence of a cobalt catalyst allows the reduction of oxygen more readily than if the catalyst was not present. In chapter 3 the effect of immobilising the catalyst in a number or polymers to protect the catalyst was shown to have a variable effectiveness, PVP and PVC seemed to be most effective though layer thickness proved to be an important issue.

8.2 Photoelectrochemical cells using visible light

In chapter 4, model photoelectrochemical cells based on the TiO_2 coated ink as anode and a cobalt catalyst loaded cathode were studied and these were shown to work effectively as photoelectrochemical cells using model light conditions. It was found that the cells behaved as batteries when connected in series and in parallel. In chapter 5 using a relatively low energy light source, namely a tungsten lamp, KHP was degraded a little though the concentration of ascorbic acid was significantly decreased from 10 ppm to 0 ppm using the photo electrochemical cell; compared to the control that only degraded to 8 ppm. This indicated that there was a positive influence of using photoelectrochemistry compared to photochemistry. As the work in chapter 4 was achieved with a non-platinum catalyst, the results are good.

8.3 Photoelectrochemical cells using UV light

For two cases in chapter 5 the photo electrochemical cell produced a greater degradation of the organic substrate than an unconnected TiO_2 coated electrode. This

happened in the case of HHP and Bz using a 400 W mercury arc lamp; and isopropanol using a 150 W Xe lamp.

In addition there was a decrease in the organic concentration when the cell was exposed to daylight showing that the system can be used in normal environmental conditions.

Particularly encouraging was the decrease in catechol concentration for a connected cell where the concentration dropped from 64 to 10 ppm, while for the unconnected TiO_2 electrode the concentration dropped from 60 to 50 ppm in daylight.

There are no precious metals used in chapter 5 so the results are good. Simple electrode configurations are employed that are cheap and easily expandable. Such electrodes can be used for cleaning trace organics from water using daylight as the source.

8.4 Model for the adsorption of organic compounds

In an effort to model the system, finite difference simulation method was employed to model the Langmuir Hinshelwood adsorption system applied to formic acid system. There is a linear increase in steady state current with increasing concentration of formic acid concentration both from model and experimental results.

A typical voltammetric profile of a bulk solution redox reaction would yield a peak. The steady state current in the presence of light for formic acid oxidation indicates a more complex situation. That the experimental voltammetric profile is a steady state current is indicative of a kinetically controlled process.

The model is an attempt to apply a Langmuir Hinshelwood model to voltammetry, a system which has been proposed in the literature for 4-chlorophenol [1], benzoic acid [2], erythrosine (a synthetic dye) [3] and oxalic acid [4] as test compounds.

8.5 Novelty of this work

Currently there is a group in Japan actively pursuing research into photoelectrochemical cells. This group published a paper based on a light assisted photoelectrochemical cell after this work began [5]. TiO_2 was annealed onto a fluoride doped tin oxide glass electrode which was irradiated with a 500 W Xe lamp (0.5 W cm^{-2}) in the aqueous organic. The wide variety of substrates tested ranged from biomass like polysaccharides, proteins, lignin and cellulose to simple alcohols and sugars, ammonia, urea and even synthetic polymers like PEG and poly(acrylamide). The electrons produced travelled through a resistance towards the positive oxygen sparged air cathode made of Pt/Pt black, where O_2 was reduced. Evolved gases (N_2, H_2, O_2 and CO_2) were analysed by gas chromatography, and compounds underwent mineralisation.

The work was promising because of the vast amount of organics incinerated by the photo-assisted cell, and large currents were produced. They used more expensive electrodes and light sources, with very small volumes involved but achieved some very good results.

This year a group in Italy presented a twin cell for the oxidation of either FA or copper at the anode and Cu^{2+} reduction or else O_2 reduction at an air cathode [6]. The work was similar to what has been done here, but the anodic compartment consisted of a copper anode, FA and a TiO_2 suspension.

There were two other studies this year (from the one group) of a photoelectrochemical cell used to degrade organics such as simple alcohols, ammonia, urea and detergents [7, 8]. The anode consisted of fluorinated ITO coated with TiO_2 doped with CdS (to make it more visible light active) while the cathode also contained TiO_2 but was sprinkled with Pt nanoparticles, aerobically producing electricity while anaerobically producing hydrogen from the reduction of H^+ that were photogenerated at the anode.

What really sets this project apart from the others is the carbon ink upon flexible anodes being used in conjunction with an air cathode.

8.6 Future work

Future work would include the correlation of the current flowing through the cell with the consumption of the organic components. In this case it would demonstrate that photoactivity is responsible for the decrease in the organic components.

Scale up of the cells and the use of the cells in an out door environment would also be of benefit. It is evident that when some compounds (e.g. catechol) are degraded that TiO_2 is fouled and the aim would be that the accumulated charge be used in cleaning the adsorbed organics off the passified TiO_2 sites.

8.7 References

[1] H. Ted Chang, Nan-Min Wu, Faqing Zhu, *Water Research*, **34**, 2 (2000) 407 – 416

[2] T. Velegraki, D. Mantzavinos, *Chemical Engineering Journal* **140**, Issues 1-3, (2008) 15 - 21 doi:10.1016/j.cej.2007.08.026

[3] M.A. Hasnat, M.M. Uddin, A.J.F. Samed, S.S. Alam, S. Hossain, *Journal of Hazardous Materials*, **147** (2007) 471 – 477

[4] T.A. McMurray, J.A. Byrne, P.S.M. Dunlop, J.G.M. Winkelman, B.R. Eggins, E.T. McAdams, *Applied Catalysis*, *A, General*, **262**, (2004), 105

[5] M. Kaneko, J. Nemoto, H. Ueno, N. Gokan, K. Ohnuki, M. Horikawa, R. Saito, T. Shibata, *Electrochemistry Communications*, **8** (2006) 336 – 340

[6] M. Canterino, I. Di Somma, R. Marotta, R. Andreozzi, V. Caprio, Energy recovery in wastewater decontamination: Simultaneous photocatalytic oxidation of an organic substrate and electricity generation, *Water Research* (2009) doi:10.1016/j.watres.2009.03.012

[7] M. Antoniadou, P. Lianos, *Journal of Photochemistry and Photobiology A: Chemistry*, **204** (2009) 69 – 74

[8] M. Antoniadou, P. Lianos, Photoelectrochemical oxidation of organic substances over nanocrystalline titania: Optimisation of the photoelectrochemical cell, *Catalysis Today* (2009) doi:10.1016/jcattod.2009.02.024

Appendix A

Finite difference methods

Appendix A – Finite difference methods

9.1 Introduction

This section is designed to introduce some numerical methods for solving mass transport equations for specific electrochemical systems. Unlike some of the theoretical approaches, numerical methods are considerably more straightforward and require only some knowledge of programming. For a typical mass transport situation, the equation to be solved is [1]:

$$\frac{\partial c}{\partial t} = \frac{\partial^2 c}{\partial x^2} \pm \text{other} \qquad 9.1$$

where the partial derivatives correspond to the diffusion process while the "other" term corresponds to concentration changes with time due to migration, convection or chemical reactions. In equation 9.1, *c* is the concentration, *t* is time and *x* is distance away from the electrode.

However in the first instance, the "other" term will be neglected. The aim is to solve equation 9.1 and to determine an expression for the concentration which is generally as a function of distance away from the electrode and time; $c_{(x,t)}$. If an expression for concentration is found then it is possible to determine the current readily.

Analytical techniques may be used in a variety of instances to determine explicit expressions for concentration profiles. Generally analytical methods may be applied for simple mechanisms but for more complicated problems, numerical methods are required. The key to these numerical methods involves discretisation of the system.

For example, in figure 9.1 the expected concentration profiles for a species in solution close to an electrode are shown where initially there is a concentration c* in

solution. Then the cell is switched on or a step potential applied so that the concentration at the electrode surface is forced to zero. Because of this, species from a little further out diffuse in toward the electrode to remove this difference in concentration. This diffusion is characterised by equation 9.1; and should equation 9.1 be solved, the series of concentration profiles $c_{(x,t)}$, shown in figure 9.1 may be found.

For these methods, the concentrations are evaluated at specific points in time and positions in distance. Finite difference methods therefore involve the application of a grid with distance and time increments *h* and *k* respectively. So rather than ending up with the complete profile, a digitised profile at particular distances and times is obtained. This incurs an error which however may be quantified.

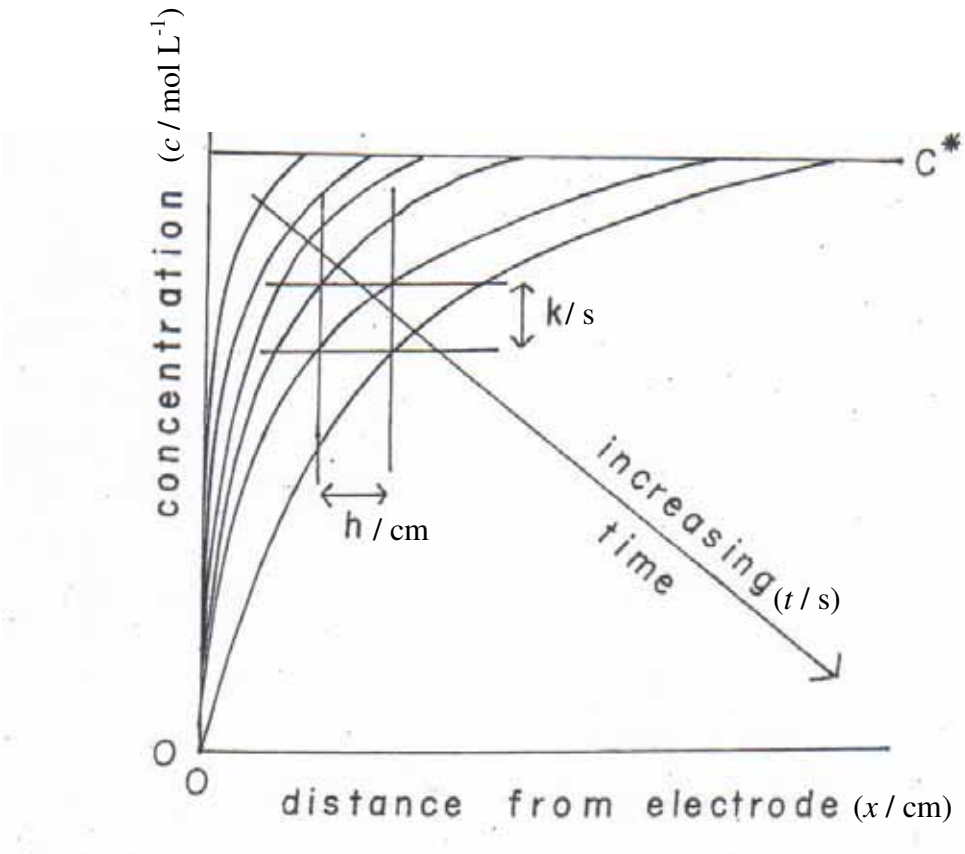

Figure 9.1: A representation of the decrease in concentration as a function of time and distance away from the electrode surface. The time increment is *k* and the distance increment is *h*.

The numerical technique is derived from a Taylors expansion which states that concentration at a position i+h may be determined if the concentration at the point i, and the various derivatives of that concentration at the point i are known:

$$c_{i+h} = c_i + h\,c_i' + h^2\frac{c_i''}{2!} + h^3\frac{c_i'''}{3} + \ldots\ldots \qquad 9.2$$

where h is the distance away form the point i to the point i+h and the dashes represent the derivatives. This expression may be applied either for distance (along the x Axis of the grid in figure 9.1) or time; (along the y Axis of the grid in figure 9.1); since for a particular distance, the concentration decreases as a function of time. An expression related to equation (9.2) is also possible for a distance in the other direction:

$$c_{i-h} = c_i - h\,c_i' + h^2\frac{c_i''}{2!} - h^3\frac{c_i'''}{3!} + \ldots\ldots\ldots \qquad 9.3$$

These expressions are derived from a theory which says that it is possible to extrapolate a function to a position i + h if it is known at i and if it's tendency to change (the derivative terms) are also known. A similar expression to equation 9.2 may be written for the time Axis as

$$c_{t+k} = c_t + k\,c_t' + k^2\frac{c_t''}{2!} + k^3\frac{c_t'''}{3!} + \ldots\ldots \qquad 9.4$$

where k is the time interval. It is possible by algebraically combining equations 9.2 - 9.4 to obtain a digitised form of equation 9.1.

From expression 9.4, one can obtain an approximate expression for $(dC)/(dt)$ by neglecting the third and remaining terms from the series in equation 9.4

$$c_t' = \frac{dc}{dt} \approx \frac{(c_{t+k} - c_t)}{k} \qquad 9.5$$

It can be seen that this is not a true equality. However at least it is an approximate expression for the derivative and the error may be quantified. Furthermore by adding equations 9.2 and 9.3, one can obtain the second derivative since

$$c_{i+h} + c_{i-h} \approx 2c_i + h^2 c_i'' \qquad 9.6$$

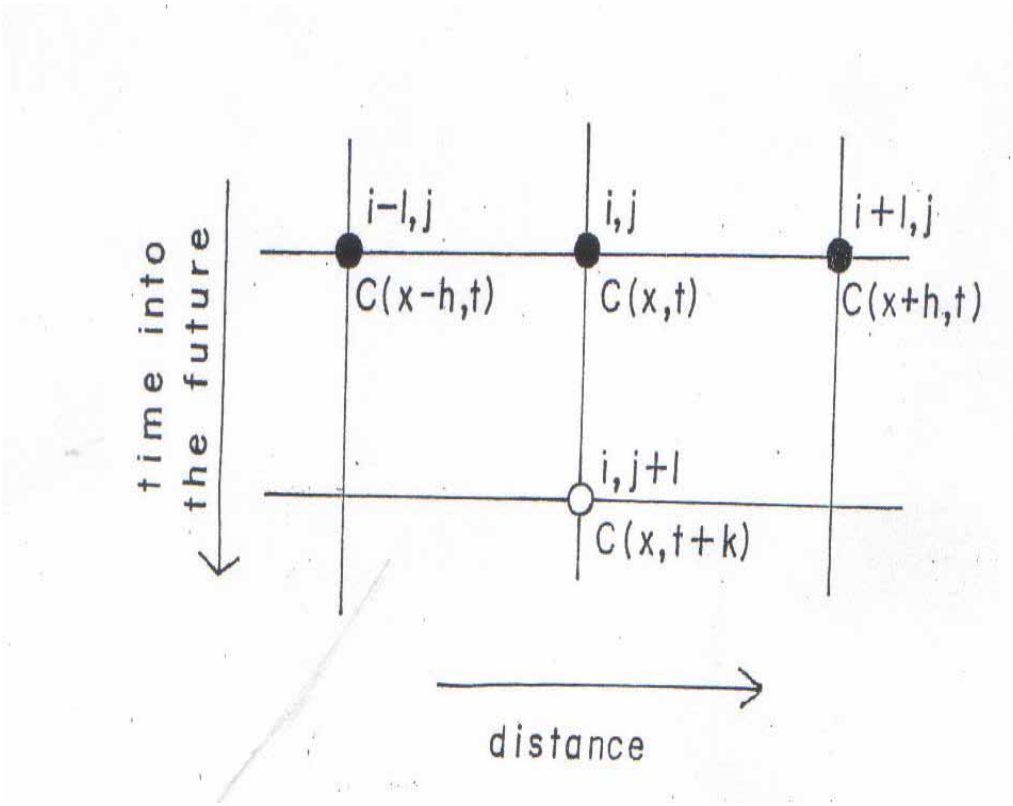

Figure 9.2: The distance time grid for the finite difference method

and therefore

$$c''_i = \frac{d^2 c_i}{dx^2} \approx \frac{(c_{i+h} + c_{i-h} - 2c_i)}{h^2} \qquad 9.7$$

By a further approximation it is possible to substitute equations 9.5 and 9.7 into equation 9.1 by assuming that the full derivatives are equal to the partial derivatives. In this manner equation 9.1 becomes:

$$\frac{(c_{t+k} - c_t)}{k} = D\,\frac{(c_{i+h} + c_{i-h} - 2c_i)}{h^2} \qquad 9.8$$

where D is the diffusion coefficient. Since concentration is both a function of time and distance, let us generalise the notation according to figure 9.2, where i,j represents the concentration at a position i and time t and $c_{i+1,j}$ represents the concentration at a position i+h and a time t. Thus equation 9.8 may be written as:

$$c_{i,j+1} = c_{ij} + D\mathrm{k}\,\frac{(c_{i+1,j} + c_{i-1,j} - 2c_{i,j})}{h^2} \qquad 9.9$$

Looking at equation 9.9 and figure 9.2, it can be seen that information at a particular time j maybe used in order to project into the future so as to get information at a time j+1. In the diagram the concentration at the full circles are known and the concentrations at the open circle may be evaluated.

In order to use this method, it is necessary to have somewhere to start from and this consists of a boundary condition. For example at the electrode surface in figure 9.1, we may set a potential so that the concentration of the redox species is always zero, thus it would be possible to extend out from this.

A nice aspect of equation 9.9 is that the units 'work out'. Since *k* is in seconds, *h* is in cm and the diffusion coefficient *D* is in $cm^2\,sec^{-1}$, the parameter

$\frac{D\mathrm{k}}{h^2} = D\mathrm{m}$ is unitless.

Furthermore it is possible to ratio all concentrations to the initial bulk concentration c* to obtain dimensionless concentrations C = c/c*.

Thus:

$$C_{i,j+1} = C_{i,j} + D_m(C_{i+1,j} + C_{i-1,j} - 2C_{i,j}) \qquad 9.10$$

Using this technique to probe into the future one point at a time is called the explicit method. It suffers from the problem that the value of D_m may not be greater than 0.5, otherwise the method is unstable [2].

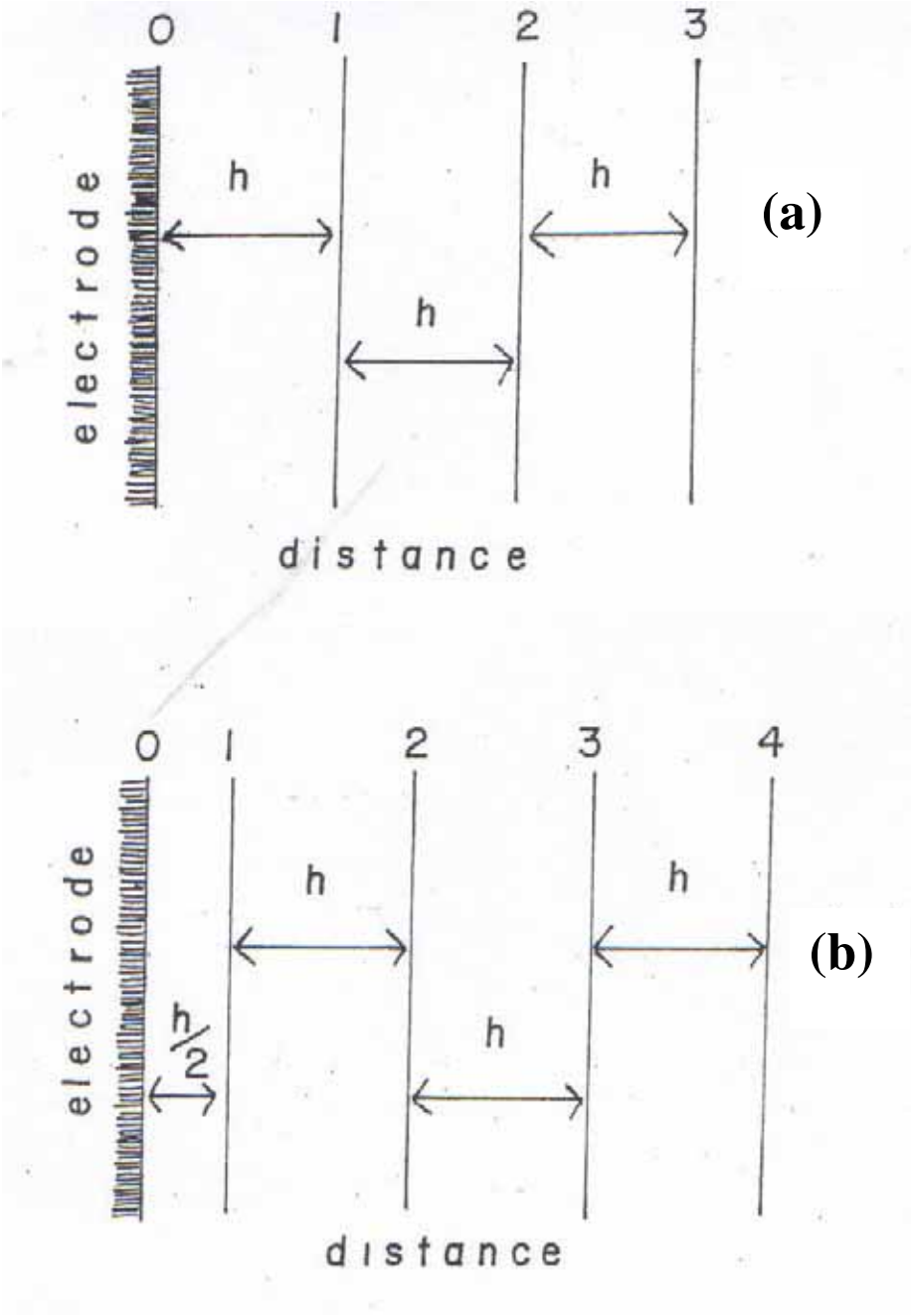

Figure 9.3: Equal (a) and unequal (b) distance spacings used in the finite difference method.

Since this method is widely used in electrochemistry, and since the concentration profile at the electrode surface is more important than out in bulk solution, a trick has been applied in order to better characterise the profile close to the electrode. By decreasing the distance interval closer to the electrode as shown in figure 9.3 (b), it would be hoped to obtain a better indication of the concentration profile rather than in figure 9.3 (a) where the distance intervals are equal. An estimate of equation 9.9 applied to what happens closer to the electrode, namely the derivative evaluated at the point 1 in figure 9.3 (b), is [2, 3]:

$$\left(\frac{C_{1,j+1} - C_{1,j}}{k}\right) = \frac{D}{h}\left(\frac{C_{2,j} - C_{1,j}}{h} - \frac{C_{1,j} - C_{0,j}}{h/2}\right) \qquad 9.11$$

or

$$C_{1,j+1} = C_{1,j} + D_m(C_{2,j} - 3\,C_{1,j} + 2C_{0,j}) \qquad 9.12$$

where the right hand side of equation 9.11 represents the average of two slopes. A problem is encountered at this point. Although equation 9.12 is quoted widely and used frequently in the literature [4], it suffers from the problem that it is asymmetric [5].

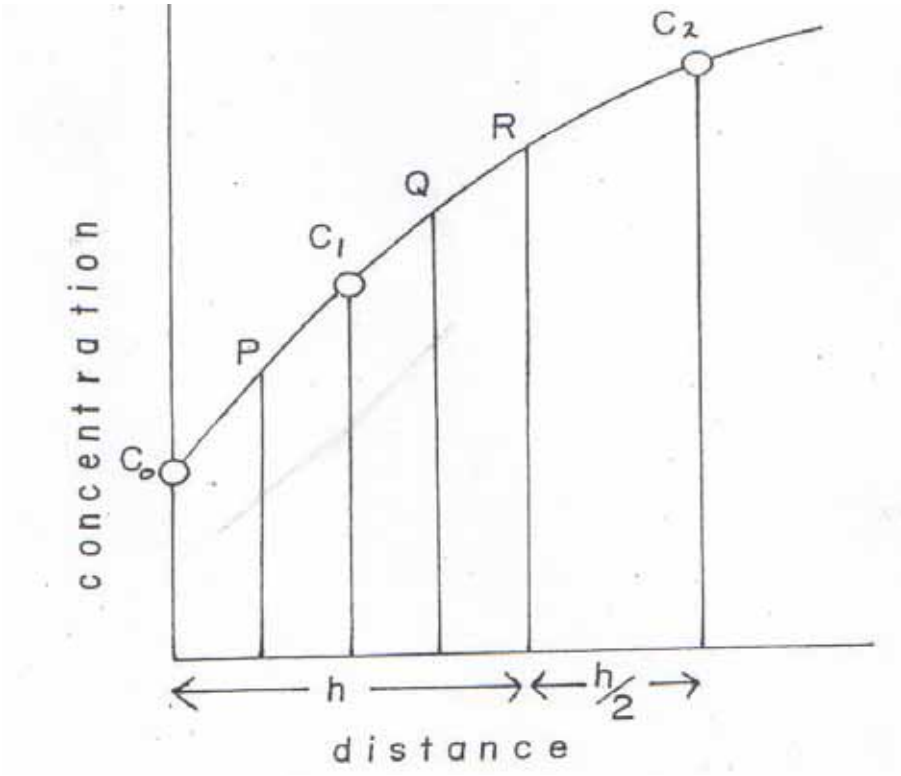

Figure 9.4: Expanded view of the unequal distance spacings to show the problem of asymmetry

A more detailed expansion of figure 9.3 (b) is shown in figure 9.4. The slope at the point P located at a distance 0.25 h is $2\frac{(C_1-C_0)}{h}$

The slope at the point R located at a distance h away from the electrode is

$$\frac{(C_2 - C_1)}{h}$$

and the slope at the point Q located a distance 0.75 h away from the electrode is given by

$$2\,\frac{(C_2 - C_0)}{3h}$$

It is possible to get two different estimates of the second derivative. The difference in slopes between R and P (located at 0.625 h away from the electrode) is

$$C'' = 4\,\frac{(C_2 - 3\,C_1 + 2\,C_0)}{3h^2} \qquad 9.13$$

while the difference between slopes between Q and P located at the point C_1 is also given by the above equation.

There is a factor of 1.33 difference between equations 9.12 and 9.13; a fact that has not received a great amount of attention. Britz [2] comments that although equation 9.12 is 'wrong', better results are obtained from it than the technically correct equation 9.13. By leaving out the factor 1.33, implicitly a fudge factor 0.75 is included for which there is no justification. Britz [2] comments that it is better to use equal intervals close to the interface i.e.

$$C_{1,j+1} = C_{1,j} + Dm\,(C_{2,j} + C_{0,j} - 2C_{1,j}) \qquad 9.14$$

rather than using a 0.5 h interval close to the electrode.

9.2 Cyclic voltammetry using the implicit method

From above, the following has been shown

$$C_{i,j+1} = Ci,j + D_m\,(C_{i+1,j} - 2\,C_{i,j} + C_{i-1,j}) \qquad 9.15$$

as may be seen in figure 9.2. The reverse of the above is also valid:

$$C_{i,j+1} + D_m\,(C_{i+1,j+1} - 2\,C_{i,j+1} + C_{i-1,j+1}) = -\,C_{i,j} \qquad 9.16$$

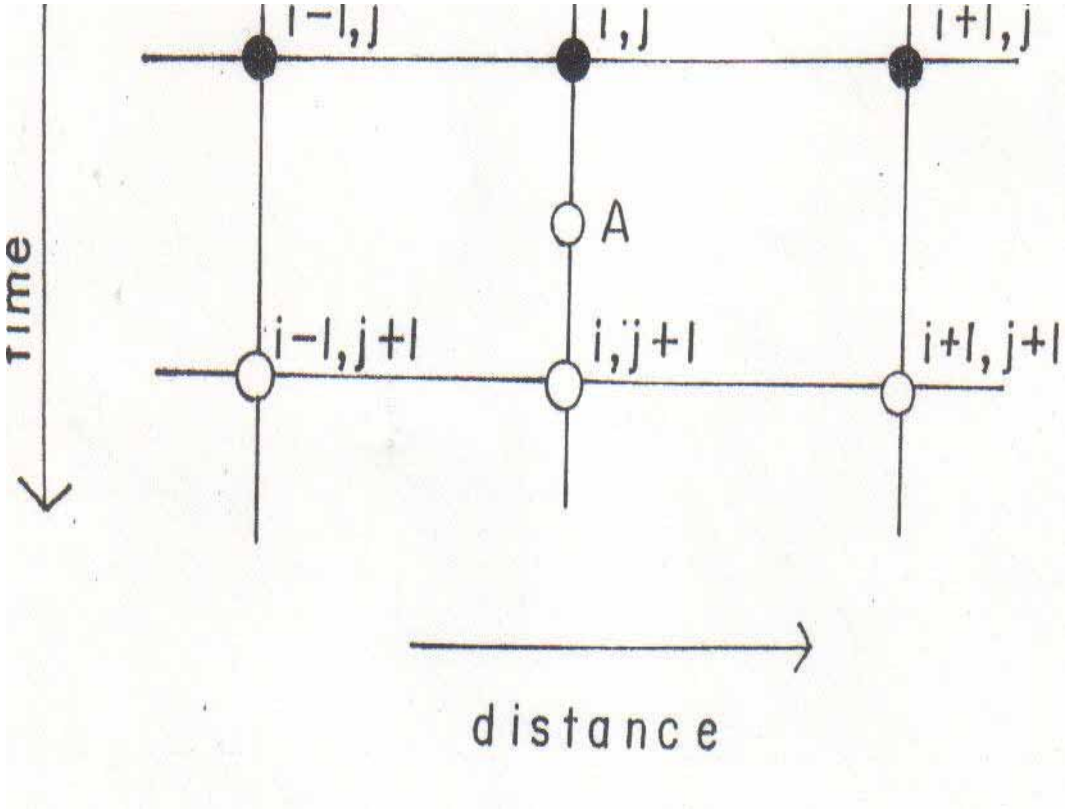

Figure 9.5: Distance time grid for the Crank Nicholson technique.

At the point A in figure 9.5, the term dC/dt may be approximated as

$$\frac{dC}{dt} = \frac{C_{i,j+1} - C_{i,j}}{k} \qquad 9.17$$

Also at the point A the C'' term may be an average of equations 9.10 and 9.16, that is:

$$\frac{C_{i,j+1} - C_{i,j}}{k} = \frac{D}{2}\left[\frac{C_{i+1,j+1} + C_{i-1,j+1} - 2C_{i,j+1}}{h^2} + \frac{C_{i+1,j} + C_{i-1,j} - 2C_{i,j}}{h^2}\right] \qquad 9.18$$

which becomes equation 9.19:

$$(2 + 2\,D_m)C_{i,j+1} - D_m C_{i+1,j+1} - D_m C_{i-1,j+1} = D_m C_{i+1,j} + D_m\,C_{i-1,j} - (2\,D_m - 2)\,C_{i,j}$$

Everything on the right hand side is known and it is possible to set up a series of algebraic equations to determine concentration on the left hand side. In the case of

the explicit method we were progressing forward in time for each distance point, whereas in this case we progress by determining the concentrations at all the distances simultaneously at each time increment. The resulting series of equations may be shown in matrix form as:

$$\begin{Vmatrix} (2+2Dm) & -Dm & 0 & 0 & 0 \\ -Dm & (2+2Dm) & -Dm & 0 & 0 \\ 0 & ... & ... & .. & 0 \\ 0 & 0 & -Dm & (2+2Dm) & -Dm \\ 0 & 0 & 0 & -Dm & (2+2Dm) \end{Vmatrix} \begin{Vmatrix} C_{1,j+1} \\ C_{2,j+1} \\ .. \\ C_{N-1,J+1} \\ C_{NJ+1} \end{Vmatrix} =$$

$$\begin{Vmatrix} (2-2Dm) & Dm & 0 & 0 & 0 \\ Dm & (2-2Dm) & Dm & 0 & 0 \\ 0 & ... & ... & .. & 0 \\ 0 & 0 & Dm & (2-2Dm) & Dm \\ 0 & 0 & 0 & Dm & (2-2Dm) \end{Vmatrix} \begin{Vmatrix} C_{1,j} \\ C_{2,j} \\ .. \\ C_{N-1,j} \\ C_{NJ} \end{Vmatrix} = \begin{Vmatrix} k_1 \\ k_2 \\ ... \\ k_{N-1} \\ k_N \end{Vmatrix} \qquad 9.20$$

It should be noted that in addition to these N points there are also two boundary points at the electrode surface and also at in bulk solution. Since these boundary conditions are known at all times then the right hand side has to be modified as follows:

$$\begin{Vmatrix} (2+2Dm) & -Dm & 0 & 0 & 0 \\ -Dm & (2+2Dm) & -Dm & 0 & 0 \\ 0 & ... & ... & .. & 0 \\ 0 & 0 & -Dm & (2+2Dm) & -Dm \\ 0 & 0 & 0 & -Dm & (2+2Dm) \end{Vmatrix} \begin{Vmatrix} C_{1,j+1} \\ C_{2,j+1} \\ .. \\ C_{N-1,J+1} \\ C_{NJ+1} \end{Vmatrix} = \begin{Vmatrix} k_1 + D_m(C_{0,j} + C_{0,j+1}) \\ k_2 \\ .. \\ .. \\ k_{N-1} \\ k_N + D_m(C_{N+1,j} + C_{N+1,j+1}) \end{Vmatrix} \qquad 9.21$$

In this manner the boundary conditions are included. The above sets of equations are tridiagonal and may be solved by using the Thomas Algorithm [2].

Booman and Pence used implicit methods for kinetic complications for bulk solution reactions [6] and Heinze *et al*. [7] used the Crank Nicolson method for cyclic

voltammetry. Lasia [8] employed it for examining dimerisation. A review of the Crank Nicolson methods has appeared [9].

9.3 References

[1] D. Britz, Digital Simulation in Electrochemistry, Springer, Verlag, Berlin (1981)

[2] S.W. Feldberg, in Electroanalytical Chemistry, A.J. Bard (ed.), volume 3, pp. 199-249, M. Dekker, New York (1969)

[3] J.R. Sandifer, R.P. Buck, *Journal of Electroanalytical Chemistry*, **49** (1974) 161

[4] The Southampton Electrochemistry Group, Instrumental Methods in Electrochemistry, Ellis Horwood, Chichester (1985)

[5] M.K. Hanafey, R.L. Scott, T.H. Ridgeway, C.N. Reilly, *Analytical Chemistry*, **50** (1978) 116

[6] G.L. Boomen, D.T. Pence, *Analytical Chemistry*, **37** (1965) 1366

[7] J. Heinze, M. Storzbach, J. Mortensen, *Journal of Electroanalytical Chemistry*, **165** (1984) 61

[8] A. Lasia, *Journal of Electroanalytical Chemistry*, **146** (1983) 397

[9] M. Storzbach, J. Heinze, *Journal of Electroanalytical Chemistry* **346** (1993) 1

Appendix B

FORTRAN program used to programme the Langmuir Hinshelwood model for the voltammetry of a reversible system

Appendix B - FORTRAN program used to programme the Langmuir Hinshelwood model for the voltammetry of a reversible system

```
c     CYCLIC VOLTAMMETRY OF A BULK SPECIED WHICH INCLUDES
ADSORPTION KINETIC
c     TERMS
c     THIS USES THE CRANK NICHOLSON IMPLICIT METHOD
c     JUNE 25TH 2008
      IMPLICIT REAL*8(A-H,O-Y)
      IMPLICIT REAL*4(Z)
      DIMENSION W(100), RMAT(250000), G(500),PCHI(22000)
      DIMENSION FONEW(500),FOOLD(500), FROLD(500), FRNEW(500)
      DIMENSION FBOLD(500), FBNEW(500),RKB(500)
      DIMENSION RKO(500), RKR(500), RNEW(500), RK(500), WZ(50000)
c      OPEN(UNIT=5,FILE='F:\TT.DAT',STATUS='OLD')
      OPEN(UNIT=6,FILE='C:\J75.DAT',STATUS='NEW')
c     this programme was written for reduction
      VI=0.3D0
      VF=-0.3D0
c     s is the scan rate
      S=0.001D0
      T=2.D0*(VI-VF)/S                    (= time)
      EI=VI/0.02569D0
      EF=VF/0.02569D0
c      DM=0.005D0
      DIFF = 6.0D-6
      CB0=1.D-2
      L=9999
      DIST=DSQRT(3.D0*DIFF*T)    (δ = √πDt )
      RH=DIST/(1.D 1)
      RKT=T/(1250)
      DM=RKT*DIFF/((RH**2)*2)
c     LANGMUIR CONST IS RLK. EQUILIBRIUM CONST IS REK
c     RD IS THE DIMENSIONLESS FACTOR TIME/DIST**2
      RKL=1.0D-3
      RKB1= 7.0D-3
c      RD=DM/DIFF
      RKDD=RKL*RKT/CB0
      RKD=RKB1*CB0
c      READ(5,60)DM,L
      WRITE(6,60)DM,L
   60 FORMAT(F10.2,I6)
      DELTAE=(EF-EI)/FLOAT(L)
      EMOD=EI
c     the total number of segments is LT2
      DO 10 J=1,200
      FOOLD(J)=0.D0
      FBOLD(J)=1.D0
      FROLD(J)=0.D0
   10 CONTINUE
```

```
      LT2=2*L
      DO 20 I=1,LT2
      ZI=SQRT(FLOAT(I))
      ZDM=DSQRT(DM)
      N=IFIX(6*ZI*ZDM)+1
      NX=N-1
c     RIGHT HAND SIDE MATRIX CALCULATION
      DO 16 LL=1,N
      DO 16 K=1,N
   16 RMAT((LL-1)*N+K)=0.D0
      DO 17 LL=1,N
   17 RMAT((LL-1)*N+LL)=2.D0*(1.D0-DM)
      DO 14 LL=1,NX
      RMAT((LL-1)*N+LL+1)=DM
   14 RMAT(LL*N+LL)=DM
c     CALCULATE THE RHS FOR THE THOMAS ALGORITHM
      DO 18 LL=1,N
      RKO(LL)=0.D0
      RKR(LL)=0.D0
      RKB(LL)=0.D0
   18 CONTINUE
      DO 19 K=1,N
      DO 45 LL=1,N
      RKB(K)=RMAT((LL-1)*N+K)*FBOLD(LL)+RKB(K)
      RKO(K)=RMAT((LL-1)*N+K)*FOOLD(LL)+RKO(K)
   45 RKR(K)=RMAT((LL-1)*N+K)*FROLD(LL)+RKR(K)
      RKB(K)=RKB(K)-RKDD*RKD*FBOLD(K)/
     1(1.D0+RKD*FBOLD(K))
      RKO(K)=RKO(K)+RKDD*RKD*FBOLD(K)/
     1(1.D0+RKD*FBOLD(K))
      RKR(K)=RKR(K)
   19 CONTINUE
c     BECAUSE K GOES FROM 1 TO N,THE KINETC TERM IS OK
c     RECALCULATE MATRIX FOR THE LEFT HAND SIDE.
      DO 30 LL=1,N
   30 RMAT((LL-1)*N+LL)=2.D0*(1.D0+DM)
      DO 21 LL=1,NX
      RMAT((LL-1)*N+LL+1)=-DM
   21 RMAT(LL*N+LL)=-DM
c     calculate the old and new surface concentrations
      RATIO=DEXP(EMOD)
      DRSURF=(FOOLD(1)+FROLD(1))/(1.D0+RATIO)
      DOSURF=RATIO*DRSURF
      EMOD=EMOD+DELTAE
      RATIO=DEXP(EMOD)
      FRSURF=(FOOLD(1)+FROLD(1))/(1.D0+RATIO)
      FOSURF=RATIO*FRSURF
      FONEW(1)=FOOLD(1)+DM*(FOSURF-2*FOOLD(1)+FOOLD(2))
      FRNEW(1)=FROLD(1)+DM*(FRSURF-2*FROLD(1)+FROLD(2))
      FONEW(N)=FOOLD(N)+DM*(FOOLD(N-1)-2*FOOLD(N))
```

```
      FRNEW(N)=FROLD(N)+DM*(FROLD(N-1)-2*FROLD(N))
      FBNEW(1)=FBOLD(1)+DM*(1.D0-2*FBOLD(1)+FBOLD(2))
      FBNEW(N)=FBOLD(N)+DM*(FBOLD(N-1)-2*FBOLD(N)+1.D0)
c      FIX UP THE BOUNDARY CONDITIONS....
      RKO(1)=RKO(1)+DM*(DOSURF+FOSURF)
      RKR(1)=RKR(1)+DM*(DRSURF+FRSURF)
      RKB(N)=RKB(N)+DM*2.D0
      RKO(N)=RKO(N)
      RKR(N)=RKR(N)
      CALL THOMAS(FRNEW,RKR,RMAT,N)
      CALL THOMAS(FONEW,RKO,RMAT,N)
      CALL THOMAS(FBNEW,RKB,RMAT,N)
c     CALCULAE THE DIMENSIONLESS CURRENT
      FACT=SQRT(DM*FLOAT(L))/(1.D0+RATIO)
      WZ(I)=FACT*(FONEW(1)-RATIO*FRNEW(1))
      PCHI(I)=WZ(I)/DSQRT(EI-EF)
c     RESET COINCENTRATUIOINS
      DO 40 J=1,N
      FOOLD(J)=FONEW(J)
      FROLD(J)=FRNEW(J)
      FBOLD(J)=FBNEW(J)
   40 CONTINUE
c     TEST FOR SWEEP DIRECTION.
      IF (I.EQ.L)DELTAE=-DELTAE
   20 CONTINUE
c     OPUTPUT DATA
      DELTAE=-DELTAE
      EMOD=EI
      WRITE(6,88)N
      WRITE(6,89)RH
      WRITE(6,90)RKT
      WRITE(6,91)DM
      WRITE(6,92)RKD
      WRITE(6,93)RKDD
      WRITE(6,94)S
      WRITE(6,95)T
   89 FORMAT('RH = ',F11.4)
   90 FORMAT('RK = ',F11.4)
   91 FORMAT('DM = ',F11.4)
   92 FORMAT('RKD = ',F11.4)
   93 FORMAT('RKDD = ',F11.4)
   94 FORMAT('S = ',F11.4)
   95 FORMAT('T = ',F11.4)
      DO 50 I=1,LT2
      EMOD=EMOD+DELTAE
      V=EMOD*0.02569D0
c     SWITCH THE VOLTAGE TO PRETEND OXIDATION
      V=-V
   88 FORMAT( 'LARGEST NUMBER OF POINTS' ,I4)
      WRITE(6,100)V,PCHI(I)
```

```
c      WRITE(6,100)FOOLD(3),FBOLD(3)
       IF(I.EQ.L)DELTAE=-DELTAE
   50 CONTINUE
  100 FORMAT(F11.4,',',F12.9)
c      CLOSE( UNIT = 5)
       CLOSE( UNIT = 6)
       STOP
       END
c     FOR SOLVING TRIDIAGONAL MATRIX
       SUBROUTINE THOMAS(RNEW,RK,RMAT,N)
       IMPLICIT REAL*8(A-H,O-Z)
       DIMENSION W(500), RMAT(250000),G(500)
       DIMENSION RNEW(500),RK(500)
       W(1)=RMAT(N+1)/RMAT(1)
       G(1)=RK(1)/RMAT(1)
       DO 10 I=2,N
       W(I)=RMAT(I*N+I)/(RMAT((I-1)*N+I)-RMAT((I-2)*N+I)*W(I-1))
    10 G(I)=(RK(I)-RMAT((I-2)*N+I)*G(I-1))/(RMAT((I-1)*N+I)-
      1RMAT((I-2)*N+I)*W(I-1))
       RNEW(N)=G(N)
       N11=N-1
       DO 20 I=1,N11
       J=N-I
    20 RNEW(J)=G(J)-W(J)*RNEW(J+1)
       RETURN
       END
```

Appendix C – Publications and presentations

Poster presentations

- '*Photo assisted fuel cell based on carbon ink*', P. Enright, J.F. Cassidy, A.J. Betts, poster presented at 58th Irish Universities Colloquium, National University of Ireland Galway, (14th - 16th June 2006)
- '*A study of a photoelectrochemical cell*' P. Enright, J.F. Cassidy, A.J. Betts, F. Touati, K.G. McGuigan, poster presented at 57th annual meeting of International Society of Electrochemistry, Edinburgh, (August 27th – September 1st 2006)

Oral Presentations

- *Immobilised TiO_2 layers for water remediation*', P. Enright, J.F. Cassidy, A.J. Betts, presentation at international conference on Materials Energy and Design (MED 06), DIT Bolton St, Dublin (March 14th – 17th 2006).
- '*Novel photoassisted fuel cell*' P. Enright, A.J. Betts, J.F. Cassidy, talk at 59th Irish Universities Chemistry Colloquium in Dublin City University, (13th – 15th June 2007)

Publications

- 'Evaluation of a naive model for square wave voltammetry at a microdisk electrode', P. Enright, J.F. Cassidy, A.J. Betts, *Journal of Electroanalytical Chemistry,* **619 - 620** (2008) 206 – 208
- 'An environmentally friendly fuel cell' F. Touati, L. Ceyssens, J.F. Cassidy, K.G. McGuigan, A.J. Betts, P. Enright (submitted)
- 'A model for cyclic voltammetry with a Langmuir Hinshelwood pre step applied to the formic acid system', P. Enright, J.F. Cassidy, A.J. Betts, (in preparation)
- 'Remediation of organic compounds in wastewater *via* a photoelectrochemical cell using near UV and visible light irradiated titania' P. Enright, J.F. Cassidy, A.J. Betts, (in preparation)